AD NUMBER

AD866981

NEW LIMITATION CHANGE

TO

Approved for public release, distribution unlimited

FROM

Distribution authorized to U.S. Gov't. agencies and their contractors; Critical Technology; DEC 1969. Other requests shall be referred to US Army Aviation Material Laboratories, Fort Eustis, VA 23604.

AUTHORITY

USAAMRDL ltr, 13 Nov 1973

AD

USAAVLABS TECHNICAL REPORT 69-92

HOT CORROSION RESISTANCE OF MATERIALS FOR SMALL GAS TURBINE RECUPERATORS

By

G. Curbishley

W. Larson

D. W. McGrath

E. W. Gellersen

December 1969

U. S. ARMY AVIATION MATERIEL LABORATORIES
FORT EUSTIS, VIRGINIA

CONTRACT DAAJ02-67-C-0048
THE GARRETT CORPORATION
AIRESEARCH MANUFACTURING COMPANY
LOS ANGELES, CALIFORNIA

DISCLAIMERS

The findings in this report are not to be construed as an official Department of the Army position unless so designated by other authorized documents.

When Government drawings, specifications, or other data are used for any purpose other than in connection with a definitely related Government procurement operation, the United States Government thereby incurs no responsibility nor any obligation whatsoever; and the fact that the Government may have formulated, furnished, or in any way supplied the said drawings, specifications, or other data is not to be regarded by implication or otherwise as in any manner licensing the holder or any other person or corporation, or conveying any rights or permission, to manufacture, use, or sell any patented invention that may in any way be related thereto.

Trade names cited in this report do not constitute an official endorsement or approval of the use of such commercial hardware or software.

DISPOSITION INSTRUCTIONS

Destroy this report when no longer needed. Do not return it to the originator.

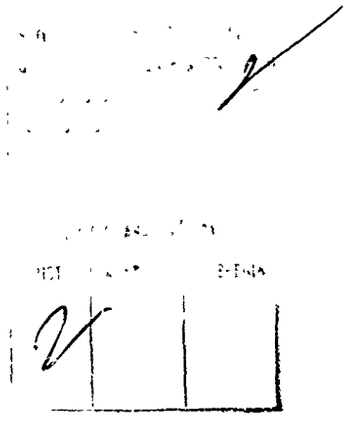

DEPARTMENT OF THE ARMY
U S ARMY AVIATION MATERIEL LABORATORIES
FORT EUSTIS, VIRGINIA 23604

The object of this contractual effort was to investigate the ability of potential gas turbine engine recuperator materials to resist hot corrosion in a corrosive engine operating environment. A secondary objective was to consider the hot corrosion phenomenon in light of the data generated by this effort as compared to existing theories of the mechanism of hot corrosion.

This report was prepared by the AiResearch Manufacturing Company of the Garrett Corporation under the terms of Contract DAAJ02-67-C-0048. It presents the method of selection of candidate recuperator materials and braze alloys, descriptions of the tests performed, and an evaluation and analysis of these tests.

This report has been reviewed by technical personnel of this command, and the conclusions contained herein are concurred in by this command.

Project 1G162203D144
Contract DAAJ02-67-C-0048
USAAVLABS Technical Report 69-92
December 1969

HOT CORROSION RESISTANCE OF MATERIALS FOR SMALL GAS TURBINE RECUPERATORS

Final Report

AiResearch Report 69-5351

By
G. Curbishley
W. Larson
D. W. McGrath
E. W. Gellersen

Prepared by
The Garrett Corporation
AiResearch Manufacturing Company
Los Angeles, California

for
U. S. ARMY AVIATION MATERIEL LABORATORIES
FORT EUSTIS, VIRGINIA

ABSTRACT

This report describes the results of a two-year program entitled "Investigation of Materials to Resist Hot Corrosion in Small Gas Turbine Engine Recuperators" conducted by AiResearch, a division of The Garrett Corporation, for the U.S. Army Aviation Materiel Laboratories, Fort Eustis, Virginia, under Contract No. DAAJ02-67-C-0048.

The objectives of the program were:

1. To determine the hot corrosion resistance and rupture strengths of thin-wall tube materials from which economic lightweight recuperators could be constructed and to verify these data by exposing a test recuperator to typical operating conditions including sea-salt contaminated products of combustion of JP-4 fuel

2. To investigate hot corrosion mechanisms at temperatures below 1500°F.

The following five tubing materials were selected on the basis of economics, corrosion resistance, and mechanical properties:

Hastelloy X

Inconel 625

N-155

Incoloy 800

Type 347 stainless steel

Three types of brazing alloys (nickel-based, nickel manganese-based, and gold-based) were selected for evaluation on the basis of known corrosion resistance and mechanical properties.

Compatible brazing alloy/tube material combinations and optimum brazing temperatures were first determined by the metallurgical examination of brazed, simulated tube/header joints.

The corrosion resistance of the selected brazing alloy was then determined by exposing simulated tube-header joints to synthetic gas turbine exhaust products at 1500°F.

Based on these preliminary results, tube material/braze material combinations were then selected and subjected to stress-rupture tests in a cyclic hot corrosion test rig at temperatures between 1100° and 1500°F for periods of up to 1000 hr.

A recuperator fabricated from two of the candidates selected above, N-155 brazed with Nicrobraz 200 and Incoloy 800 brazed with Coast Metals 50B, was then operated in the sea-salt contaminated exhaust of a JP-4 fueled combustor for a period of 500 hr. Conditions were such as to maintain the majority of the tubes between 900° and 1500°F.

The hot corrosion mechanisms were studied, and the results of the cyclic hot corrosion tests and the recuperator tests were compared.

The brazing alloy evaluation showed the nickel-chromium alloys to be more resistant to hot corrosion than the gold-base alloys or manganese-base alloys.

A Larson-Miller plot of the cyclic hot corrosion test data indicates that Inconel 625 is the best tube material; Hastelloy X and N-155 are second choices. These three tubing materials well exceeded the selected recuperator operating requir ments. Incoloy 800 only marginally exceeded the requirements. Type 347 stainless steel had inadequate hot corrosion resistance at temperatures higher than 1300°F.

The recuperator tests showed good qualitative comparison to the cyclic hot corrosion test except that Incoloy 800 was found to be equal to N-155 in corrosion resistance. Both tests showed Incoloy 800 and N-155 to be subject to localized oxidation, which may limit their usefulness in recuperators.

This study program proved satisfactory in identifying and evaluating tube material and braze alloys for recuperator applications.

TABLE OF CONTENTS

TABLE OF CONTENTS (Continued)

LIST OF ILLUSTRATIONS

LIST OF ILLUSTRATIONS (Continued)

LIST OF ILLUSTRATIONS (Continued)

LIST OF ILLUSTRATIONS (Continued)

LIST OF ILLUSTRATIONS (Continued)

LIST OF ILLUSTRATIONS (Continued)

LIST OF ILLUSTRATIONS (Continued)

LIST OF ILLUSTRATIONS (Continued)

LIST OF ILLUSTRATIONS (Continued)

LIST OF ILLUSTRATIONS (Continued)

LIST OF ILLUSTRATIONS (Continued)

LIST OF ILLUSTRATIONS (Continued)

LIST OF TABLES

LIST OF TABLES (Continued)

LIST OF TABLES (Continued)

INTRODUCTION

The U.S. Army's increased interest in recuperators for airborne and portable turboshaft engines has made the selection of materials and fabrication processes for optimum design highly significant and critical. Recuperators are attractive from standpoints of both increased range per load of fuel and potentially lower overall costs resulting from fuel savings. The major recuperator design requirements are

1. Low weight
2. Low cost
3. Long life (that is, low maintenance)

These objectives must be met with materials that resist the hot corrosion caused by hot combustion products. Hot corrosion is defined as the attack on metal alloy components caused directly or indirectly by contact with products of combustion of gas turbine engines. Included in this term are all synergistic effects that contribute to hot corrosion, such as sulfidation, oxidation, erosion, stress-corrosion, and both static and cyclic stresses.

The literature indicates that most corrosion investigations for gas turbine engine materials have been for temperatures above 1500°F. Materials that withstand this environment will, of course, sustain the 900° to 1500°F temperature of the recuperator. High-temperature alloys, however, are not necessarily good heat exchanger core materials and are often extremely expensive, less available, and more difficult to fabricate than lower-strength alloys. As a result, there is a serious lack of data on suitable recuperator materials that resist hot corrosion attack in the 900° to 1500°F environment.

U.S. Army Aviation Materiel Laboratories initiated a 21-month program to obtain fundamental data on materials and joining processes that withstand corrosive combustion products at recuperator temperatures. This document is the final report of that program.

The program was organized into seven work tasks that were divided into two phases:

Phase I Initial Material Evaluation and Selection

- Task A Selection of Candidate Base Metals and Filler Metals
- Task B Material Procurements
- Task C Preliminary Brazing Tests
- Task D Cyclic Hot Corrosion Tests

Phase II Experimental and Verification Tests

Task A Design and Fabrication of Recuperator Test Cores

Task B Recuperator Test

Task C Final Metallurgical Evaluations

Each work task is described in a separate section of the report. A summary discussion of the total program and the program conclusions and recommendations are presented in the last section of the report.

Since gas turbine cores are of brazed construction, the program was directed to identify suitable structural alloys and brazing filler metals. Tests were conducted on alloys and filler metals selected from a large number of potential candidates. The following typical recuperator operating conditions were selected to establish test conditions for the program:

	100-Percent Power	60-Percent Power
Gas inlet temperature	1214°F	1358°F
Gas inlet pressure	15.6 psia	15.2 psia
Air inlet temperature	759°F	645°F
Air inlet pressure	206 psia	139 psia

The target minimum life expectancy for a recuperator was 5000 hr distributed over the following operating envelope:

Power (percent)	Time at Power (percent)
100	15
75	45
55	25
35	10
Idle	5

SELECTION OF CANDIDATE TUBING MATERIALS

FACTORS AFFECTING MATERIAL SELECTION

Many factors need to be considered in the selection of appropriate materials for recuperator construction. Some of the most significant considerations are:

1. Economics of manufacture
2. Environmental compatibility
3. Mechanical properties

In this program, the materials selected for study were (1) those materials that would contribute most to an understanding of the fundamental principles of hot corrosion of thin-wall tubing, and (2) those alloys most suitable for the manufacture of reliable, lightweight, and economical recuperators. Since the ultimate purpose of the program was to generate information that could be applied to the design and manufacture of hardware, greater emphasis was directed to the latter requirement. Table I shows the nominal chemical composition of the alloys considered as candidates. The materials listed are those that have found application in recuperators and in gas turbine engines.

ECONOMICS OF MANUFACTURE

Cost is a factor of prime importance in almost all recuperators. To provide an economic advantage, the life cycle costs of a recuperated engine-powered aircraft must be less than that of an unrecuperated engine-powered aircraft. Within this limitation, the choice between materials must be made by trading off the cost of original and replacement units against design life, ease of replacement, and desired reliability.

Manufacturing costs are based on two considerations: first, the capability of the material to be drawn into a small-diameter, thin-wall tube; and second, the ease of manufacture of a recuperator from that tubing. Since initial material selection was based on the suitability of the material for efficient recuperator production, several alloys were eliminated because of the difficulties of forming them into such thin-wall tubing in production quantities at competitive prices. These materials were Udimet 500, Udimet 700, and AiResist 213. Udimet 500 and 700 are nickel-base alloys containing high proportions of aluminum and titanium. These elements impart the necessary mechanical properties to the material, but they also cause a decrease in ductility. This low ductility coupled with high yield strength makes the production of thin-wall tubing from these alloys uneconomical. A further drawback to the Udimet alloys is that their high strengths are developed by complex heat treatment. AiResist 213 is a cobalt-base alloy containing additions of aluminum and yttrium. Both of these elements

TABLE I. CHEMICAL COMPOSITION OF CANDIDATE TUBING ALLOYS

		Nominal Chemical Composition, Weight Percent												
Group	Alloy	C	Mn	Si	Cr	Ni	Co	Mo	W	Cb+Ta	Fe	Ti	Al	Others
I	Type 347 stainless steel	0.08*	0.40	1.00*	18.0	11.0	-	-	-	0.80	Bal	-	-	-
	Type 430 stainless steel	0.07	0.45	0.50	17.0	0.30	-	-	-	-	Bal	-	-	-
	Armco 21-6-9	0.05*	9.0	1.0	21.0	6.0	-	-	-	-	Bal	-	-	0.5 N_2
II	L-605	0.10	1.5	0.50	20.0	10.0	Bal	-	5.0	-	-	-	-	-
	N-155	0.15	1.5	0.50	21.0	20.0	20.0	3.0	2.5	1.0	Bal	-	-	-
	AiResist 213	0.15	0.10*	0.20*	19.0	0.50*	Bal	-	5.0	6.5	0.50*	-	3.5	0.15 Zr, 0.10 Yt
III	Inconel 600	0.04	0.20	0.20	16.0	Bal	-	-	-	-	7.0	-	-	-
	Incoloy 800	0.04	0.75	0.35	20.0	32.0	-	-	-	-	Bal	0.30	0.30	-
	Incoloy 825	0.05	1.0	0.50	21.0	42.0	-	3.0	-	-	Bal	-	-	2.2 Cu
IV	Hastelloy X	0.10	0.50	0.50	22.0	Bal	1.5	9.0	0.60	-	18.5	-	-	-
	Hastelloy C	0.08*	0.75	0.75	15.5	Bal	2.0	16.0	4.0	-	5.5	-	-	-
	Hastelloy F	0.05*	1.0	0.75	22.0	Bal	2.0	6.5	0.75	2.0	20.0	-	-	-
	Inconel 625	0.05	0.15	0.30	22.0	Bal	-	9.0	-	4.0	3.0	0.20	0.20	-
V	Inconel 718	0.04	0.20	0.30	18.5	Bal	-	3.0	-	5.0	18.5	0.90	0.40	-
	Udimet 500	0.08	-	-	18.0	Bal	18.5	4.0	-	-	-	2.9	2.9	0.05 Zr
	Udimet 700	0.08	-	-	15.0	Bal	18.5	5.2	-	-	-	3.5	4.3	0.03 B
	TD Nickel	-	-	-	-	Bal	-	-	-	-	-	-	-	2.2 ThO_2

*Indicates maximum allowed

greatly improve the hot corrosion resistance of the alloy. AiResearch 213 has been drawn into thin-wall tubing, but is difficult to work because of low temperature age hardening characteristics, which are currently under study. Although further improvements in cold workability are anticipated, tubing prices will still be high, and the use of the alloy would not be warranted at temperatures of 1500°F and below. The ease with which alloys can be drawn into thin-wall tubing is reflected in the costs. Table II gives some idea of the costs of 0.125-in.-OD by 0.0035-in.-wall tube purchased in 50,000-ft quantities.

ENVIRONMENTAL COMPATIBILITY

One of the most important requirements of a recuperator material is that it must not suffer excessive or unacceptable degradation when exposed to its operating environment. That is, the degradation must not be so severe as to cause failure before the expiration of the design life. Since mechanical properties are invariably degraded by environmental attack and by metallurgical changes such as aging reactions and carbide precipitation, measuring the properties of new, unexposed material is not sufficient. Metallurgical stability and hot corrosion resistance cannot be considered apart; they are important in evaluating mechanical properties.

Hot corrosion is a process of chemical attack at elevated temperatures by atmospheres containing either oxygen, sulfur, sea salts, or combinations of these corrodents. Although there are many conflicting theories explaining the mechanism of hot corrosion, all investigators agree that susceptibility to attack is inversely proportional to the amount of chromium in the alloy. Generally speaking, cobalt-base superalloys are superior to iron-base alloys, which in turn are better than nickel-base alloys in resisting hot corrosion. The severity of hot corrosion increases with increasing temperature up to about 1950°F, but most theories suggest that attack would be negligible below 1200°F. It is also postulated that hot corrosion rates are dependent on the stresses imposed on the alloys.

It was considered that all the candidates would have sufficient hot corrosion resistance at 900°F, but at higher temperatures up to 1500°F some of the alloys would have little resistance to sulfur-bearing gases containing ingested sea salts (such as found in marine atmospheres). The most susceptible to attack would be TD Nickel, because this alloy contains neither chromium nor any other element that affords protection at 1500°F. Furthermore, it has no mechanical properties advantages in this temperature range. Three other alloys that have lower chromium content and may suffer corrosion over prolonged periods of exposure to hot corrosive atmospheres are Hastelloy C, Inconel 600, and type 430 stainless steel, all of which have about 15 percent chromium. Such low chromium contents probably would not protect these alloys at 1500°F in marine atmospheres, particularly the first two, which are nickel-base alloys. Hastelloy C may also be unsuitable because some authorities claim that a high molybdenum content will adversely affect oxidation resistance.

TABLE II. CONSIDERATIONS FOR SELECTING CANDIDATE MATERIALS

Alloy	Temperature at Which 3.4 ksi Produces Rupture In 1000 hr (°F)	Hot Corrosion Resistance	Tube Fabricability	Brazing Compatibility	Costs (50,000 ft Lots) $/100 ft	Alloy Selected
Type 347 stainless steel	1550	Poor	Good	Good	34	X
Type 430 stainless steel	1200	Poor	Good	Good		
Armco 21-6-9	1450	Poor	Good	Good		
L-605	1800	Good	Good	Good	111	
N-155	1750	Good	Good	Good	87	X
AiResist 213	1775	Excellent	Fair	Good		
Inconel 600	1600	Fair	Good	Good	37	
Incoloy 800	1500	Fair	Good	Good	37	X
Incoloy 825	1600	Fair	Good	Good	41	
Hastelloy X	1800	Good	Good	Good	107	X
Hastelloy C	1700	Fair	Good	Good		
Hastelloy F	1700	Good	Good	Good		
Inconel 625	1800	Good	Good	Good	46	X
Inconel 718	1600	Good	Fair	Good		
Udimet 500	1850	Fair	Poor	Good		
Udimet 700	1850	Fair	Poor	Good		
TD Nickel	2000	Poor	Good	Fair		

MECHANICAL PROPERTIES

The reference power system requirements presented in the introduction show a maximum gas temperature at the inlet to the recuperator of 1350°F and a maximum air inlet pressure of 206 psia. This pressure represents a calculated hoop stress of 3400 psi on the 0.125-in.-OD by 0.0035-in.-wall tubing where

$$\sigma = \frac{Pd}{2t}$$

σ = hoop stress in tube wall (psi)

P = internal tube pressure (psig)

d = outside diameter of tube (in.)

t = tube wall thickness (in.)

For this investigation, the recuperator design life was taken to be 5000 hr under these operating conditions. To take care of uprating and future developments, the testing program was planned to acquire data at temperatures up to 1500°F. Consequently, the mechanical properties of the candidate materials were evaluated at this temperature.

The alloys considered were grouped according to their chemical compositions, and their 5000-hr stress rupture properties at 1500°F were compared. Because of the lack of information concerning the stress rupture properties of tubes, data for sheet materials were compared. Table II indicates the salient features of the alloys considered as candidates.

Group I: Stainless Steels

Type 347 Stainless Steel

Type 347 stainless steel is one of the least expensive of the candidate materials. It is widely used in recuperators and has provided excellent performance at lower temperatures. In this alloy, the presence of columbium minimizes the carbide precipitation in the grain boundaries and increases corrosion resistance. Type 347 is readily drawn into tube form and is easily brazed. It has good oxidation resistance at moderate temperatures and relatively good corrosion resistance; in the cold drawn condition, however, it can be susceptible to stress corrosion cracking in chloride solutions. Since this alloy has proved successful in recuperator applications operating below 1300°F, one of the objectives of the program was to determine the suitability of the material at higher temperatures under hot, corrosive conditions.

Type 430 Stainless Steel

AISI type 430 is a low-carbon, high-chromium ferritic steel possessing good resistance to oxidation and corrosion at elevated temperatures. It is lower in cost than type 347 and has been used in turbine ducting. It also has good room-temperature strength and ductility, but it has only one-half the yield strength of type 347 at 1200°F. The stress rupture properties of the alloy are also low.

Armco 21-6-9

The cost of Armco 21-6-9 is comparable to that of type 347 stainless steel, and its yield strength is much higher. This alloy is an austenitic steel and reportedly has excellent resistance to attack from products of combustion, particularly from leaded gasolines. With its high chromium content, it should have good resistance to hot corrosion. Since it is available in sheet form and its fabricability is similar to that of type 347 stainless steel, the production of high-quality welded tubing from Armco 21-6-9 should present no difficulty.

Comparison of Group I Alloys

Figure 1 presents the stress rupture properties of the stainless steels as a function of temperature. These data show that type 347 is the only one of the candidate stainless steel materials that has sufficient strength throughout the required temperature range. A 5000-hr stress-rupture strength of greater than 3.4 ksi was considered as the minimum requirement for materials to be considered for this program. Armco 21-6-9 appears to have insufficient strength above 1300°F, and type 430 could be used only at temperatures below about 1100°F. For these reasons, the latter two materials were omitted from the testing program.

Group II: Iron-Cobalt and Cobalt-Base Alloys

L-605

L-605 (Haynes 25) is a cobalt-base superalloy with good strength and excellent hot corrosion resistance in the 1000° to 1500°F temperature range. Its main application is at temperatures of 1700° to 2000°F, where it is stronger than most wrought nickel-base superalloys. It offers no strength advantage over Inconel 625 (discussed under Group IV alloys) at temperatures below 1100°F, however; because it has lower ductility, it is not expected to have comparable low-cycle (thermal) fatigue performance. Fabricability of the alloy is good, but its greater work hardening tendency makes tube forming difficult. L-605 would be an ideal material to use in applications requiring higher strength.

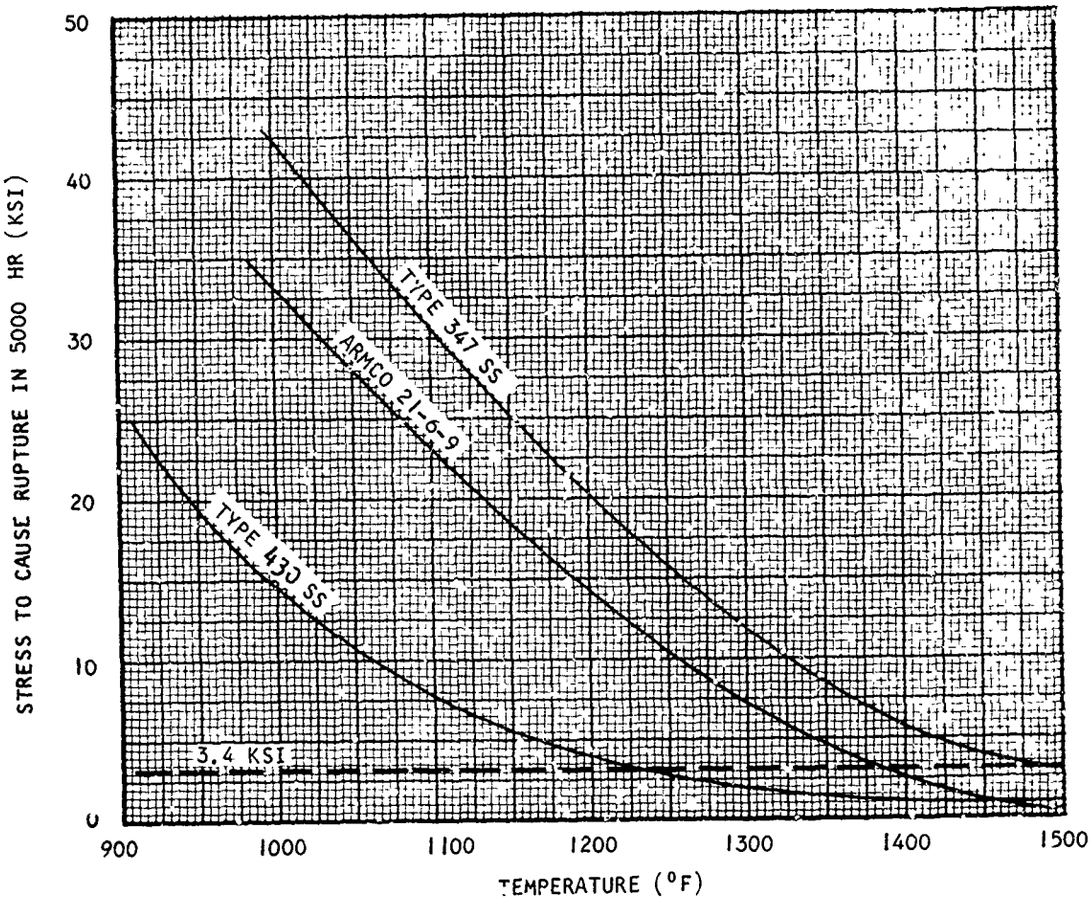

Figure 1. 5000-hr Stress-Rupture Properties of Stainless Steels (Armco Stainless Steels: Data for Sheet Material).

N-155

N-155 is an alloy containing 20 percent chromium, cobalt, and nickel, with the balance iron. Small amounts of tungsten, molybdenum, and columbium are also present. The high content of chromium and cobalt should contribute to good hot corrosion resistance. The alloy is widely used in gas turbine engines and is available as thin-wall tubing. N-155 has good forming, welding, and brazing characteristics. It is a moderate-cost alloy with moderate strength but only fair ductility. If hot corrosion of nickel-base alloys (Group IV) presents a problem, then N-155 is a good alternative tubing alloy.

Comparison of Group II Alloys

There is very little difference between the 5000-hr stress-rupture properties of N-155 and those of L-605 at temperatures to 1500°F (see Figure 2). However, N-155 costs approximately 20 percent less than L-605, so there is no real justification in using the more expensive alloy.

Group III: Nickel-Chromium and Nickel-Chromium-Iron Base Alloys

Inconel 600

Inconel 600 is a low-cost nickel-base alloy containing 15 percent chromium and having good oxidation and corrosion resistance. The 15 percent chromium, however, may be insufficient to impart good hot corrosion resistance at 1500°F. Because of the absence of molybdenum to provide solid solution hardening, this alloy has only medium strength. It has somewhat better rolling, drawing, and forming properties than Inconel 625 or Hastelloy X.

Incoloy 800

Incoloy 800 is a low-cost iron-base superalloy containing 32 percent nickel and 21 percent chromium. The high percentage of nickel stabilizes the austenitic structure even after prolonged exposure at elevated temperatures. Nickel renders the alloy practically immune to stress corrosion cracking in chloride ion environments. Because of its chromium content, the alloy displays good resistance to hot corrosion and oxidation. Mechanical properties at 1000° to 1500°F are comparable to type 347 stainless steel. Fabrication, welding, and brazing characteristics are very good.

Incoloy 825

Incoloy 825 is similar to Incoloy 800 except that the nickel content is higher, and small amounts of copper and molybdenum have been added to improve resistance to corrosion by sulfuric and sulfurous acids. The alloy displays exceptional resistance to seawater corrosion and is nearly immune from stress corrosion cracking.

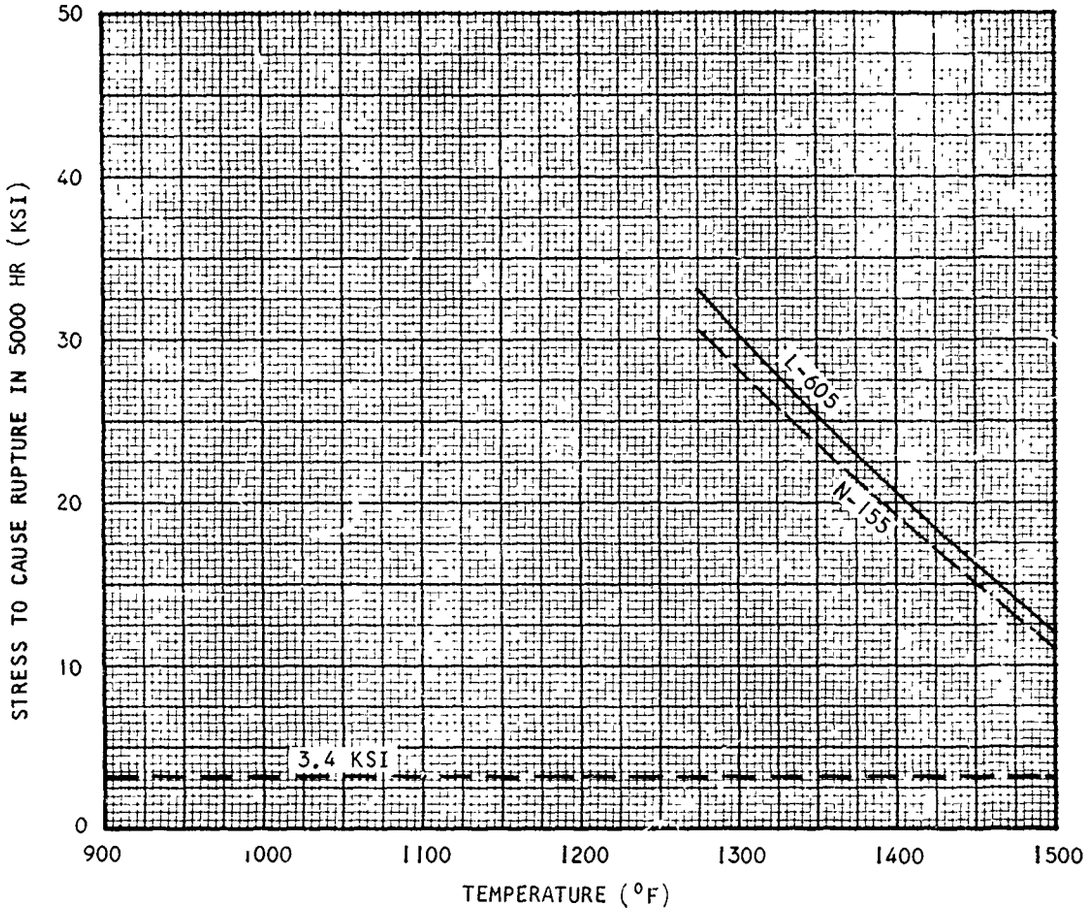

Figure 2. 5000-hr Stress-Rupture Properties of Iron-Cobalt and Cobalt-Base Alloys (Union Carbide Corporation: Data for Sheet Materials).

Comparison of Group III Alloys

Inconel 600 has the lowest 5000-hr stress-rupture strength in this group. It also has the lowest amount of chromium and a high nickel content, indicating that its hot corrosion resistance would probably be inferior to the Incoloy alloys. Although Incoloy 825 has slightly better properties than Incoloy 800, they should have almost identical life under dynamic, hot corrosion conditions. Since Incoloy 825 is more expensive, Incoloy 800 is recommended. As can be seen from Figure 3, the stress-rupture properties of Inconel 600 are inferior to those of the Incoloy alloys.

Group IV: Nickel-Base Alloys Containing Chromium and Molybdenum

Hastelloy X

Hastelloy X is a favorite nickel-base sheet-metal alloy for use in combustion liners and hot ducting of gas turbine engines. It is moderately priced and readily available. Its mechanical properties are much better than those of type 347 stainless steel, and it has excellent hot corrosion resistance. Hastelloy X has very good forming, welding, and brazing characteristics. AiResearch has used this alloy in making tubes 0.125-in.-OD by 0.003-in.-wall to operate in an air-to-hydrogen heat exchanger at 1550°F (Contract AF 33(615)1926).

Hastelloy C

Excellent room-temperature corrosion resistance is the outstanding feature of this nickel-base alloy. It is very similar to Hastelloy X, but it has a higher molybdenum and tungsten content, which may adversely affect the hot corrosion resistance. Also, the chromium content of Hastelloy C is lower than that of Hastelloy X, indicating that the latter will have superior hot corrosion resistance. The fabricability of Hastelloy C is similar to that of Hastelloy X.

Hastelloy F

The chemical composition and mechanical properties of Hastelloy F are very similar to those of Hastelloy X. The main differeneces are the lower carbon content and the addition of columbium and tantalum to Hastelloy F to minimize grain boundary carbide precipitation. Consequently, this alloy has better resistance to corrosive acids and alkaline solutions, corrosive gases, and stress corrosion cracking. In the 1000° to 1500°F temperature range, however, the mechanical strength and ductility of Hastelloy F are slightly lower than those of Hastelloy X.

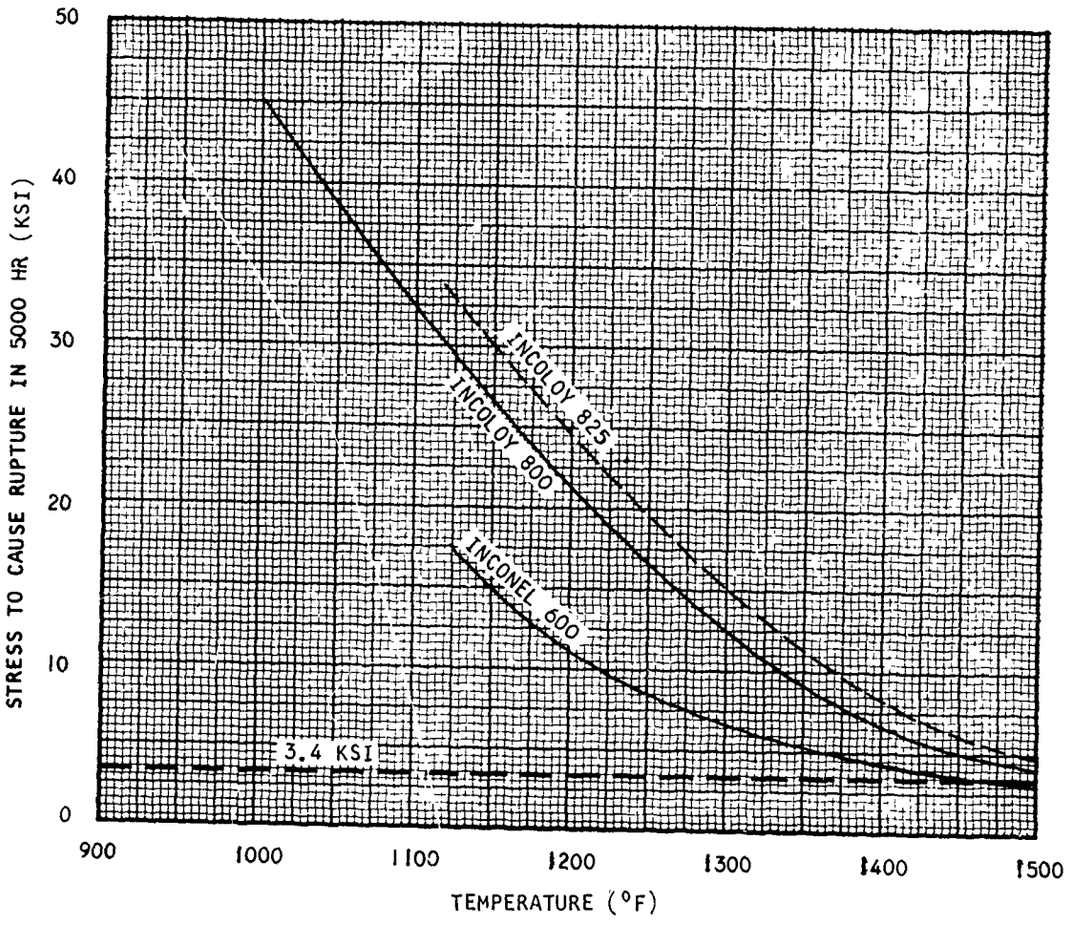

Figure 3. 5000-hr Stress-Rupture Properties of Nickel-Chromium and Nickel-Chromium Iron Alloys (Huntington Alloys: Data for Sheet Material).

Inconel 625

At 1500°F, Inconel 625 has better stress-rupture properties than Hastelloy X and comparable oxidation resistance. Its distinguishing feature is the improved ductility at elevated temperatures. Resistance to low-cycle fatigue failure should be good. This alloy has excellent fabricability and is currently used in a number of hot ducting applications in turbine engines.

Comparison of Group IV Alloys

Although there is not much difference in the mechanical properties of these materials, particularly at 1500°F, Inconel 625 is the strongest alloy in this group. This may be seen from the four curves presented in Figure 4. The high strength of Hastelloy C is attributed to the high molybdenum content of this alloy, but its combination of molybdenum and chromium may be such that its hot corrosion resistance may not be as good as that of the other alloys in this group. Since there appears to be very little difference between Hastelloy X and F, the former was preferred because of widespread experience in fabricating and brazing of this alloy.

Inconel 625 has higher strength and lower cost than Hastelloy X, but brazing with other than the gold-base brazing alloys may be more difficult, in which case its advantages in strength and economy may be lost. Hastelloy X has excellent properties and hot corrosion resistance and can be brazed without undue difficulty. Although this alloy is more expensive than Inconel 625, its use may prove to be more economical if the lower cost nickel-base brazing alloys can be utilized. Both of these alloys were selected for investigation.

Group V: Heat-Treatable Alloys

Inconel 718

Inconel 718 is a high-strength, nickel-base alloy used predominantly at temperatures below 1200°F; at temperatures above this, the alloy averages with a corresponding lowering of stress-rupture strength and ductility. (Low ductility results in poor low-cycle fatigue performance.) Compared with most precipitation hardening alloys, the fabricability of Inconel 718 is good, but it is not generally equal to that of the solid-solution hardening alloys. Inconel 718 offers no real advantage in the temperature range of interest.

Udimet 500

Udimet 500 is a highly alloyed nickel-base alloy with very good mechanical properties at elevated temperatures. It has some ductility and, with difficulty, has been rolled into sheet form. The alloy has good hot corrosion resistance.

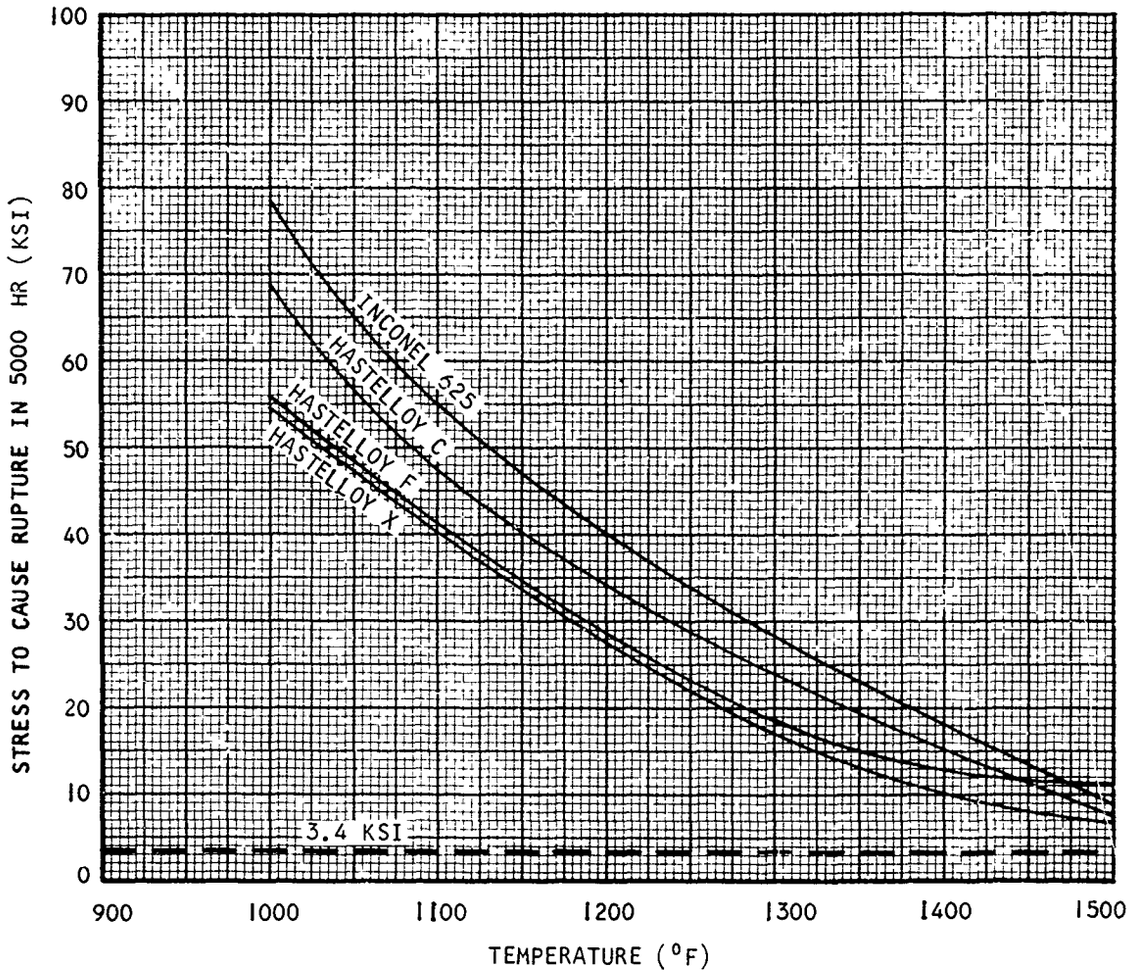

Figure 4. 5000-hr Stress-Rupture Properties of Nickel-Base/Chromium Molybdenum Alloys (International Nickel Company: Data for Sheet Material).

Udimet 700

Udimet 700 is similar to Udimet 500, and derives its higher strength from the addition of more aluminum and titanium. It is not generally available in sheet form, but it is used as forged gas turbine disks.

Comparison of Group V Alloys

The relatively high aluminum and titanium contents of the two Udimet alloys impart the necessary strength to the materials in the 1000° to 1500°F temperature range of interest, but they also cause a considerable decrease in ductility. This fact and the high yield strength of these alloys make the production of thin-wall tubing impracticable. A further drawback to the precipitation hardening alloys is that their high strengths are developed by complex heat treatments that are not conducive to economical recuperator manufacturing practice.

Group VI: TD Nickel

TD Nickel is a high-temperature alloy that derives its high-temperature strength from the addition of finely dispersed thoria (ThO_2) particles in a matrix of essentially pure nickel. It has higher mechanical strength than nickel- or cobalt-base alloys at temperatures above 2000°F, but it offers no advantages at temperatures up to 1500°F. TD Nickel has good forming characteristics at room temperature and high thermal conductivity. Although this feature is desirable in a recuperator, the poor weldability and low ductility at 1500°F limit its use in this application. As explained earlier, because of the poor hot corrosion resistance of uncoated TD Nickel, this material is not recommended for use in gas turbine engine recuperators. It is not considered feasible to coat 0.0035-in.-wall tubing.

Materials Selected

Based on considerations of recuperator manufacturing economics and the mechanical and chemical properties of the candidate alloys, the following materials were selected for further investigation:

1. Type 347 stainless steel
2. N-155
3. Incoloy 800
4. Hastelloy X
5. Inconel 625

At least one alloy was chosen from each of the first four groups of alloys. No materials were selected from groups V and VI because of the inadequacies of these alloys. The purpose of dividing the materials into groups was to compare the hot corrosion characteristics of the different types of alloys. Hastelloy X and Inconel 625 were both selected from the same group to take advantage of the excellent properties of each alloy.

JOINING METHODS

Tube-header joints are a major consideration in fabricating tubular recuperators. An example of this type of heat exchanger is shown in Figure 5. Of the three major methods of obtaining sound tube-header joints (brazing, fusion welding, and diffusion bonding), brazing is the most practical, economical, and reliable. This is especially true when small tubing sizes are involved because the tooling needed for brazing is much simpler than that required for fusion welding or diffusion bonding. Since fusion welding and diffusion bonding are both extremely time-consuming, they are not economical for manufacturing thin-wall tubular heat exchangers. The most logical approach to joining, therefore, is by brazing.

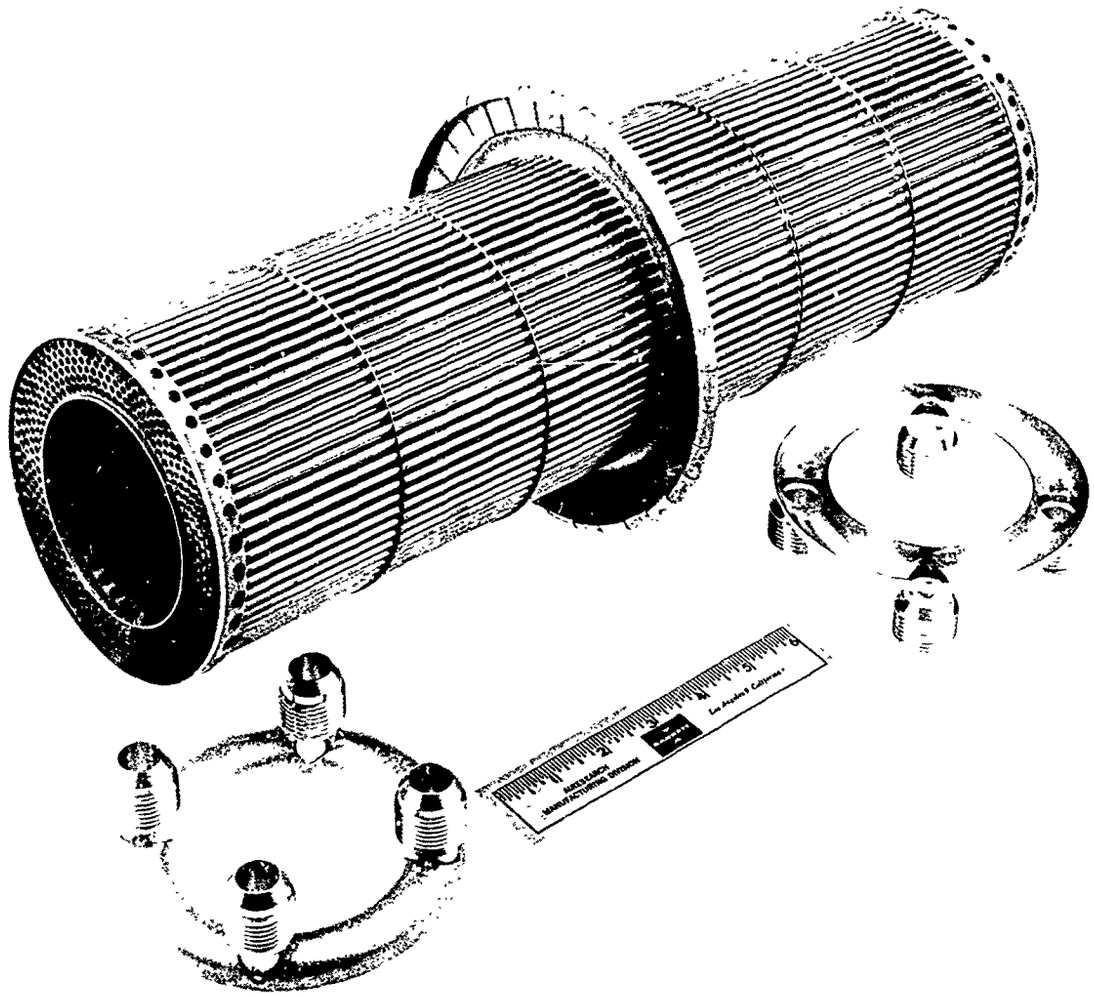

Figure 5. Example of Tubular Heat Exchanger With Brazed Tube-Header Joints.

SELECTION OF FILLER METALS

BRAZING ALLOY SELECTION

The brazing alloy selected must satisfy the following criteria:

1. The brazing temperature must be compatible with the base material; that is, there should be no excessive grain growth or carbide precipitation within the parent metal as a result of the brazing cycle.

2. There should be a minimum of penetration and erosion into the base metal.

3. The brazing alloy must wet the base metal and flow into the joint.

4. The tubes should not be seriously embrittled by the diffusion of the brazing alloy into the base metal.

5. The joints must have adequate strength and hot corrosion resistance to give satisfactory service reliability.

6. The galvanic potential between the base material and filler metals should be low, and the base metal should preferably be anodic since it will have a much greater surface area.

The filler metals for brazing tubular heat exchanger assemblies were selected on the basis of previous experience with thin-wall tubing and data contained in published reports of company-sponsored or Government-funded R & D programs. In addition, the results, conclusions, and recommendations of The Boeing Company in their brazing work associated with small gas turbine engine recuperator research[1] were considered.

BRAZING ALLOYS

The normal silver-base alloys such as 72Ag-28Cu and 85Ag-15Mn have poor strength at temperatures above 900°F. Although the addition of palladium and manganese to silver (Palmansil 5) increases the elevated-temperature strength of joints, oxidation resistance is still inadequate for the intended use. Copper-base alloys such as 93Cu-7P, 86Cu-8P-6Ag, 95Cu-5Si, and 63Cu-22Mn-10Co-5Ni also have poor strength at elevated temperatures, and their inadequate oxidation resistance renders them unsuitable for operation in the 900° to 1500°F temperature range. Manganese-base alloys (70Mn-30Ni, 67Mn-16Ni-16Co-1B) have better strength and oxidation resistance than the silver- and copper-base materials, but their corrosion resistance under the anticipated service conditions is still insufficient.

Nickel-base filler metals containing silicon, boron, and chromium have good strength and corrosion resistance up to 1500°F, but diffusion (intergranular penetration and solutioning) may be excessive for 3.5-mil-wall tubing. Reducing or eliminating the boron content (Nicrobraz 30 or General Electric J-8100) reduces the degree of penetration. Boron, which is added to the braze alloy as a melting temperature depressant, can be effectively replaced by manganese as in Nicrobraz 65, which is generally less harmful because it does not cause intergranular penetration.

Gold-base alloys have excellent corrosion resistance and strength in the temperature range of interest. Additions of palladium and nickel (Palniro 1, Palniro 7) increase the elevated-temperature strength. These alloys generally have lower hardness, better ductility, and less tendency toward interalloying and intergranular penetration than the nickel-base alloys.

For the reasons indicated above, the nickel-base, nickel-manganese-base, and gold-base alloys were the only types considered suitable as braze alloys for this program. The candidate filler metals selected for brazing the nickel- and cobalt-base superalloys, the austenitic stainless steels, and the iron-base superalloys are presented in Table III. Their nominal chemical compositions and brazing characteristics are also shown.

TABLE III. CANDIDATE BRAZING FILLER METALS

Brazing Filler Metal	Spec.*	Nominal Chemical Composition of Brazing Filler Metals										Normal Brazing Temp (°F)	Compatible Base Metals	Characteristics
		Au	Pd	Ni	Cr	B	Si	P	C	Mn	Others			
Palniro 4; AGC 4	-	30	34	36		-	-	-	-	-	-	2170	A	Limited diffusion into base metal (0.5 to 1.0 mil), excellent wettability, good high-temperature strength, oxidation-corrosion resistance, good ductility.
Palniro 1; AGC 1	-	50	25	25	-	-	-	-	-	-	-	2070	A	Limited diffusion into base metal (1.0 to 1.5 mils), other characteristics similar to Palniro 4.
Palniro 7; AGC 7	-	70	8	22	-	-	-	-	-	-	-	1950	A,B,C	Low diffusion into base metal (0.5 mil), other characteristics similar to Palniro 4.
J-8100	BNI-5	-	-	71	19	-	10	-	0.10***	-	-	2150	A	Limited diffusion into base metal (0.5 to 1.5 mils), good wettability, good high-temperature strength, good oxidation-corrosion resistance.
Nicrobraz 135	4779	-	-	94	-	2	3 5	-	0.06***	-	-	2000	A	Low diffusion into base metal (0.5 to 1.0 mil), good wettability, good high-temperature strength, good oxidation-corrosion resistance.
Nicrobraz 65	-	-	-	65	-	-	7	-	-	?3	4 Cu	1975	A,B,C	Low diffusion into base metal (0.5 mil), good wettability, good high-temperature strength, good oxidation-corrosion resistance.
Nicrobraz 200	-	-	-	bal	7.0	3.2	4.5	-	0.10	-	6% W, 3% Fe	1950 2050 2150	A	Limited diffusion into base metal (1.0 to 2.5 mils), good wettability, high-temperature strength and oxidation resistance. Recommended by Boeing in their study[1] because of its good brazability and low cost.
Coast Metals 508	-	-		bal	-	1.5	2.6	-	-	-	-	2000 2100	-	Lower B content
Englehard 135	-	-	21	48	-	-	-	-	-	31	-	2150	-	Medium strength at elevated temperatures, good corrosion and oxidation resistance, minimum diffusion into base metal, good joint strength.

*A = Nickel-base superalloys; e.g., Hastelloy X, Inconel 625, Hastelloy C.
B = Iron-base superalloys; e.g., Incoloy 800, Incoloy 825
C = Austenitic stainless steels; e.g., Type 347 stainless steel, Armco 21-6-9.

**Specifications: All numbers (e.g., 4777) = AMS Specification; Letters and numbers (e.g., BNI-5) = ASTM Specifications

***Maximum content

TUBE MATERIAL PROCUREMENT

To aid in the initial selection of tubing materials, a tentative material specification, Heat Resistant Tubing, was drafted. Four manufacturers of small-diameter tubing were contacted and asked to estimate the costs of 100-, 200-, and 50,000-ft lots of the tubes manufactured according to the requirements of the tentative specification. Since most of the industry lacks experience in drawing small-diameter, thin-wall tubing in these materials, the initial response was poor. The purpose of the program was explained to each manufacturer, but only two vendors submitted written quotations, and only one of these was able to estimate prices for all tubing materials requested. The other quoted only four of the alloys. The third vendor gave prices for two materials, and the fourth manufacturer declined to submit a quotation. Delivery times and costs were analyzed, and tubing orders were placed with two of the four vendors originally contacted.

A major procurement problem was encountered with the production of Inconel 625. Although 200 ft of tubing was ordered, only 48 ft of short tube lengths was available for shipment because stringers in the raw material caused considerable splitting in the final redraw. Metallographic examination revealed that the outside surface of the tubing contained numerous longitudinal cracks, often extending to a length of 0.75 in. and a depth of 0.001 in. The distribution of the cracks was such that all specimens prepared from nine randomly selected tube areas exhibited some degree of unsoundness. Figure 6 shows a transverse section of tubing containing such a defect. Despite these cracks, the tubing was used for the evaluation of brazing characteristics in the first phase of testing.

A second batch of material was received, and inspection of the tubes showed that these also had surface defects. Microstructural examination revealed what appeared to be foreign particles impressed into the surface (Figure 7). It appeared that alloying occurred between the particles and the Inconel 625 during annealing. The supplier was requested to analyze this tubing, and his report confirmed that the surface imperfections were widespread. Identification of the contaminant was hampered by the difficult etching characteristics of the thin-wall tubing. However, a review of the manufacturing history indicated that the contamination occurred in finishing processes. It was also concluded from the unusual nature of the defect that it was an isolated occurrence and that there should be no inherent difficulty in manufacturing thin-wall tubing from Inconel 625. The entire second consignment was rejected and returned to the vendor.

A second supply source of Inconel 625 tubing was found, and the lot received from this source was found to be free from imperfections. The samples used in the cyclic hot corrosion test were prepared from this batch.

Figure 6. Inconel 625 Tube Wall Section (First Lot).

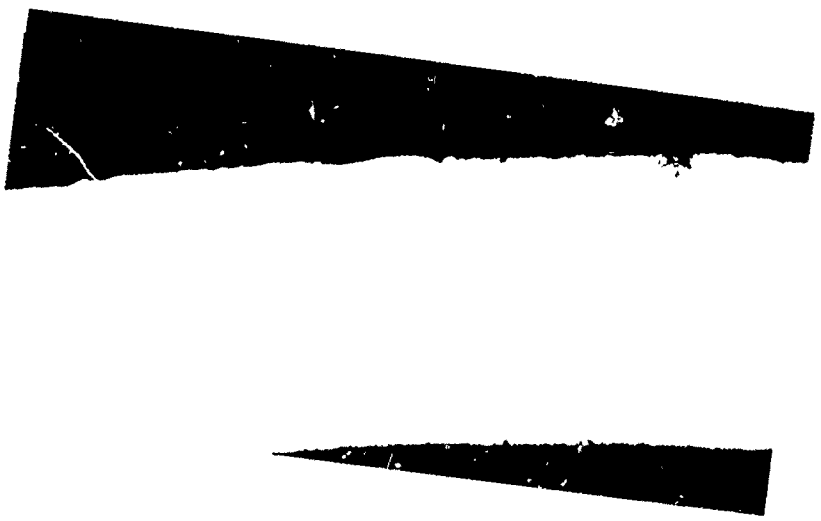

Figure 7. Inconel 625 Tube Wall Section (Second Lot).

PRELIMINARY BRAZING EVALUATION

A relatively simple comparative test was devised to determine the compatibility of the brazing alloys with the tubing materials. Washers with 0.375-in. OD, 0.125-in. ID, and 0.032-in. thickness were produced from the same alloys as the tubing materials and were brazed midway along 1-in. tube sample lengths. The brazing alloy/tube material combinations considered most suitable for recuperator application are given in Table IV. Brazing conditions are also tabulated with respect to temperature, time, and atmosphere. In most instances, the brazing temperatures were selected from manufacturer's recommendations, but for some cases were modified according to AiResearch experience with the alloys.

Optimum brazing temperature is often a compromise between the degree of alloy penetration associated with high temperatures and the lack of filler metal fluidity caused by low temperatures. As explained earlier, penetration was anticipated to be the major problem in brazing 0.0035-in.-wall tubes. Consequently, lower brazing temperatures were tried to assess the penetration and flow characteristics of the alloys.

A common hold time of 10 min was chosen for all brazing operations. This was considered to be the most practical time for production line brazing of recuperators; hence, the results of the preliminary tests would become a useful guide to brazing characteristics under production line conditions. Brazing was carried out under vacuum except for Englehard 135 and Nicrobraz 65, which contain manganese. Manganese volatilizes rapidly in vacuum brazing and causes furnace contamination, possible difficulty with wetting flow, and skull formation. These two alloys were therefore brazed in hydrogen.

After brazing, the tubes were sectioned longitudinally through the brazed joint and prepared for examination. The results of the metallographic evaluation are summarized in Tables V through IX. Photomicrographs illustrating the brazing characteristics at each temperature for all the combinations of filler metals and tubing materials are presented in Appendix I. Electron microprobe analyses were also carried out on selected samples to ascertain the diffusion characteristics of the brazing alloys. Appendix III contains the details of these analyses.

The results are discussed in detail in the Selection of Brazing Alloys for Cyclic Hot Corrosion Testing section of this report. Briefly, N-155 and Hastelloy X had the best brazing characteristics, followed closely by type 347 stainless steel and Incoloy 800. Although the Incoloy 800 had a dull surface appearance caused by oxidation during brazing, it still brazed fairly well. The first consignment of Inconel 625 had a surface appearance similar to that of Incoloy 800, but wetting and filleting were poorer. This was probably associated with the manufacturing imperfections found in the first batch of tubing, because a subsequent batch of Inconel 625 used for the cyclic hot corrosion test was brazed without any problems.

TABLE IV. SELECTION OF BRAZING ALLOYS FOR PRELIMINARY EVALUATION

Brazing Alloy	Brazing* Temperature (°F)	Base Metal Tubing and Washers				
		Hastelloy X	Inconel 625	Incoloy 800	N-155	347SS
Palniro 4	2150, 2175, 2200	X	-	-	X	-
J-8100	2125, 2150, 2175	X	X	-	X	-
Palniro 1	2050, 2075, 2100	X	-	-	X	-
Engelhard 135**	2075, 2100, 2125	-	X	-	-	-
Nicrobraz 200	1925, 1950, 1975	-	-	-	X	-
Nicrobraz 135	1975, 2000, 2025	X	X	X	-	X
Nicrobraz 65**	1925, 1950, 1975	-	X	X	-	X
Palniro 7	1925, 1950, 1975	-	-	X	-	X
Coast Metals 50B	2025, 2050, 2075	-	-	X	-	X

*10-min hold time at brazing temperature.

**Braze in hydrogen atmosphere; all other brazing can be done in vacuum.

TABLE V. BRAZING CHARACTERISTICS OF HASTELLOY X TUBE-HEADER JOINTS

Brazing Alloy	Brazing Temperature (°F)	Visual Observations*			Micro**	
		Surface Condition	Wetting (Flow)	Filleting	Alloying Into Tube Wall (percent)	Penetration (mils)
Palniro 4	2200	C	E	E	80	1/4
	2175	C	E	E	60	1/2
	2150	C	E	E	20	1/4
J-8100	2175	C	E	E	100	-
	2150	C	E	E	40	1/2
	2125	C	E	E	40	1/2
Palniro 1	2100	C	E	E	75	1/4
	2075	C	E	E	10	1/4
	2050	C	E	E	10	1/4
Nicrobraz 135	2025	C	G	E	70	1
	2000	C	G	G-E	60	1
	1975	C	G	G	50	1

*C = Clean
G = Good
E = Excellent

**Example of measurements for brazed tube-header joints.

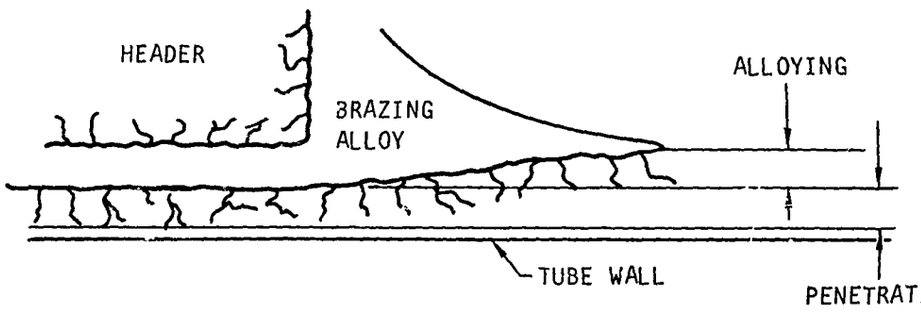

TABLE VI. BRAZING CHARACTERISTICS OF INCONEL 625 TUBE-HEADER JOINTS

Brazing Alloy	Brazing Temperature (°F)	Visual Observations*			Micro	
		Surface Condition	Wetting (Flow)	Filleting	Alloying Into Tube Wall (percent)	Penetration (mils)
J-8100	2175	D	G	F	100	None
	2150	D	G	P-F	70	None
	2125	D	G	P	60	None
Engelhard 135	2125	D	F	F-G	Slight	None
	2100	D	F	F	Slight	None
	2075	D	F	F	Slight	None
Nicrobraz 135	2025	D	P-F	P	**	**
	2000	D	P-F	P	None	1
	1975	D	P	P	None	1
Nicrobraz 65	1975	D	G	G	20	None
	1950	D	F	G	20	None
	1925	C	P	P	20	None

*C = Clean
D = Dull (oxide film)
E = Excellent
G = Good
F = Fair
P = Poor

**Inadequate brazing alloy in joint

TABLE VII. BRAZING CHARACTERISTICS OF INCOLOY 800 TUBE-HEADER JOINTS

Brazing Alloy	Brazing Temperature (°F)	Visual Observations*			Micro	
		Surface Condition	Wetting (Flow)	Filleting	Alloying Into Tube Wall (percent)	Penetration (mils)
Nicrobraz 135	2025	D	G	E	50	None
	2000	C	G	E	20	None
	1975	D	F-G	G	20	None
Nicrobraz 65	1975	C	G	F	10	None
	1950	D	G	G	None	None
	1925	D	P	P	None	None
Palniro 7	1975	D	F	G	10	None
	1950	D	G	G	10	None
	1925	D	G	E	20	None
Coast Metals 50B	2075	D	G	G	50	None
	2050	D	G	G	40	None
	2025	D	G	G	30	None

*C = Clean
D = Dull (oxide film)
E = Excellent
G = Good
P = Poor

TABLE VIII. BRAZING CHARACTERISTICS OF MULTIMET N-155 TUBE-HEADER JOINTS

Brazing Alloy	Brazing Temperature (°F)	Visual Observations*			Micro	
		Surface Condition	Wetting (Flow)	Filleting	Alloying Into Tube Wall (percent)	Penetration (mils)
Palniro 4	2200	C	E	E	80	1/2
	2175	C	E	E	60	1/2
	2150	C	E	E	20	1/2
J-8100	2175	C	E	E	50	1/4
	2150	C	E	E	50	1/4
	2125	C	E	E	50	1/4
Palniro 1	2100	C	E	E	70	1/4
	2075	C	E	E	30	1/4
	2050	C	E	E	20	1/4
Nicrobraz 200	1975	C	G	G-E	15	Slight
	1950	C	G-E	G-E	10	Slight
	1925	C	G	G-E	5	Slight

*C = Clean
G = Good
E = Excellent

TABLE IX. BRAZING CHARACTERISTICS TYPE 347 STAINLESS STEEL TUBE-HEADER JOINTS

Brazing Alloy	Brazing Temperature (°F)	Visual Observations*			Micro	
		Surface Condition	Wetting (Flow)	Filleting	Alloying Into Tube Wall (percent)	Penetration (mils)
Nicrobraz 135	2025	D	G	G	30	2-1/2**
	2000	D	G	G	30	2-1/2**
	1975	C	E	G	30	2-1/2**
Nicrobraz 65 (AMI 930)	1975	C	E	G	10	None
	1950	C	G	G	Slight	None
	1925	Brazing alloy did not melt at this temperature				
Palniro 7	1975	C	E	E	25	None
	1950	C	G	G	20	1/2
	1925	C	G	G	25	None
Coast Metals 50B	2075	D	G	G	60	1-1/2**
	2050	D	G	G	30	2-1/2**
	2025	D	G	G	10	3**

*C = Clean
D = Dull (oxide film)
E = Excellent
G = Good
P = Poor

**Penetrated through wall

STATIC HOT CORROSION TESTS AND RESULTS

Static tests were performed to determine the high-temperature corrosion resistance of the simulated tube-header joints used in the preliminary brazing evaluation. The identical brazed samples were heated in a furnace retort containing an atmosphere similar to that based on the exhaust of a gas turbine engine operating in a marine atmosphere.

TEST ENVIRONMENT

The amount of sea salt ingested by a gas turbine engine located near sea-water appears to be subject to many variables. The average sea-salt aerosol concentration, however, has been measured[2] and found to be proportional to the absolute wind velocity above the water. Figure 8 shows that the total sea-salt concentration is approximately 1.0 ppm at wind velocities of 40 kn. To accelerate the corrosion process during the preliminary test, the solution was injected into the gas stream and controlled to produce a concentration of sea salts one order of magnitude greater than the above concentration, or 10 ppm.

JP-4 fuel used by turbojet engines contains a maximum of 0.4-percent sulfur. These engines operate efficiently at air-fuel ratios of about 50 to 1. Under such circumstances the turbine exhaust gases contain about 160-ppm sulfur dioxide (weight percent). The typical analysis of the remainder of the gas in volume percent is 3.8-percent carbon dioxide, 4.1-percent water, 77.4-percent nitrogen, 0.2-percent carbon monoxide, and 14.5-percent oxygen. Under startup conditions, the air-fuel ratio is lower and incomplete combustion takes place. The composition of the turbine exhaust gases is complex and unstable but is about 2.8-percent carbon dioxide, 3.5-percent water, 10.5-percent oxygen, 15.1-percent carbon monoxide, 9.5-percent hydrogen, 61.8-percent nitrogen, and about 320-ppm hydrogen sulfide.

Simplified compositions of these mixtures (void of hazardous combinations of gases) were passed through the retort containing the test specimens. The gas compositions used were as follows:

Oxidizing Gas	Reducing Gas
4-percent carbon dioxide	3.5-percent carbon dioxide
15-percent oxygen	19-percent carbon monoxide
81-percent nitrogen	77.5-percent nitrogen
150-ppm sulfur dioxide	320-ppm hydrogen sulfide
10-ppm sea salts	10-ppm sea salts

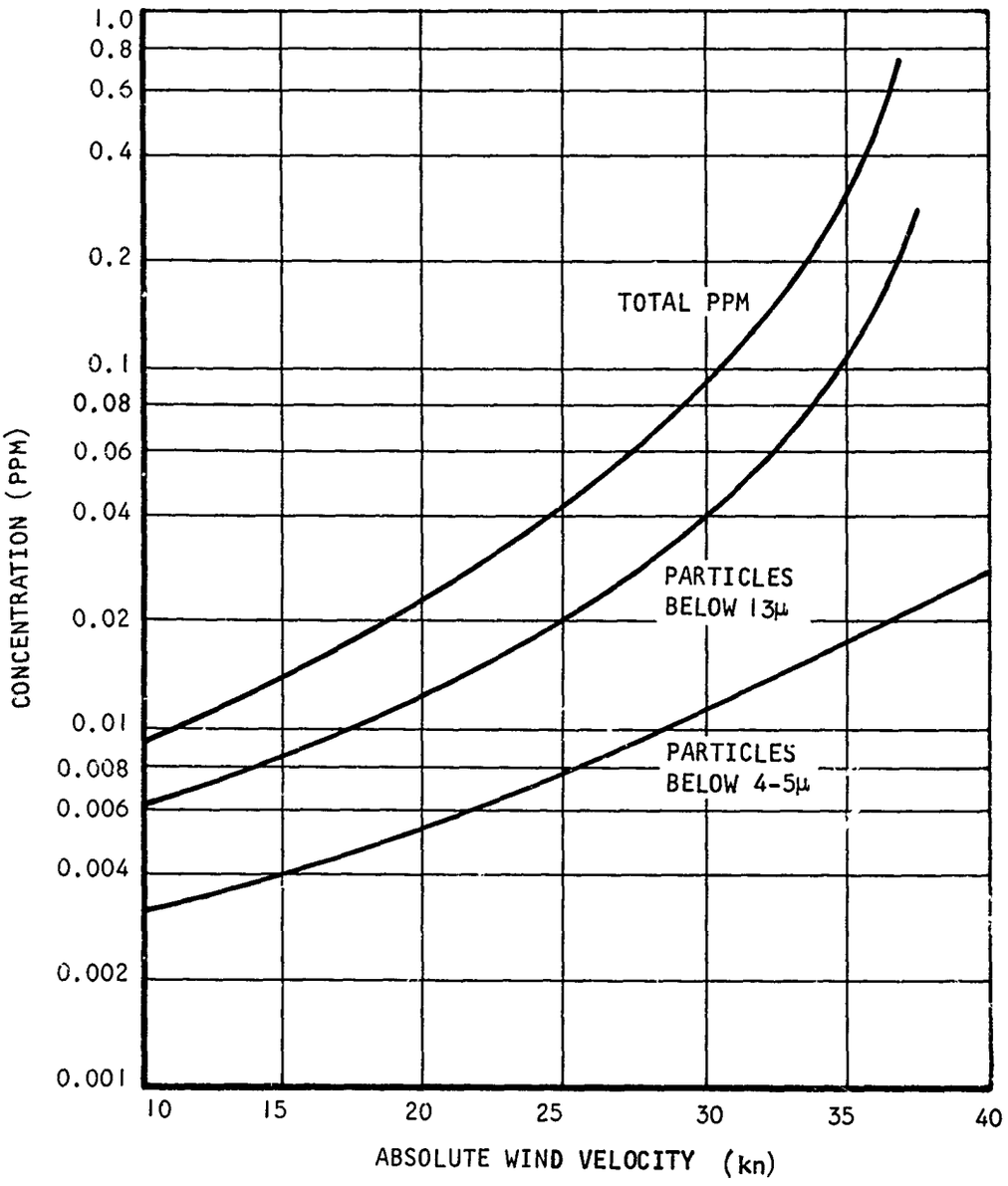

Figure 8. Average Sea-Salt Concentration in Air.

TEST SETUP

The retort depicted in Figure 9 was built to hold the brazed tube-header specimens such that the hot corrosion gases would impinge upon and engulf all pieces equally. The specimens were mounted on a wire screen with their longitudinal axes parallel to the direction of flow. (See Figure 10.) Temperature inside the retort was monitored by a chromel-alumel thermocouple attached to the wire screen. A schematic layout of the test apparatus is shown in Figure 11, and a general view of the test rig is shown in Figure 12.

TESTING

The sea salts were injected into the furnace retort by a process similar to paint spraying. Gases, flowing at a controlled rate, atomized a solution of sea salts as the solution emerged from a capillary tube. Control was effected by metering the gas delivered to the injector and by the concentration of sea salts in the solution. A nitrogen flow rate of 8 ft^3/hr was maintained throughout the test. Two ft^3/hr of reducing gas and 80 ml/hr of hydrogen sulfide were introduced for 30 min at the beginning of each 25-hr cycle. During the remainder of the cycle, oxidizing gas was added at the rate of 2 ft^3/hr, and sulfur dioxide was added at the rate of 40 ml/hr. During the entire 100 hr of testing, sea-salt solution, made according to Specification ASTM D665-60, Procedure B (see Table X), was injected into the gas stream at the rate of 66 ml/hr to produce 10-ppm sea salts in the retort atmosphere. The furnace was maintained at a constant temperature of 1500°F. Material combinations evaluated in the test were identical to those used for the preliminary brazing evaluation. Only one brazing condition was chosen for this experiment: the median brazing temperature for each combination shown in Table IV.

Evaluation of Static Hot Corrosion Test Results

The 1-in.-long tube-header samples were sectioned longitudinally, and their microstructures were examined for the effects of the static hot corrosion test. Photomicrographs of the brazed joints in the unetched condition are shown in Figures 13 through 17. These figures show the resistance of the various tube material/filler metal combinations to the corrosive atmospheres at 1500°F for 100 hr.

With the exception of type 347 stainless steel, none of the tube-header joints showed more than superficial corrosion. The stainless steel, however, was more heavily oxidized, as can be seen in Figure 17. Palniro 4, J-8100, Palniro 1, Palniro 7, and Nicrobraz 200 filler metals were not attacked by the sulfurous atmosphere. Nicrobraz 135 and Coast Metals 50B suffered moderate attack, and Nicrobraz 65 and Englehard 135 were both severely corroded.

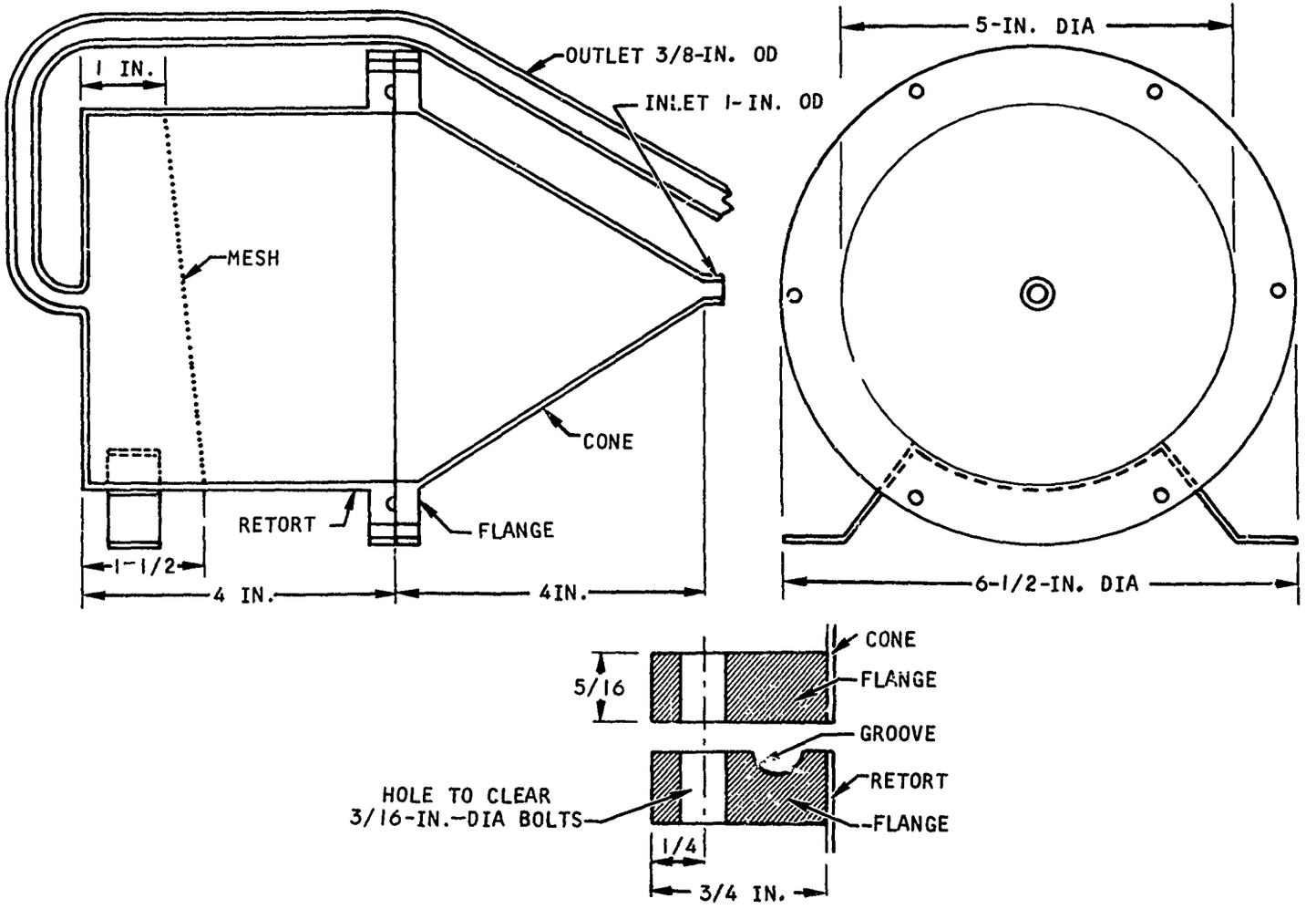

Figure 9. Static Hot Corrosion Test Rig.

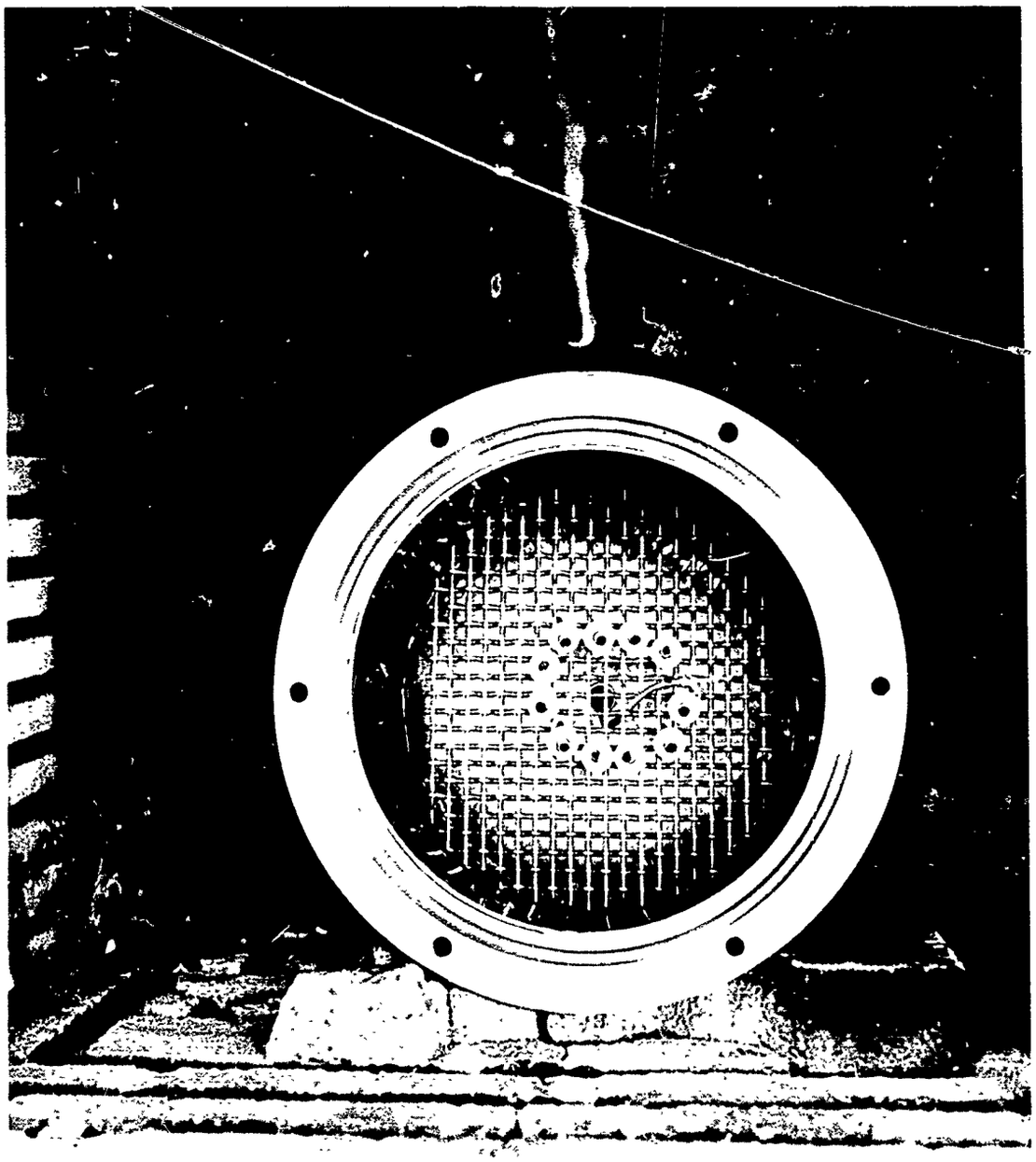

Figure 10. Test Specimens Mounted in Static Hot Corrosion Test Retort.

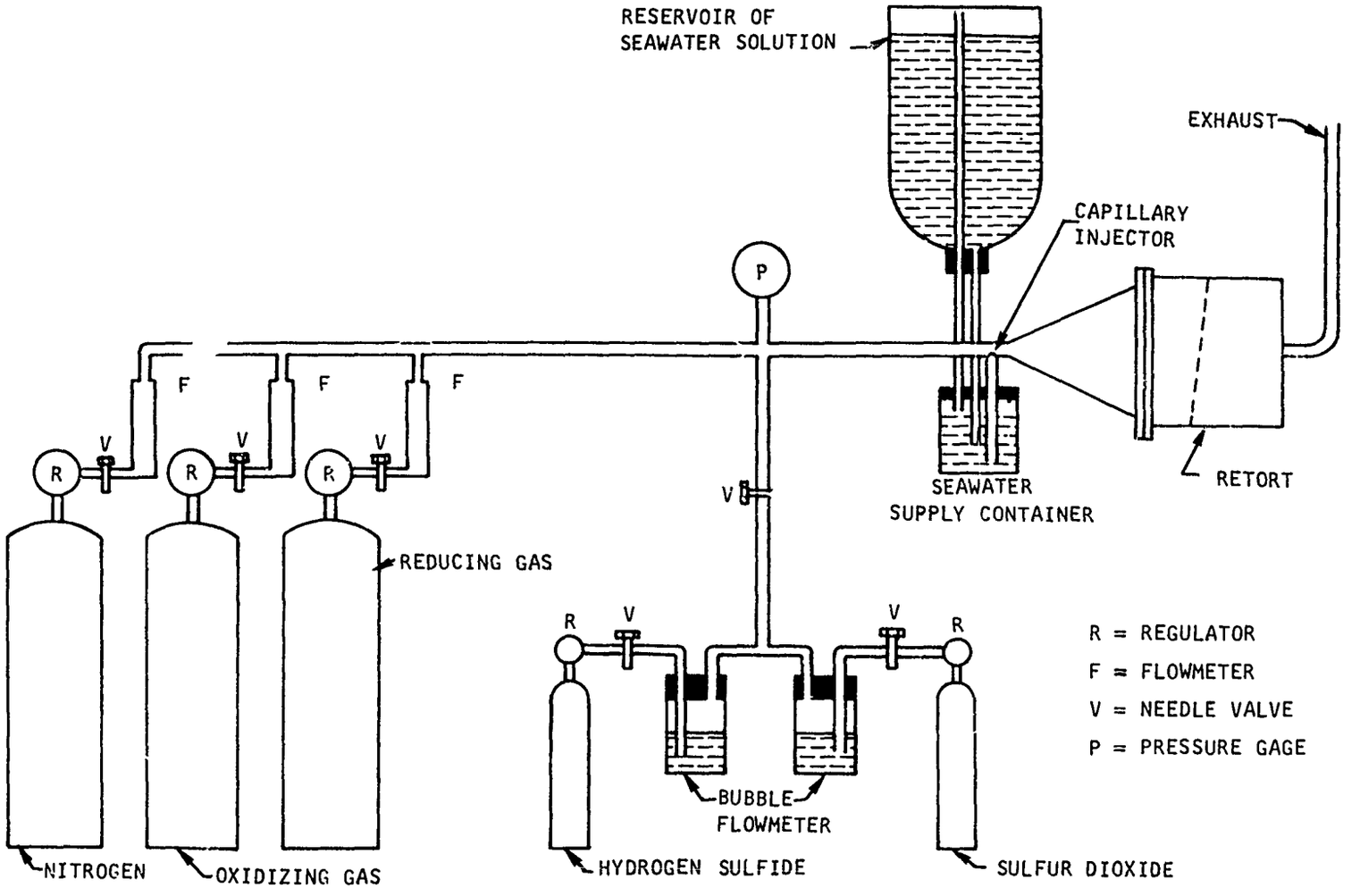

Figure 11. Schematic of Static Hot Corrosion Test Apparatus.

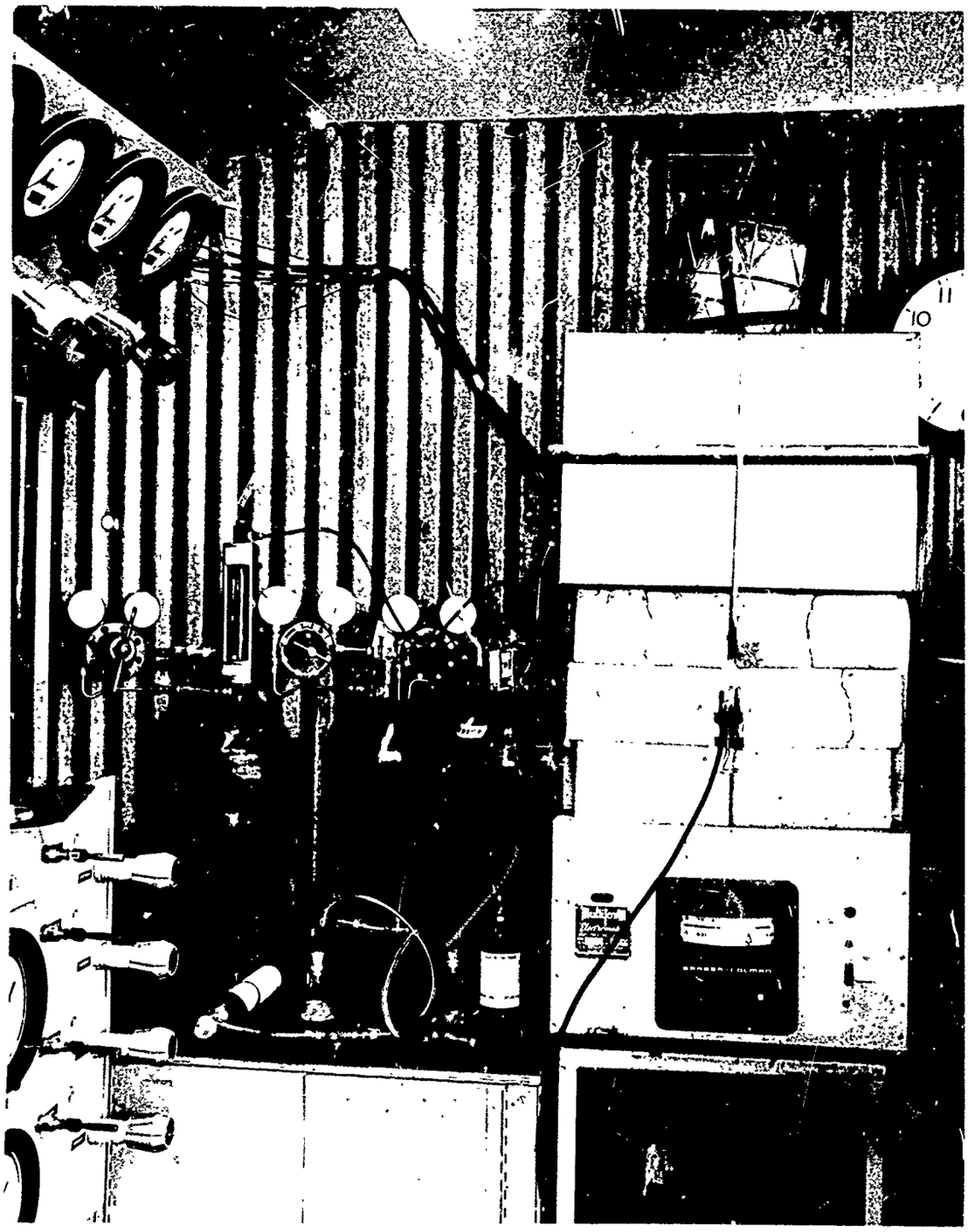

Figure 12. General View of Static Hot Corrosion Test Rig.

TABLE X. COMPOSITION OF SYNTHETIC SEAWATER

Salt (a)	Formula	Composition, gm/l (b)
Sodium chloride	NaCl	24.54
Magnesium chloride	$MgCl_2.6H_2O$	11.10
Sodium sulfate	Na_2SO_4	4.09
Calcium chloride	$CaCl_2$	1.16
Potassium chloride	KCl	0.69
Sodium bicarbonate	$NaHCO_3$	0.20
Potassium bromide	KBr	0.10
Boric acid	H_3BO_3	0.03
Strontium chloride	$SrCl_2.6H_2O$	0.04
Sodium fluoride	NaF	0.003
Total		41.953

(a) Use cp chemicals.

(b) Use distilled water.

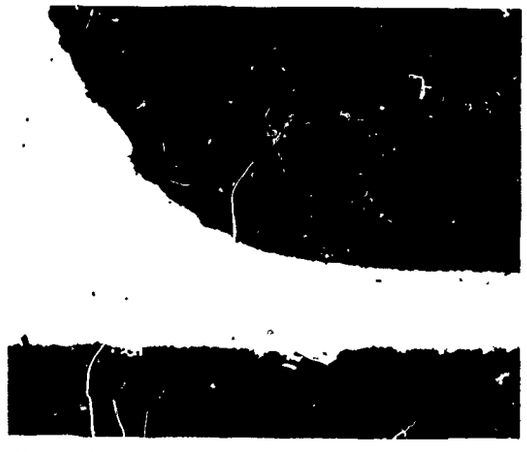

MAG = X150

a. PALNIRO 4 BRAZING ALLOY, VACUUM BRAZED AT 2170°F WITH HOLD TIME OF 10 MIN. NO CORROSION OF PALNIRO 4.
UNETCHED

MAG = X150

b. J-8100 BRAZING ALLOY, VACUUM BRAZED AT 2150°F WITH HOLD TIME OF 10 MIN. NO CORROSION OF J-8100.
UNETCHED

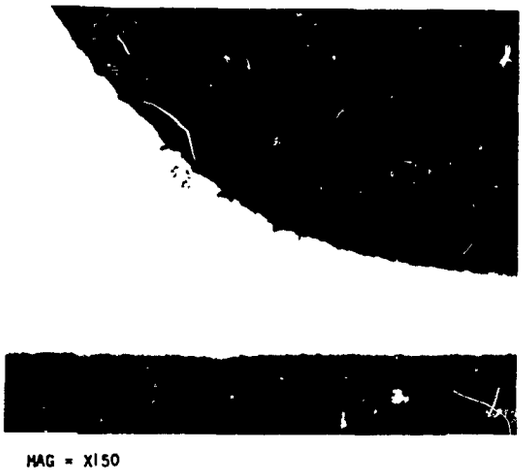

MAG = X150

c. PALNIRO 1 BRAZING ALLOY, VACUUM BRAZED AT 2070°F WITH HOLD TIME OF 10 MIN. NO CORROSION OF PALNIRO 1.
UNETCHED

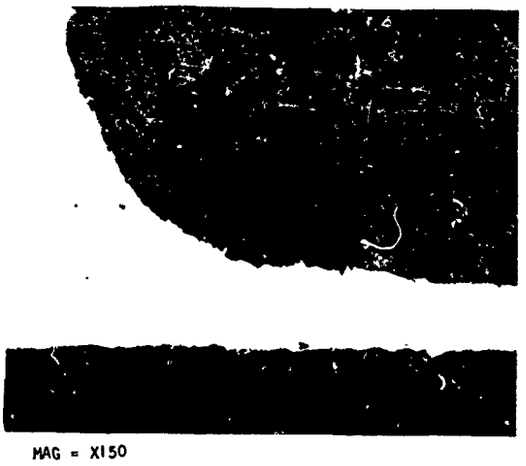

MAG = X150

d. NICROBRAZ 135 BRAZING ALLOY, VACUUM BRAZED AT 2000°F WITH HOLD TIME OF 10 MIN. SOME CORROSION OF NICROBRAZ 135 NOTED.
UNETCHED

NOTE: PHOTOS HAVE BEEN REDUCED TO 66%.

Figure 13. Hastelloy X Tube-Header Joints After 100 hr at 1500°F, Static Hot Corrosion Test.

MAG = X150

a. J-8100 BRAZING ALLOY. VACUUM BRAZED AT 2150°F WITH HOLD TIME OF 10 MIN. NO CORROSION OF J-8100 NOTED. UNETCHED

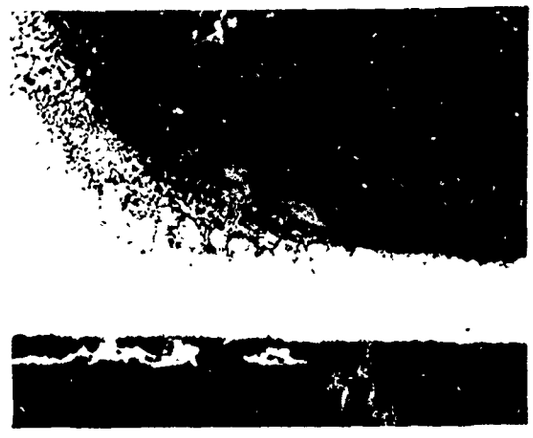

MAG = X150

b. ENGELHARD 135 BRAZING ALLOY. BRAZED AT 2100°F IN HYDROGEN ATMOSPHERE WITH 10 MIN HOLD TIME. EXTENSIVE CORROSION OF ENGLEHARD 135 OCCURRED. UNETCHED

MAG = X150

c NICROBRAZ 135 BRAZING ALLOY. VACUUM BRAZED AT 2000°F WITH HOLD TIME OF 10 MIN. SOME CORROSION OF NICROBRAZ 135 NOTED UNETCHED

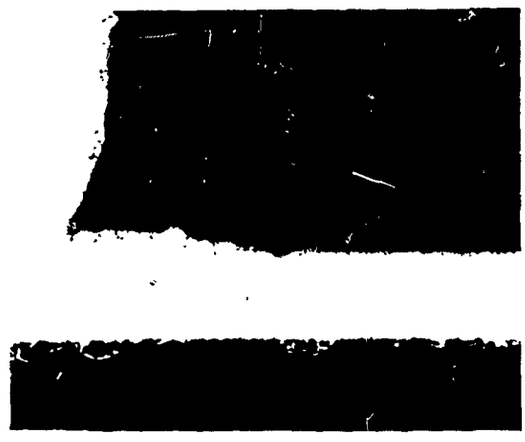

MAG = X150

d. NICROBRAZ 65 BRAZING ALLOY. BRAZED AT 1950°F IN HYDROGEN WITH HOLD TIME OF 10 MIN. HEAVY CORROSION OF NICROBRAZ 65. UNETCHED

NOTE: PHOTOS HAVE BEEN REDUCED TO 67%.

Figure 14. Inconel 625 Tube-Header Joints After 100 hr at 1500°F, Static Hot Corrosion Test.

MAG = X150

a. NICROBRAZ 135 BRAZING ALLOY, VACUUM BRAZED AT 2000°F WITH 10 MIN HOLD TIME. SOME CORROSION OF NICROBRAZ 135 NOTED. UNETCHED

MAG = X150

b. NICROBRAZ 65 BRAZING ALLOY, BRAZED AT 1950°F IN HYDROGEN WITH 10 MIN HOLD TIME. EXTENSIVE CORROSION OF NICROBRAZ 65. UNETCHED

MAG = X150

c. PALNIRO 7 BRAZING ALLOY, VACUUM BRAZED AT 1950°F WITH 10 MIN HOLD TIME. NO CORROSION OF PALNIRO 7 NOTED. UNETCHED

MAG = X150

d. COAST METALS 50B BRAZING ALLOY, VACUUM BRAZED AT 2050°F WITH 10 MIN HOLD TIME. SOME CORROSION OF 50B NOTED. UNETCHED

NOTE: PHOTOS HAVE BEEN REDUCED TO 67%.

Figure 15. Incoloy 800 Tube-Header Joints After 100 hr at 1500°F, Static Hot Corrosion Test.

MAG = X150

a. PALNIRO 4 BRAZING ALLOY. VACUUM BRAZED AT 2175°F WITH 10 MIN HOLD TIME. NEGLIGIBLE CORROSION OF PALNIRO 4 NOTED UNETCHED

MAG - X150

b. J-8100 BRAZING ALLOY. VACUUM BRAZED AT 2150°F WITH 10 MIN HOLD TIME. NO CORROSION OF J-8100 NOTED. UNETCHED

MAG = X150

c. PALNIRO 1 BRAZING ALLOY. VACUUM BRAZED AT 2075°F WITH 10 MIN HOLD TIME. NO CORROSION OF PLANIRO 1 NOTED. UNETCHED

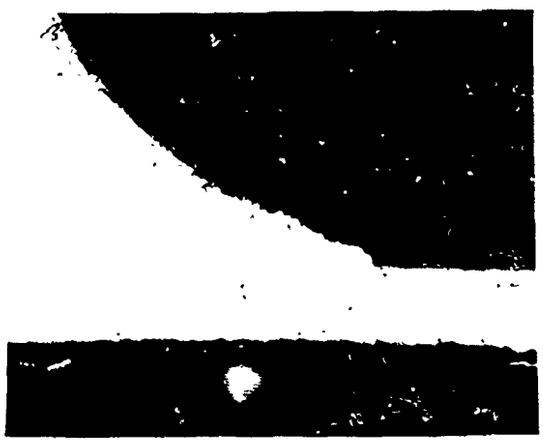

MAG = X150

d. NICROBRAZ 200 BRAZING ALLOY. VACUUM BRAZED AT 1950°F WITH 10 MIN HOLD TIME. SLIGHT CORROSION OF NICROBRAZ 200 NOTED. UNETCHED

NOTE PHOTOS HAVE BEEN REDUCED TO 67%.

Figure 16. N-155 Tube-Header Joints After 100 hr at 1500°F, Static Hot Corrosion Test.

MAG = X150

a. NICROBRAZ 135 BRAZING ALLOY, VACUUM BRAZED AT 2000°F WITH 10 MIN HOLD TIME. SOME CORROSION OF NICROBRAZ 135 NOTED.
UNETCHED

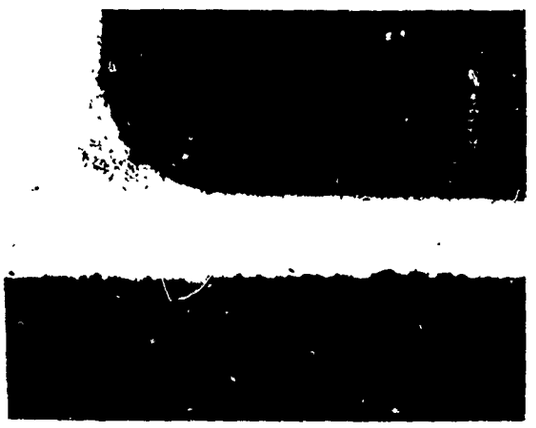

MAG = X150

b. NICROBRAZ 65 BRAZING ALLOY, BRAZED AT 1950°F IN HYDROGEN WITH 10 MIN HOLD TIME. CORROSION OF NICROBRAZ 65 NOTED.
UNETCHED

MAG = X150

c. PALNIRO 7 BRAZING ALLOY, VACUUM BRAZED AT 1950°F WITH 10 MIN HOLD TIME. NO CORROSION OF PALNIRO 7 NOTED.
UNETCHED

MAG = X150

d. COAST METALS 50B BRAZING ALLOY, VACUUM BRAZED AT 2050°F WITH 10 MIN HOLD TIME. SOME CORROSION OF 50B NOTED.
UNETCHED

NOTE: PHOTOS HAVE BEEN REDUCED TO 67%.

Figure 17. Type 347 Stainless Steel Tube-Header Joints at 1500°F, Static Hot Corrosion Test.

SELECTION OF BRAZING ALLOYS FOR CYCLIC HOT CORROSION TESTING

The selection of two brazing alloys for each of the four candidate tubing materials for the cyclic hot corrosion tests was based on the following:

1. Brazing characteristics for each brazing alloy/tubing material combination at the three temperatures used in brazing
2. Effect of brazing temperature on tubing material
3. Results of the 1500°F, 100-hr static hot corrosion tests

On the basis of the hot corrosion tests, Englehard 135 and Nicrobraz 65 were eliminated because of poor corrosion resistance. Coast Metals 50B and Nicrobraz 135 had satisfactory hot corrosion resistance and brazing characteristics, warranting consideration for the cyclic temperature tests. All the Palniro brazing alloys, J-8100, and Nicrobraz 200 had excellent hot corrosion resistance and brazing characteristics.

Both Palniro 4 and J-8100 were brazed at high temperatures (2175° and 2150°F, respectively), and grain growth occurred in base metals brazed at these temperatures. Grain coarsening, however, was more severe with Palniro 4. Very large grains are considered to be undesirable because of the possibility of decreased low-cycle fatigue resistance. In addition, Palniro 4 has no advantage over Palniro 1 (brazed at 2070°F) with respect to joint strength at 1300° to 1500°F. Palniro 4 was therefore eliminated as a candidate.

The final selection is shown in Table XI, and the alloys for each of the tubing materials are further discussed below.

Hastelloy X

Palniro 1 had excellent brazing characteristics as noted in Table V. It also had excellent hot corrosion resistance. The 2075°F brazing temperature permitted the retention of a fine-grained structure. J-8100 also had good brazing characteristics and excellent hot corrosion resistance, although satisfactory alloying was greater than with Palniro 1. Grain growth occurred in Hastelloy X when brazed with J-8100. A fine-grained structure has better tensile and fatigue properties but lower stress-rupture properties. Selection of these two brazing alloys afforded a comparison of the fine- and coarse-grained materials. These two brazing alloys were previously evaluated for a similar application in a lightweight heat exchanger operating at 1540°F maximum temperature. Both alloys performed equally well in axial-tensile and axial-fatigue tests at room temperature and at 1540°F.

TABLE XI. SELECTION OF BRAZING ALLOYS FOR CYCLIC HOT CORROSION TESTING

Tubing	Brazing Alloy	Brazing Temperature (°F)*
Hastelloy X	Palniro 1	2075
	J-8100	2150
Incoloy 800	Palniro 7	1950
	Coast Metals 50B	2050
N-155	Palniro 1	2075
	Nicrobraz 200	1950
Type 347 stainless steel	Palniro 7	1950
	Nicrobraz 135	2000
Inconel 625	J-8100	2125
	Nicrobraz 135	2000

*Hold time of 10 min, vacuum furnace brazing.

Incoloy 800

The basis for selecting Palniro 7 for Incoloy 800 was its excellent brazing characteristics, hot corrosion resistance, and retention of a fine grain structure. Coast Metals 50B permitted some grain growth in Incoloy 800, alloyed somewhat more than Nicrobraz 135, but penetrated less than Nicrobraz 135. Within the brazing temperature evaluated, Coast Metals 50B had less overall alloying and penetration with Incoloy 800 than Nicrobraz 135 and was selected as the second choice.

N-155

Palniro 1 had good brazing characteristics and excellent hot corrosion resistance. It was selected for brazing N-155 for the same reasons that it was selected for brazing Hastelloy X. Nicrobraz 200 also had good brazing characteristics and excellent hot corrosion resistance. Alloying and penetration of the N-155 by Nicrobraz 200 was only about 0.001 in., which should be satisfactory for this application.

Type 347 Stainless Steel

Palniro 7 was an obvious first choice because of its excellent brazing characteristics and hot corrosion resistance. Nicrobraz 135 and Coast Metals 50B had similar brazing characteristics and hot corrosion resistance. Because of its lower brazing temperature, the Nicrobraz 135 (2000°F) was more compatible with the annealing temperature of type 347 stainless steel (1950°F maximum) than 50B (2050°F). Grain size of the stainless steel tubing was larger for the 50B brazing cycle than for the Palniro 7 cycle. Nicrobraz 135 was selected as the second choice.

Inconel 625

Despite the interalloying between J-8100 and Inconel 625, the joints should have adequate strength, particularly if the lower brazing temperature of 2125°F is used. The lack of wettability observed on the batch of Inconel 625 tubes tested in the preliminary brazing tests was probably associated with the process of that particular batch of tubing. No problems were observed on the consignment of tubes provided by an alternate supplier, and tube samples prepared for cyclic hot corrosion/stress rupture testing exhibited good wettability. A penetration of 0.001 in. was detected on Inconel 625 joints made with Nicrobraz 135, but nevertheless these two brazing alloys were selected for cyclic hot corrosion testing because of their better hot corrosion resistance. Therefore, the necessary test samples were brazed at 2000°F for Nicrobraz 135 and at 2125°F for J-8100.

CYCLIC HOT CORROSION TESTING

The objective of this task was to develop stress-rupture information which, when correlated with the reference power system design requirements, would indicate the two most likely candidates for subsequent combustor testing. A secondary objective of the testing was to evaluate the phenomenological effects of hot corrosion on the tube-header joints and to determine their comparative corrosion resistance.

TESTING PROCEDURE

Washers with 0.375-in. OD's were brazed 10 in. from the closed ends of 22-in. lengths of sample tubing using the filler materials and brazing conditions shown in Table XI. These tubes were then assembled in the test rig and tested at temperatures of 1500°, 1300°, and 1100°F (1200°F for Inconel 625). Thermal cycling was introduced every 2 hr. Cold nitrogen gas was admitted from a liquid source into the test rig for 1 min, thus reducing the temperature of tubes 500° to 600°F below the test temperature, after which the tubes were allowed to return to the temperature of the test. Oxidizing gas consisting of 4-percent carbon dioxide, 15-percent oxygen, 81-percent nitrogen, and 150-ppm sulfur dioxide constituted the testing atmosphere before cooling. The reducing gas consisting of 3.5-percent carbon dioxide, 19-percent carbon monoxide, 77.5-percent nitrogen, and 350-ppm hydrogen sulfide was passed over the tubes during the temperature recovery period. A sea-salt solution was injected into the gas stream at the inlet to the furnace retort, and a concentration of 5-ppm sea salts was maintained in the gases throughout the entire test. The tubes were pressurized with nitrogen containing 1-percent oxygen to provide stress levels predetermined to cause failure in 75, 300, and 1000 hr of testing at each temperature. Details of the test rig and the testing procedure are described in Appendix II.

The results of the tests are depicted in Figures 18 through 22, which show the stress-rupture properties of the various material combinations at the indicated temperatures. Care must be taken in extrapolating these curves to times beyond that of the maximum exposure, particularly in the case of Incoloy 800 and type 347 stainless steel. Straight lines were constructed through the minimum data points at each temperature and stress level except when the effects of hot corrosion were more pronounced. The straight-line relationship cannot be maintained at extended times of exposure. At these points, the extent of corrosion will have weakened the alloy such that it will not be able to contain even the lowest pressure.

COMPARISON OF STRESS-RUPTURE DATA

Hastelloy X

At 1100°F, the pressures necessary to produce hoop stresses high enough to cause failure in less than 300 hr were greater than the test rig capacity. Consequently, only one stress level was tested at this temperature. The

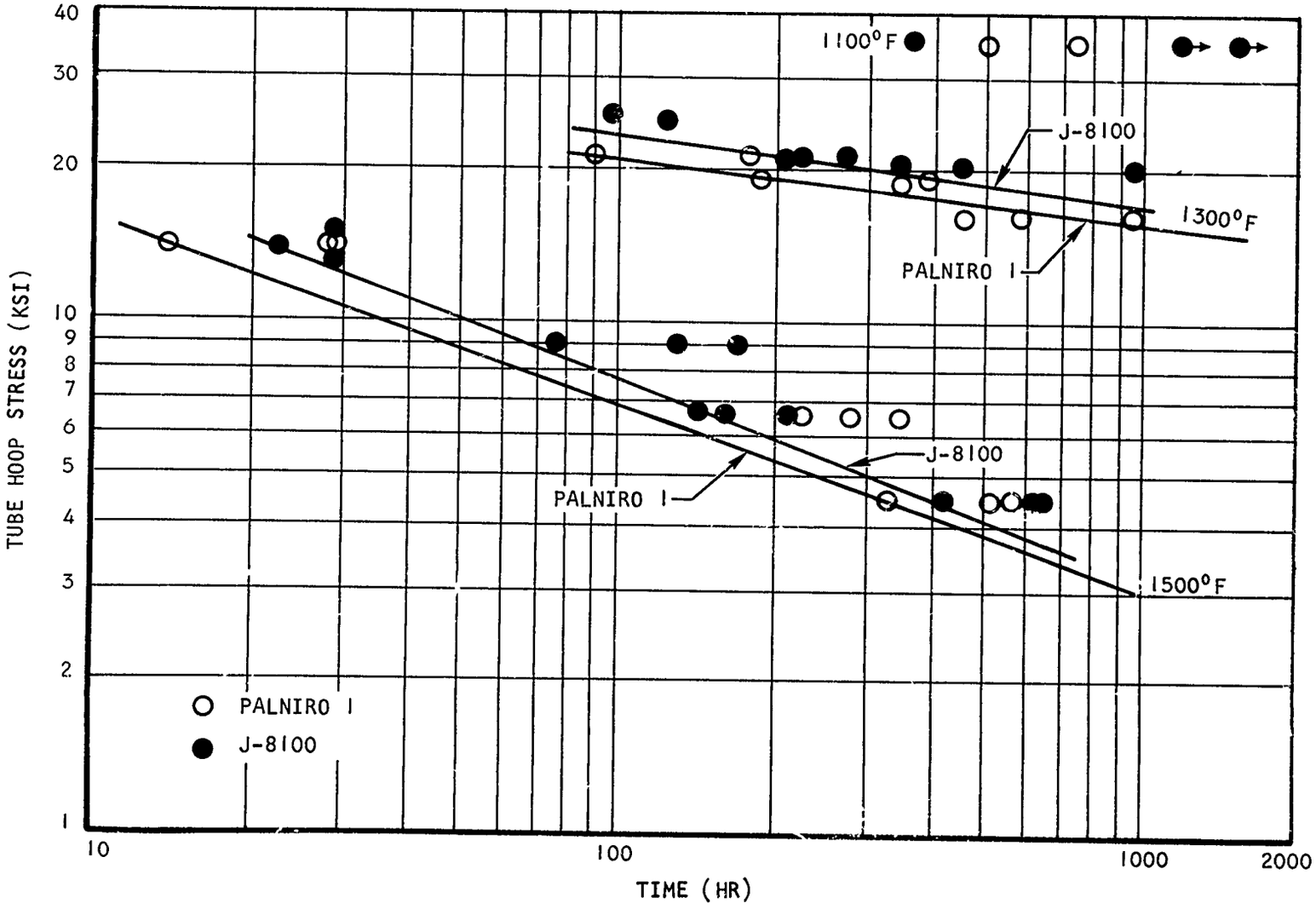

Figure 18. Cyclic Hot Corrosion/Stress-Rupture Data, Hastelloy X Tubing.

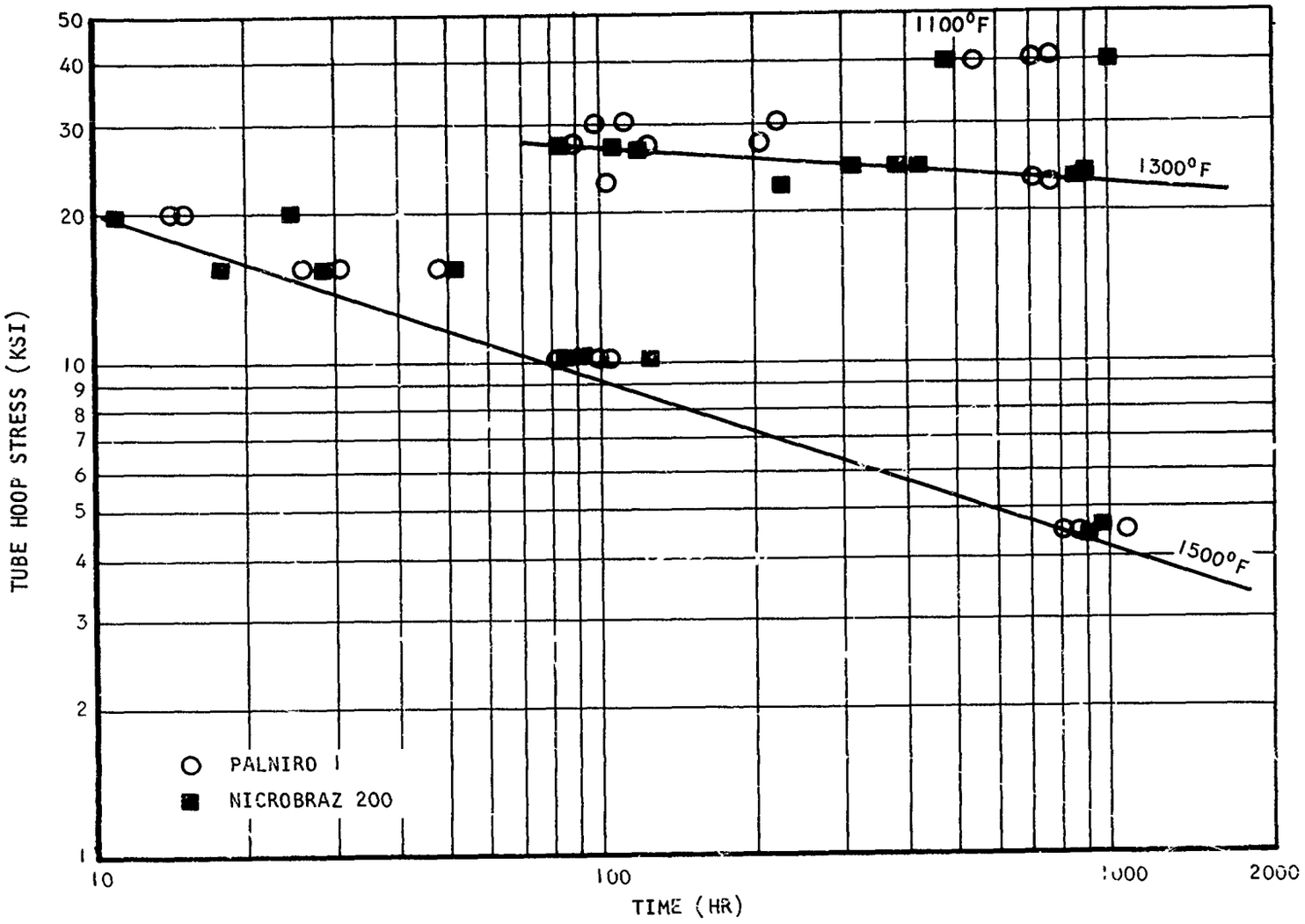

Figure 19. Cyclic Hot Corrosion/Stress-Rupture Data, N-155 Tubing.

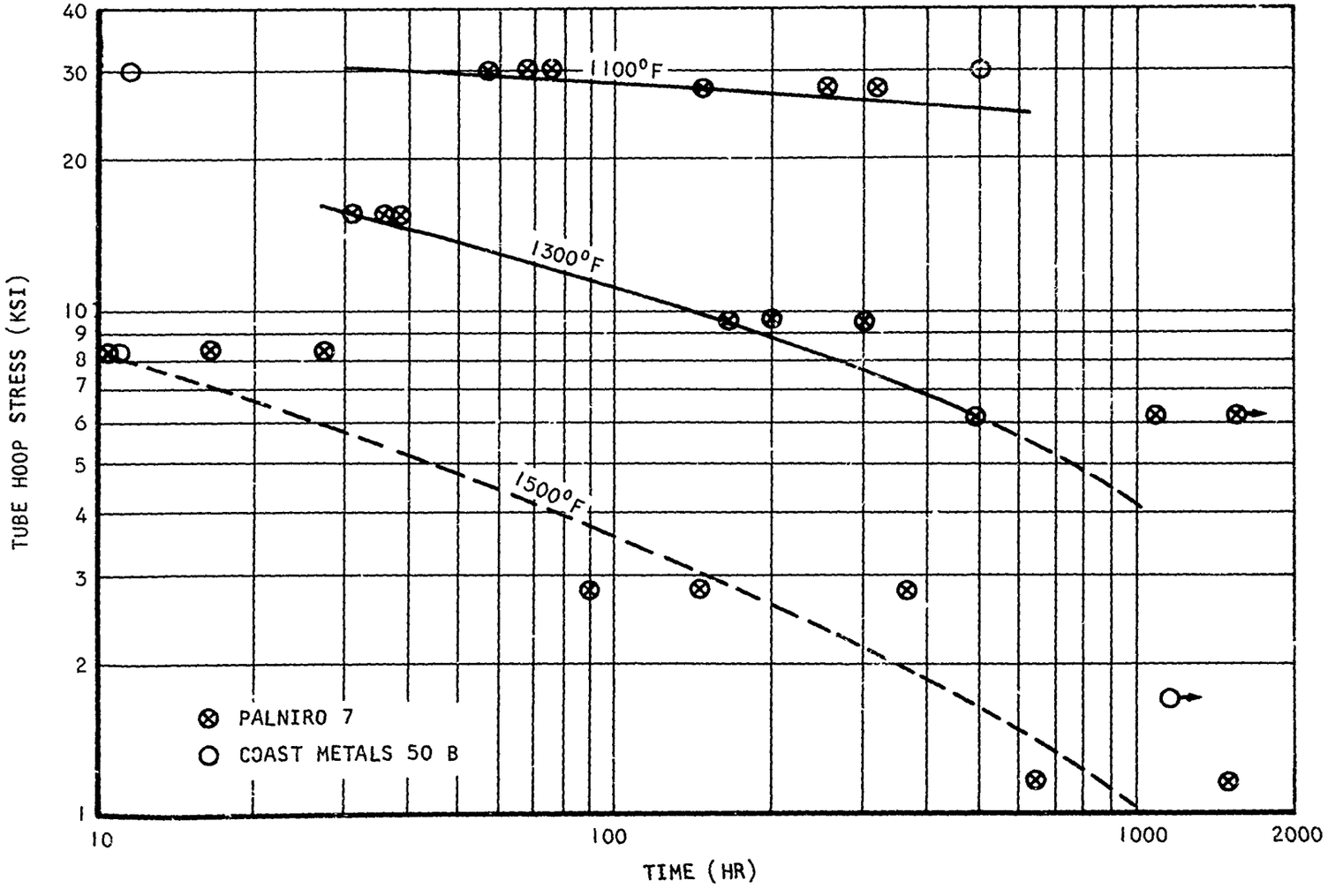

Figure 20. Cyclic Hot Corrosion/Stress-Rupture Data, Incoloy 800 Tubing.

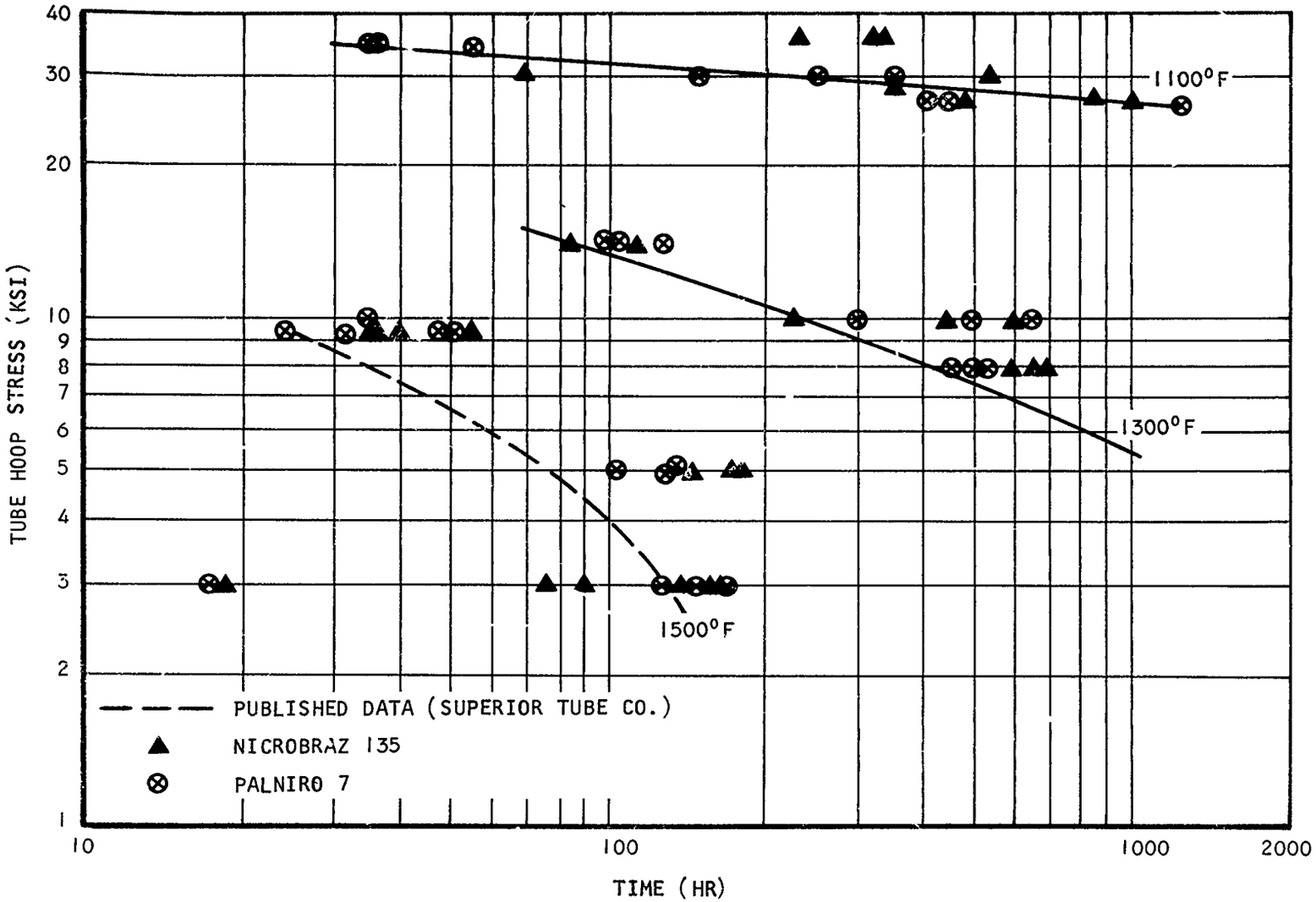

Figure 21. Cyclic Hot Corrosion/Stress-Rupture Data, Type 347 Stainless Steel.

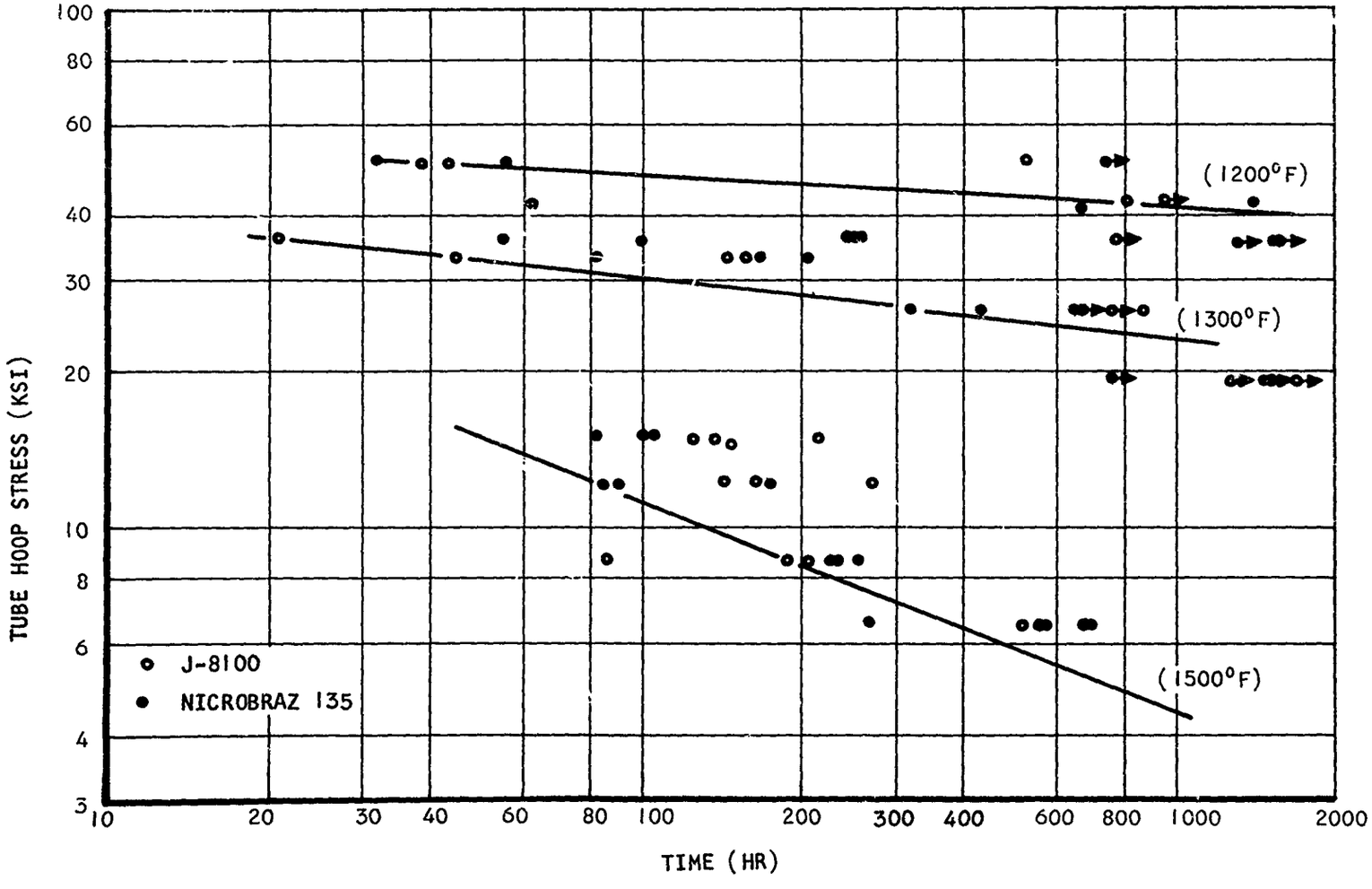

Figure 22. Cyclic Hot Corrosion/Stress-Rupture Data, Inconel 625 Tubing.

wide scatter of results shown in Figure 18 was obtained in the virtual absence of corrosion and indicates that rupture time was so sensitive to tube pressure that small changes in pressure resulted in large differences in rupture time.

Data collected for the 1300°F test condition suggest that tubes brazed with J-8100 have slightly better stress-rupture properties than those brazed with Palniro 1. This trend was also observed at the 1500°F test condition.

N-155

The same problems associated with Hastelloy X were experienced with N-155; that is, the pressures required to cause early failure at 1100°F were greater than the capacity of the test rig. Consequently, only one stress level was tested at this temperature. The results presented in Figure 19 indicate no significant differences between the brazing alloys used. Some scatter of results is prevalent, and the shallow slope of the curve for the 1300°F condition indicates that small changes of stress would greatly influence rupture time at this temperature.

Incoloy 800

Data obtained for Incoloy 800 tubes (Figure 20) show that a wide scatter band exists at 1500°F, particularly at low pressures. No significant differences were observed between the brazing alloys used. The departure from the straight-line relationship at 1300° and 1500°F is attributed to the effects of hot corrosion.

Type 347 Stainless Steel

Although two heat numbers of type 347 stainless steel tubing were tested, the results at 1500°F indicate that early failure would occur no matter how small the applied stress. (See Figure 21.) Microstructural evidence clearly shows that at this temperature, corrosion of type 347 stainless steel was proceeding at a rapid rate. At lower temperatures (1300° and 1100°F), good relationships between the log stress and the log time were observed.

Inconel 625

Because of the delays caused early in the program by the lack of good quality Inconel 625 tubing, this alloy was tested after testing of the other materials had been completed. Consequently, some modifications to the test rig were permitted so that higher pressures could be used to test this higher strength alloy. Even so, since testing at 1100°F would have been impractical, 1200°F was selected as the lowest testing temperature for this material. At this low temperature and at 1300°F, the characteristic shallow curves shown in Figure 22 were observed, indicating the extreme sensitivity of rupture time as a function of small changes in stress. Some scatter of results was obtained at 1500°F, but a fairly reliable extrapolation of the stress rupture properties at 1000 hr could still be made.

To compare the relative stress-rupture properties of the material combinations, data taken from the stress-time plots are summarized in Table XII. From this summary it can be seen that the descending order of relative stress-rupture properties is as follows:

1. Inconel 625
2. N-155
3. Hastelloy X brazed with J-8100
4. Hastelloy X brazed with Palniro I
5. Type 347 stainless steel
6. Incoloy 800

EXAMINATION OF HOT CORROSION PROPERTIES

All the failed tubes were examined visually, and approximately 40 percent of the samples were submitted for metallographical examination. Details of these examinations are presented in Appendix II, which indicates that hot corrosion had occurred by different processes in the various tube materials. In some cases, the oxidant had diffused through the oxide layer and reacted with the metal atoms; in other cases, the metal appeared to have diffused outward through the oxide film and reacted with the corrosive environment. Oxidation products were detected to be either in the grain boundaries, randomly distributed within the area of attack, or built up in layer formation on the surfaces of the corroded tubes. Electron microprobe analyses were carried out on selected samples of tubing materials to obtain a better understanding of the hot corrosion mechanisms. Details of the microprobe analyses are found in Appendix III.

COMPARISON OF HOT CORROSION PROPERTIES

Hastelloy X

Grain boundary attack was clearly evident after Hastelloy X was submitted to high stress levels for both the 1500° and 1300°F conditions. No appreciable oxide layer was detected on any sample examined, but in some cases the grain boundaries were so severely attacked that the tube wall was almost penetrated. This type of corrosion is illustrated in Figure 23, which shows Hastelloy X after 204 hr at 1300°F and 0.8 ksi. Concentration of the attack in the grain boundaries is not surprising with such high stresses involved. Loss of cohesive strength at the grain boundaries is the normal mode of stress-rupture failure; consequently, the effects of hot corrosion may have been slight. Microprobe analysis identified the corrosion product as a chromium oxide phase, free of nickel or iron oxides, which adhered to a metal layer depleted in chromium content. No sulfides were associated with the oxide.

TABLE XII. RESULTS OF CYCLIC HOT CORROSION/STRESS-RUPTURE TESTS

Temperature (°F)	Time to Rupture (hr)	Approximate Stress-Rupture Values (ksi)					
		Hastelloy X/ Palniro I	Hastelloy X/ J-8100	N-155	Incoloy 800	TYPE 347 SS	Inconel 625
1100	100	-	-	-	28	32	-
	1000	35	35	40	25	25	-
1200	100	-	-	-	-	-	47
	1000	-	-	-	-	-	41
1300	100	21	25	30	12	14	30
	1000	15	18	21	4	5.5	26
1500	100	7	7.5	9	3.5	5	11
	1000	3	3.5	4	1.0	-	4.5

At high temperatures the Palniro 1 braze alloy was corroded only slightly at first, but to an approximate depth of 1.5 mils after 341 hr at 1500°F. The incidence of failure at the simulated braze joint was greater with this filler metal than with J-8100, which was subject only to slight corrosion (about 0.1 mil) after almost a 1000-hr exposure.

N-155

At 1500°F and high stresses, N-155 oxidation occurred along the grain boundaries and resulted in the ultimate stress-rupture failure of the tube. The material also appeared to be subject to "wart" attack. On isolated tubes, severe corrosion occurred over a limited tube surface area, which resulted in a relatively massive oxide spot that in some cases almost penetrated the tube wall thickness. With the exception of these "warts," oxidation was, in general, slight at low stresses or low temperatures. Electron microprobe analysis identified the oxide as a mixture of iron, chromium, cobalt, and possible manganese oxides. No sulfides were detected. Figure 24 depicts the type of oxide layer found on N-155 tubing material.

The incidence of failure at the simulated tube-header joint was greater for tubes brazed with Palniro 1 than for those brazed with Nicrobraz 200. As previously observed, Palniro 1 was susceptible to corrosion after prolonged exposure; Nicrobraz 200 was also oxidized after a 1000-hr exposure at 1500°F. At lower temperatures, no oxidation of either brazing alloy was detected.

Incoloy 800

The surface oxide layer was never more than superficial on this alloy, except in isolated instances where warts were produced. At 1500°F, the tubes generally became porous, the degree of porosity increasing with increasing exposure time or increasing stress. Figure 25 shows a sample of Incoloy 800 after 812 hr at 1500°F and 2.8 ksi. Microprobe scans across the tube wall thickness confirmed that internal oxidation had occurred. Porosity was not so evident at 1300°F, but layer formation was more prevalent. In some cases oxidation had occurred at the Palniro 7 tube-alloy interface, which resulted in massive oxide layers containing numerous islands of unoxidized metal. Chromium oxide was again identified as the principal product of corrosion, although iron-, nickel-, and manganese-oxides were also detected in the layer. The metal was covered with chromium oxide, which in turn was covered with iron oxide. Sulfides were entirely absent. Except at 1100°F, Palniro 7 was badly oxidized if exposed for periods in excess of 100 hr, whereas Coast Metals 50B was only slightly corroded after 1171 hr at 1500°F.

Type 347 Stainless Steel

Type 347 stainless steel was severely oxidized under most circumstances at 1300° and 1500°F. Figure 26 shows the typical layer formation of the oxide. The oxide rarely exhibited any preference for grain boundary sites. Even

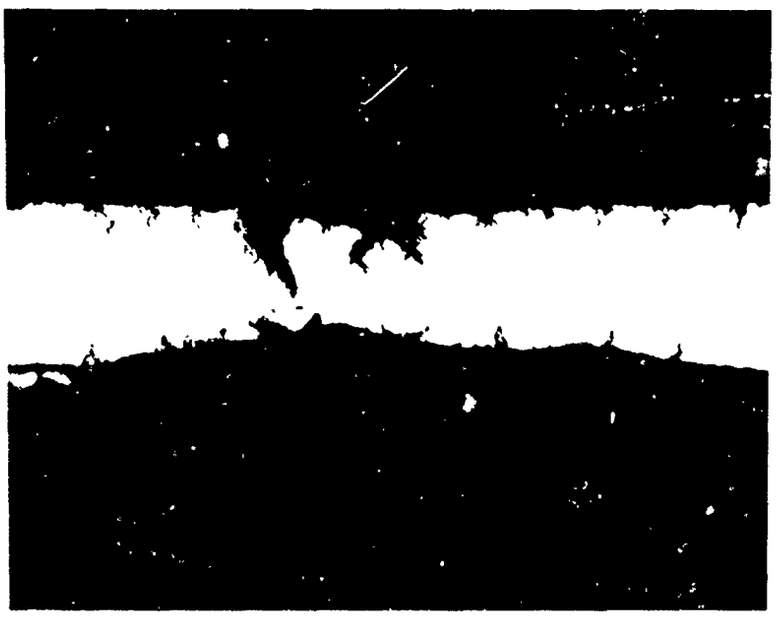

MAG = X230

Figure 23. Hastelloy X After a 204-hr Exposure at 1300°F and 20.8 ksi.

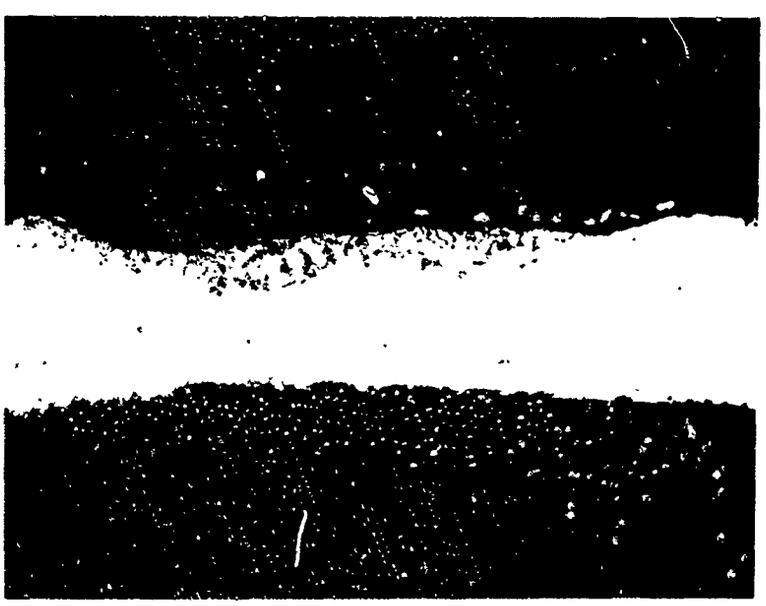

MAG = X250

NOTE: FIGURES REDUCED TO 95%.

Figure 24. N-155 After a 87.9-hr Exposure at 1300°F and 26.7 ksi.

MAG = X250

Figure 25. Incoloy 800 After 812 hr at 1500°F and 2.8 ksi.

MAG = X250

NOTE: FIGURES REDUCED TO 95%.

Figure 26. Type 347 Stainless Steel After 77.4 hr at 1500°F and 3.0 ksi.

at 1100°F, some oxidation was observed after 1238 hr on the test rig. Microprobe analysis across the oxide layer showed that the inner film of nickel-iron oxides was covered by a chromium-oxide layer. A third, outermost layer of iron oxide was also detected at 1500°F. The Palniro 7 brazing alloy was extensively oxidized, even after quite short exposures at the two higher temperatures. No oxidation of the filler metal was observed at 1100°F except after prolonged (1238 hr) exposure. Some slight intergranular oxidation of the Nicrobraz 135 was detected at the longer exposure times and high temperatures.

Inconel 625

Little or no oxide layer was found on Inconel 625 tubes. Failure along the oxidized grain boundaries resulted from high pressure levels at 1300° and 1500°F. Microprobe analysis showed that the surface oxide film was approximately 5μ thick and consisted essentially of chromium oxide. Extending below the oxide layer was a zone of metal depleted of molybdenum, nickel, and chromium. X-ray scanning displays illustrated that no sulfides were associated with the corroded areas. The brazing alloys (J-8100 and Nicrobraz 135) were slightly oxidized, but failure never occurred at the simulated tube-header joint. Figure 27 shows the most severe case of oxidation observed for Inconel 625 tubing.

SELECTION OF MATERIALS FOR RECUPERATOR MANUFACTURE

Operating data for the reference power system are presented graphically in Figure 28. Table XIII was constructed by converting the pressure data into hoop stress in the recuperator tube and Larson-Miller indexes for the selected power settings. These indexes are conservative since they were calculated from the gas temperatures, whereas in practice the recuperator metal remains at a lower temperature.

TABLE XIII. TYPICAL TURBINE ENGINE OPERATING DATA

Point	Percent	Time at Power (hr)*	Compressor Discharge Pressure (psia)	Turbine Discharge Temperature (°F)	Tube Hoop Stress (ksi)	Larson-Miller Index
A	100	750	206	1214	3.4	38.0
B	75	2250	165	1310	2.9	40.8
C	55	1250	130	1365	2.3	42.2
D	35	500	97	1400	1.7	42.2

*Portion of 5000-hr total operating time

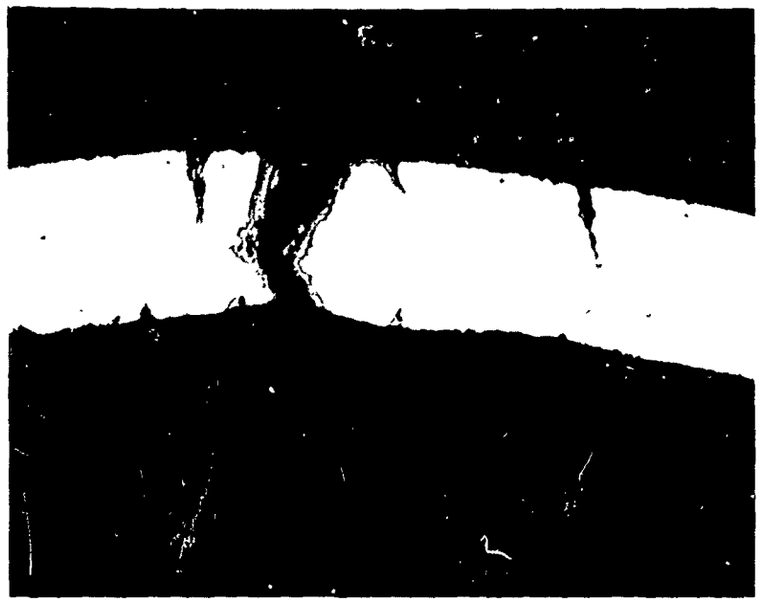

MAG = X250

NOTE: FIGURE REDUCED TO 95%.

Figure 27. Inconel 625 After 146 hr at 1500°F and 12.1 ksi.

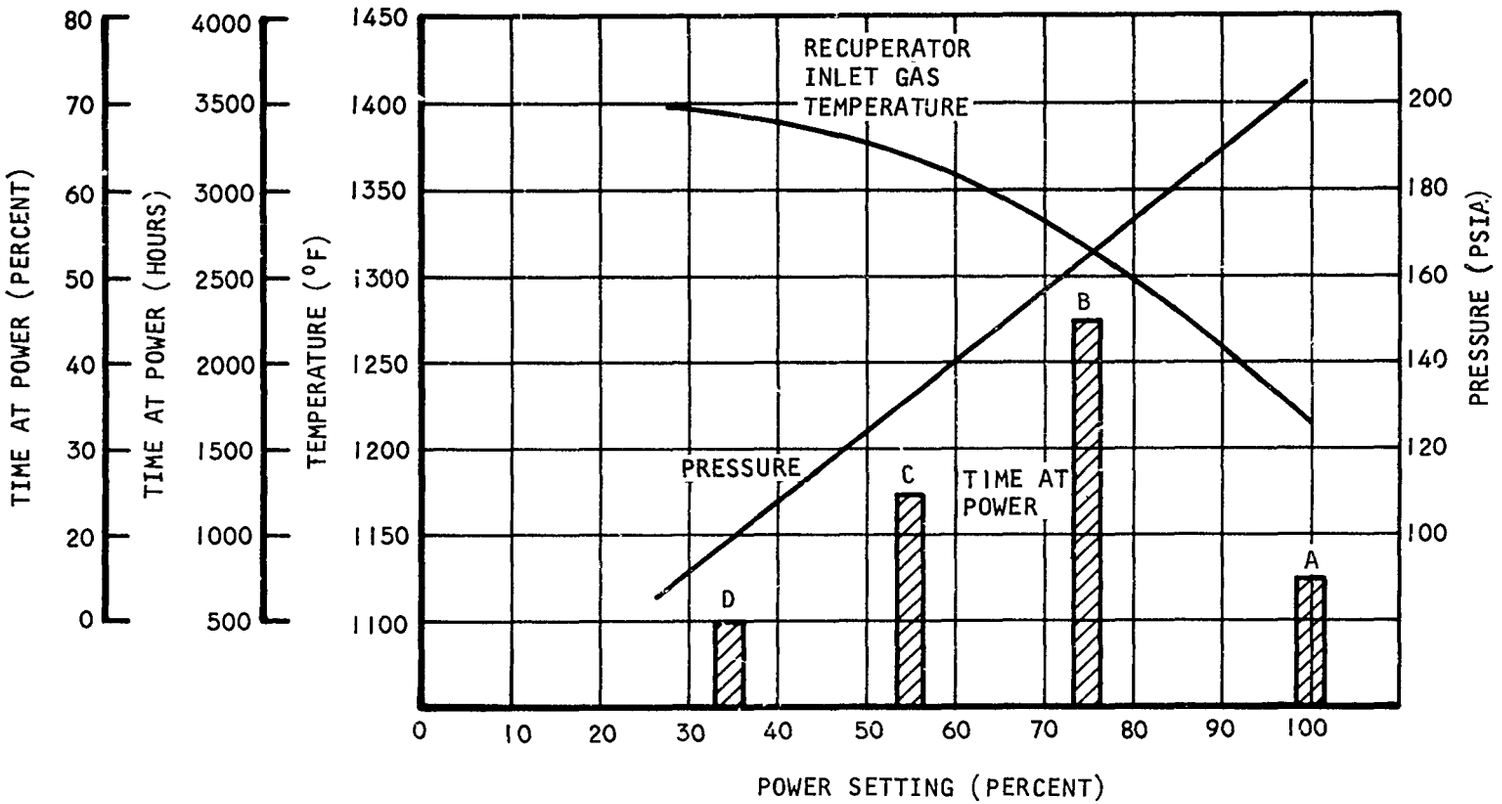

Figure 28. Typical Gas Turbine Engine Operating Data.

Data points A, B, C, and D were then superimposed on the Larson-Miller plots for stress rupture of the five materials constructed from the cyclic hot corrosion stress-rupture results. There are some limitations to this technique of comparing the actual data gleaned from testing to the actual requirements of a recuperator. With some reservations, however, some comparison of the relative suitability of each material can be attempted.

Figures 29 through 33 illustrate the Larson-Miller plots of each tubing alloy with the four data points superimposed on them. It is apparent that the straight-line relationship between log stress and the Larson-Miller index was not achieved and that a marked lowering of stress values occurred at high indexes. This degradation is attributed to the effects of corrosion, which will be more pronounced at higher temperatures. Consequently, the absolute values derived from these graphs may not be accurate, and extrapolation to times or temperatures beyond those in the tests would be questionable. Also, representing the typical gas turbine engine operating data as four separate points is not an accurate representation of the true operating conditions, since each point corresponds to a time and temperature condition for each stress level. The recuperator will be subjected to the cumulative effects of these various exposure levels; this has not been accounted for in the compilation of the graphs.

The proximity of the curve to the data points was taken as a measure of the suitability of the material. The curves for Hastelloy X, N-155, and Inconel 625 were well above the data points representing the operating conditions. The Incoloy 800 curve was perilously close, but still above, and the type 347 stainless steel curve was below these data points. This indicates that the first three materials would be adequate to meet operating conditions and that the latter two would probably have insufficient strength and/or corrosion resistance to survive the reference operating conditions.

Metallurgical examination of the failed tubes also indicated that the three high-strength alloys were most resistant to hot corrosion and that type 347 stainless steel was attacked most rapidly at 1500°F.

It was decided that a low-cost tubing material should be included in the recuperator test rig. Inconel 625, the obvious candidate, was not selected because at that time all the stress-rupture data was not available on this material as a result of the delay in testing caused by the unavailability of good quality tubing. The choice of a low-cost material, therefore, had to be made between Incoloy 800 and type 347 stainless steel.

Considerable experience has been gained using type 347 stainless steel as a recuperator material for operations at lower temperatures. Boeing[1] had previously concluded that this material was unsuitable for 1500°F applications in hot corrosive environments. It was believed, therefore, that little would be learned from testing this alloy. On the other hand, Incoloy 800 has not been used in recuperators and did show some slight advantages over type 347 stainless steel in that it appeared to have better

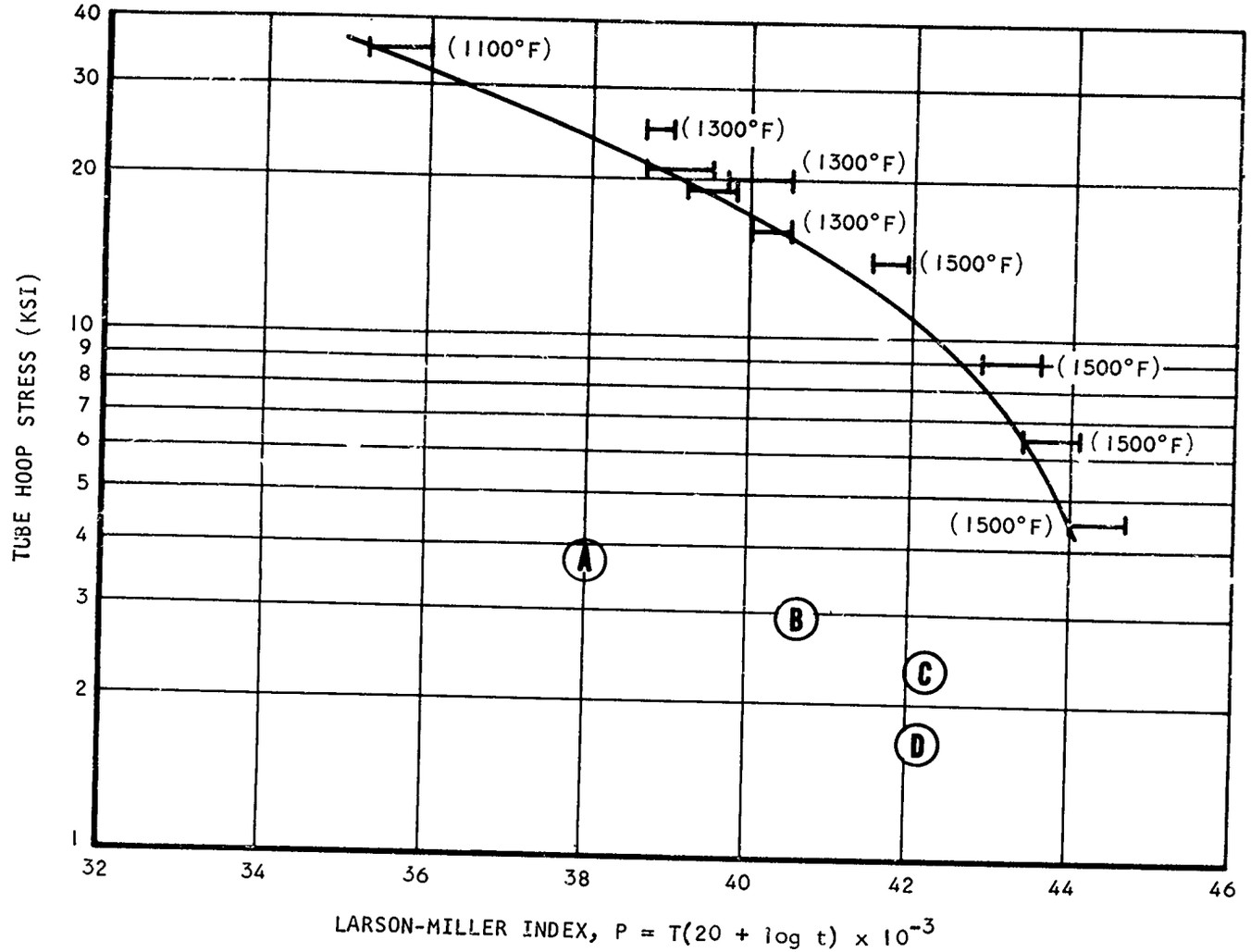

Figure 29. Hastelloy X Tubing, Cyclic Hot Corrosion/Stress-Rupture Data.

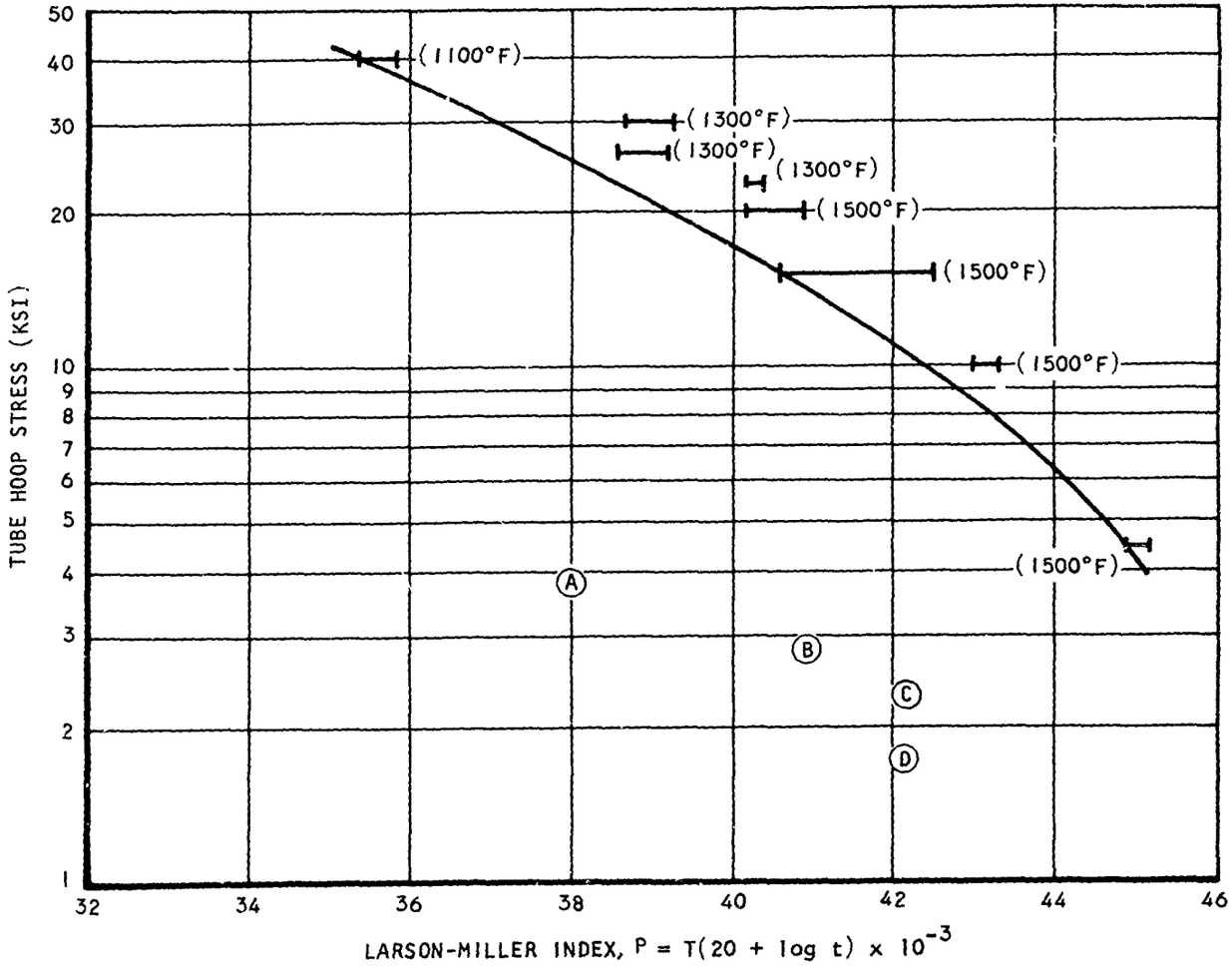

Figure 30. Multimet N-155 Tubing, Cyclic Hot Corrosion/Stress-Rupture Data.

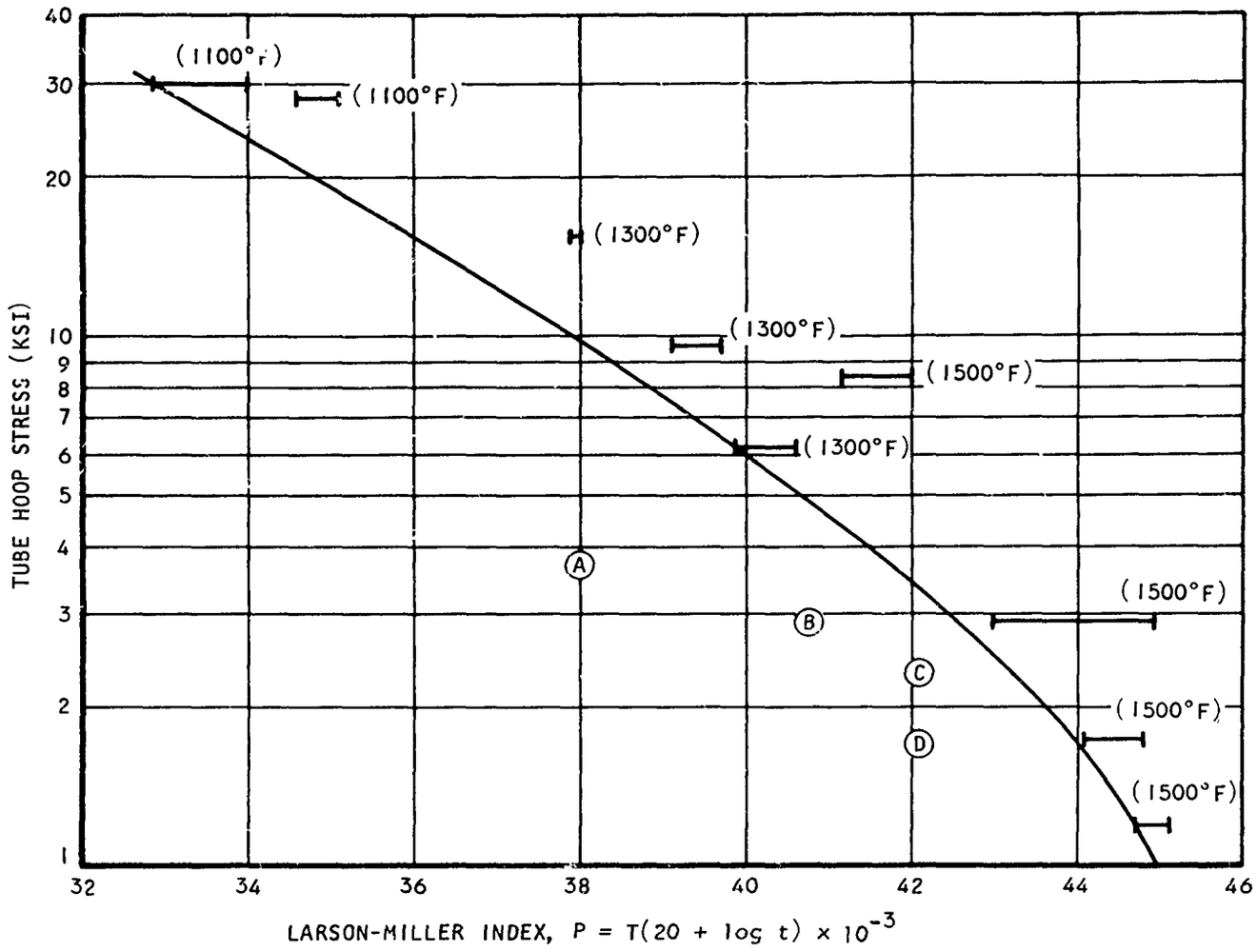

Figure 31. Incoloy 800 Tubing, Cyclic Hot Corrosion/Stress-Rupture Data.

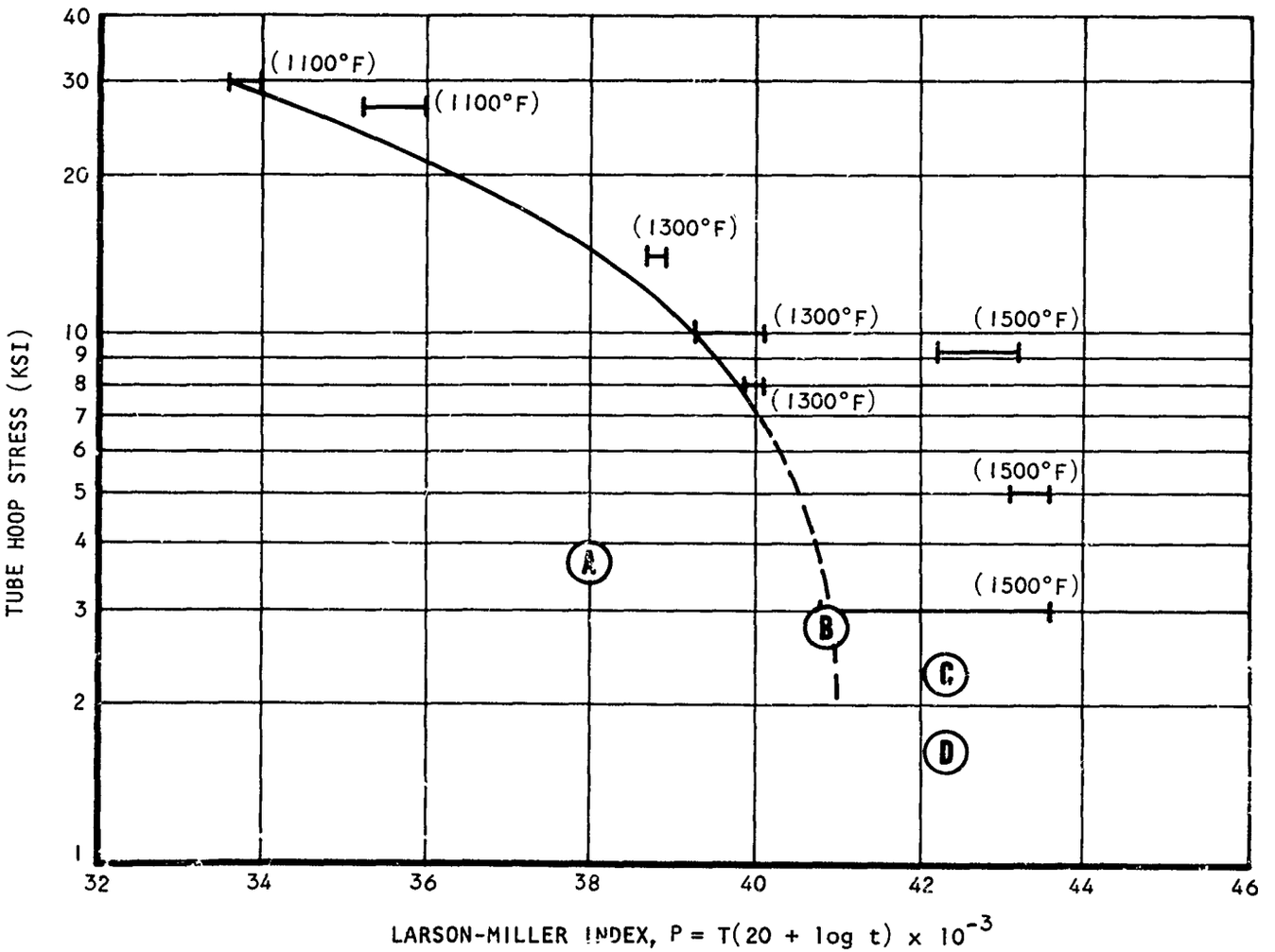

Figure 32. Type 347 Stainless Steel Tubing, Cyclic Hot Corrosion/Stress-Rupture Data.

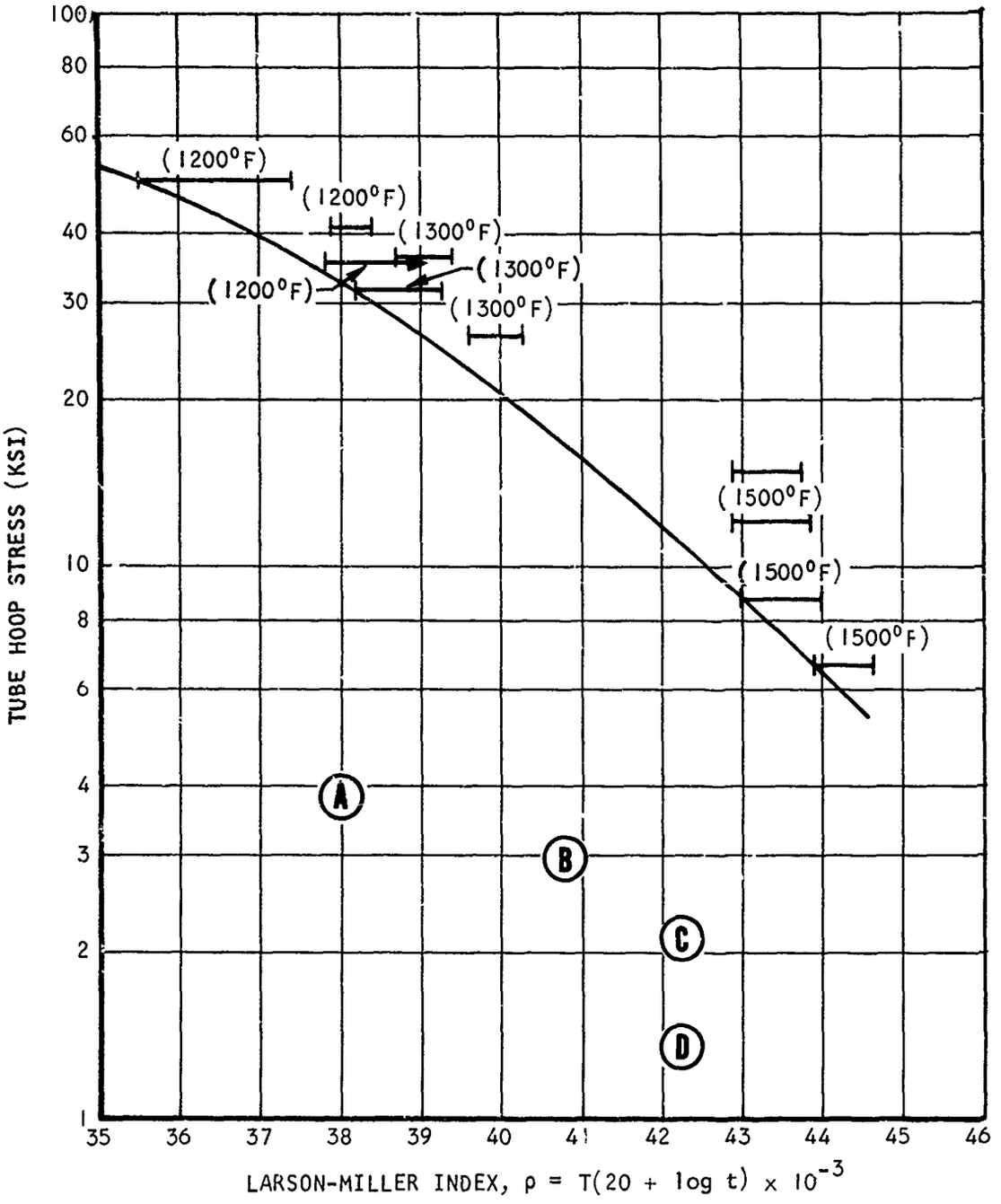

Figure 33. Inconel 625 Tubing, Cyclic Hot Corrosion/ Stress-Rupture Data.

hot corrosion resistance at low pressures and temperatures. Comparison of the Larson-Miller curves of Figures 31 and 32 also shows Incoloy 800 to be marginally better.

Since there was very little difference in strength or hot corrosion resistance of N-155 and Hastelloy X, the latter alloy was discarded because of its higher cost.

The two materials selected for recuperator construction and dynamic testing were Incoloy 800 and N-155.

In general, the palladium-nickel-gold series of brazing alloys had been more susceptible to hot corrosion than the less expensive nickel-chromium base alloy. Consequently, there was little justification in selecting the noble metal series of brazing alloys. Nicrobraz 200 and Coast Metals 50B were chosen as filler metals for constructing the N-155 and Incoloy 800 recuperator modules.

DESIGN AND FABRICATION OF RECUPERATOR TEST CORES

A recuperator test core was designed and fabricated using 0.125-in.-dia tubes of both Incoloy 800 and N-155. When operated in the exhaust of a JP-4-fueled burner, the cores experienced the range of conditions of the specified gas turbine engine recuperator.

RECUPERATOR DESIGN

The recuperator was designed to meet the following problem statement:

Hot gas pressure drop	0.5 psi
Hot gas inlet temperature	1800°F
Hot gas flow	over tubes
Cooling air inlet pressure	125 psig
Cooling air inlet temperature	760°F
Maximum tube temperature	1500°F
Minimum tube temperature	900°F

The tube was specified as 0.125 in. dia by 0.0035 in. wall and 0.125 in. dia by 0.005 in. wall. Tubes of two wall thicknesses were selected to investigate the effect of stress on hot corrosion, and dimpled tubes were included to investigate the effects of cold working on hot corrosion. Small-diameter tubing means more heat transfer surface available per unit volume, resulting in a compact heat exchanger design. The minimum practical diameter used for tubing today is 0.125 in. dia. Reducing the diameter further results in significant cost increase for both the tubing and its manufacture into heat exchangers.

Tubing spacing was optimized at 1.50 D by 1.25 D staggered (see Figure 34).

This tube spacing has good heat transfer and pressure drop characteristics and results in a compact design. By reiterative calculation, the core geometry, discussed below, and a cooling flow of 60 lb/min, were determined. These satisfied the above problem statement.

Facility problems resulted in only 20 lb/min of cooling air being available. By reducing both the cooling air and the hot gas inlet temperature, however, it was possible to maintain the majority of the tubes within the critical temperature range of 1500° to 900°F.

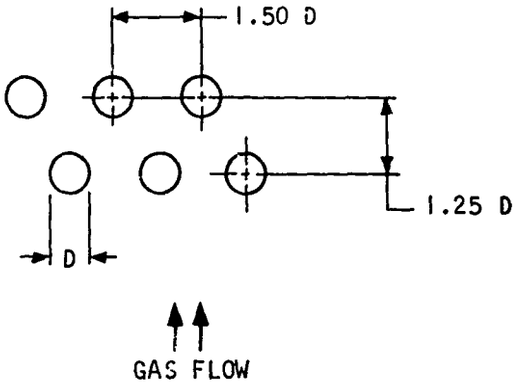

Figure 34. Tube Pattern.

RECUPERATOR FABRICATION

The recuperator was a crossflow tubular design of typical recuperator construction (see Figure 34). A novel feature of this heat exchanger was that the unit was divided into 10 modules, each capable of being removed and replaced. Five modules were fabricated from Multimet N-155 tubing and five from Incoloy 800 tubing. Each module had eighty 6-in.-long tubes, half of 0.005-in.-wall thickness and the other half of 0.0035-in.-wall thickness. The rows were arranged in a staggered pattern, four tubes per row (two plain, two dimpled), 20 rows deep, in the hot gas direction. The overall core dimensions were:

No flow	9.4 in.
Cold flow	6.0 in.
Hot flow	3.1 in.

Fabrication of the recuperator followed normal practice except that each module was built separately. The tubes were stacked between headers with the assistance of a stacking fixture. The selected braze alloy (Nicrobraz 200 for the Multimet N-155 tubes and Coast Metals 50B for the Incoloy 800 tubes) was slurried onto the external header faces. The assemblies were then vacuum brazed, the N-155 unit at 1950°F with a hold time of 10 min and the Incoloy 800 unit at 2050°F with a hold time of 10 min. Inlet and outlet pans with connectors for coolant lines were then welded on to complete the assembly of a single module. Each module was then pressure tested to 100 psig to ensure that all brazed and welded joints were leak-proof. The final test unit assembly, shown in Figures 35, 36, and 37, was produced by tack welding the 10 modules together and adding the side plates and spacers.

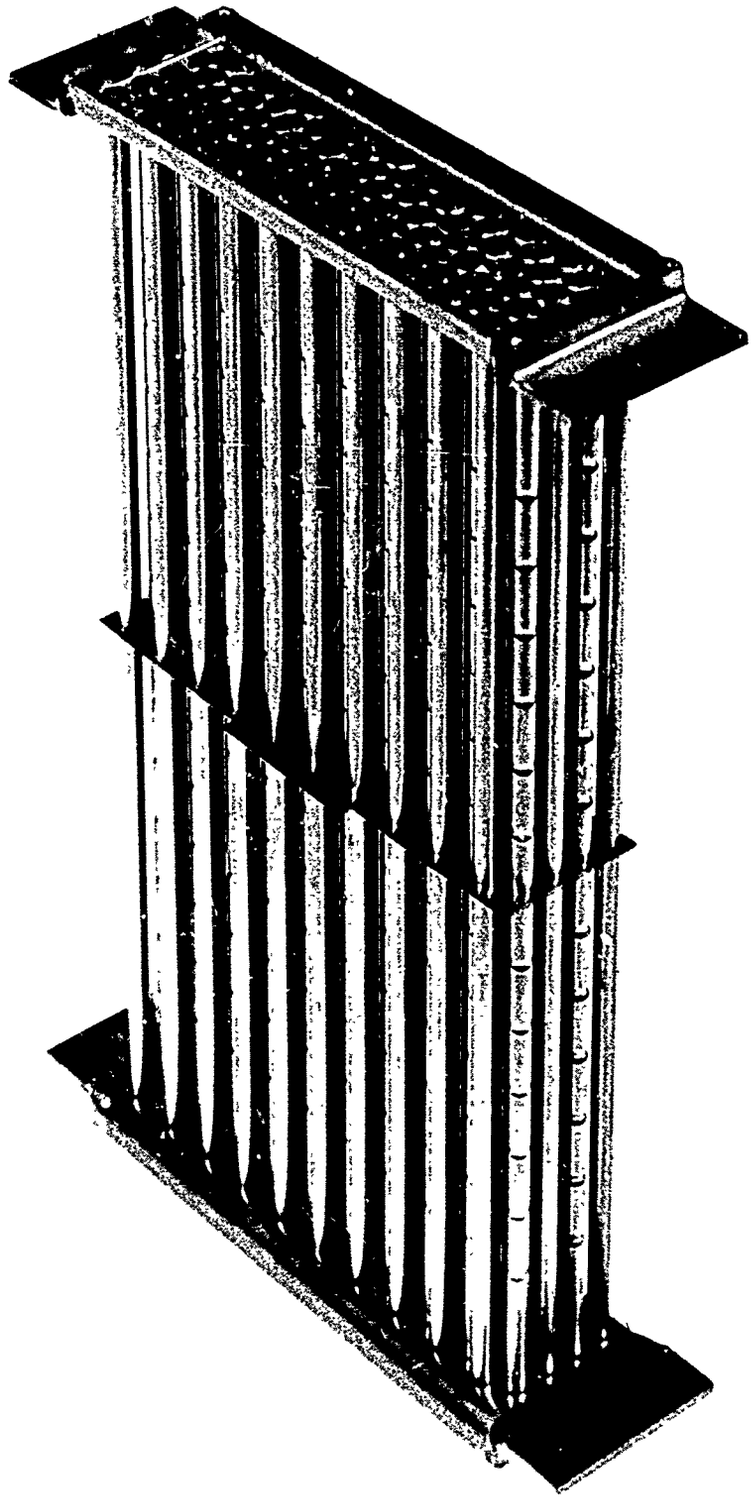

Figure 35. Recuperator Module.

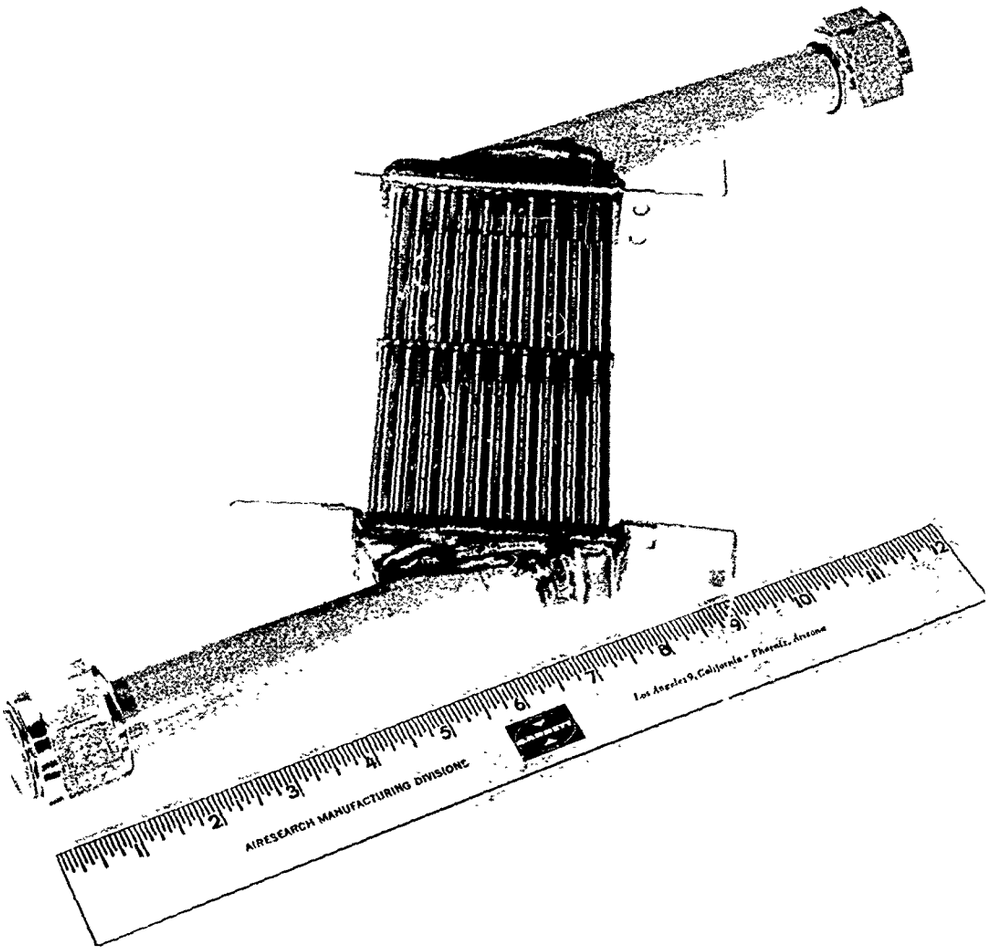

Figure 36. Recuperator Module Assembly.

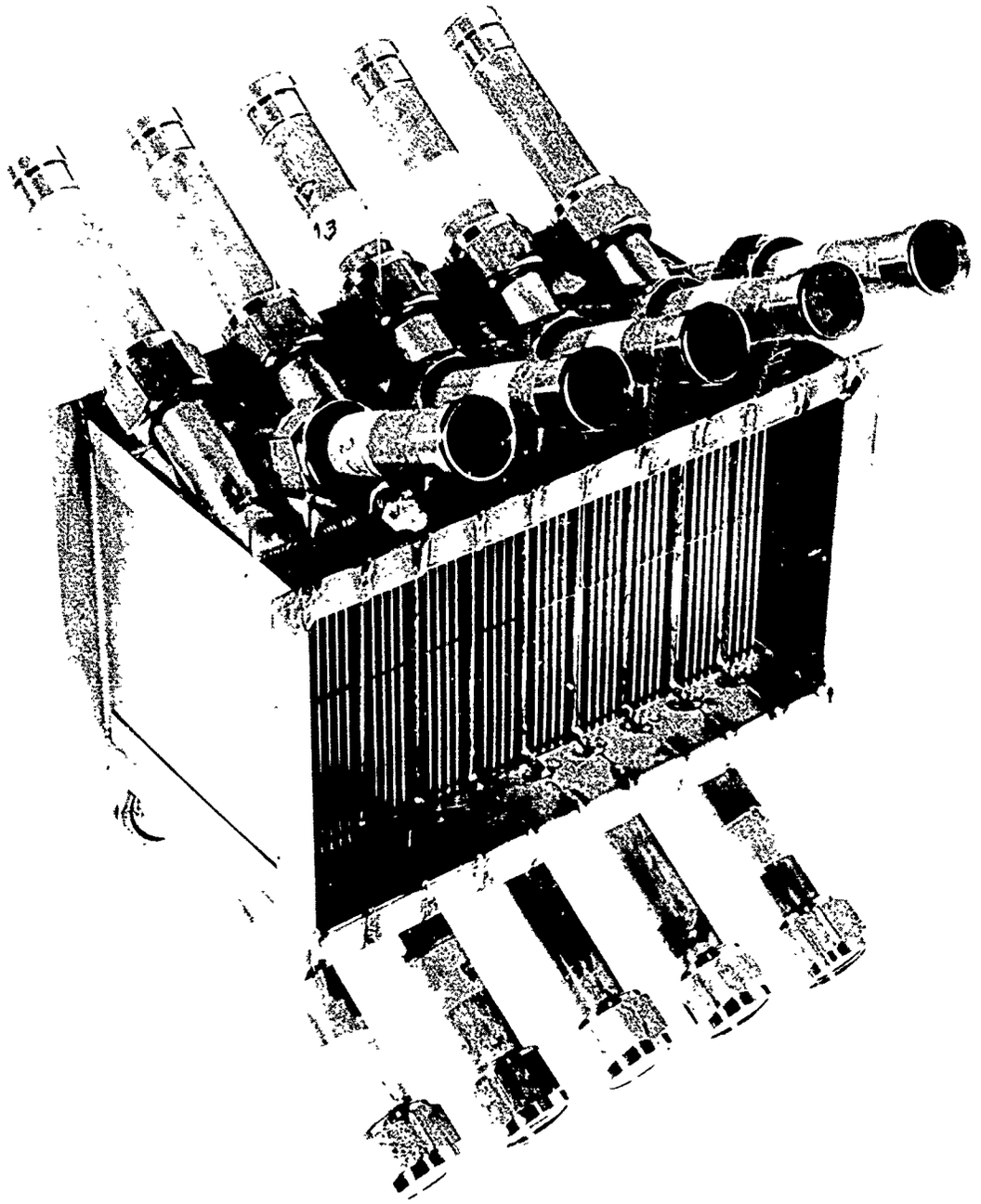

Figure 37. Recuperator Assembly.

RECUPERATOR TEST

The recuperator hot corrosion test was performed to verify the results and conclusions of the cyclic hot corrosion/stress-rupture tests and to evaluate the differences, if any, between testing in dynamic and static gas environments. Evaluation of the differences between the two tests is necessary to provide confidence in the predictions of the static test and to provide a basis, if necessary, for applying correction factors to static test results.

TEST EQUIPMENT

The hot corrosion dynamic testing was conducted at Component Evaluation Laboratories (CEL) of South El Monte, California. An overall diagram of the test setup is shown in Figure 38, and a detailed diagram of the test section showing duct dimensions and thermocouple locations is shown in Figure 39.

The combustor section consisted of a Roots blower supplying air through an orifice section and a control valve to the combustor. Fuel (JP-4 as specified in MIL-F-5624C) and salt solution (as specified in ASTM D665), each from a separate pressurized supply, were filtered through two 10μ filters and metered through flowmeters before being combined in a mixing tee just prior to entering the combustor.

The exhaust gases from the combustor were expanded and passed through a turbulator, to promote uniform flow and temperature distribution, and then through the test heat exchangers. All portions of the combustor and ducting exposed to hot gases were fabricated from Inconel 600.

Cooling air from a compressor was passed through a water trap, an oil filter, and then through a gas-fired furnace that controlled the air temperature at the desired level. The hot air was then distributed by means of a manifold to all 10 heat exchanger modules, which were arranged in parallel. Bellows were provided between the manifold and the modules to allow for thermal expansion and to prevent transmission of undue stress to the recuperator. The recuperator flange and combustor duct were designed for quick disconnection to allow the inspection of inlet and outlet faces of the heat exchanger.

All test instrumentation used in the test program was certified to comply with the accuracies and calibration procedures of MIL-C-45662A, with traceability to the National Bureau of Standards. Photographs of the combustor test rig are shown in Figures 40 and 41.

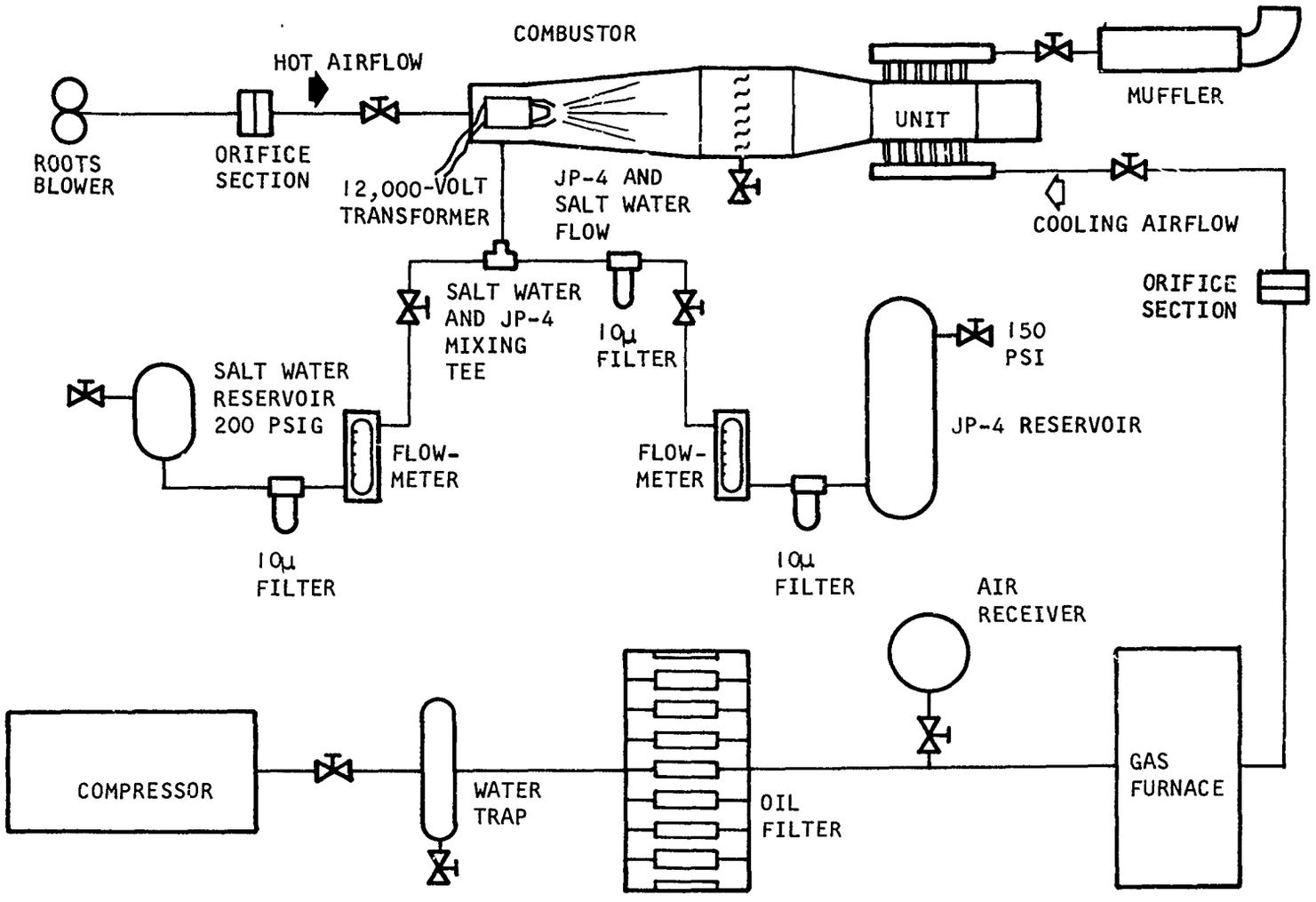

Figure 38. Schematic Diagram of Recuperator Test Setup.

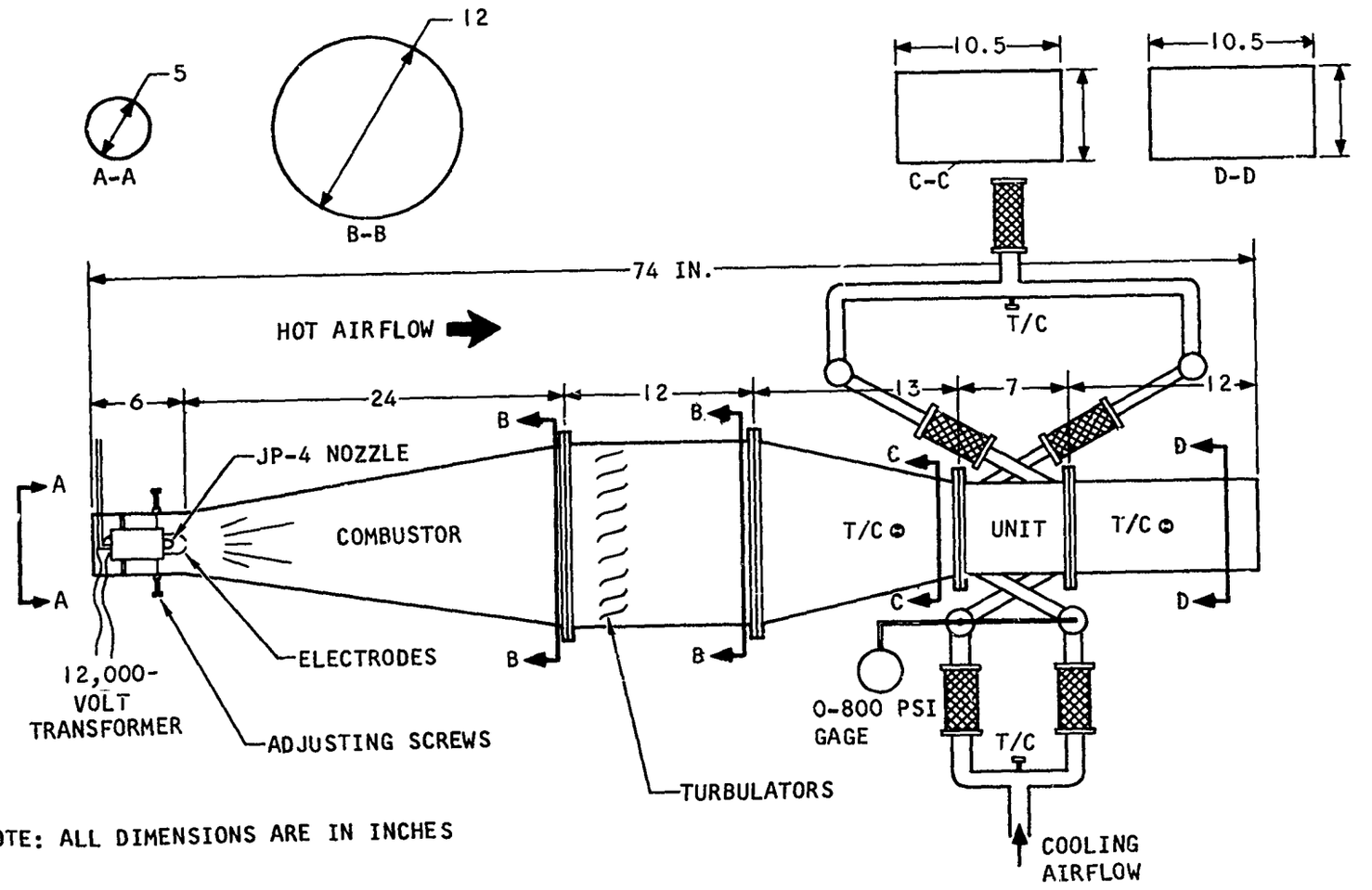

Figure 39. Detailed Diagram of Test Section.

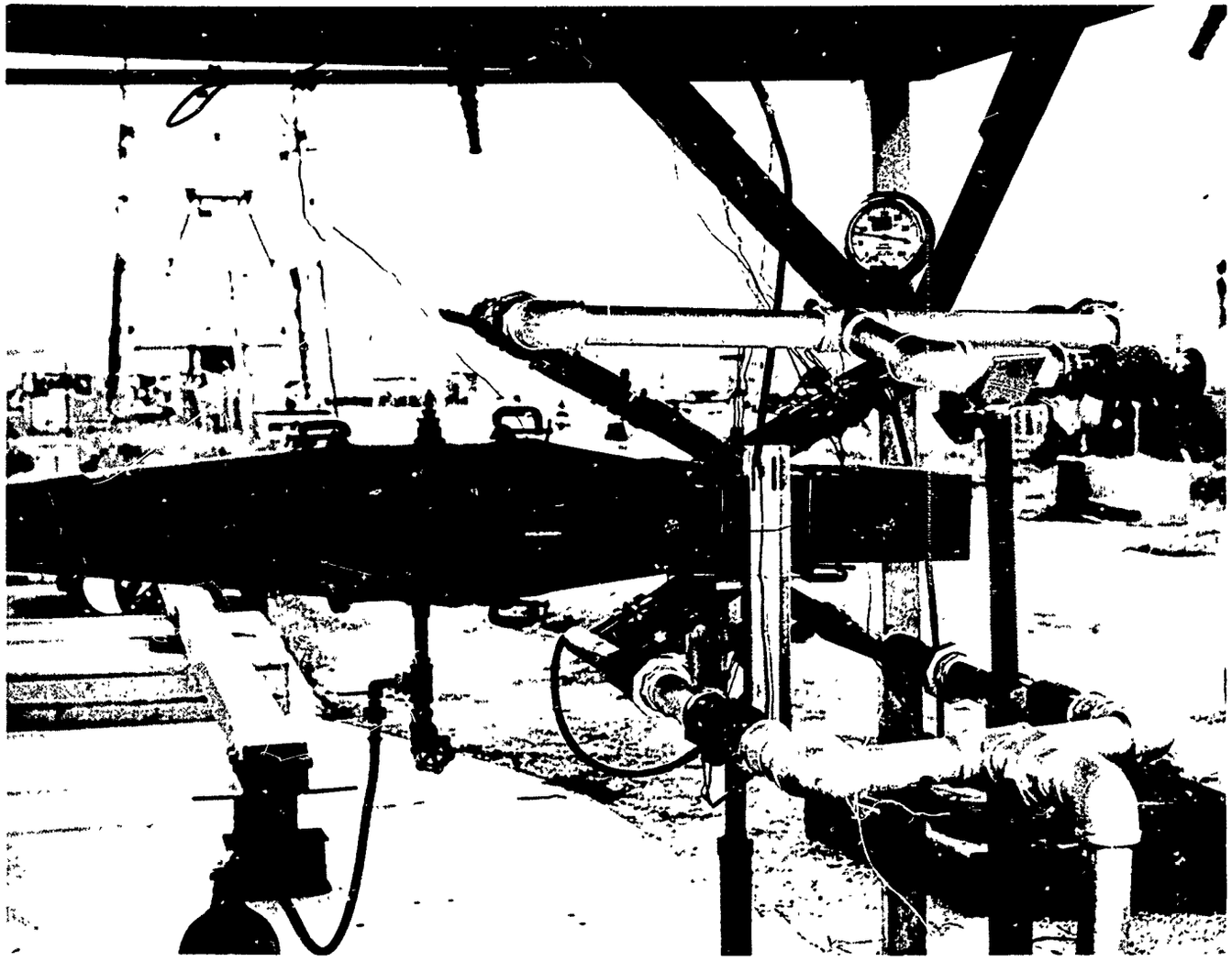

Figure 40. Recuperator Hot Corrosion Test Setup (Closeup of Ducting and Recuperator).

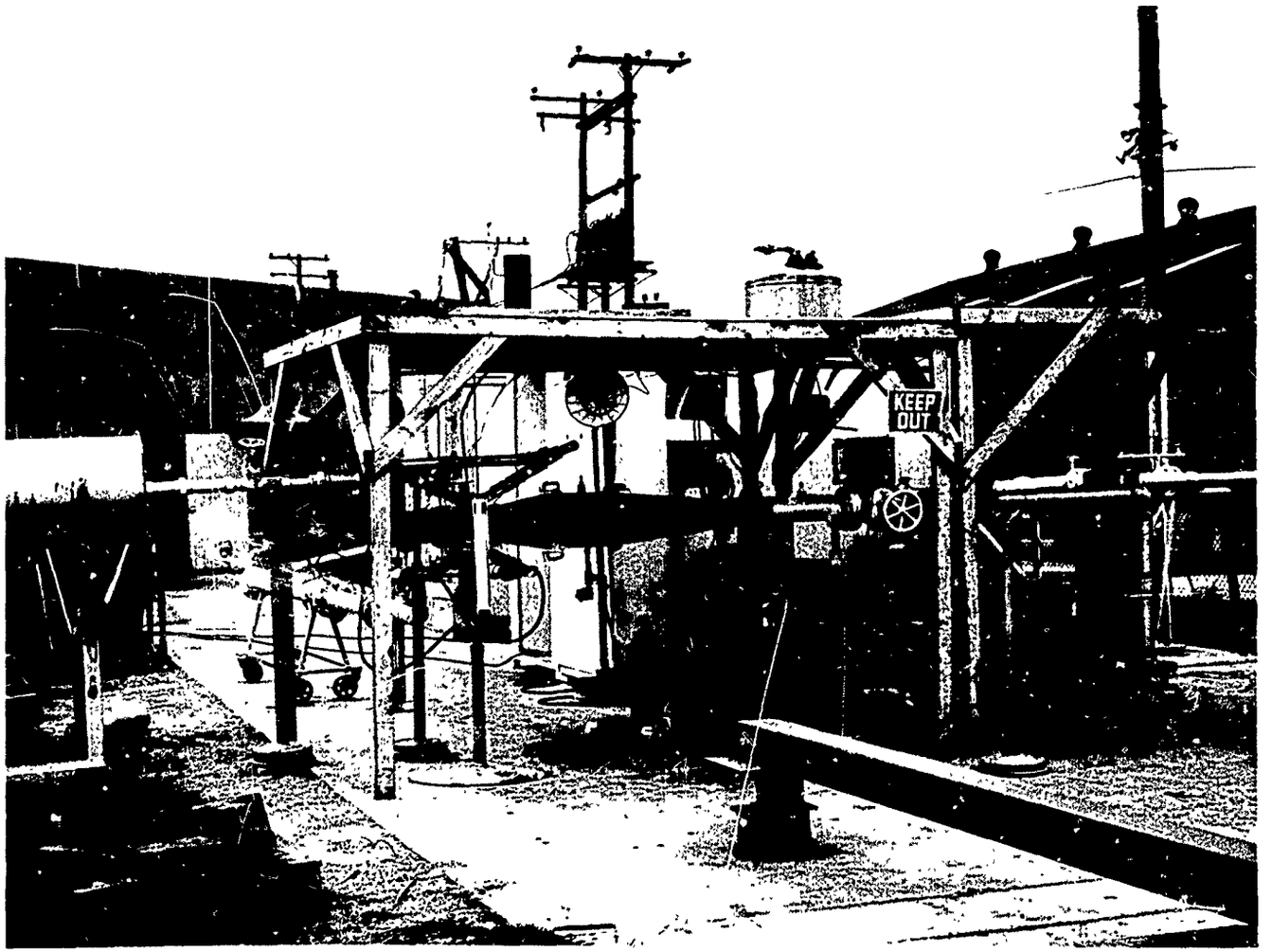

Figure 41. General View of Recuperator Hot Corrosion Test Setup.

TEST PROCEDURE

The test conditions experienced by the recuperator modules are summarized in Table XIV; these represent the steady-state test condition. Approximately every 4 hr, the hot-gas inlet temperature was reduced by 500°F and then returned to the original condition over a period of 10 min. The reduction in inlet hot-gas temperature was executed by reducing the fuel flow to the combustor.

Temperature Measurements

The recorded inlet gas temperatures are in considerable error. The measurements were made with a 1/8-in.-OD stainless steel sheathed chromel-alumel thermocouple inserted midway in the duct 5 in. upstream of the heat exchanger face. The duct walls were unlagged and approximately 400°F cooler than the gas stream. The heavily oxidized thermocouple would have an emissivity of approximately 0.85 and, in conjunction with the cold duct walls, would produce a radiation error resulting in the thermocouple's indicating a temperature approximately 100°F cooler than the true gas temperature.

The tube temperatures were measured by chromel-alumel thermocouples welded to the tube wall and protected by a thin layer (< 0.030 in.) of Cerabond (major constituent Al_2O_3). The insulation provided by this Cerabond is calculated to produce a measured temperature < 10°F below the true tube temperature. The thermocouple was located 1.0 in. from the header to prevent conduction-induced temperature errors.

The inlet hot-gas temperature profile was taken at intervals, and a typical result is shown in Table XV. It is evident that the outermost modules were receiving cooler gas than those in the center, resulting in a similar distribution in tube temperature from module to module.

Core Module Test Histories

Figure 42 displays the history of the test cores exposed in the rig and also shows the salt concentrations in the combustor exhaust stream. Both are shown as a function of rig test time. In each of the 10 core module positions, from one to three test cores were exposed. A serial number, for example, (6-2), was assigned to each test core module depending upon its position in the rig and its sequential order of exposure in that position. For example, after 36 hr, all the modules in positions 4 through 8 were removed and replaced with new, unexposed modules.

The initial salt concentration in the combustor exhaust was set at 5 ppm to correspond to that used in the cyclic hot corrosion test. After 36 hr, however, unexpected severe corrosion was observed.

To determine whether or not the salt was the cause of this corrosion, the most severely corroded modules were replaced and the next 36 hr were run without salt injection. Only minor corrosion was experienced in this period,

TABLE XIV. RECUPERATOR TEST CONDITIONS

Hot Gas			Cooling Air			Indicated Tube Temperature (°F)							
						Front Row				Rear Row			
						Maximum		Minimum		Maximum		Minimum	
Time Period (hr)	Flow (lb/min)	Maximum-Indicated Temperature (°F)	Flow (lb/min)	Temperature (°F)	Pressure (psig)	A*	B*	A	B	A	B	A	B
0 to 36	23 to 25	1440 to 1460	19 to 20	420 to 450	90 to 100	1390	1350	-	-	1100	-	700	650
36 to 72	23 to 25	1475 to 1500	19 to 20	420 to 450	90 to 90	1500	-	1250	1320	1100	-	-	1050
72 to 229	19 to 20	1475 to 1500	18 to 20	650 to 700	80 to 90	1510	1480	1000	-	1075	1075	730	730
229 to 367	19 to 20	1475 to 1500	19 to 20	650 to 700	105 to 120	-	-	-	930	1230	-	750	750
367 to 500	19 to 20	1475 to 1500	14 to 15	600 to 650	17** to 18	-	-	-	910	-	-	730	730

*Thermocouple location 0 to 72 hr A = Module 3 B = Module 8
72 to 500 hr A = Module 4 B = Module 6

**Air pressure reduced due to excessive leakage at high pressure.

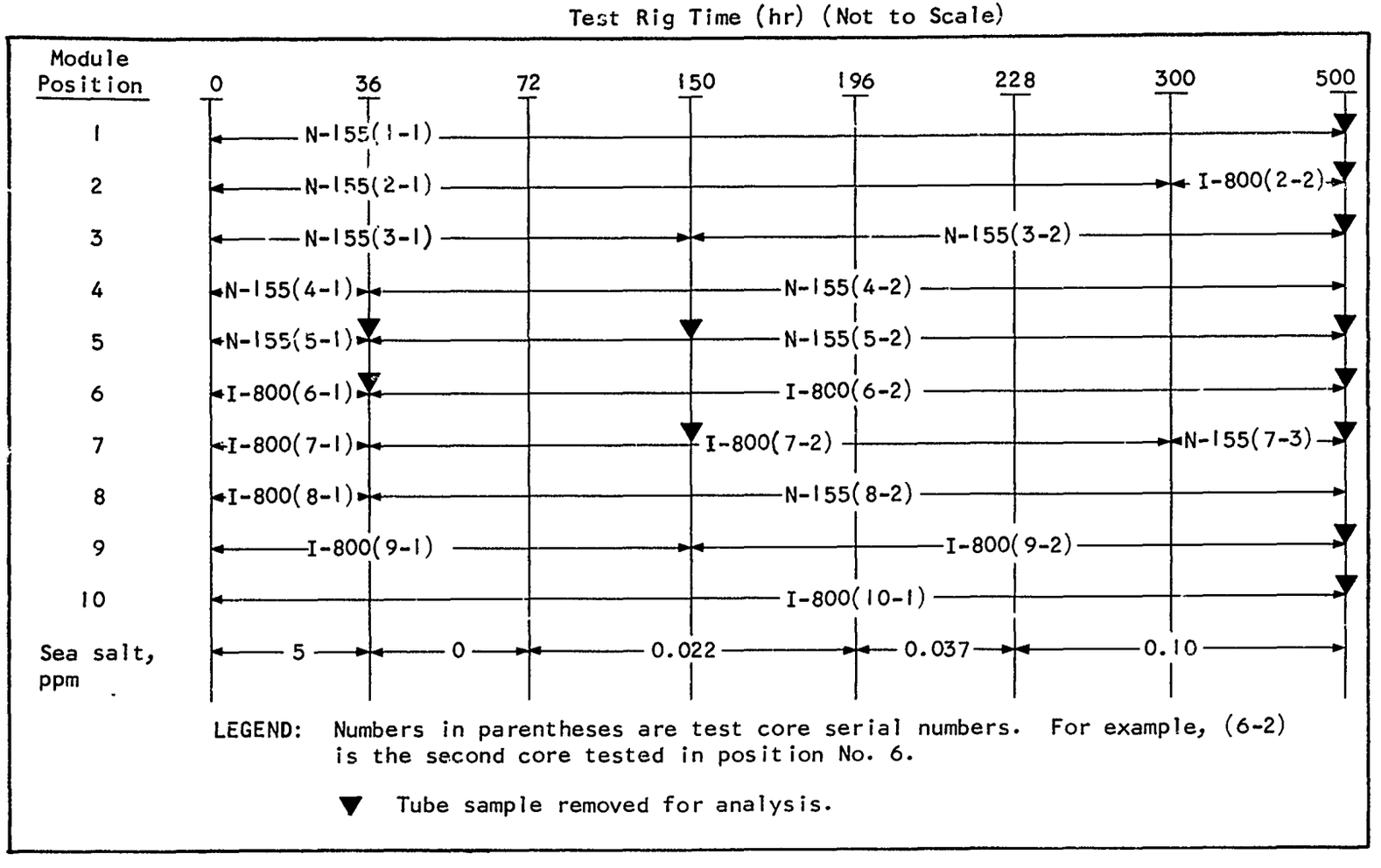

Figure 42. Core Module Test History.

TABLE XV. HOT-GAS INLET TEMPERATURE PROFILE	
Module Number	Indicated Temperature (°F)
1	1420
2	1450
3	1480
4	1490
5	1500
6	1500
7	1490
8	1470
9	1460
10	1435

indicating that the salt had influenced the corrosion rate. The reason for the unexpected increase in corrosion rate over that experienced in the cyclic hot corrosion test is discussed in the following section.

It was decided to set a more realistic salt concentration than the initial 5 ppm. The initial concentration corresponded to 5 times the sea-salt concentration recorded on the deck of a destroyer in a 40-kn wind (see Figure 8). The salt concentration, therefore, was set at 0.022 ppm, corresponding to a 20-kn wind. After a period of operation at this level, where no serious corrosion was exhibited, the salt concentration was revised to 0.10 ppm, corresponding to a 30-kn wind, and was maintained at that level for the duration of the test.

Salt Concentration

Sea-salt concentrations in the combustion gas were controlled by adjusting the injection flow rates and solution strengths. During the first 36 hr, sea-salt solution was injected upstream of the combustor; during the second 36 hr of rig time, no salt was injected. For the remainder of the test, the salt solution was injected into the JP-4 fuel line. Table XVI shows a salt exposure history for each module.

The salt concentrations in the gas stream were changed several times, as indicated in Table XVII.

TABLE XVI. EXPOSURE HOURS VS SALT CONCENTRATION

Position No.	Module No.	Tube Alloy	Salt Concentration (ppm)					Total Exposure (hr)
			5.0	0	0.022	0.037	0.10	
1	1-1	N-155	36	36	124	32	272	500
2	2-1	N-155	36	36	124	32	72	300
	2-2	I-800	-	-	-	-	200	200
3	3-1	N-155	36	36	78	-	-	150
	3-2	N-155	-	-	46	32	272	350
4	4-1	N-155	36	-	-	-	-	36
	4-2	N-155	-	36	124	32	272	464
5	5-1	N-155	36	-	-	-	-	36
	5-2	N-155	-	36	124	32	272	464
6	6-1	I-800	36	-	-	-	-	36
	6-2	I-800	-	36	124	32	272	464
7	7-1	I-800	36	-	-	-	-	36
	7-2	I-800	-	36	124	32	72	264
	7-3	N-155	-	-	-	-	200	200
8	8-1	I-800	36	-	-	-	-	36
	8-2	N-155	-	36	124	32	272	464
9	9-1	I-800	36	36	78	-	-	150
	9-2	I-800	-	-	46	32	272	350
10	10-1	I-800	36	36	124	32	272	500

TABLE XVII. SALT WATER CONCENTRATION HISTORY

Time on Rig (hr)	Hot-Gas Flow Rate (lb/min)	Salt Concentration in Hot Gas (ppm)	Total Rig Time (percent)
0 to 36	23 to 25	5	7.2
36 to 72	23 to 25	0	7.2
72 to 196	19 to 20	0.022	24.8
196 to 228	19 to 20	0.037	6.4
228 to 355	19 to 20	0.10	54.4
355 to 500	19 to 20	0.10	

EXAMINATION OF RECUPERATOR TUBES

At predetermined times during the test, the combustor rig was stopped and the recuperator was visually examined. If damage was indicated, tubes were taken from the modules for more detailed metallurgical evaluation. The dynamic conditions that prevailed during the tests were similar to the anticipated service conditions. The purpose of the metallurgical examination was to observe the effects of the dynamic test conditions on the hot corrosion behavior of the two tubing materials, to correlate the findings with those of the cyclic hot corrosion test, and then to determine the reliability of the data gleaned from the earlier experiments.

Apart from the variables introduced during the course of the test run (for example, salt concentration, temperature, gas flow rates, and time), tubes of two different dimensions, 0.0035- and 0.005-in. wall thickness, were built into the recuperator, and both sizes of tubing were present in both the plain and the dimpled condition. A secondary purpose of the investigation was to observe the hot corrosion characteristics of these different tubing forms.

Specimens were examined from tubes exposed under the conditions tabulated in Table XVIII.

Tubes were taken from both the hot inlet face and the cold outlet face of the recuperator. Each tube was sectioned at 1-in. intervals, resulting in 12 temperature stations being examined metallographically on each module.

The results of the recuperator test are summarized in Table XIX and are discussed in detail below.

EXAMINATION OF RECUPERATOR AFTER 36-HR EXPOSURE TO 5-PPM SEA SALTS

Preliminary visual examination of the heat exchanger at this stage indicated that gross corrosion had taken place. The general appearance of the hot (upstream) and cold (downstream) faces is shown in Figures 43 and 44. A white deposit observed on the hot face was identified as sea salts. Warts were also present on the cold face of the Incoloy 800 modules.

Metallurgical Examination of Incoloy 800 Tubes (Module 6-1)

At 675°F, no oxide layer was observed, but as temperature was increased, a thin oxide layer was detected at 975°F. The thickest oxide layer was observed at the highest exposure temperature of 1370°F. At the lower temperatures, however, warts were observed. A section through such an area is shown in Figure 45. This shows gross oxidation occurring at a local site while adjacent surfaces remain virtually uncorroded. At higher temperatures (on the hot face of the recuperator), such phenomena were not observed. Instead, the outer surfaces were covered with an oxide layer

TABLE XVIII. CONDITIONS OF EXPOSURE OF TUBES FOR MICROSTRUCTURAL EXAMINATION

Material	Module Number	Micro Specimen Number	Total Time on Test (hr)	Salt Concentration (ppm)	Temperature (°F)
N-155	(5-1)	17279		5.0	675
		17280	36	5	1370
	(5-2)	16911			730
		16909	36	0	1500
	(5-2)	17114			730
		17175	114	0.02	1500
	(7-3)	17297			740
		17298	200	0.10	1480
	(3-2)	17293			715
		17294	350	up to 0.10	1460
	(5-2)	17287			730
		17288	464	up to 0.10	1500
	(1-1)	17302-1		5.0 (36 hr)	700
				0.0 (36 hr)	
		17302-4	500	up to 0.1 (428 hr)	1445
Incoloy 800	(6-1)	17283			675
		17284	36	5.0	1370
	(6-2)	16913			730
		16912	36	0	1500
	(7-2)	17171			730
		17172	114	0.02	1500
	(2-2)	17299			715
		17300	200	0.10	1460
	(9-2)	17295			715
		17296	350	up to 0.10	1460
	(6-2)	17290			780
		17291	464	up to 0.10	1500
	(10-1)	17301-1		5.0 (36 hr)	700
				0.0 (36 hr)	
		17301-4	500	up to 0.1 (428 hr)	1445

TABLE XIX. SUMMARY OF RECUPERATOR TEST RESULTS

Exposure Conditions		Incoloy 800		N-155	
Time (hr)	Sea-Salt Concentration (ppm)	Hot Face*	Cold Face	Hot Face	Cold Face
36	5	0.4-mil oxide	No appreciable oxide layer: warts	0.8-mil oxide	No appreciable oxide layer: warts
36	0	No oxidation	No oxidation	No oxidation	No oxidation
114	0.022 maximum	1.0-mil oxide	No oxidation	0.3-mil oxide	No oxidation
200	0.1	0.6-mil oxide	No oxidation	0.4-mil oxide	No oxidation
350	0.1 maximum	0.1-mil oxide	No oxidation	0.4-mil oxide	No oxidation
464	0.1 maximum	0.6-mil oxide	No oxidation	0.5-mil oxide	No oxidation
500	5 to 0 to 0.1	0.6-mil oxide	Thin oxide:warts	0.3-mil oxide	Thin oxide:warts

*Hot face temperature varied according to location of tubes in recuperator, which must be considered when making comparisons.

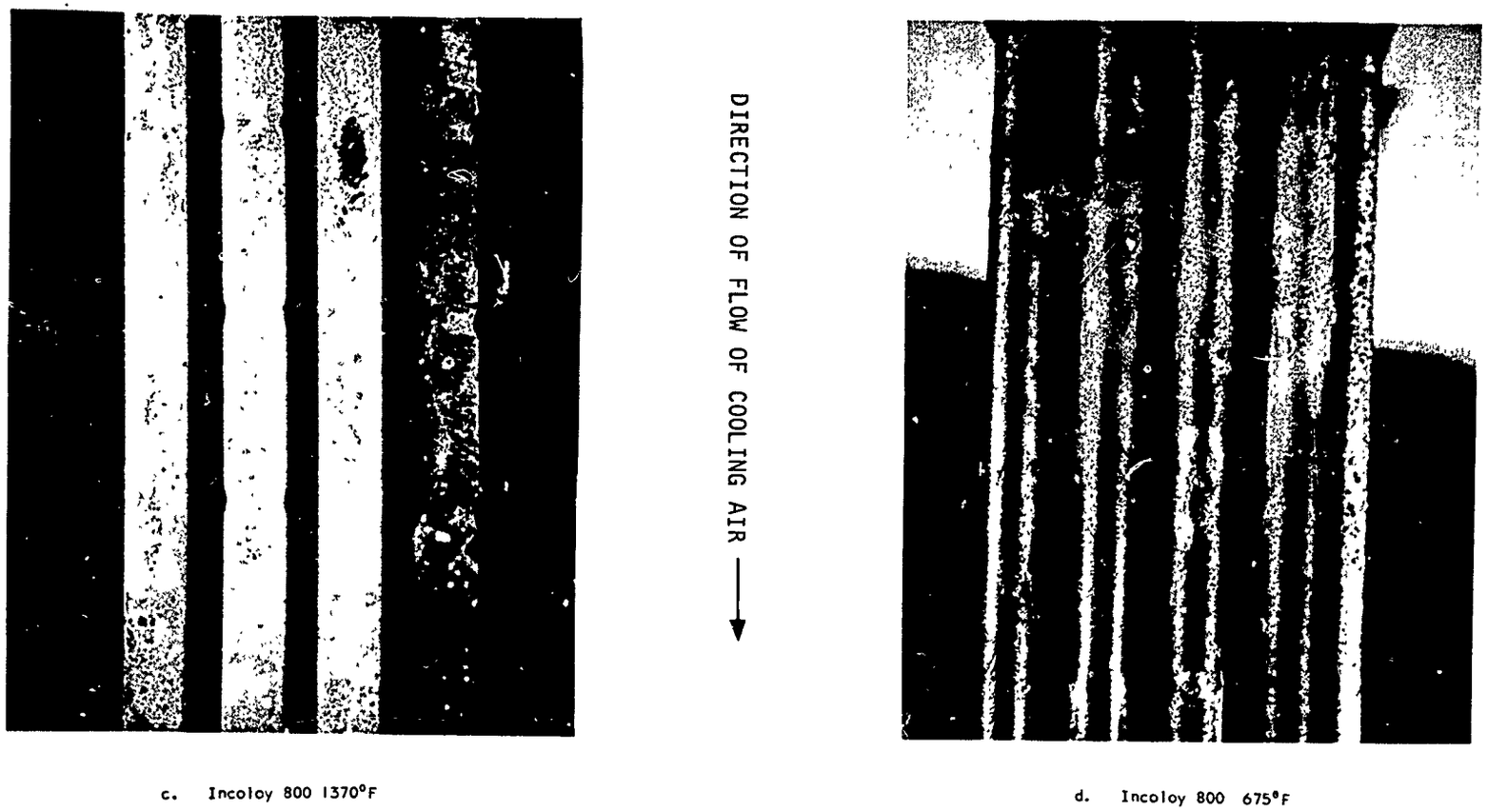

c. Incoloy 800 1370°F

d. Incoloy 800 675°F

Figure 43. Appearance of Incoloy 800 Recuperator Tubes After 36-hr Exposure to 5-ppm Sea Salts (Module 5-1).

a. N-155 1375°F

DIRECTION OF FLOW OF COOLING AIR ⟶

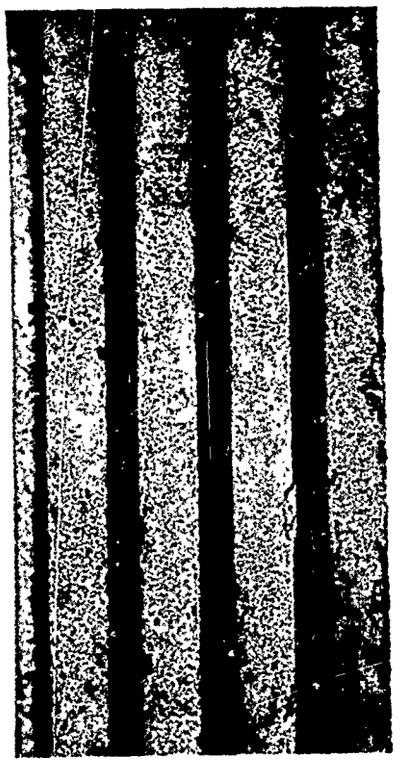

b. N-155 675°F

Figure 44. Appearance of N-155 Recuperator Tubes After 36-hr Exposure to 5-ppm Sea Salts (Module 6-1).

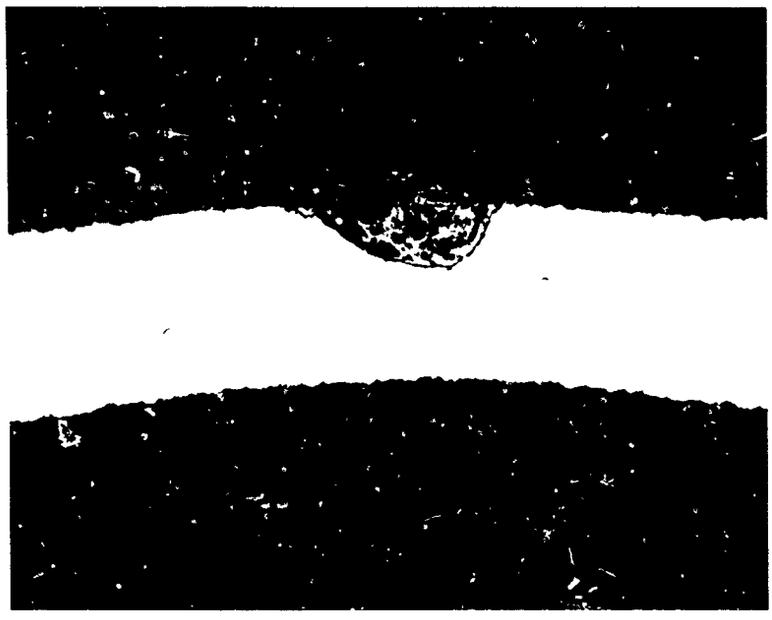

MAG = X250

a. 675°F

MAG = X250

b. 1370°F

NOTE: FIGURES REDUCED TO 95%.

Figure 45. Incoloy 800 Exposed for 36 hr to 5 ppm Sea Salts in Recuperator Test Rig (Module 6-1).

approximately 0.4 mil thick, with slight evidence of intergranular penetration. No oxide layer was detected on the inside surfaces of the tube. Microprobe analysis confirmed the thickness of the oxide and indicated that there was a chromium-depleted layer underlying the chromium-oxide layer. Iron and nickel oxides also were present; sulfides were not. No internal oxidation was observed, nor was any oxide found on the inside surfaces of the tube.

Metallurgical Examination of N-155 Tubes (Module 5-1)

No oxide layer was detected on tubes heated to temperatures below 900°F, nor on the inside surfaces which had not been exposed to the sea-salt impregnated atmosphere. A layer of oxide approximately 0.8 mil thick covered the portion of the tube heated to the highest temperature of 1370°F. Warts also were observed on the tubes exposed at low temperatures. An area of severe erosion is depicted in Figure 46, which shows that in an isolated spot on the tube the metal had been removed so that only about 1 mil of unaffected material remained. As far as could be ascertained, no oxide layer was associated with the phenomenon. Microprobe analysis showed that the tube was covered with a layer of chromium oxide and that the metal was depleted in chromium adjacent to the oxide film.

EXAMINATION OF RECUPERATOR AFTER 36-HR EXPOSURE TO ZERO SEA SALTS

To obtain a comparison with the 5-ppm sea-salt injection run, the heat exchanger, containing previously unexposed modules, was run for 36 hr with no sea-salt ingestion. Visual examination showed that the tubes were discolored only by interference tints, indicating that only slight oxidation had taken place.

Metallurgical Examination of Incoloy 800 Tubes

As predicted from the visual observations, no oxide layers were detected on any sample examined.

Metallurgical Examination of N-155 Tubes

No oxide film was observed on either the inside or the outside surfaces of the tubes examined, regardless of the temperature of exposure.

EXAMINATION OF RECUPERATOR AFTER 114-HR EXPOSURE

The first 36 hr of this test were completed with no sea-salt solution injected into the JP-4 fuel. For the balance of the time, 0.022-ppm sea salts were present in the hot-gas stream. To monitor the corrosion rates, tubes were removed from other modules that had a total test time of 114 hr, and these samples were prepared for metallurgical examination.

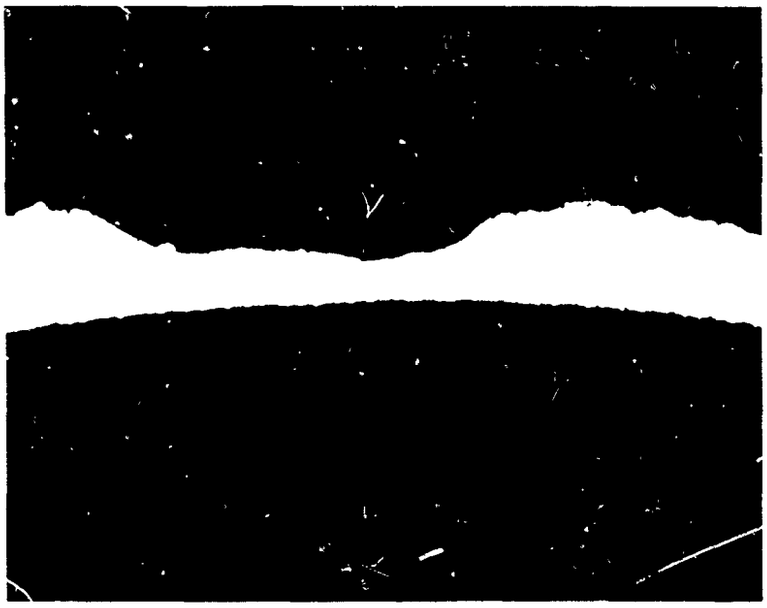

MAG = X250

a. 675°F

MAG = X250

b. 1370°F

NOTE: FIGURES REDUCED TO 95%.

Figure 46. N-155 Exposed for 36 hr to 5 ppm Sea Salts in Recuperator Test Rig (Module 5-1).

Metallurgical Examination of Incoloy 800 Tubes (Module 7-2)

Oxide layers were not evident on samples exposed to temperatures of less than 930°F. Figure 47 shows some evidence of intergranular penetration on a section of a 5-mil tube heated to 1500°F with the oxide layer penetrating approximately 1.0 mil. Slight oxidation was observed on the inside surface of the tube exposed to the cooling air.

A more detailed microprobe analysis on this sample revealed that the chromium oxide adjacent to the metal contained nickel oxide (and was probably a spinel) and was covered by a layer of iron oxide.

Metallurgical Examination of N-155 Tubes (Module 5-2)

Electron microprobe analysis showed that the oxide layer was only 0.3 mil thick on the outside of the tube and consisted essentially of chromium oxide.

EXAMINATION OF RECUPERATOR AFTER 200-HR EXPOSURE

After 200 hr of exposure, the hot face tubes were oxidized, but not severely, and the cold face was only discolored by interference tints. Sea-salt concentration had been maintained at 0.1 ppm for the duration of this exposure.

Metallurgical Examination of Incoloy 800 Tubes (Module 2-2)

A slight oxide film was observed on the portion of the tube heated to 1050°F. The thickness of the layer increased at each successive temperature and reached its maximum thickness of about 0.6 mil at the highest temperature of exposure. Some intergranular oxidation was observed, and oxide was also detected on the bore of the tube, but in much less quantity than the surfaces exposed to the burner exhaust. (See Figure 48.) Microprobe analysis confirmed the thickness of the oxide film.

Metallurgical Examination of N-155 Tubes (Module 7-3)

No oxide layers could be seen on the portion of the tubes heated to 740°F, and the thickness of the film was only 0.4 mil at the point of highest temperature. Figure 49 illustrates the extent of oxidation on a 5-mil tube and shows the relative extent of oxidation on the inner and outer surfaces of the tube. Confirmation of the oxide thickness was established by microprobe analysis.

EXAMINATION OF RECUPERATOR AFTER 350-HR EXPOSURE

Modules (3-2) and (9-2) were put on test at the 150-hr mark when 0.022-ppm sea salts were admitted into the test rig. After less than 50 hr, the salt concentration was increased to 0.037 ppm for 32 hr and then increased again to 0.1 ppm for the balance of the testing. Little oxidation had

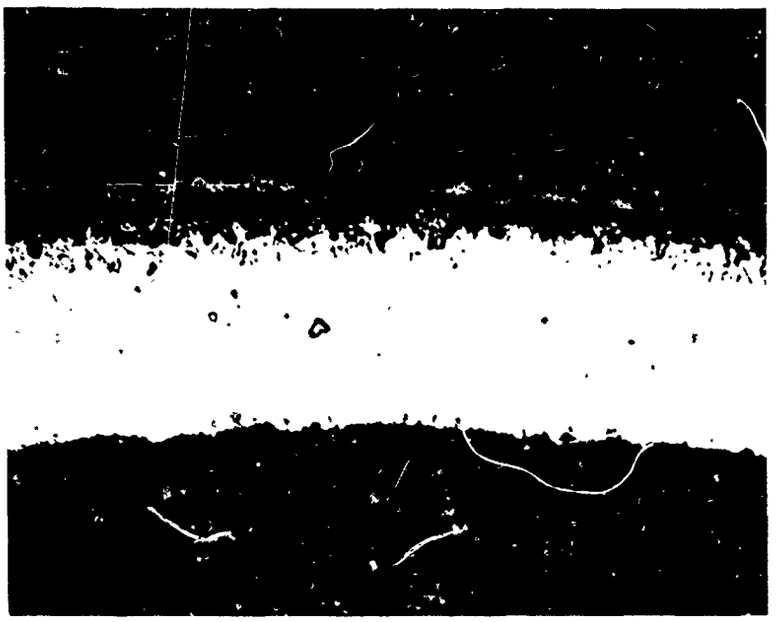

MAG = X250

Figure 47. Incoloy 800 Exposed for 114 hr at 1500°F to 0.02-ppm Sea Salts in Recuperator Rig (5-mil Tube, Module 7-2).

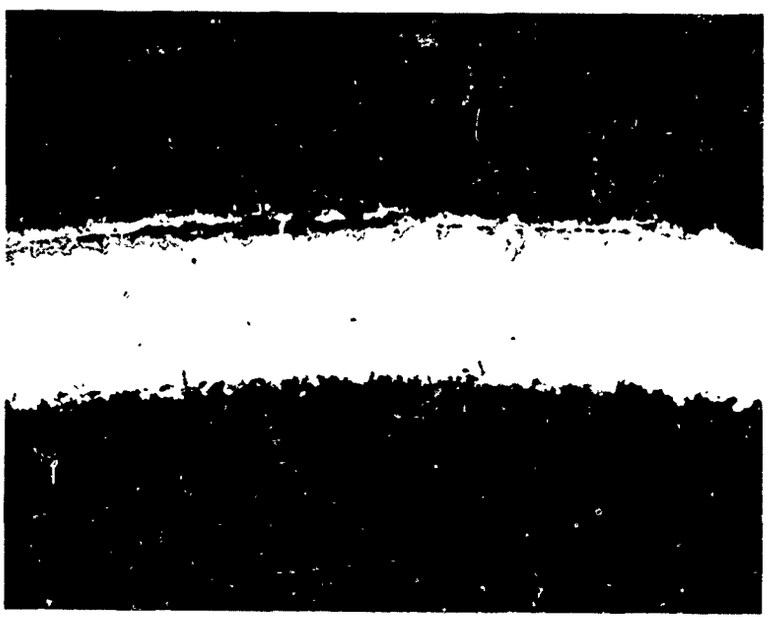

MAG = X250

NOTE: FIGURES REDUCED TO 95%.

Figure 48. Incoloy 800 Exposed for 200 hr at 1460°F to 0.1-ppm Sea Salts in Recuperator Test Rig (3.5-mil Tube, Module 2-2).

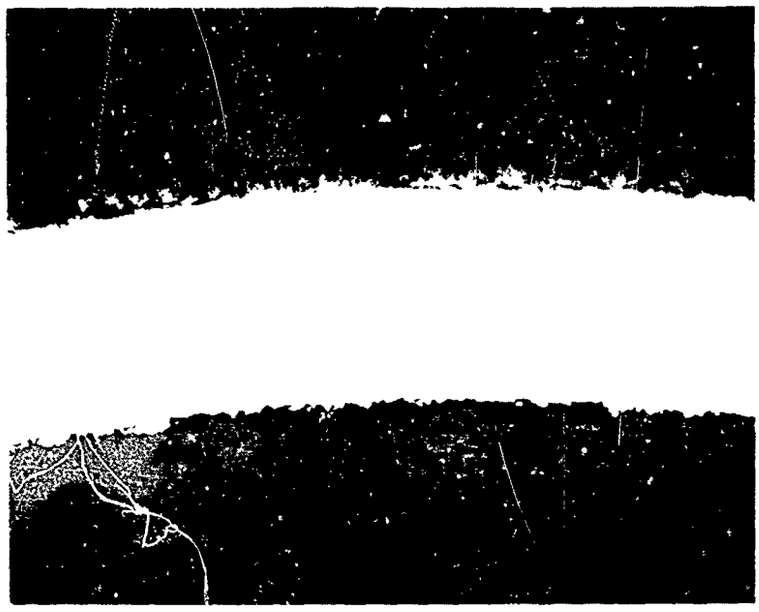

MAG = X250

Figure 49. N-155 Exposed for 200 hr at 1500°F to 0.1 ppm Sea Salts in Recuperator Test Rig (5-mil Tube, Module 7-3).

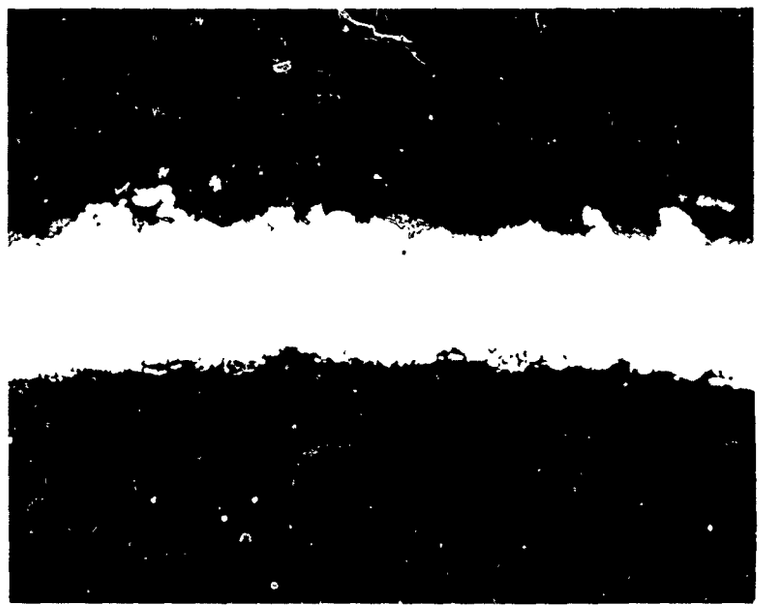

NOTE: FIGURES REDUCED TO 95%.

MAG = X250

Figure 50. N-155 Exposed for 350 hr at 1480°F to a Maximum of 0.1-ppm Sea Salts in Recuperator Rig (3.5-mil Tube, Module 3-2).

occurred on the Incoloy 800 module (9-2). One factor contributing to this was that the temperature of the hot gas admitted to this portion of the heat exchanger was 40°F below nominal, resulting in a maximum tube temperature of 1460°F. Little corrosion had occurred on the N-155 module (3-2).

Metallurgical Examination of Incoloy 800 Tubes (Module 9-2)

Specimens prepared from the Incoloy 800 module (9-2) confirmed that the tube temperature had been somewhat lower than planned because the oxide film on the section prepared from the hottest zone measured less than 0.1 mil.

Metallurgical Examination of N-155 (Module 3-2)

The surface of the tube in the vicinity of the microsection appeared to be quite roughened. A discontinuous oxide film was observed, about 0.4 mil deep in places. This roughening could have been the result of some localized corrosion-erosion effect, for it was not found on any other section of the tube examined. Some intergranular oxidation of the inside surface of the tube is shown in Figure 50.

EXAMINATION OF RECUPERATOR AFTER 464-HR EXPOSURE

After 464 hr of exposure, the hot face of the heat exchanger did not appear to be badly oxidized, and the cold face did not have any visible oxide on the coolest 2 or 3 in. of tubing. Sea-salt injection was varied from zero to 0.1 ppm during testing of these modules. For the first 36 hr no salt was added, followed by a period of 124 hr at 0.022 ppm, 32 hr at 0.037, and the final 272 hr at 0.10 ppm sea salts.

Metallurgical Examination of Incoloy 800 Tubes (Module 6-2)

An oxide layer approximately 0.6 mil thick was observed on the portion of the tube heated to 1500°F, and some intergranular penetration had occurred on the outside, and to a lesser extent on the inside, tube surfaces (see Figure 51). Microprobe analysis confirmed the oxide thickness.

Metallurgical Examination of N-155 Tubes (Module 5-2)

Figure 52 shows that the oxide layer was 0.5 mil thick on the outside surface and that some intergranular oxide penetration occurred on the bore of the tube. No internal oxidation was detected, and microprobe analysis indicated that no oxygen had penetrated beyond the oxide film.

EXAMINATION OF RECUPERATOR AT THE COMPLETION OF TESTING

Modules (1-1) and (10-1) remained on test throughout the experiment; however, the temperature of the hot gases flowing through these modules was approximately 60°F lower than it was in the other areas of the heat exchanger. During the course of the experiment, some tubes did develop leaks, but these were generally found in the cooler sections and were associated with the warts.

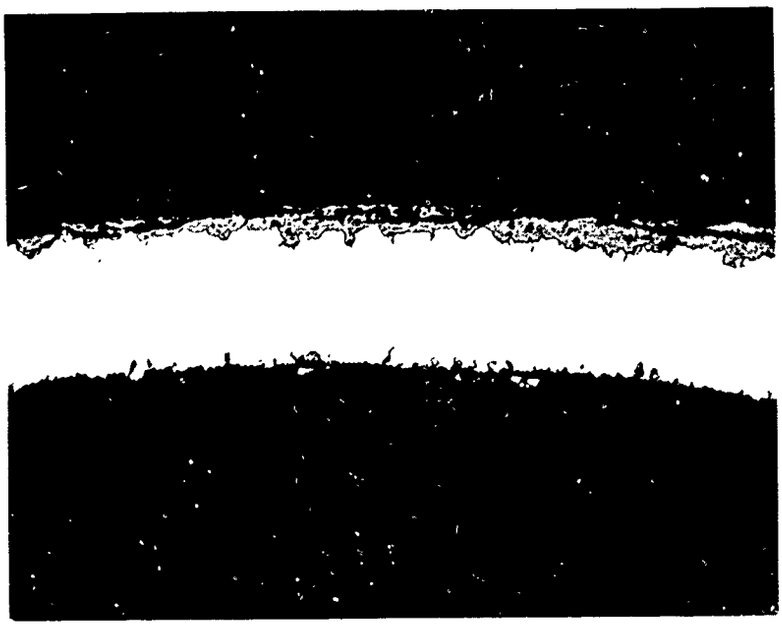

MAG = X250

Figure 51. Incoloy 800 Exposed for 464 hr at 1500°F to 0.1-ppm Maximum Sea Salts in Recuperator Test Rig (Module 6-2).

MAG = X250

NOTE: FIGURES REDUCED TO 95%.

Figure 52. N-155 Exposed for 464 hr at 1500°F to 0.1-ppm Maximum Sea Salts in Recuperator Test Rig (Module 5-2).

Metallurgical Examination of Incoloy 800 Tubes (Module 10-1)

In spite of the blackened appearance of the tubes and the presence of a loosely adherent oxide film, the extent of corrosive attack was not severe, except for the warts. At 900°F, the oxide film was extremely thin but had caused some slight roughening of both the inside and outside surfaces of the tube (see Figure 53). Microprobe analysis of the oxide film on the hottest portion of the tube showed that the film consisted of nickel-chromium oxide covered by iron oxide and that the total thickness of corrosion products was 0.6 mil. The loosely adherent scale was scraped from the tubes and identified spectrographically as iron oxide.

Metallurgical Examination of N-155 Tubes (Module 1-1)

Samples prepared from the coolest sections of the module were covered by a very thin layer of oxide, as can be seen in Figure 54a. The highest temperature portion of the tube was also covered with oxide about 0.3 mil thick. Figure 54b shows a section of the tube prepared from an area adjacent to the failure site. From this it can be seen that internal oxidation had occurred along the grain boundaries from the outside surface of the tube, and intergranular penetration was also evident on the bore of the tube. Microprobe analysis taken through a wart area indicated that it was composed principally of chromium oxide.

METALLURGICAL EXAMINATION OF DIMPLED TUBES

Longitudinal sections were prepared from dimpled tubes taken from modules (5-1), (6-1), (4-2), and (8-2) after exposure for 36 hr to 5-ppm sea salts and 464 hr to a lower concentration of sea salts, respectively. The visual appearance of the tubes was identical to that of adjacent undimpled tubes, and metallographical examination confirmed that the oxide layers were the same composition and extended to the same thickness as the films found on corresponding plain tubes. No undue intergranular penetration was observed in the vicinity of the dimples.

COMPARISON OF 3.5-MIL- AND 5-MIL-THICK TUBE WALLS

Random samples of both sizes of tubing were examined for most of the exposure conditions, but no differences in the corrosion characteristics could be found.

MAG = X250

a. 700°F (3.5-mil Tube)

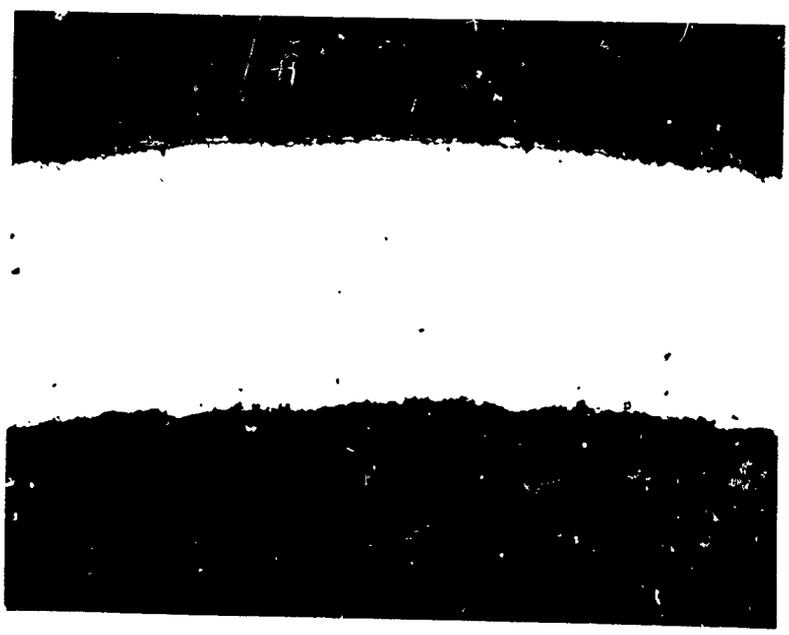

NOTE: FIGURES REDUCED TO 95%.

MAG = X250

b. 1445 °F (5-mil Tube)

Figure 53. Incoloy 800 After 500 hr Exposure in Recuperator Test Rig (Module 10-1).

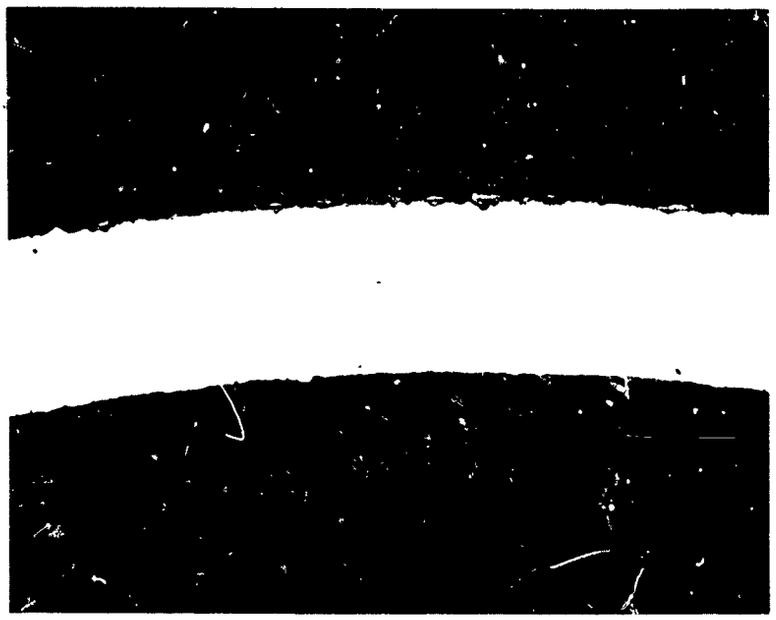

MAG - X250

a. 700°F

MAG = X250

NOTE: FIGURES REDUCED TO 95%.

b. 1445°F

Figure 54. N-155 After 500-hr Exposure in Recuperator Test Rig (Module 1-1).

DISCUSSION

MECHANISMS OF HOT CORROSION

Nickel- and cobalt-base superalloys are corroded at a rapid rate in the presence of sea salts at elevated temperatures. This type of corrosion caused considerable concern when it first appeared in gas turbine equipment more than a decade ago. Because the phenomenon occurred in many guises, and under what at first appeared to be widely dissimilar circumstances, metallurgists had difficulty relating the problems to a common cause. Although the nature of the corrosion was not understood in these early days, many common factors were observed. It appeared that the attack predominated on components that were heated to the highest temperatures in the engine (such as nozzle vanes, turbine blades, and combustion chambers), but the "black plague," as it was termed, was rarely observed on installations that operated away from the sea. The same type of attack had recurred many years previously on iron-chromium and iron-nickel-chromium steels and stainless steels in equipment burning low-grade fuel oils (that is, fuel oils high in sulfur and fuel ash content), but many metallurgists were nevertheless surprised to detect such severe hot corrosion in gas turbine equipment that used higher grade fuels and were constructed from nickel-base superalloys, which were supposed to have better corrosion-resistant properties. The problem eventually became so severe that serious temperature limitations and service life restrictions were imposed on equipment that was to operate in marine environments. At one time, limiting the sulfur content of marine turbine fuel was even considered. Although some work had already been undertaken on the study of fuel ash corrosion, the appearance of hot corrosion in marine gas turbine engines precipitated widespread investigations into the causes, fundamental mechanisms, and cures of this corrosion problem.

It was apparent that corrosion was proceeding by a process of sulfidation. The classical work of Simons et. al[3] in this country, and Shirley and his co-workers [4, 5] in England, established that molten slag reactions of alkali metal salts and the sulfur content of the fuel produced rapid rates of sulfur corrosion. Consequently, it was believed that the degree of corrosion would be related to the sulfur content of the fuel. The various mechanisms for hot corrosion that they and subsequent workers proposed during the next few years differed considerably in detail, but there was general agreement that three basic conditions must be satisfied before appreciable attack could occur. These conditions were:

1. The presence of a molten slag, composed principally of sodium sulfate
2. The destruction of the protective oxide film on the surface of the metal
3. A temperature high enough to promote and maintain the reactions

It was thought that the slag that promoted sulfidation was formed by the reaction of sulfur in the fuel and sea salts ingested with the intake air. Sykes and Shirley[4] confirmed that this reaction was in fact taking place, resulting in the formation of sodium sulfate, the chief cause of the attack. Several workers, however, were quick to recognize that sodium sulfate alone was not responsible for such catastrophic corrosion rates. The observations of early investigators[3, 4, 5, 6] indicated that sodium sulfate alone was innocuous and that sodium chloride was an essential ingredient of the molten slag to produce rapid corrosion rates. More recent work by General Electric[7] however, suggests that chlorides or other extraneous reducing agents are not necessary for corrosion to proceed. Other investigators[8,9] believed that carbon also catalyzed the reaction between the sodium sulfate and the metal surface. It was established that sodium chloride played a dual role in the process of sulfidation by providing the essential raw material for the production of sodium sulfate and then by fluxing with this sodium sulfate to form a eutectic salt having a low melting point.

It was then believed that this slag penetrated the protective oxide layer present on the surfaces of superalloys, bringing the molten sodium sulfate into contact with the metal surface. Some workers contended that the penetration was a result of the natural porosity of the chromium-oxide layer, particularly under reducing conditions.[10] Others[11] suggested that the atomic lattice of the oxide was permeable to chloride ions, but the most widely accepted theory was that the fused sodium sulfate/sodium chloride salt fluxed with the oxide to form a slag of low melting point. This liquid phase cannot offer any resistance to the diffusion of oxygen and sulfur ions to the surface of the metal.

During the early sixties, theories of sulfidation began to be developed. Danek[12] reported that several investigators postulated that the sulfur reacted with the chromium, the major oxidation resistant element in the superalloy, resulting in the removal of the chromium. Hence, the surface of the metal, being depleted of chromium, permits more rapid oxidation and subsequent exfoliation removal of this oxide layer. Thus, a new metal surface was exposed for further reaction with oxygen and sulfur. The oxidizing agents required to sustain this process were available from the decomposition of the sulfate slag. A slight variation to this mechanism was proposed by other workers, who suggested that the chromium sulfide also oxidized along with the chromium-depleted layer. This type of attack has also been observed by Lucas[13] under conditions of thermal cycling in sodium sulfate/sodium chloride mixtures; and in its studies of sulfidation mechanism on superalloys, General Electric[7,14] concluded that oxidation of the chromium sulfide contributed toward the catastrophic attack observed.

A theory advanced by Hancock[15] proposed that sulfur attack on nickel alloys containing 20-percent chromium proceeded by the formation of both chromium

and nickel sulfides. At temperatures above 1200°F, the nickel/nickel-sulfide eutectic became liquid, causing accelerated corrosion of the alloy. During cooling from the operating temperature, the nickel sulfide can be reduced by chromium, but this reaction is controlled by the diffusion characteristics of chromium and sulfur in the alloy.

Danek[12] also reported a fourth theory that had been developed by many workers who postulated that the low-melting-point nickel/nickel sulfide that formed initially was able to penetrate otherwise protective oxide layers, attack the matrix metal, and eventually be oxidized by the decomposition of sodium sulfate. The reaction is autocatalytic and hence very destructive. The reaction in its simplest form has been written[3]:

$$Na_2SO_4 + 3Ni \quad Na_2O + 3NiO + S \qquad (1)$$

$$3Ni + 2S \quad Ni_3S_2 \qquad (2)$$

$$Na_2SO_4 + Ni_3S_2 \quad 3NiO + Na_2O + 3S \qquad (3)$$

The "sulfur" produced in Equation (3) is then available to react with more nickel to continue the destruction of the nickel. (The reactions would proceed in the same manner with chromium, cobalt, or iron substituted for Ni in Equation (1).)

It also was evident from early investigations[16] that reducing atmospheres were more corrosive than oxidizing environments and that alternate oxidizing and reducing conditions were particularly damaging.[6] It was universally agreed that chromium had a beneficial effect on the resistance of superalloys to sulfur attack, but much confusion existed as to the status of other alloying elements. Lewis and Smith[17] concluded that aluminum and niobium were also beneficial to nickel-chromium alloys. Belgian researchers[18] proposed that aluminum improved the sulfur corrosion resistance of cobalt-base alloys. It was suggested that the reason for this improvement lies in the fact that aluminum does not form a stable sulfide and is therefore always available for oxide formation, resulting in the buildup of an aluminum-oxide-rich spinel, permitting the chromium to react with the sulfur to form an impervious barrier. More recent work[19], however, has indicated that high aluminum contents can be detrimental to sulfur corrosion resistance. Carbon[16] and molybdenum[18] were also considered to be harmful, but there is much conflicting evidence of the effects of other alloying elements. In any event, their effects are secondary to the overriding influence of chromium. Davin and Coutsouradis[18] showed that cobalt-base alloys were superior in sulfidation resistance to nickel- and iron-base alloys containing equivalent amounts of chromium. These findings have been substantiated in more recent investigations.[7,19,21,22] The superiority of cobalt-chromium alloys is attributed to the smaller molecular volume of cobalt sulfide, the slower diffusion rate of cobalt, and the relatively high melting point of the cobalt/cobalt-sulfide eutectic.

Nevertheless, other workers[8, 17] could not substantiate these findings and concluded that cobalt alloys, or cobalt additions to nickel-chromium alloys, at best only marginally improved sulfidation resistance.

More recent research efforts have been directed toward improving the hot corrosion resistance of superalloys, either by coating the alloys or by developing new alloys. The impregnation of the metal surface with aluminum or aluminum-chromium mixtures has received the most widespread attention, and now many patented processes are available for treating superalloys to extend their life in hot corrosive environments.

The most significant advances in developing alloys to resist hot corrosion have been made by adding small amounts of rare earth elements to modified compositions of cobalt-base alloys. Research at AiResearch and General Electric[23] has resulted in commercial cobalt-base alloys, containing yttrium and lanthanum, respectively, having specifically designed hot corrosion resistance up to 2000°F.

Contrary to what at first was popular belief, decreasing the sulfur concentration in the fuel did not significantly reduce the extent of hot corrosion in the presence of sea salt. Bergman[14] calculated that the sodium sulfate present in the ingested sea salts was sufficient to sustain attack even if the fuel was sulfur-free. Other workers[21, 22] have reported results of tests comparing the degree of corrosion with the fuel sulfur content. While high sulfurs did in some instances cause a slightly greater degree of attack, substantial attack was also observed with low sulfur fuels in the presence of sea salt. It was concluded that the amount of sulfur in the fuel affected neither the mode nor the intensity of attack in sea-salt environments. In recent years, only one company[24,25] has disagreed with this. From this research, it was concluded that a reduction in fuel sulfur from 0.16 to 0.02 percent resulted in a marked decrease in attack on about twelve superalloys.

Most of the earlier experiments were carried out in crucibles of molten salt mixtures in which metal samples were totally or partially immersed. Such tests were useful in establishing which salt mixtures were most harmful and in determining the temperature range of corrosive attack. While they were useful in grading classes of materials according to their corrosion resistance, they were too insensitive to predict life expectancy of engineering components. Burner rigs were developed, into which controlled amounts of salts could be added and qualitative (and often quantitative) comparisons of materials could be made. At first, copious quantities of salts were thought to be necessary, and 200 ppm injected into the burner was not uncommon. As hot corrosion mechanisms became more clearly understood, lower and lower sea-salt concentrations were used until 1 to 10 ppm became almost standard. When it was discovered that sea salt alone could cause hot corrosion and indeed was believed to be the primary causative agent in hot corrosion, it became apparent that even smaller quantities could have a significant effect; more recent experiments using 0.01 to

0.1-ppm sea-salt concentration have caused hot corrosion to occur. Haryslak and Pollini,[2] in fact, measured the sea-salt aerosol content at destroyer deck height at various wind velocities and found approximately 1 ppm at a 40-kn wind speed (see Figure 8).

Considerable effort has been made in determining the thermodynamic and kinetic reaction of the various hot corrosion models. Although a number of mechanisms have been proposed, no single system clearly defines the role of sodium chloride, delineates the conditions at which sodium sulfate will form, or explains how metal sulfides are formed in highly oxidizing atmospheres. De Crescente and Bornstein[26] showed, by thermodynamic considerations, the relationship between the condensation point of sodium sulfate, concentration of sodium chloride, and pressure. Figure 55, taken from Quigg's and Schirmer's report[27], indicates the conditions under which sodium sulfate exists as a vapor, when it is supposed to be innocuous, and the conditions that can cause it to condense and attack the metal. From this it can be seen that certain combinations of pressure and temperature can cause condensation at quite low concentrations of sodium sulfate. There was also disagreement among researchers concerning the effects of temperature on the sulfidation process. The majority have reported that the most severe attack occurs at temperatures from 1760° to 1830°F, with a decrease in the sulfidation rate above this temperature. Danek quotes several authorities who detected no sulfidation at temperatures in excess of 2000°F. The explanation for this is that slag had vaporized at this temperature, and since the liquid sodium sulfate was not in contact with the metal, corrosion proceeded by the process of oxidation only.

The rate of attack at lower temperatures, however, is not so clearly definable. Some tests[14,22] have failed to produce significant sulfidation at temperatures as high as 1500°F; yet other workers[5] have reported attack at temperatures as low as 1100°F. Steverding[28] found that fuels containing 0.4 percent sulfur did not produce significant corrosion on nickel below 950°F. Davin and Coutsouradis[20] observed no attack on nickel-chromium alloys in gaseous sulfur dioxide or hydrogen sulfide at temperatures below the nickel/nickel-sulfide eutectic temperature of 1200°F.

From all the mass of apparently contradictory observations and deductions that have been made by hundreds of workers throughout the past decade, it is difficult to present a clear picture of the precise mechanism and cure for hot corrosion. Attack is attributable to sodium sulfate, which is present to the extent of 11 percent in sea salts, sufficient, many claim, to cause corrosion. Sodium sulfate can also be formed by the reaction of the sulfur content of the fuel with sodium chloride, either ingested with the intake air or present as a fuel contaminant. Sulfidation is always more severe in reducing atmospheres, or in an environment that is alternately reducing and oxidizing (typical of a gas turbine engine). The sulfate is most aggressive at temperatures in the range from 1750° to 1850°F, and sodium chloride, while in itself innocuous, does appear to assist the

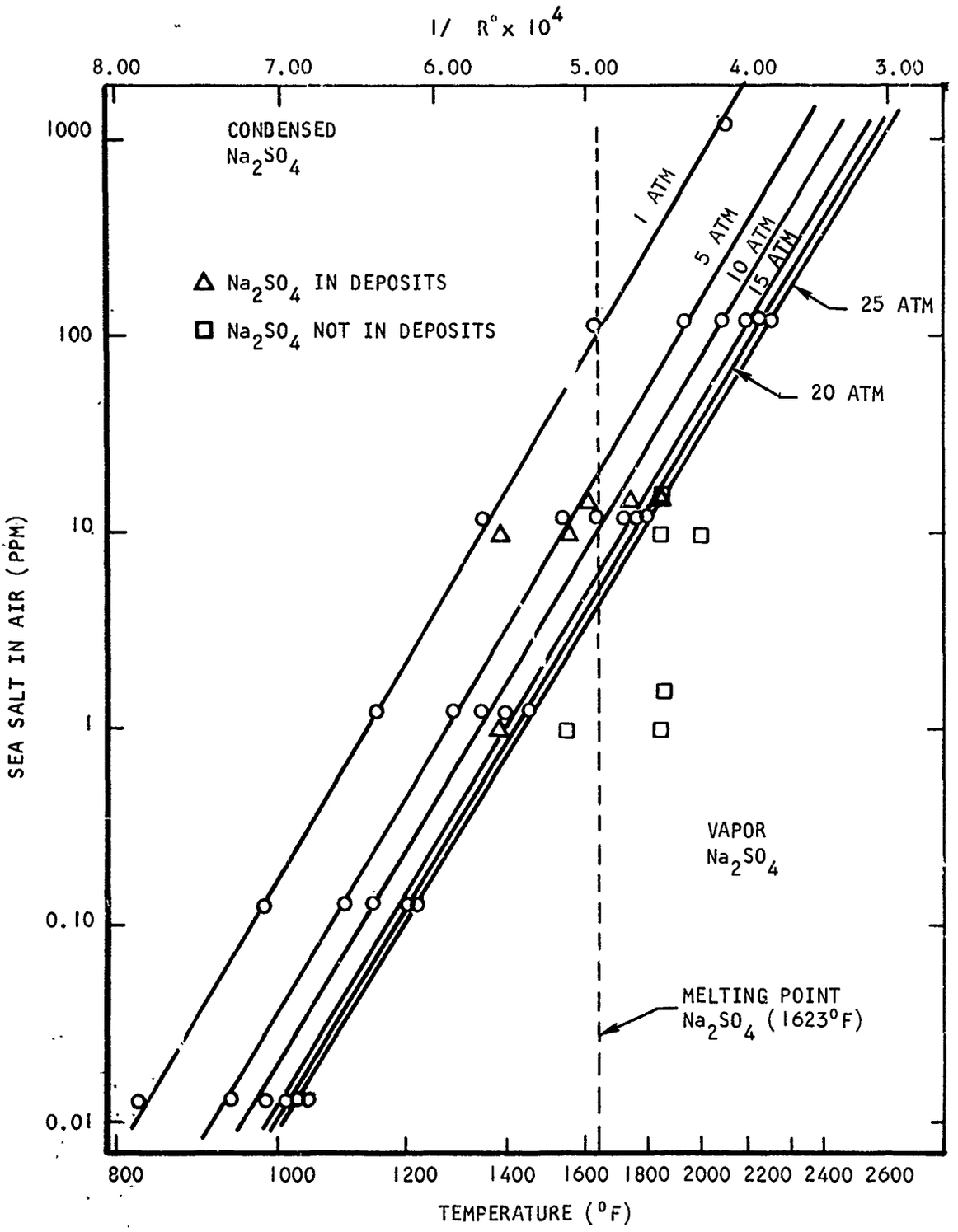

Figure 55. Phase Relationship for Sodium Sulfate.

sulfate in attack. Nickel-base alloys are most susceptible to attack, and the consensus is that cobalt-base alloys have the greatest resistance. Additions of chromium are beneficial, but there is widespread lack of agreement as to the effects of other alloying elements. The amount of sulfur in the fuel is irrelevant to the extent of hot corrosion. Even if uneconomically low (0.02 percent) fuel sulfur levels were achieved, there is no guarantee that the sea salt alone will not cause serious attack, even when present in such small amounts as 0.1 ppm. There appears to have been very little investigation in the 900° to 1500°F temperature range.

BRAZING ALLOY CHARACTERISTICS

In the manufacture of recuperators, the brazing alloy is an important item of consideration. The joints between the tubes and the header plate must have a high degree of integrity if the recuperator is to continue to operate efficiently. Some of the service conditions that the joint must withstand include static stresses imposed by pressure differentials and thermal expansion, and dynamic stresses resulting from vibration, thermal gradients, and alternating expansion and contraction. Because the recuperator operates at elevated temperatures, the joints must have adequate oxidation resistance and resistance to creep. On the other hand, the alloy must have reasonable cost and good wetting and flow characteristics when brazed at a temperature that will not harm the recuperator tubing.

The initial selection of some nine alloys was an attempt to test a wide spectrum of filler metals which could be useful at the lowest practical brazing temperature. Most combinations brazed well, except that the wetting and flow characteristics of the first lot of Inconel 625 tubing were poor. Subsequent consignments of Inconel 625 tubing, however, were brazed without the slightest problem, and first-class joints were obtained. This perhaps points out the necessity of having the metal surfaces free from contaminants and thoroughly cleaned before brazing.

The 100-hr static corrosion test was merely a qualitative test to grade the relative hot corrosion resistance of the joints. Sea-salt concentration at 10 ppm was considered adequate to produce hot corrosion in such a short time on those material combinations most susceptible to attack, yet not adequate to cause everything to corrode and make comparison impossible. As a result of this test, two of the brazing alloys were eliminated from further consideration, and indications of the lesser corrosion resistance of type 347 stainless steel were observed.

Two brazing alloys were selected for each tubing material, and the 10 combinations were quantitatively evaluated by measuring their stress-rupture values and assessing their hot corrosion resistance by metallography and electron probe analysis. Longer periods of exposure to thermal-cycling conditions were a more sensitive test than the 100-hr static exposure. The

sea-salt concentration was lowered to 5 ppm to prevent excessive corrosion. As a result of this experiment, it was found that the nickel-gold-palladium alloys were more susceptible to hot corrosion than the less expensive nickel-chromium filler metals; hence, this latter type was selected for the manufacture of the recuperator tested in the products of combustion of JP-4 fuel contaminated with sea-salt solution. Because the temperature of the header of the test recuperator was considerably lower than the maximum, nominal metal temperature of 1500°F, no hot corrosion was detected on the tube-header joints after the full 500-hr exposure. It was concluded, therefore, that the brazing alloys and conditions selected for this test (Nicrobraz 200 and Coast Metals 50B) were entirely satisfactory.

HOT CORROSION IN CYCLIC HOT CORROSION TEST

Two of the tubing materials, Inconel 625 and Hastelloy X, were not affected by hot corrosion under the conditions of the cyclic hot corrosion test. Even after prolonged exposures, only superficial oxide layers were found, except in the vicinity of the failure point, where grain boundary oxidation was observed. It is believed, however, that this condition (which was more prevalent at high stresses and high temperatures) was the typical result of stress rupture, which may not have been influenced to any great extent by the injection of sea-salt solution into the furnace retort. N-155 was also quite resistant to the corrosive atmosphere, except that it was, for some reason, susceptible to intense local oxidation, which produced warts. Microprobe analysis revealed that these outgrowths were composed principally of chromium oxide but did not suggest what might have caused the phenomenon.

Incoloy 800 was also subject to wart formation, particularly in cooler sections of the tubes. Again, microprobe analysis identified the chromium-oxide composition but revealed no element that could have triggered such catastrophic growth. This alloy suffered internal oxidation (that is, the diffusion of oxygen into the metal, producing oxides well below the surface), particularly at high temperatures and high stresses. Chromium oxide was identified at these internally oxidized sites. The oxide film on the outer surfaces of the tubes was found to consist of nickel-chromium oxide (probably a spinel) covered with an outer layer of iron oxide. Corrosion had so affected the stress-rupture properties that they were only marginally better than the reference power system design requirements.

Oxidation had proceeded at such a rapid rate on type 347 stainless steel as to render it virtually useless for applications involving sea salts at temperatures of 1500°F for times longer than a few hundred hours. Two heat numbers of this tubing were tested, and both exhibited the same catastrophic attack at 1500°F. Internal oxidation was almost entirely absent on this alloy. The corrosion took place at the surface, which oxidized rapidly to form a thick layer of oxide. Even at 1300°F, oxidation was extensive. This will reduce the reliability of tubes made from this material that are used for prolonged periods in such a corrosive environment. Very little serious

oxidation was observed at 1100°F, and the alloy will undoubtedly prove to be successful if applied to components operating in marine conditions below this temperature.

A surprising feature of the products of corrosion was that no sulfides were ever detected, but undoubtedly the sea salts were contributing to the rate of oxidation because the inside surfaces of the tubes, which were not exposed to the sea salts, were generally much less severely attacked than the outside surfaces.

STRESS-RUPTURE MEASUREMENTS

The curves of stress rupture vs log time in some cases show a fairly linear relationship; in other cases, there is a decided downward bend in the curves. These curves obviously do not reflect the pure stress rupture vs time relationship that might be approached in a rupture test conducted in an inert environment. There is good reason, therefore, for conducting such tests in an actual or simulated operating environment; stress and surface attack are synergistic effects, each accelerating the other.

Even if no stress were applied, a specimen exposed to a corrosive environment would, in time, be corroded through and incapable of sustaining any load. This point in time is shown schematically in Figure 56.

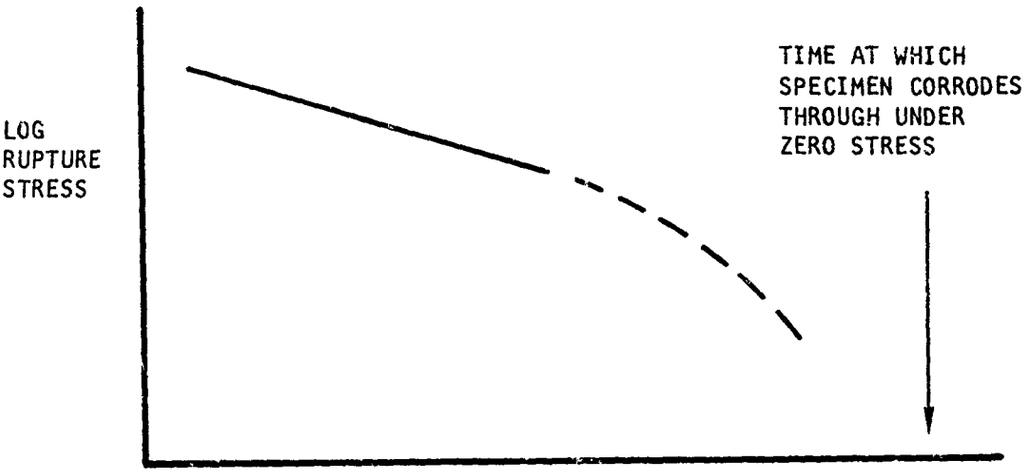

Figure 56. Phase Relationship for Sodium Sulfate.

Any extrapolation of the rupture curve shown must therefore curve downward and become asymptotic with the arrow shown in Figure 56. For this reason, no valid extrapolation can be made of the rupture curves presented in this report beyond a few hundred hours.

It might be possible to determine the zero-stress failure by simpler means than actually conducting rupture tests for longer and longer times at lower

and lower stresses. A series of specimens might be exposed under zero stress for various lengths of time and then tensile tested to determine residual strength. In this way, the zero stress failure time could be closely estimated and plotted on the existing stress-rupture curve, thereby affording a means for estimating the extrapolated shape of the curve. The validity of this technique would, of course, have to be established by actual long-term rupture testing.

In the absence of such a technique, it is erroneous to extrapolate the curves published in this report for more than a short distance, even if the plots appear to be linear. The most that can be obtained from such extrapolations is estimates of maximum possible values which, when coupled with generous safety factors, can be of definite value in feasibility studies or preliminary design studies.

HOT CORROSION RECUPERATOR TEST

Initially, 5-ppm sea salts were selected for injection into exhaust gases from the combuster so that a direct comparison could be made of the recuperator test and the cyclic hot corrosion test. After 36 hr of testing, however, numerous leaks were detected in the recuperator modules, and the test was interrupted for investigation. Preliminary visual examination showed tubes to be corroded on both the hot face (nominal maximum of 1500°F) and the cold face (nominal minimum of 900°F) of the recuperator. A thorough search was made of the possible cause of such oxidation in so short a time. Predictions made on the results of the cyclic hot corrosion test data indicated that the corrosion rate should have been negligible in so short a time. The differences between the two tests are tabulated in Table XX.

The probability that the recuperator test rig temperatures were grossly inaccurate, that salt concentrations were improper, or that unknown salts were admitted from some extraneous source was reexamined, and convincing evidence was collected to offer assurance that these factors had not contributed to the oxidation of the tubes. Significant differences between the two tests were:

1. Gas velocity
2. Salt solution flow rate
3. Vibration
4. Temperature difference between gas and metal

Previous AiResearch work indicated that corrosion rates could be increased by as much as 25 percent by increasing gas velocity. Other workers have confirmed this order by magnitude and have attributed the fact to a combined corrosion-erosion effect. Even though some evidence of this combined attack was found on a few tubes, the increased oxidation rate observed on the tubes could not be accounted for solely by this mechanism.

TABLE XX. DIFFERENCES BETWEEN THE CYCLIC HOT CORROSION TEST AND THE RECUPERATOR TEST

Condition	Cyclic Test	Recuperator Test
Gas velocity	230 ft/min	2900 ft/min
Stress	1 to 40 ksi	1 to 2 ksi
Temperature	1100° to 1500°F	900° to 1500°F
Sea salts	5 ppm	5 ppm
Salt solution flow rate	0.1 ml/min	2.7 ml/min
Gas composition	Synthetic	Products of combustion
Vibration	None	Slight
Gas temperature	Cooler	Hotter
Metal temperature	Hotter	Cooler

A major difference between the two tests was the absolute amount of sea salts admitted into the test environment. Although the concentration of contaminant in the hot gases was the same (5 ppm), because the flow rate of gases was much greater in the recuperator test, the actual influx of sea salts per unit time was correspondingly greater.

Vibration could be present in the recuperator test, induced by flame resonance, and at certain frequencies vibrational stresses could be severe. Little is known of the effects of vibration on hot corrosion rates. Examination of the failure sites and the nature of the failures, however, did not suggest that fatigue stresses had contributed to tube rupture.

The most significant difference between the two tests was the temperature difference between the gas and the metal. In the cyclic and static corrosion tests, the hot tubes were exposed to relatively cold gas; consequently, the rate of salt condensation may have been slight. In the recuperator test, however, the tubes were much cooler than the gas, and reference to de Crescente's and Bornstein's[26] thermodynamic calculations and to Schirmer's and Quigg's[21] graph, Figure 55, indicates that such conditions are conducive to sodium-sulfate condensation. Little information was available in the literature regarding sea-salt condensation, but it was postulated that if the sea salts were condensing on the tubes, and the absolute amount of sea salts injected into the recuperator was greater, then a layer of sea salts would build up on the surface of the tubes. Should the temperature of the tubes become high enough to promote and sustain the reaction, catastrophic corrosion would result.

The white deposit observed on tubes from the recuperator at this stage was identified as a sodium chloride/sodium sulfate mixture, indicating that condensation could have taken place. Microprobe analysis, however, showed that the products of corrosion contained no sulfides. To test the veracity of this hypothesis, that is, that salt condensation was responsible for the rapid corrosion, the recuperator test was restarted using new, unexposed modules in the central stations. After 36 hr of exposure with no salt ingestion whatever, the modules were again examined. No salt deposits were detected, and the corrosion was so slight that the tubes were only discolored by interference tints. This confirmed that the amount of sea salts injected during the initial testing period was the primary causative agent for premature failure of the tubes.

So that the test would not be completely aborted, the sea-salt concentration was reduced from 5 to 0.022 ppm. This latter figure, according to Figure 8, corresponded to the amount of sea-salt contamination in the air on the deck of a ship in a wind velocity of 20 knots. A further period of testing at this low level did produce some slight oxidation, but it was not severe enough to show any significant differences between the two alloys on test. Ultimately, the concentration was adjusted to 0.1 ppm (equivalent to a 30-knot windspeed), and the tests were completed at this level.

It should be noted that these salt concentrations represent values found at low altitude over the sea or in immediate coastal areas. Reference to Mason's book, The Physics of Clouds,[29] indicates that there is considerable salt concentration falloff at altitude and in inland areas. Therefore, even the 0.1-ppm salt level may represent an extreme environment.

Metallographic and microprobe analyses also were used to evaluate tubes taken from recuperator modules after various exposure times. Because of the two superimposed variables of time and sea-salt concentration, it was difficult to quantitatively assess the value of any one of them. But generally speaking, long-time exposures and high salt concentrations produced a greater degree of oxidation than short-time exposures and low-salt concentrations. The chemical composition of the oxide layers formed was identical to the corresponding samples tested on the cyclic hot corrosion rig, indicating that agreement existed between the two tests from a hot corrosion standpoint.

The disturbing feature that had been repeated in the recuperator test was the tendency of both the Incoloy 800 and the N-155 to form warts. These localized areas of extreme oxidation were almost always the sites of leaks in the recuperator tubes. How and why these warts were initiated were not studied in this program, but such defects would have a high nuisance value in service if their occurrence cannot be restricted. Internal oxidation was not observed on the materials tested in the recuperator test, but that was expected in view of the lower tube pressures applied. There was not a great deal of difference between the two tube materials tested, and the extent of corrosion was the same on thick-wall (0.005-in.), thin-wall (0.0035-in.), and dimpled tubes.

Unfortunately, AiResearch did not have the opportunity of testing the Inconel 625 tubing in the recuperator test. From the cyclic hot corrosion test results, there is every reason to be optimistic about the success of this alloy as a recuperator material. It did not appear to be affected by the hot corrosive environment; it was not prone to wart formation; and the third lot of tubing, which was free from manufacturing imperfections, was brazed with J-8100 and Nicrobraz 135 without any problems. Even though the more aggressive J-8100 completely penetrated the tube wall in some instances, this did not detract from the excellent stress-rupture properties of the alloy. From a recuperator manufacturing point of view, the alloys chief advantage lies in its low cost, which is approximately 40 percent of the equivalent cost of Hastelloy X, when equivalent tubing prices are compared.

The heat exchanger test was considered to be satisfactory for comparing candidate recuperator materials, in that the test conditions of temperature, pressure, flow rate, thermal cycling, etc., were similar to the actual operating conditions of gas turbine recuperators. The cyclic hot corrosion test was useful in providing actual stress-rupture data and in duplicating the corrosion effects. Extrapolations of such test data to times and temperatures beyond the testing parameters, however, may prove to be inaccurate, particularly for type 347 stainless steel and Incoloy 800 materials.

CONCLUSIONS

A number of conclusions were reached regarding the suitability of the tested materials for use in recuperators, hot corrosion effects, test techniques, and the applicability of the test data to recuperator design. These are discussed separately.

The conclusions of this program apply only to thin-wall materials for tubular recuperators. The same materials in plate-fin heat exchangers will display different strengths and corrosion behaviors because of coatings of brazing filler metals usually present on the base metal surfaces.

MATERIALS

1. Of the five alloys tested, only Inconel 625 and Hastelloy X were suitable for use at a metal temperature of 1500°F. Inconel 625 would probably be the more reliable and economical.

2. Incoloy 800 and N-155 suffered from wart formation (localized oxidation) to such an extent that their integrity over prolonged exposure times is questionable.

3. Type 347 stainless steel was suitable for use at metal temperatures up to 1250° - 1300°F, but as temperature increased above 1300°F, the alloy suffered increasingly extensive hot corrosion damage.

4. The nickel-chromium brazing filler metals had better hot corrosion resistance than the expensive gold-base alloys. Nickel-manganese and silver-palladium-manganese filler metals tested had very poor hot corrosion resistance.

5. Brazing filler metal selection had little influence on the stress-rupture properties of the tube samples, except that Hastelloy X brazed with J-8100 was superior to Hastelloy X brazed with Palniro 1.

HOT CORROSION EFFECTS

1. Environmental attack was greatly accelerated by the introduction of sea salts into the combustor exhaust, showing that hot corrosion is definitely possible at metal temperatures of 1100° to 1500°F.

2. Sea-salt concentration had a strong effect on corrosion rate in the recuperator test but not in the static tests. This was probably due to salt condensation in the recuperator test, where the metal temperature was substantially below the gas temperature.

3. Although the formation of sulfides is generally associated with hot corrosion mechanisms, no sulfur compounds were detected in any of the corroded samples.

TEST TECHNIQUES

1. The cyclic hot corrosion test is useful in providing actual stress-rupture data and in duplicating the corrosion effects experienced in a recuperator.

2. The recuperator test is satisfactory for comparing candidate recuperator materials, in that the test conditions of temperature, pressure, flow rate, thermal cycling, etc., are similar to the actual operating conditions of gas turbine recuperators.

3. Neither of the two tests employed, by itself, gives sufficient information to completely characterize the suitability of a material for use in a recuperator. Although many similarities were noted, differences in order of ranking of materials resulted. Both tests should be used.

APPLICATION OF TEST DATA TO DESIGN

1. Extrapolations of stress-rupture data much beyond the testing parameters of time and temperature are not advisable. This is particularly true for type 347 stainless steel and Incoloy 800. The combined effects of corrosion and stress cause the rupture curves to curve downwardly, and straight-line extrapolations will be inaccurate.

2. Extrapolations should be used only to define maximum upper limitations. Coupled with generous safety factors to allow for corrosion effects, the information can be used for first approximations in the design of recuperators, or for feasibility studies.

APPENDIX I

EVALUATION OF BRAZED TUBE-HEADER JOINTS

Tube-header joints were brazed with each of the five selected materials and the four selected braze alloys. After brazing, the 1-in.-long samples were sectioned longitudinally and prepared for metallographical evaluation. The results of this examination are presented in the main body of the report. Figures 57 through 76, presented in this appendix, illustrate the microstructures of the various tube material brazing alloy combinations after brazing at the three predetermined brazing temperatures for 10 min each.

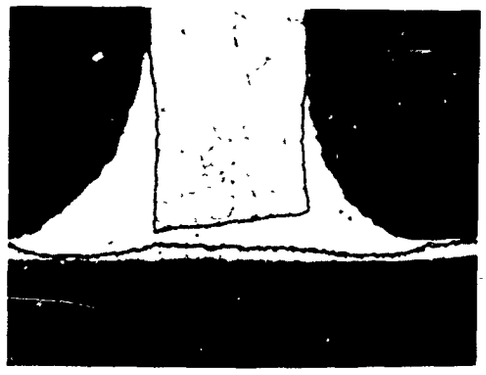

MAG = X50

a. 2200°F BRAZING TEMPERATURE.

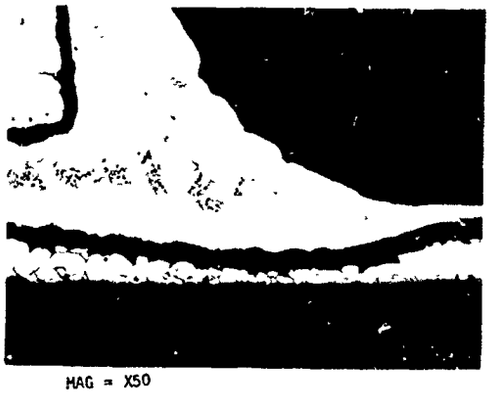

MAG = X50

b. 2200°F BRAZING TEMPERATURE.

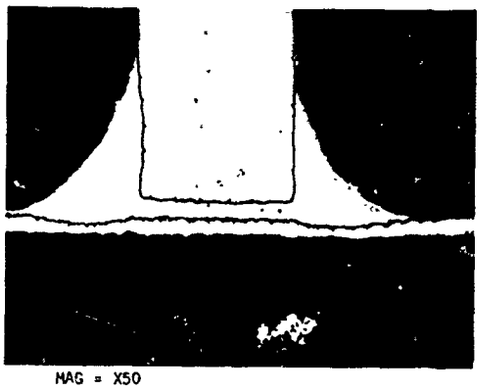

MAG = X50

c. 2175°F BRAZING TEMPERATURE.

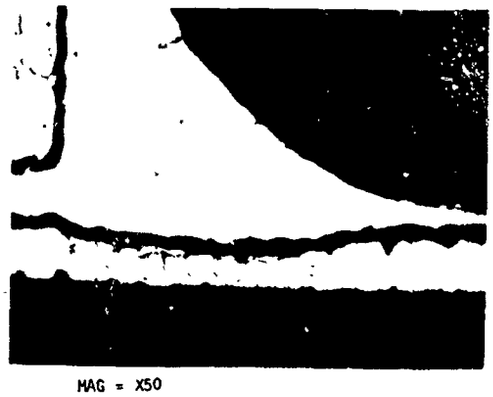

MAG = X50

d. 2175°F BRAZING TEMPERATURE.

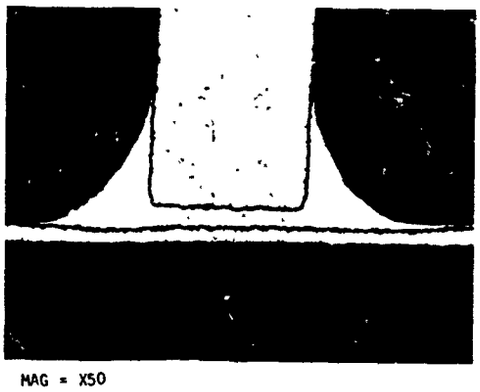

MAG = X50

e. 2150°F BRAZING TEMPERATURE.

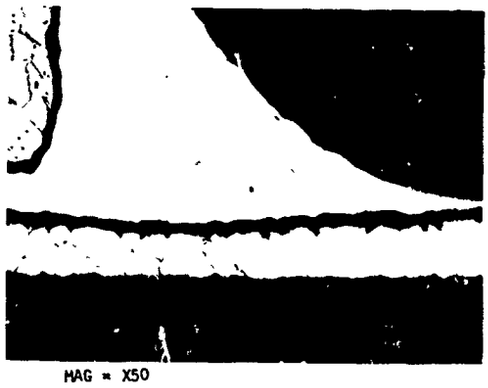

MAG = X50

f. 2150°F BRAZING TEMPERATURE.

NOTE: PHOTOS HAVE BEEN REDUCED TO 62%.

Figure 57. Photomicrographs of Hastelloy X Tube-Header Joints Brazed With Palniro 4 Brazing Alloy, in Vacuum, With a 10-Min Hold Time at Temperature. Etched With Kalling's Reagent.

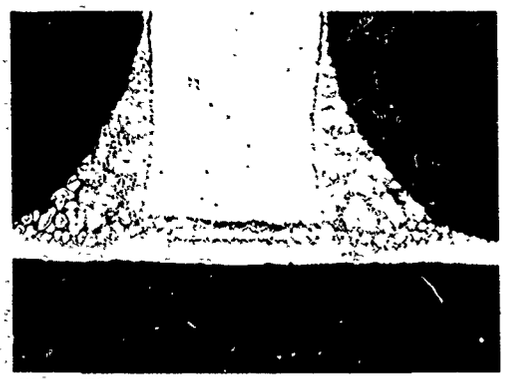

MAG = X50

a. 2175°F BRAZING TEMPERATURE.

MAG = X150

b. 2175°F BRAZING TEMPERATURE.

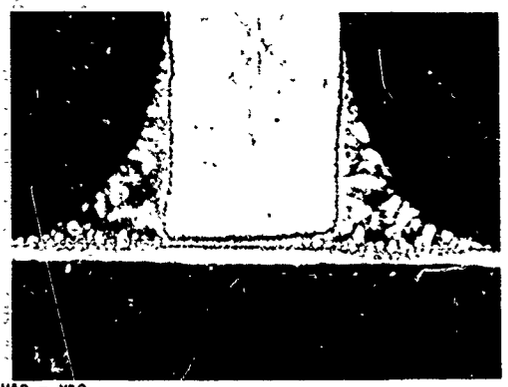

MAG = X50

c. 2150°F BRAZING TEMPERATURE.

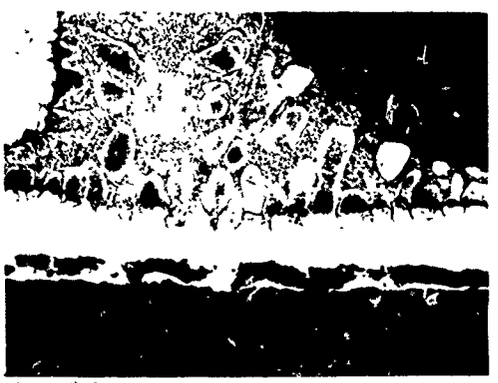

MAG = X150

d. 2150°F BRAZING TEMPERATURE.

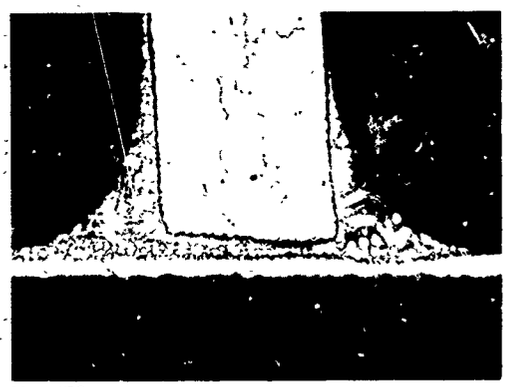

MAG = X50

e. 2125°F BRAZING TEMPERATURE.

MAG = X150

f. 2125°F BRAZING TEMPERATURE.

NOTE: PHOTOS HAVE BEEN REDUCED TO 65%.

Figure 58. Photomicrographs of Hastelloy X Tube-Header Joints Brazed With J-8100 Brazing Alloy, in Vacuum, With a 10-Min Hold Time at Temperature. Etched With Kalling's Reagent.

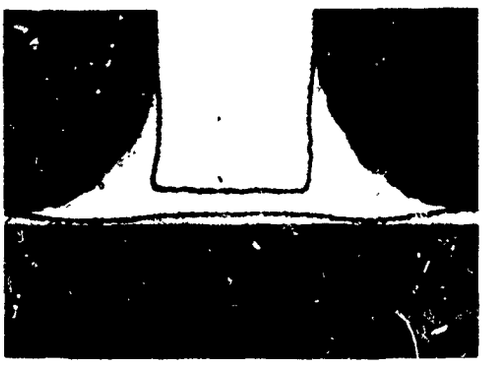

MAG = X50

a. 2100°F BRAZING TEMPERATURE.

MAG = X150

b. 2100°F BRAZING TEMPERATURE.

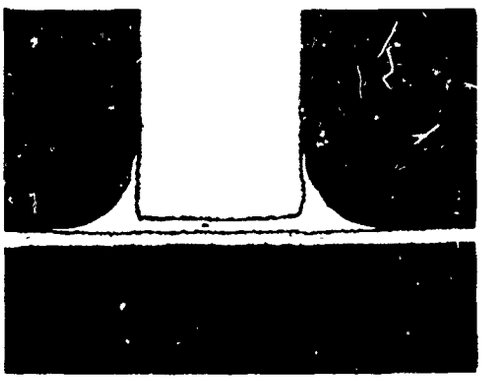

MAG = X50

c. 2075°F BRAZING TEMPERATURE.

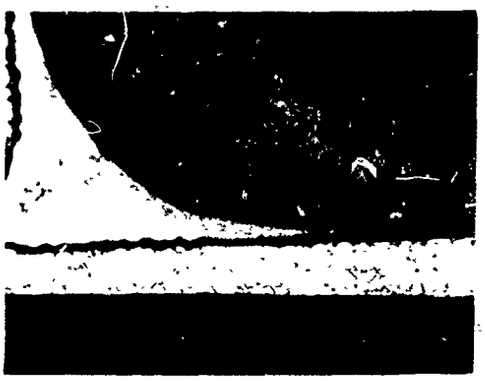

MAG = X150

d. 2075°F BRAZING TEMPERATURE.

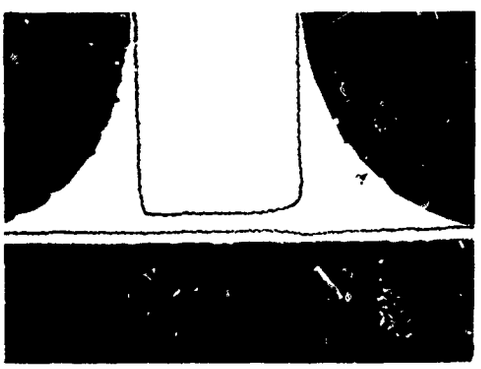

MAG = X50

e. 2050°F BRAZING TEMPERATURE.

MAG = X150

f. 2050°F BRAZING TEMPERATURE.

NOTE: PHOTOS HAVE BEEN REDUCED TO 65%.

Figure 59. Photomicrographs of Hastelloy X Tube-Header Joints Brazed With Palniro I Brazing Alloy, in Vacuum, With a 10-Min Hold Time at Temperature. Etched With Kalling's Reagent.

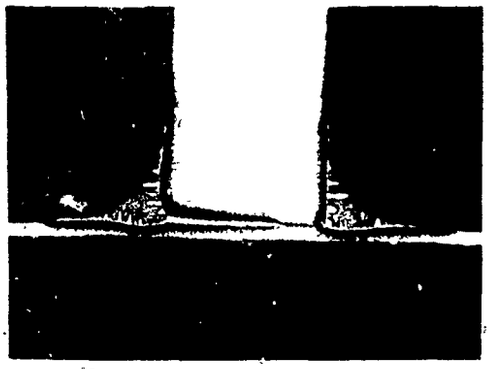

MAG = X50

a. 2025°F BRAZING TEMPERATURE.

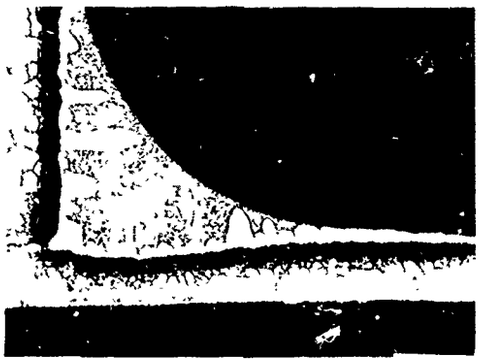

MAG = X150

b. 2025°F BRAZING TEMPERATURE.

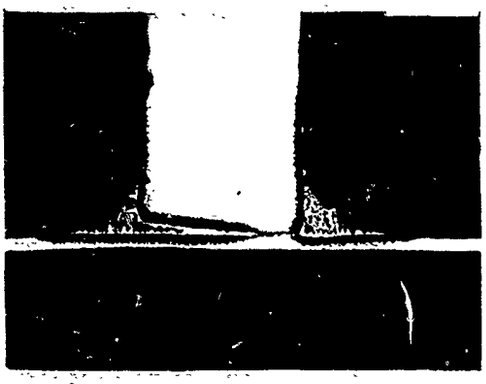

MAG = X50

c. 2000°F BRAZING TEMPERATURE.

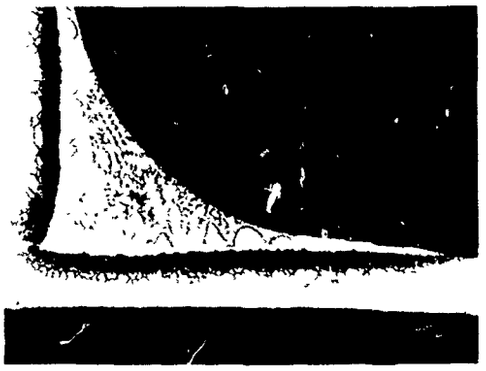

MAG = X150

d. 2000°F BRAZING TEMPERATURE.

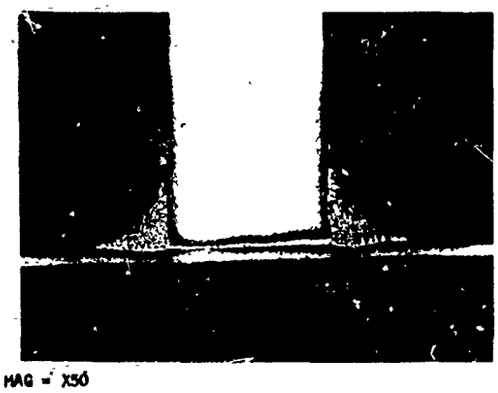

MAG = X50

e. 1975°F BRAZING TEMPERATURE.

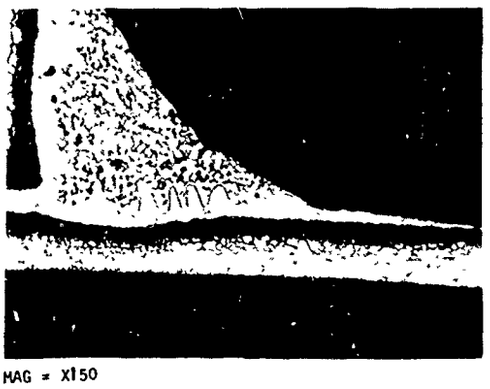

MAG = X150

f. 1975°F BRAZING TEMPERATURE.

NOTE: PHOTOS HAVE BEEN REDUCED TO 63%.

Figure 60. Photomicrographs of Hastelloy X Tube-Header Joints Brazed With Nicrobraz 135 Brazing Alloy, in Vacuum, With a 10-min Hold Time at Temperature. Etched With Kalling's Reagent.

MAG = X50

a. 2175°F BRAZING TEMPERATURE.

MAG = X50

b. 2150°F BRAZING TEMPERATURE.

MAG = X50

c. 2125°F BRAZING TEMPERATURE.

NOTE: PHOTOS HAVE BEEN REDUCED TO 74%.

Figure 61. Photomicrographs of Inconel 625 Tube-Header Joints Brazed With J-8100 Brazing Alloy, in Vacuum, With a 10-Min Hold Time at Temperature. Etched With Kalling's Reagent.

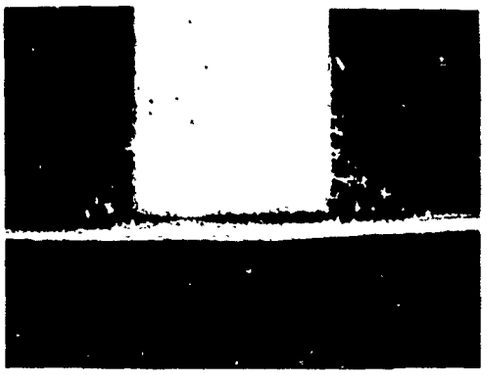

MAG = X50

a. 2125°F BRAZING TEMPERATURE.

MAG = X150

b. 2125°F BRAZING TEMPERATURE.

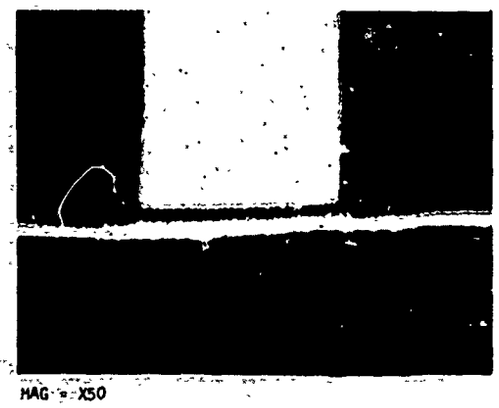

MAG = X50

c. 2100°F BRAZING TEMPERATURE.

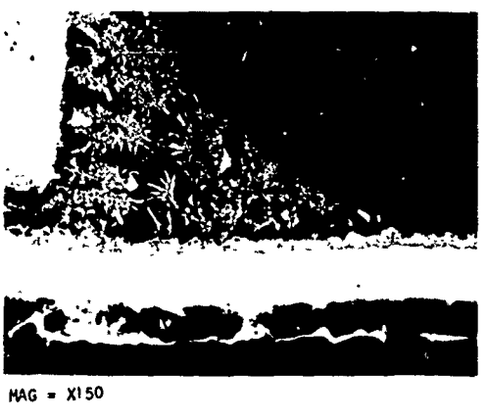

MAG = X150

d. 2100°F BRAZING TEMPERATURE.

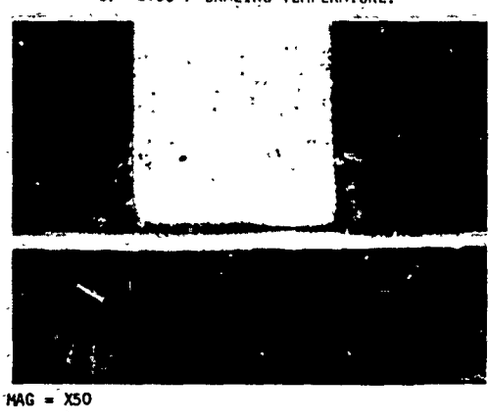

MAG = X50

e. 2075°F BRAZING TEMPERATURE.

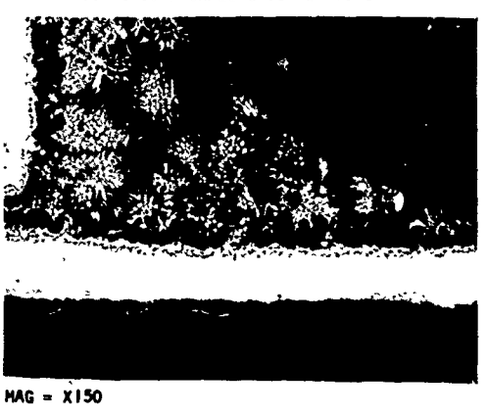

MAG = X150

f. 2075°F BRAZING TEMPERATURE.

NOTE: PHOTOS HAVE BEEN REDUCED TO 62%.

Figure 62. Photomicrographs of Inconel 625 Tube-Header Joints Brazed With Engelhard 135 Brazing Alloy, in Hydrogen, With a 10-Min Hold Time at Temperature. Etched With Kalling's Reagent.

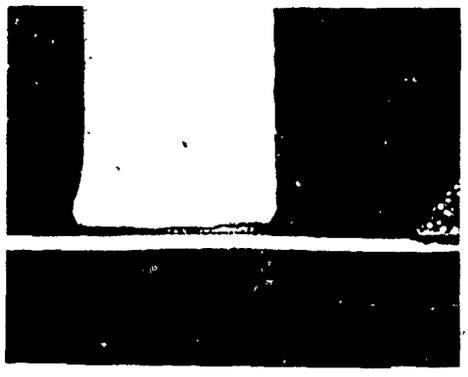

MAG = X50

a. 2025°F BRAZING TEMPERATURE.

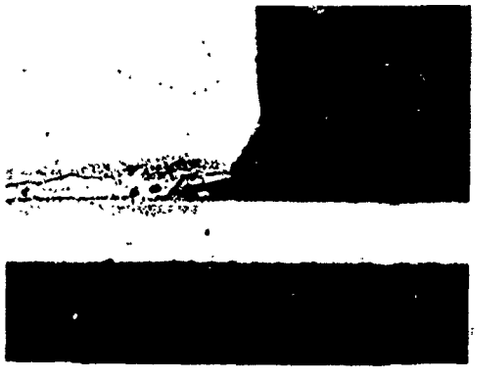

MAG = X150

b. 2025°F BRAZING TEMPERATURE.

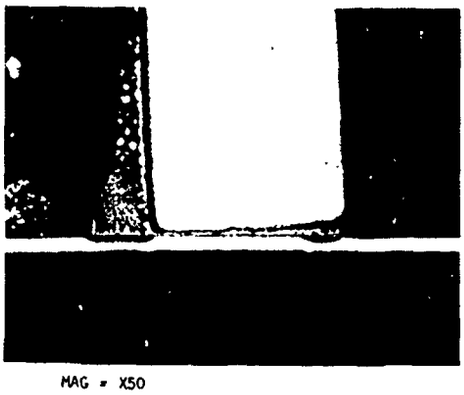

MAG = X50

c. 2000°F BRAZING TEMPERATURE.

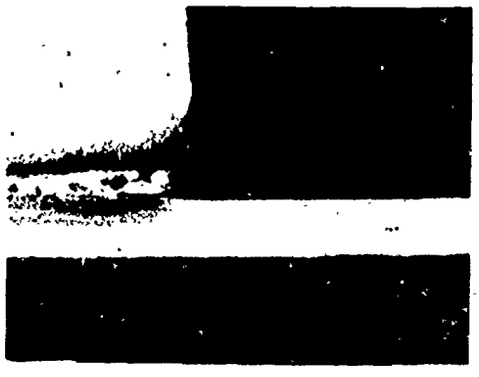

MAG = X150

d. 2000°F BRAZING TEMPERATURE.

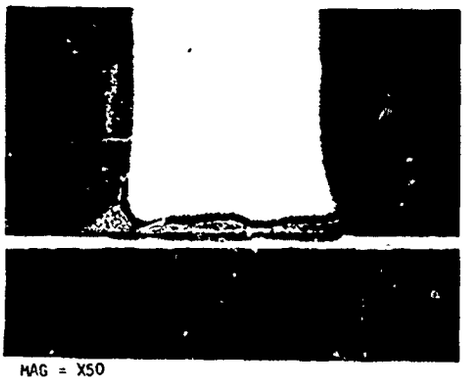

MAG = X50

e. 1975°F BRAZING TEMPERATURE.

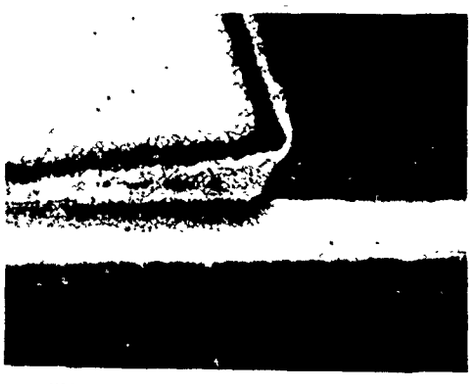

MAG = X150

f. 1975°F BRAZING TEMPERATURE.

NOTE: PHOTOS HAVE BEEN REDUCED TO 61%.

Figure 63. Photomicrographs of Inconel 625 Tube-Header Joints Brazed With Nicrobraz 135 Brazing Alloy, in Vacuum, With a 10-Min Hold Time at Temperature. Etched With Kalling's Reagent.

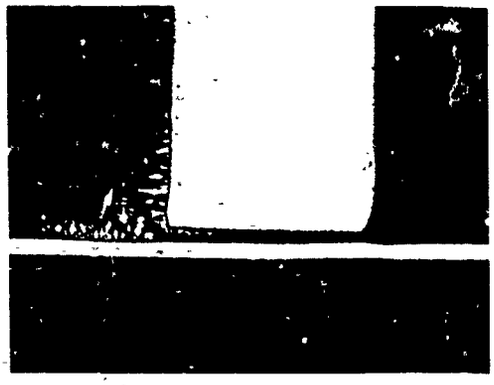

MAG = X50

a. 1975°F BRAZING TEMPERATURE.

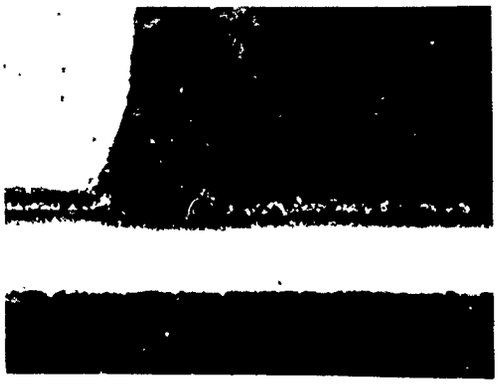

MAG = X150

b. 1975°F BRAZING TEMPERATURE.

MAG = X50

c. 1950°F BRAZING TEMPERATURE.

MAG = X150

d. 1950°F BRAZING TEMPERATURE.

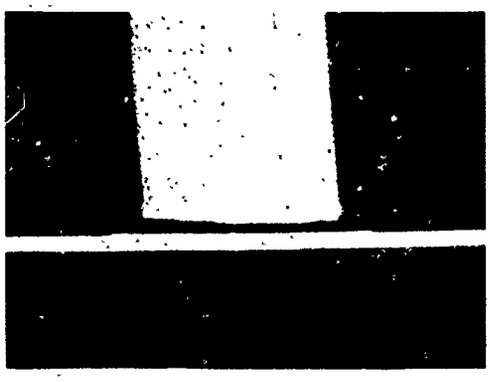

MAG = X50

e. 1925°F BRAZING TEMPERATURE.

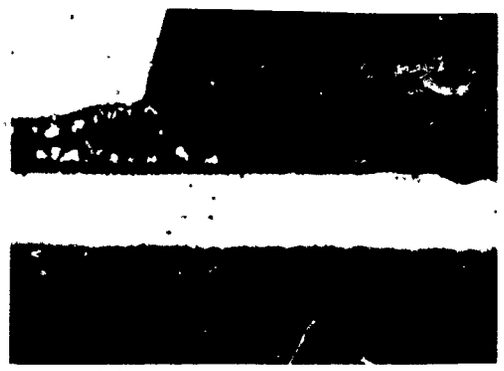

MAG = X150

f. 1925°F BRAZING TEMPERATURE.

NOTE: PHOTOS HAVE BEEN REDUCED TO 63%.

Figure 64. Photomicrographs of Inconel 625 Tube-Header Joints Brazed With Nicrobraz 65 Brazing Alloy, in Hydrogen, With a 10-Min Hold Time at Temperature. Etched With Kalling's Reagent.

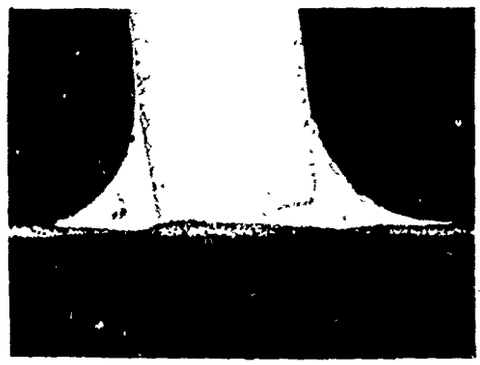

MAG = X50

a. 2025°F BRAZING TEMPERATURE.

MAG = X150

b. 2025°F BRAZING TEMPERATURE.

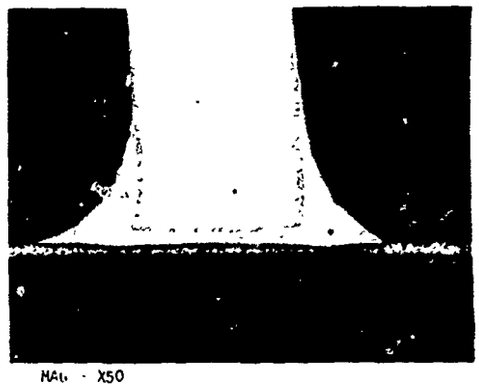

MAG = X50

c. 2000°F BRAZING TEMPERATURE.

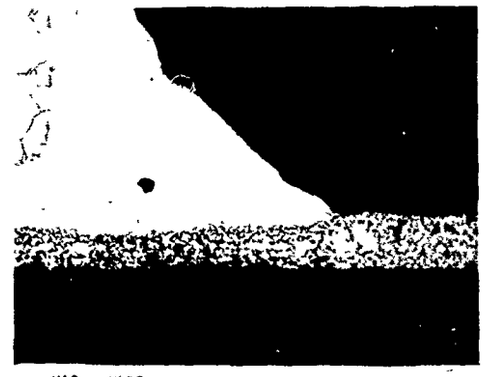

MAG = X150

d. 2000°F BRAZING TEMPERATURE.

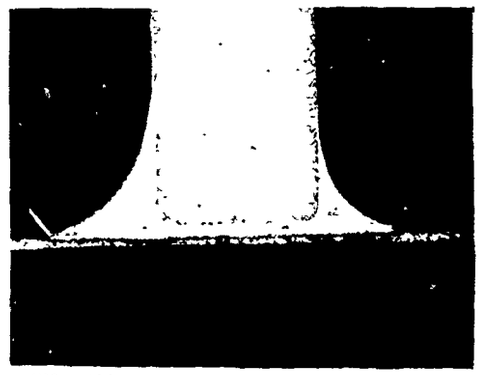

MAG = X50

e. 1975°F BRAZING TEMPERATURE.

MAG = X150

f. 1975°F BRAZING TEMPERATURE.

NOTE: PHOTOS HAVE BEEN REDUCED TO 61%.

Figure 65. Photomicrographs of Incoloy 800 Tube-Header Joints Brazed With Nicrobraz 135 Brazing Alloy, in Vacuum, With a 10-Min Hold Time at Temperature. Etched With Kalling's Reagent.

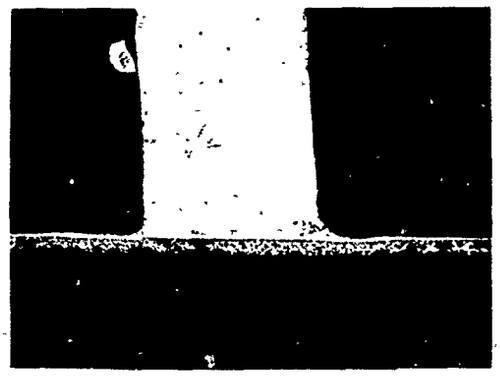

MAG = X50

a. 1975°F BRAZING TEMPERATURE

MAG = X150

b. 1975°F BRAZING TEMPERATURE

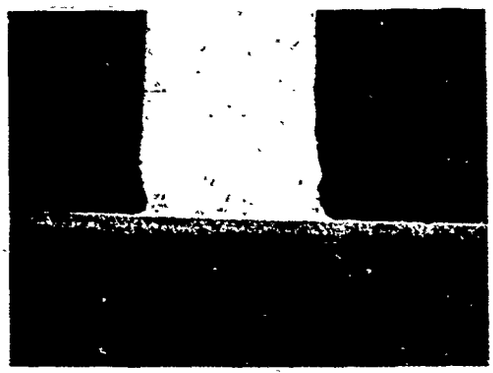

MAG = X50

c. 1950°F BRAZING TEMPERATURE

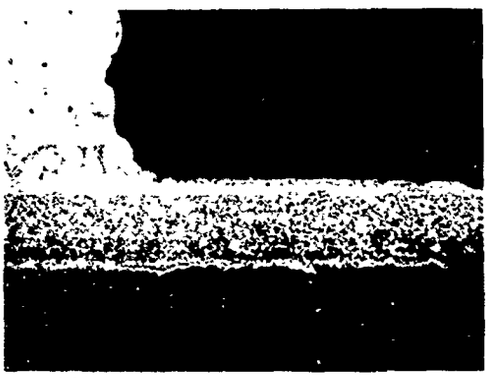

MAG = X150

d. 1950°F BRAZING TEMPERATURE

MAG = X50

e. 1925°F BRAZING TEMPERATURE

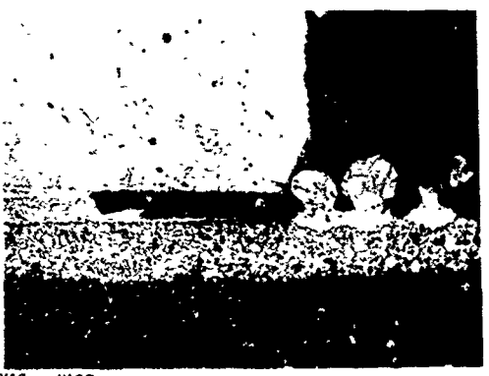

MAG = X150

f. 1925°F BRAZING TEMPERATURE

NOTE: PHOTOS HAVE BEEN REDUCED TO 63%.

Figure 66. Photomicrographs of Incoloy 800 Tube-Header Joints Brazed With Nicrobraz 65 Brazing Alloy, in Hydrogen, With a 10-Min Hold Time at Temperature. Etched With Kalling's Reagent.

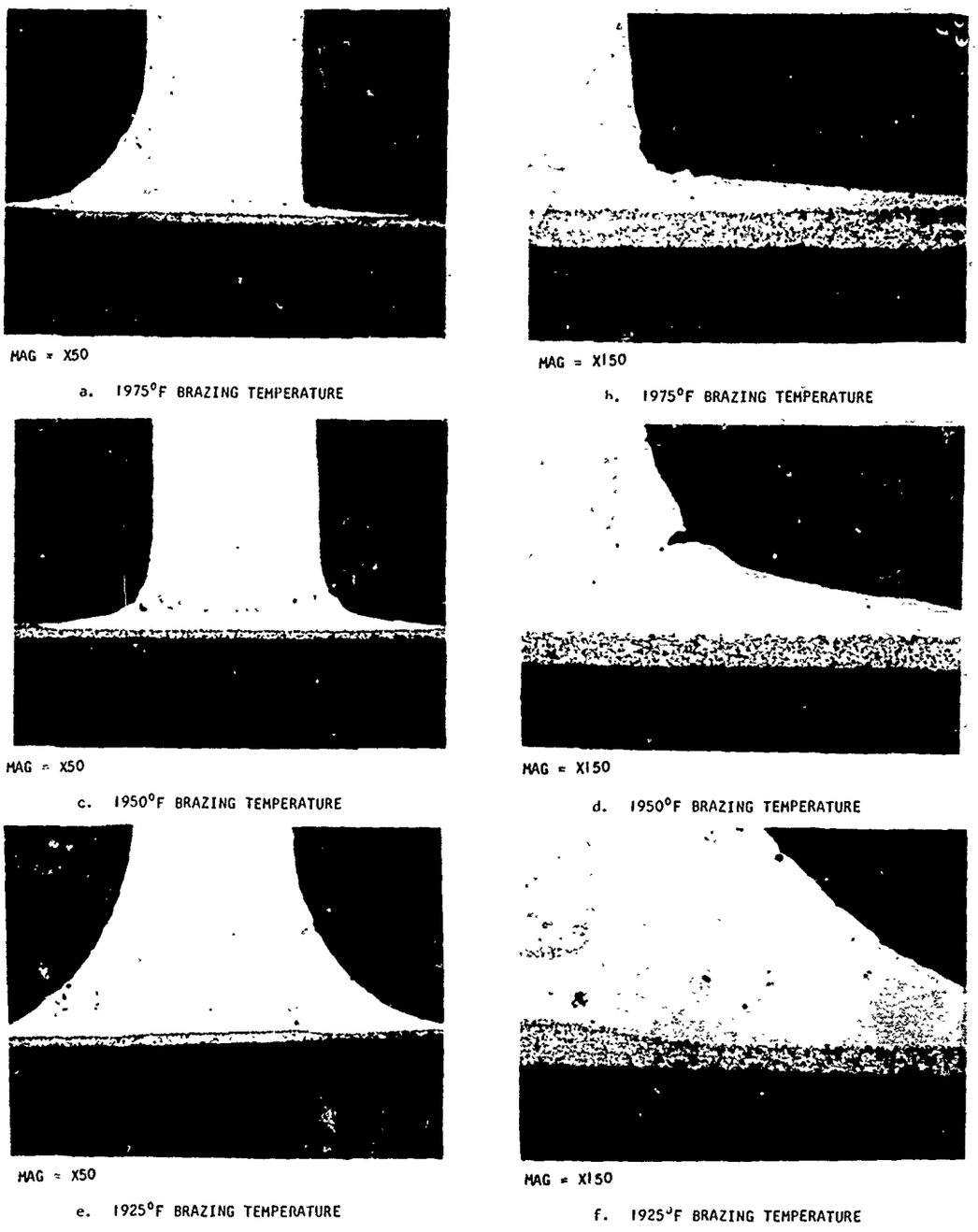

MAG = X50

a. 1975°F BRAZING TEMPERATURE

MAG = X150

b. 1975°F BRAZING TEMPERATURE

MAG = X50

c. 1950°F BRAZING TEMPERATURE

MAG = X150

d. 1950°F BRAZING TEMPERATURE

MAG = X50

e. 1925°F BRAZING TEMPERATURE

MAG = X150

f. 1925°F BRAZING TEMPERATURE

NOTE: PHOTOS HAVE BEEN REDUCED TO 61%.

Figure 67. Photomicrographs of Incoloy 800 Tube-Header Joints Brazed With Palniro 7 Brazing Alloy, in Vacuum, With a 10-Min Hold Time at Temperature. Etched With Kalling's Reagent.

MAG = X50

a. 2075°F BRAZING TEMPERATURE.

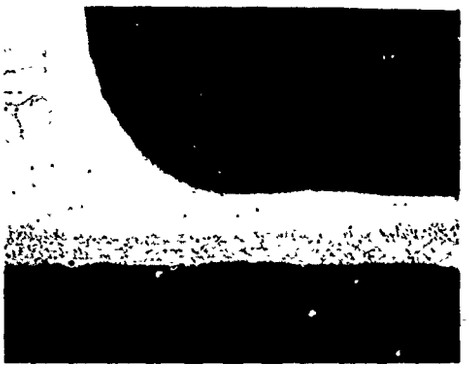

MAG = X150

b. 2075°F BRAZING TEMPERATURE.

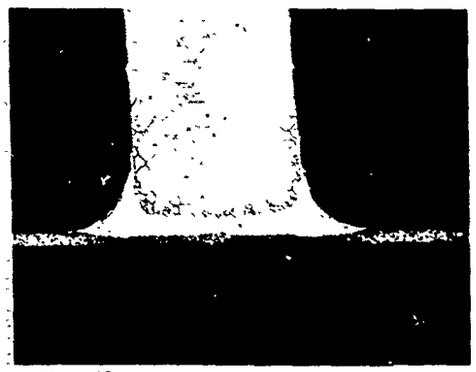

MAG = X50

c. 2050°F BRAZING TEMPERATURE.

MAG = X150

d. 2050°F BRAZING TEMPERATURE.

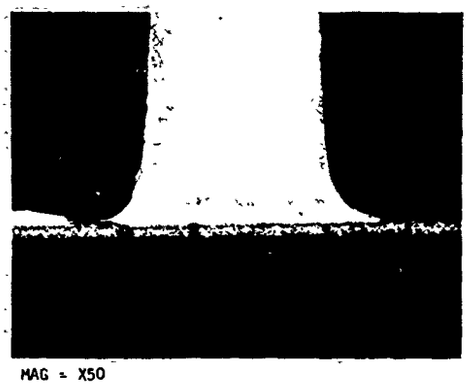

MAG = X50

e. 2025°F BRAZING TEMPERATURE.

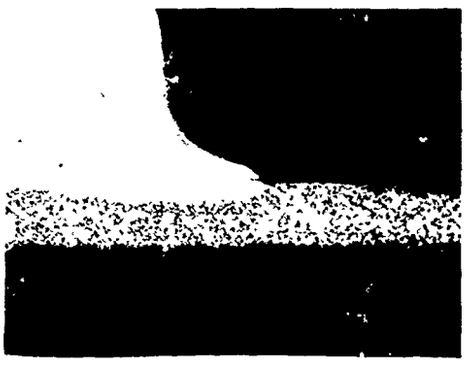

MAG = X150

f. 2025°F BRAZING TEMPERATURE.

NOTE: PHOTOS HAVE BEEN REDUCED TO 61%.

Figure 68. Photomicrographs of Incoloy 800 Tube-Header Joints Brazed With Coast Metals 50B Brazing Alloy, in Vacuum, With a 10-Min Hold Time at Temperature. Etched With Kalling's Reagent.

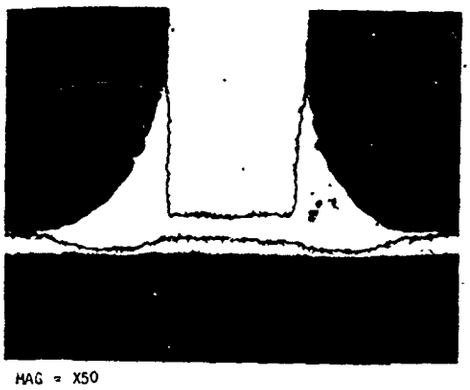

MAG = X50

a. 2200°F BRAZING TEMPERATURE.

MAG = X150

b. 2200°F BRAZING TEMPERATURE.

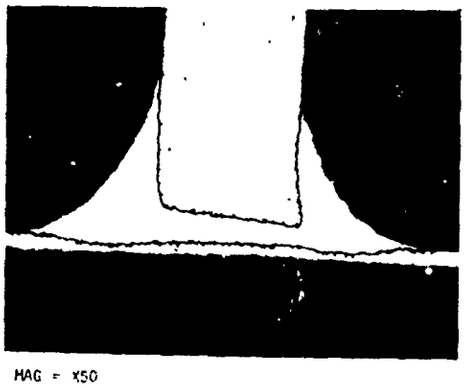

MAG = X50

c. 2175°F BRAZING TEMPERATURE.

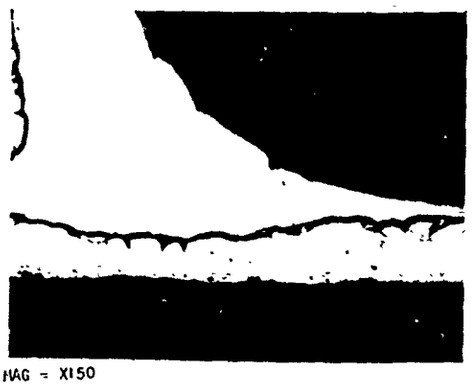

MAG = X150

d. 2175°F BRAZING TEMPERATURF.

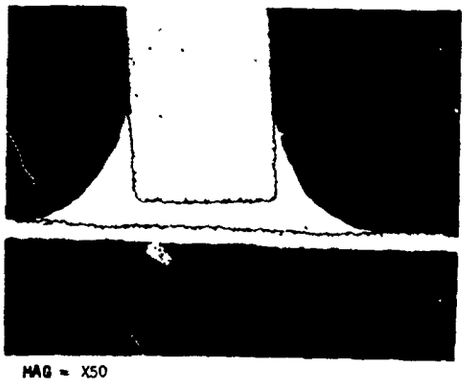

MAG = X50

e. 2150°F BRAZING TEMPERATURE.

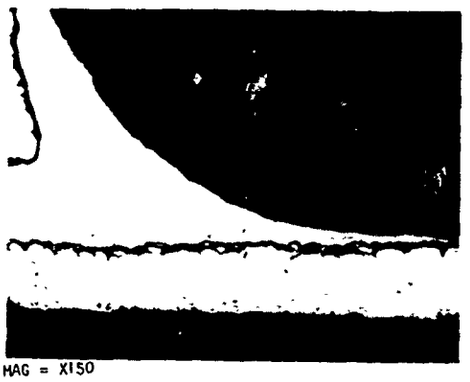

MAG = X150

f. 2150°F BRAZING TEMPERATURE.

NOTE: PHOTOS HAVE BEEN REDUCED TO 61%.

Figure 69. Photomicrographs of Multimet N-155 Tube-Header Joints Brazed With Palniro 4 Brazing Alloy, in Vacuum, With a 10-Min Hold Time at Temperature. Etched With Kalling's Reagent.

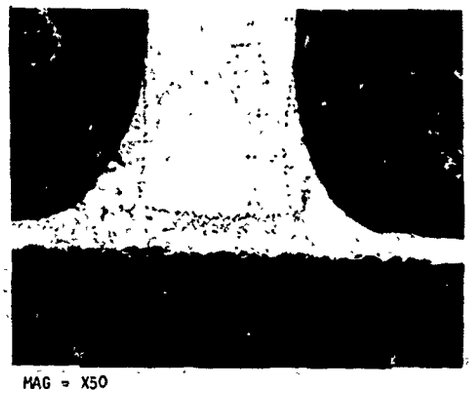

MAG = X50

a. 2175°F BRAZING TEMPERATURE.

MAG = X150

b. 2175°F BRAZING TEMPERATURE.

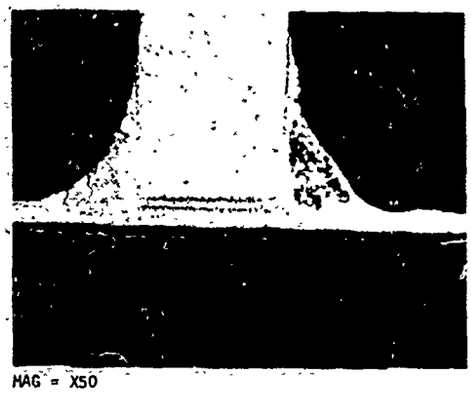

MAG = X50

c. 2150°F BRAZING TEMPERATURE.

MAG = X150

d. 2150°F BRAZING TEMPERATURE.

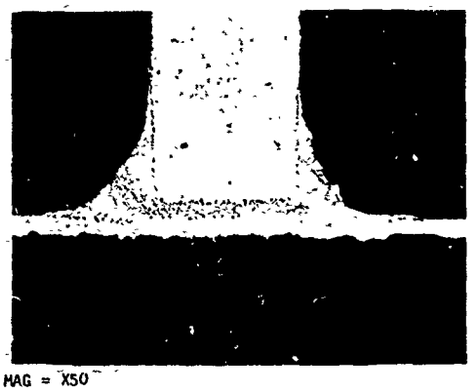

MAG = X50

e. 2125°F BRAZING TEMPERATURE.

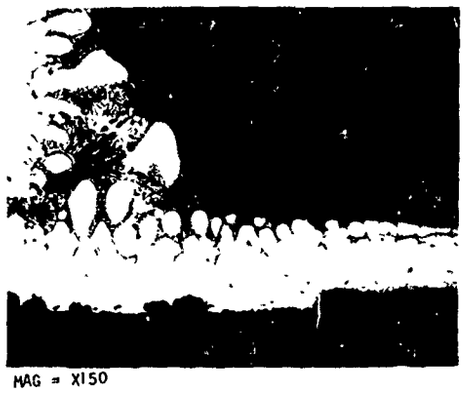

MAG = X150

f. 2125°F BRAZING TEMPERATURE.

NOTE: PHOTOS HAVE BEEN REDUCED TO 61%.

Figure 70. Photomicrographs of Multimet N-155 Tube-Header Joints Brazed With J-8100 Brazing Alloy, in Vacuum, With a 10-Min Hold Time at Temperature. Etched With Kalling's Reagent.

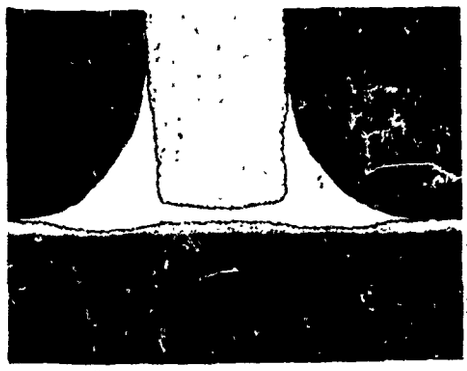

MAG = X50

a. 2100°F BRAZING TEMPERATURE.

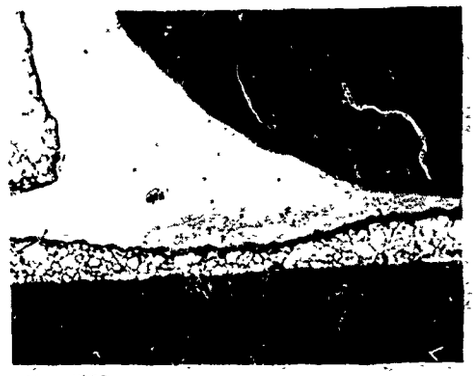

MAG = X150

b. 2100°F BRAZING TEMPERATURE.

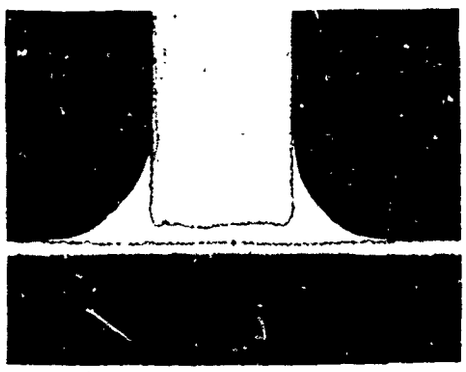

MAG = X50

c. 2075°F BRAZING TEMPERATURE.

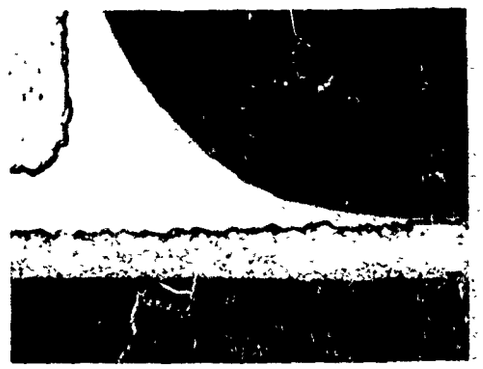

MAG = X150

d. 2075°F BRAZING TEMPERATURE.

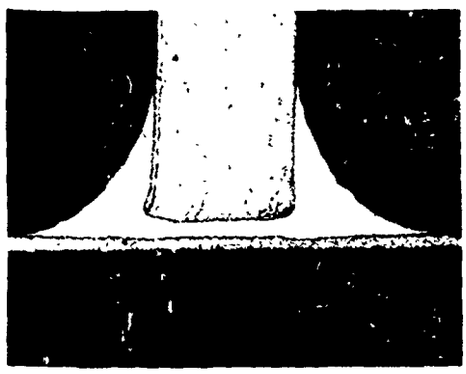

MAG = X50

e. 2025°F BRAZING TEMPERATURE.

MAG = X150

f. 2025°F BRAZING TEMPERATURE.

NOTE: PHOTOS HAVE BEEN REDUCED TO 61%.

Figure 71. Photomicrographs of Multimet N-155 Tube-Header Joints Brazed With Palniro I Brazing Alloy, in Vacuum, With a 10-Min Hold Time at Temperature. Etched With Kalling's Reagent.

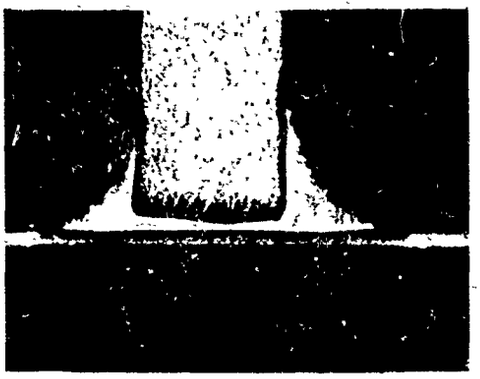

MAG = X50

a. 1975°F BRAZING TEMPERATURE.

MAG = X150

b. 1975°F BRAZING TEMPERATURE.

MAG = X50

c. 1950°F BRAZING TEMPERATURE.

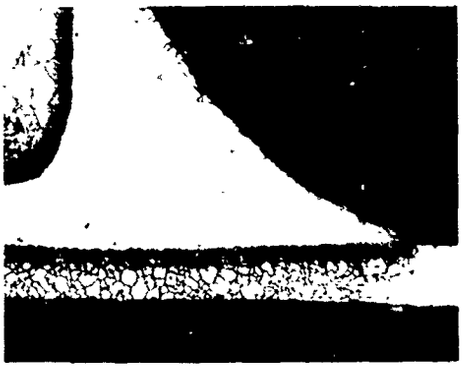

MAG = X150

d. 1950°F BRAZING TEMPERATURE.

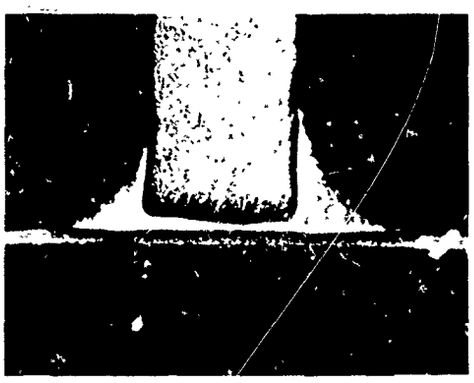

MAG = X50

e. 1925°F BRAZING TEMPERATURE.

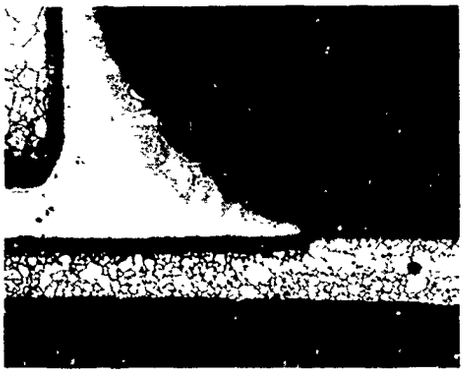

MAG = X150

f. 1925°F BRAZING TEMPERATURE.

NOTE: PHOTOS HAVE BEEN REDUCED TO 61%.

Figure 72. Photomicrographs of Multimet N-155 Tube-Header Joints Brazed With Nicrobraz 200 Brazing Alloy, in Vacuum, With a 10-Min Hold Time at Temperature. Etched With Kalling's Reagent.

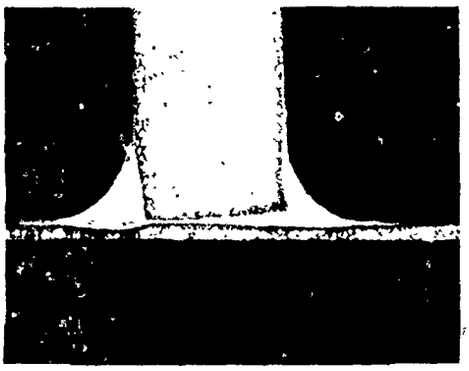

MAG = X50

a. 2025°F BRAZING TEMPERATURE.

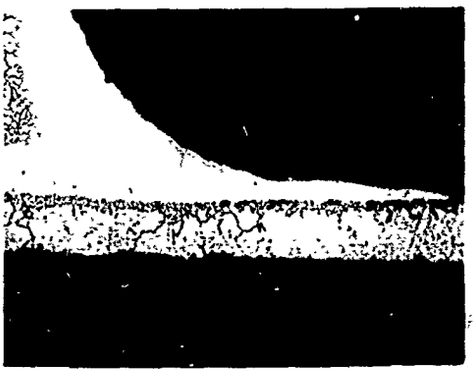

MAG = X150

b. 2025°F BRAZING TEMPERATURE.

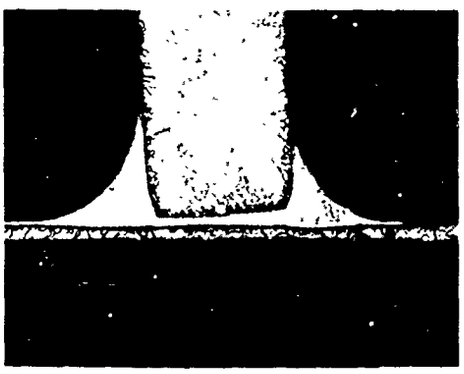

MAG = X50

c. 2000°F BRAZING TEMPERATURE.

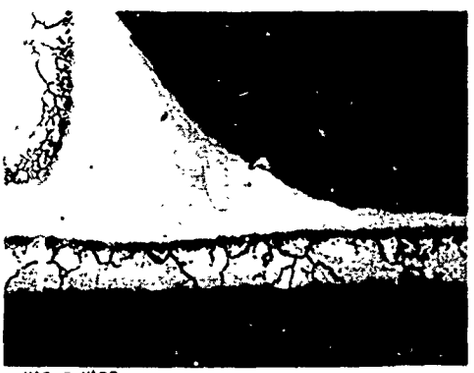

MAG = X150

d. 2000°F BRAZING TEMPERATURE.

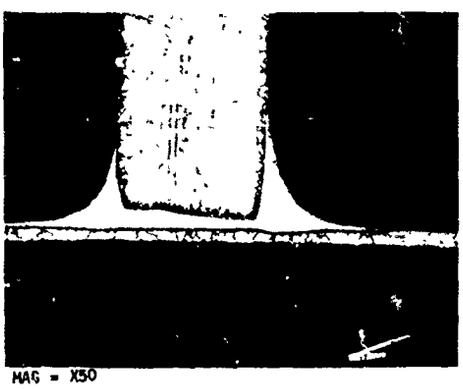

MAG = X50

e. 1975°F BRAZING TEMPERATURE.

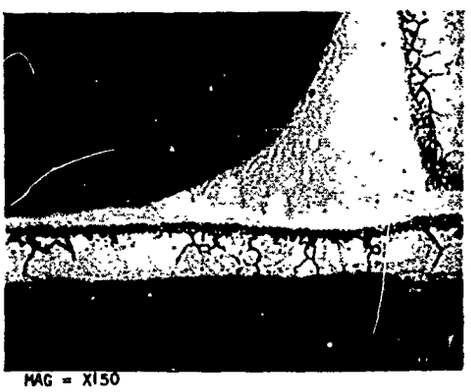

MAG = X150

f. 1975°F BRAZING TEMPERATURE.

NOTE: PHOTOS HAVE BEEN REDUCED TO 61%.

Figure 73. Photomicrographs of Type 347 Stainless Steel Tube-Header Joints Brazed With Nicrobraz 135 Brazing Alloy, in Vacuum, With a 10-Min Hold Time at Temperature. Etched With Kalling's Reagent.

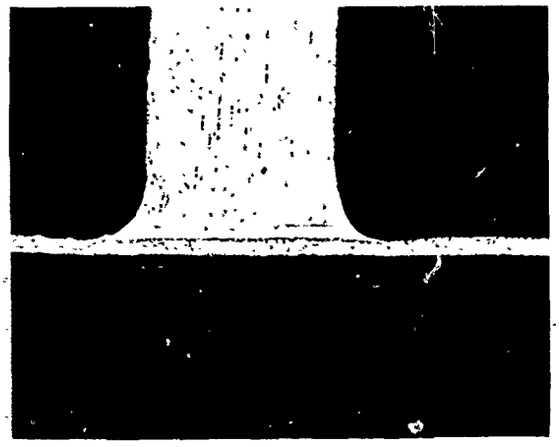

MAG = X50

a. 1975°F BRAZING TEMPERATURE.

MAG = X150

b. 1975°F BRAZING TEMPERATURE.

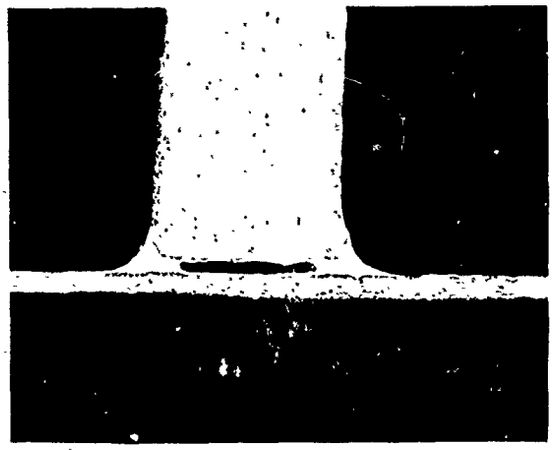

MAG = X50

c. 1950°F BRAZING TEMPERATURE.

MAG = X150

d. 1950°F BRAZING TEMPERATURE.

NOTE: PHOTOS HAVE BEEN REDUCED TO 74%.

Figure 74. Photomicrographs of Type 347 Stainless Steel Tube-Header Joints Brazed With Nicrobraz 65 Brazing Alloy, in Hydrogen, With a 10-Min Hold Time at Temperature. Etched With Kalling's Reagent.

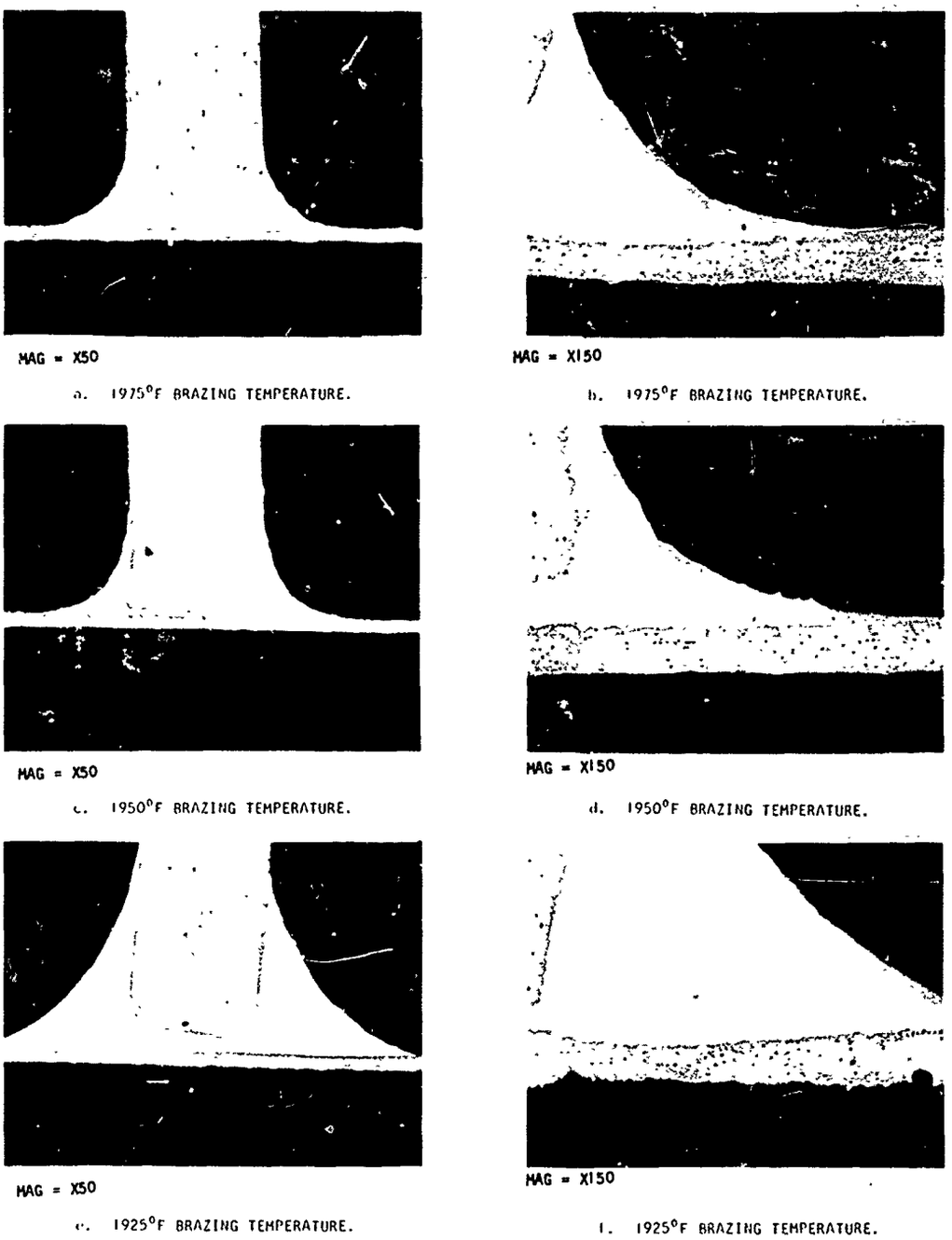

MAG = X50

a. 1975°F BRAZING TEMPERATURE.

MAG = X150

b. 1975°F BRAZING TEMPERATURE.

MAG = X50

c. 1950°F BRAZING TEMPERATURE.

MAG = X150

d. 1950°F BRAZING TEMPERATURE.

MAG = X50

e. 1925°F BRAZING TEMPERATURE.

MAG = X150

f. 1925°F BRAZING TEMPERATURE.

NOTE: PHOTOS HAVE BEEN REDUCED TO 59%.

Figure 75. Photomicrographs of Type 347 Stainless Steel Tube-Header Joints Brazed With Palniro 7 Brazing Alloy, in Vacuum, With a 10-Min Hold Time at Temperature. Etched With Kalling's Reagent.

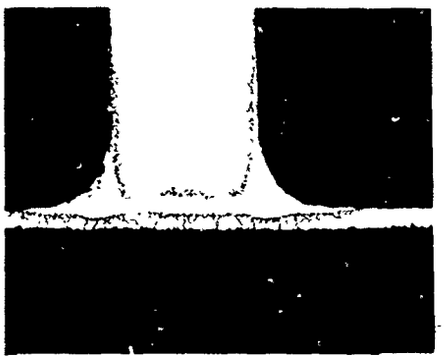

MAG = X50

a. 2075°F BRAZING TEMPERATURE.

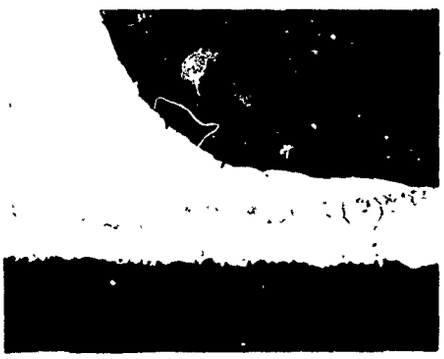

MAG = X150

b. 2075°F BRAZING TEMPERATURE

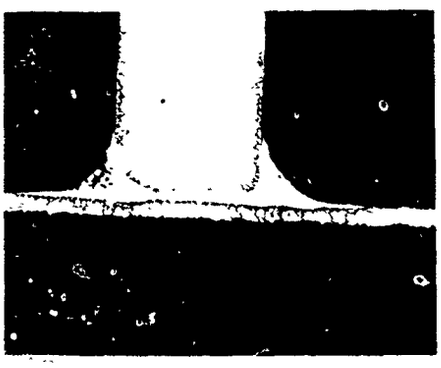

MAG = X50

c. 2050°F BRAZING TEMPERATURE.

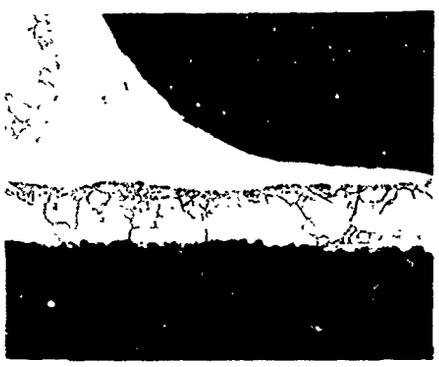

MAG = X150

d. 2050°F BRAZING TEMPERATURE.

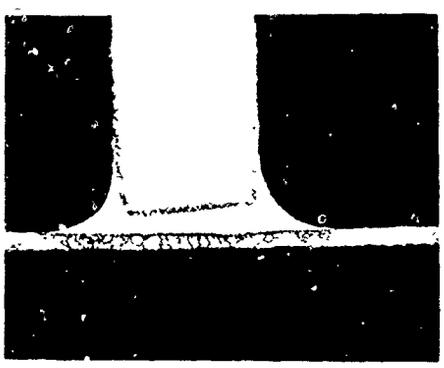

MAG = X50

e. 2025°F BRAZING TEMPERATURE.

MAG = X150

f. 2025°F BRAZING TEMPERATURE.

NOTE: PHOTOS HAVE BEEN REDUCED TO 60%.

Figure 76. Photomicrographs of Type 347 Stainless Steel Tube-Header Joints Brazed With Coast Metals 50B Brazing Alloy, in Vacuum, With a 10-Min Hold Time at Temperature. Etched With Kalling's Reagent.

APPENDIX II

CYCLIC HOT CORROSION TEST

TEST CONDITIONS

Temperature

Each material combination was tested at 1500°, 1300°, and 1100°F (except Inconel 625, which was tested at 1200°F). The highest temperature represented the maximum theoretical gas temperature anticipated across the hot face of the recuperator, while the lower temperatures were more indicative of the highest heat exchanger metal temperature which would be expected in service.

Stress and Time

At least three stress levels were applied to each tubing material-braze alloy combination at each temperature. The stress levels used were calculated to produce rupture in the tubes within 75-, 300-, and 1000-hr periods, respectively. The purpose of the test was to compile stress-rupture data from the stress-time relationship.

Thermal Cycling

During the course of the test, gas from a liquid nitrogen (LN_2) source was admitted into the furnace retort to cool the tubes by approximately one-third the testing temperature. This 500° to 600°F temperature drop was achieved in 1 min. After the cooling cycle, the tubes were allowed to reheat to the testing temperature, which took about 6 min. The cycle was repeated every 2 hr. These cooling and reheating parameters simulated the temperature changes normally occurring in the operation of a recuperated gas turbine engine.

Gas Composition

As in the previous experiment, synthetic products of combustion were used to provide the corrosive environment within the furnace retort. A reducing gas consisting of 3.5-percent carbon dioxide, 19-percent carbon monoxide, 77.5-percent nitrogen, and 350-ppm hydrogen sulfide was admitted during the 6-min reheating period of the cycle.

Oxidizing gas containing 4-percent carbon dioxide, 15-percent oxygen, 81-percent nitrogen, and 150-ppm sulfur dioxide was passed through the retort during the remainder of the time.

Sea-Salt Concentration

A sea-salt solution was injected into the gas stream at the top of the retort. Solution flow rate was controlled to maintain concentration of 5-ppm sea salts in the retort atmosphere. The sea-salt solution was prepared in accordance with Specification ASTM D665-60, Procedure B, in Table XI. This particular concentration of sea salts was approximately one order of magnitude greater than the amount measured on the deck of a ship (referring to Haryslak's and Pollini's report). A higher than normal quantity was considered necessary to produce an accelerating effect in the laboratory test.

APPARATUS

An overall picture of the test rig is shown in Figure 77.

Test Samples

Specimens were prepared by brazing washers onto the tube samples to make test pieces according to the dimensions of Figure 78. Samples were prepared from five tubing materials and brazed in accordance with the conditions specified in Table XI.

Pressure Header Plate

The tubes to be tested were attached to the pressure header plate, and pressurizing gas (nitrogen plus 1-percent oxygen) was supplied to it at eight different manifolds via pressure regulators. Each manifold had provisions for three tube attachments. Thus, 24 tubes could be simultaneously tested from any one plate (i.e., three tubes at each of eight different pressures). Figure 79 depicts the pressure header plate with all tube attachments filled.

Furnaces

Electrical resistance-wound furnaces were used to heat the tubes to the required testing temperatures. The hot zone of each furnace was determined prior to testing. A retort made from Inconel 625 sheet material was fitted inside the furnace to accommodate the tube samples and to contain the environmental gases. Temperature was maintained at the prescribed level by a sheathed thermocouple set and positioned about the axis of the furnace in the center of the hot zone, and connected to a recorder-controller. Temperature-sensitive safety devices were also incorporated into the system. A second thermocouple positioned in approximately the same place as the first was connected to a controller and set at T + 25°F. This backup device could take over control of the furnace should the first unit fail. A third, independent, system was also incorporated. This thermocouple was positioned adjacent to the windings in the refractories of the furnace and was designed to trip a millivolt alarm relay which would electrically isolate the

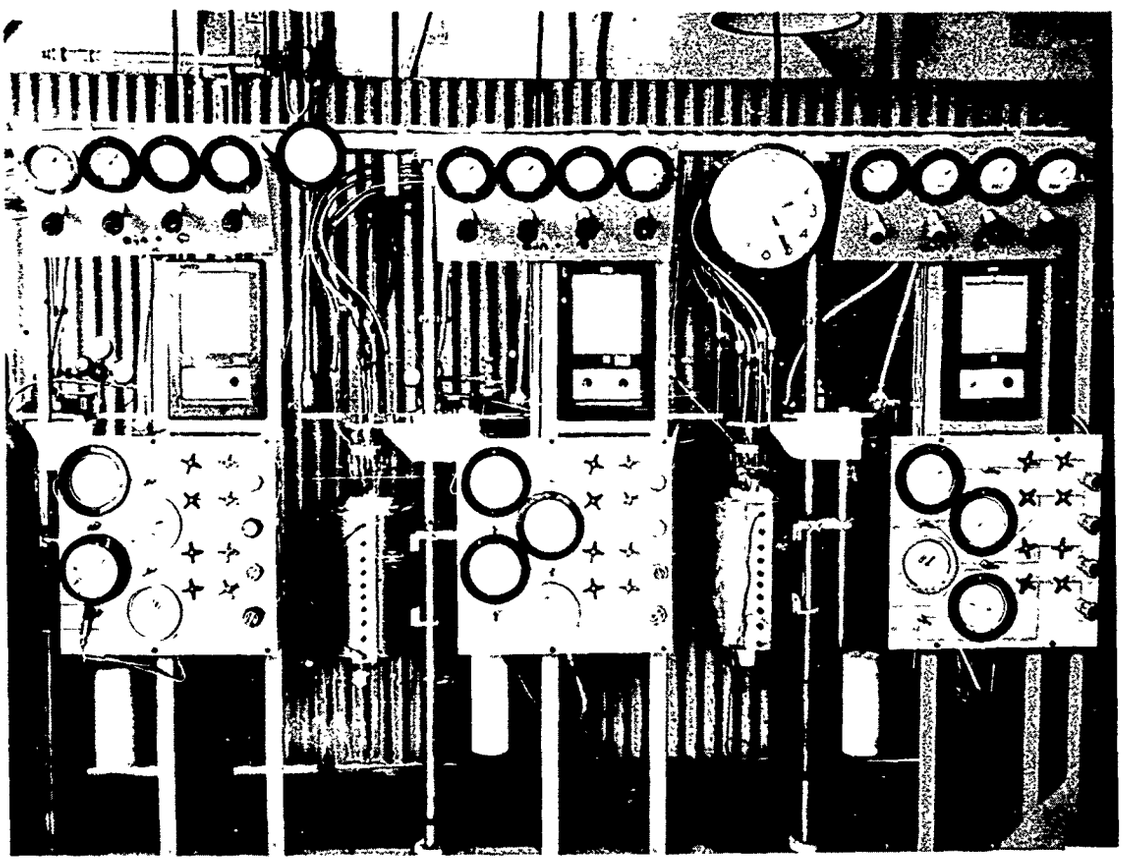

Figure 77. Tube Stress-Rupture Test Rig.

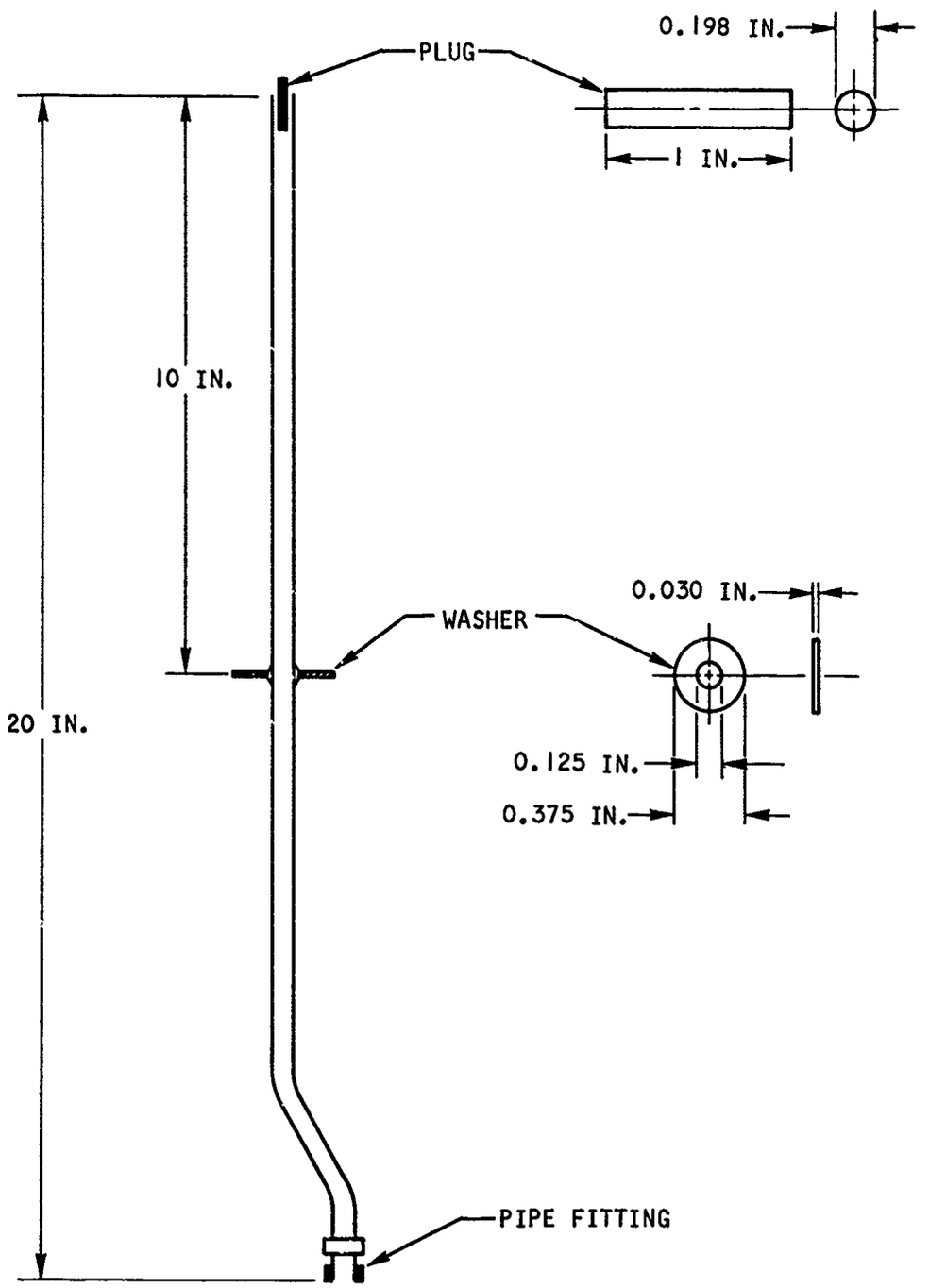

Figure 78. Schematic Diagram of Cyclic Hot Corrosion Test Sample.

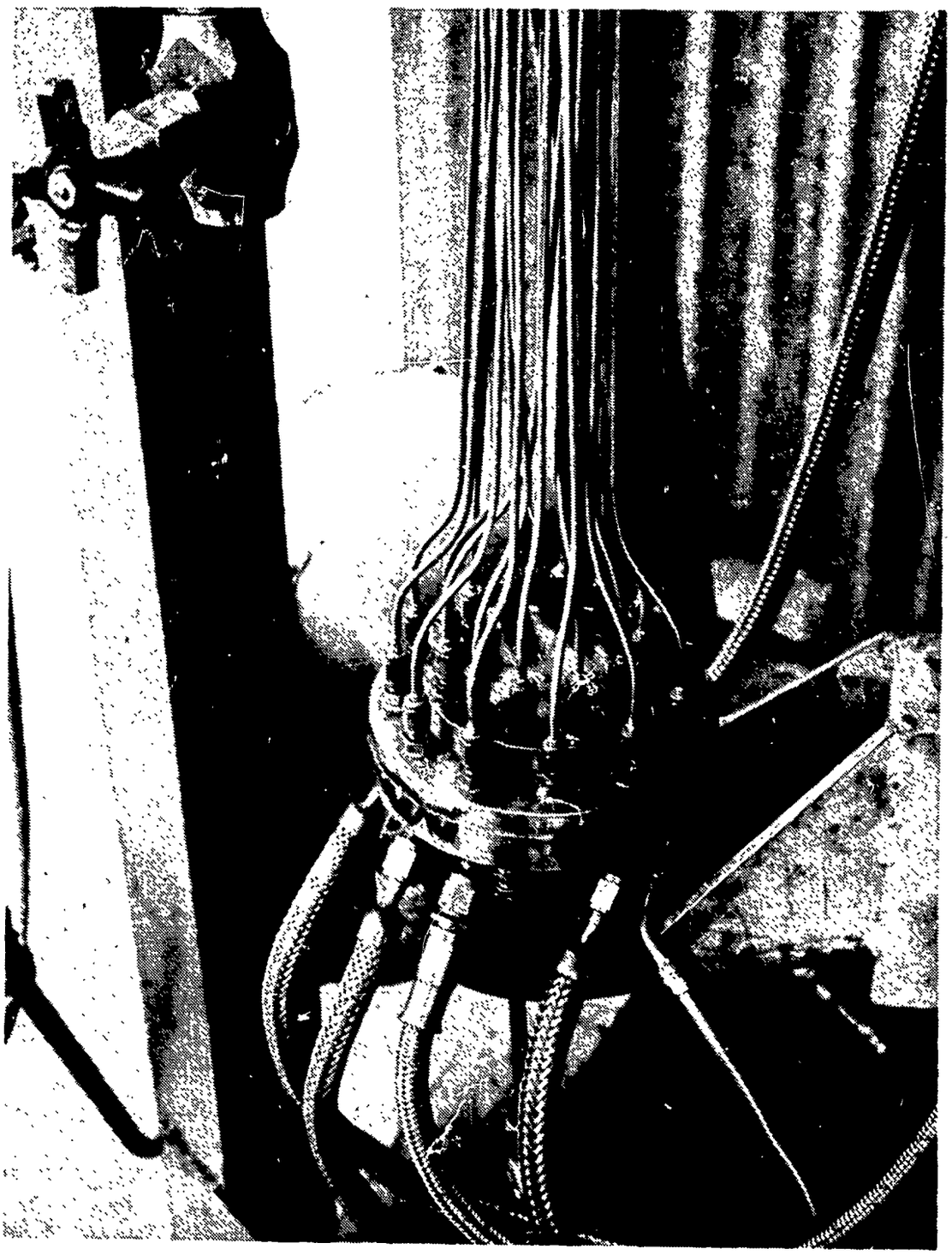

Figure 79. Pressure-Header Plate.

furnace. This third device was set to operate at T + 50°F. A schematic diagram of the furnace, retort, and thermocouple arrangement is shown in Figure 80.

Stress Control

The tubes were pressurized with nitrogen gas containing 1-percent oxygen. Air was not chosen for this purpose because a potentially explosive situation could arise if tube rupture occurred during the reducing cycle. Some oxygen was required to oxidize the inside surfaces of the tubes and achieve a more realistic simulation of the service conditions of recuperators. Pure nitrogen might result in formation of surface nitrides, particularly in alloys containing aluminum and titanium. Previous experience at AiResearch indicated that the gas chosen was previously found to contain sufficient oxygen to produce the oxidation effect.

Nitrogen gas with 1-percent oxygen was purchased in cylinders pressurized at 6000 psi and was admitted into the tubes via valves and regulators designed to maintain the desired pressure in any test manifold. Figure 81 shows the schematic layout of the tube pressurizing system. The relationship $\sigma = Pd/2t$ was used to calculate stress (σ) from the manifold pressure (P) and the dimension of the tube (d and t).

Gas Environment

As described above, the gas composition used in the furnace retort was the same as that used in the static hot corrosion test. However, the oxidizing and reducing gases for the cyclic test were purchased in cylinders pressurized to 2200 psi and 1000 psi, respectively. These concentrated gases were mixed with nitrogen in a preretort mixing chamber by flowing the gas at a predetermined flow rate and pressure and diluting it with nitrogen before admission into the retort. Figure 82 shows the layout of the gas environment system.

Sea-Salt Injection

A sea-salt solution, made in accordance with Specification ASTM D665-60, Procedure B, was diluted with deionized water and stored in a 5-gallon container. During the test, a positive, constant air pressure was supplied to the container to force the solution through a series of control valves and flowmeters into the furnace retort. The dilution factor and flow rate were adjusted to ensure that 5-ppm sea salts were admitted to the furnace atmosphere. A schematic diagram of the sea-salt solution injection system is shown in Figure 83, and a detailed sketch of the actual injector is depicted in Figure 84.

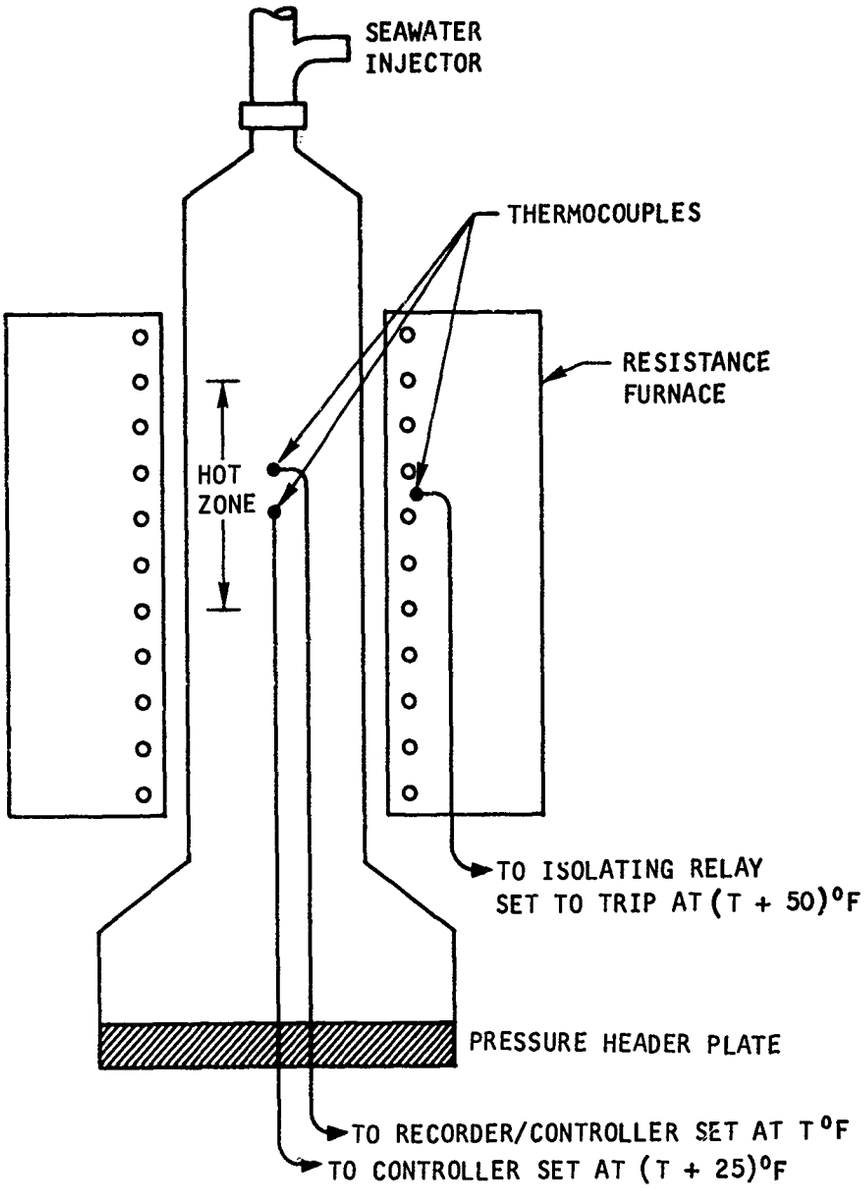

Figure 80. Schematic Diagram of Furnace Retort.

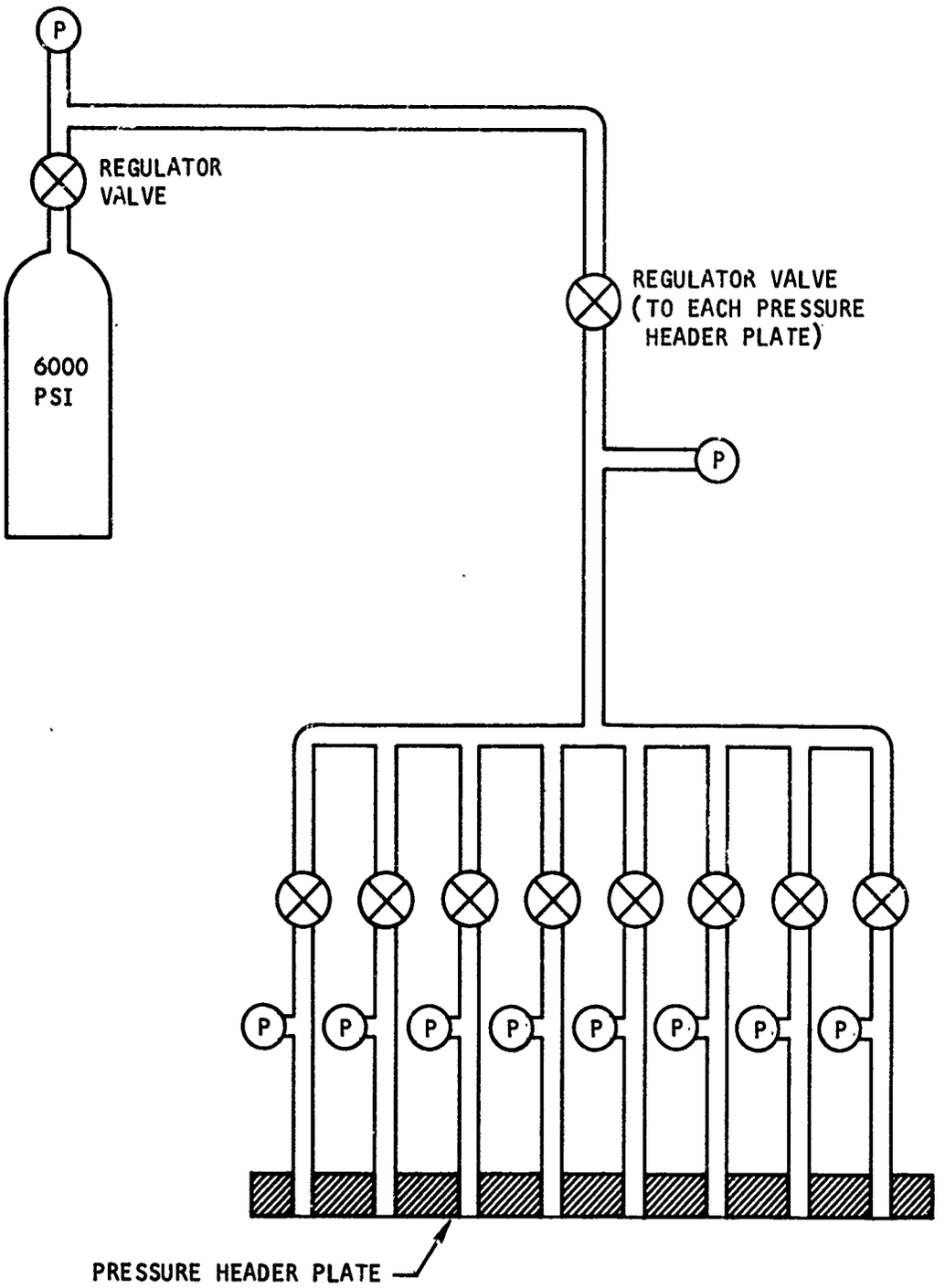

Figure 81. Schematic Diagram of Tube Pressurization System.

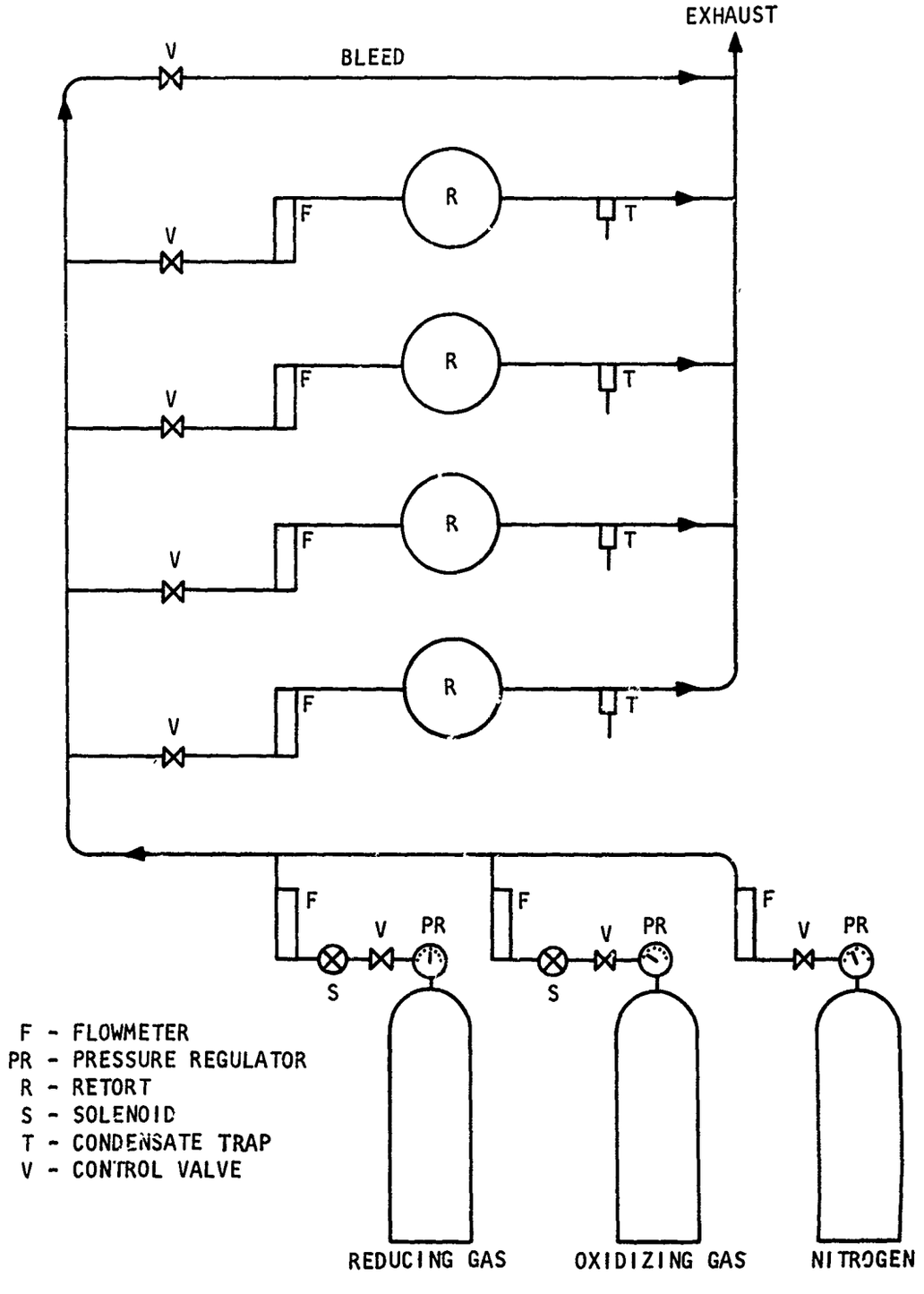

Figure 82. Schematic Diagram of Test Atmosphere Control System.

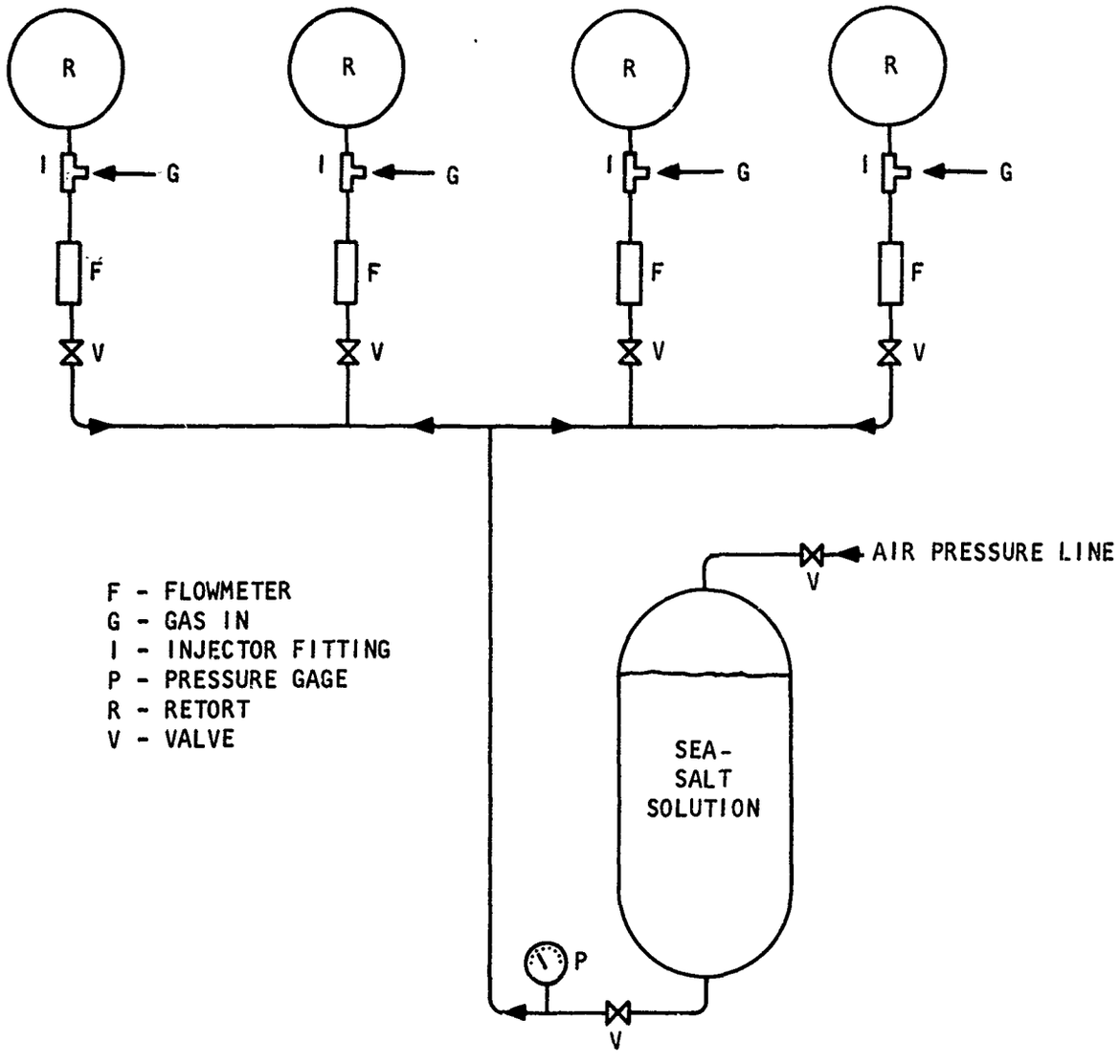

Figure 83. Schematic Diagram of Sea-Salt Solution Injection System.

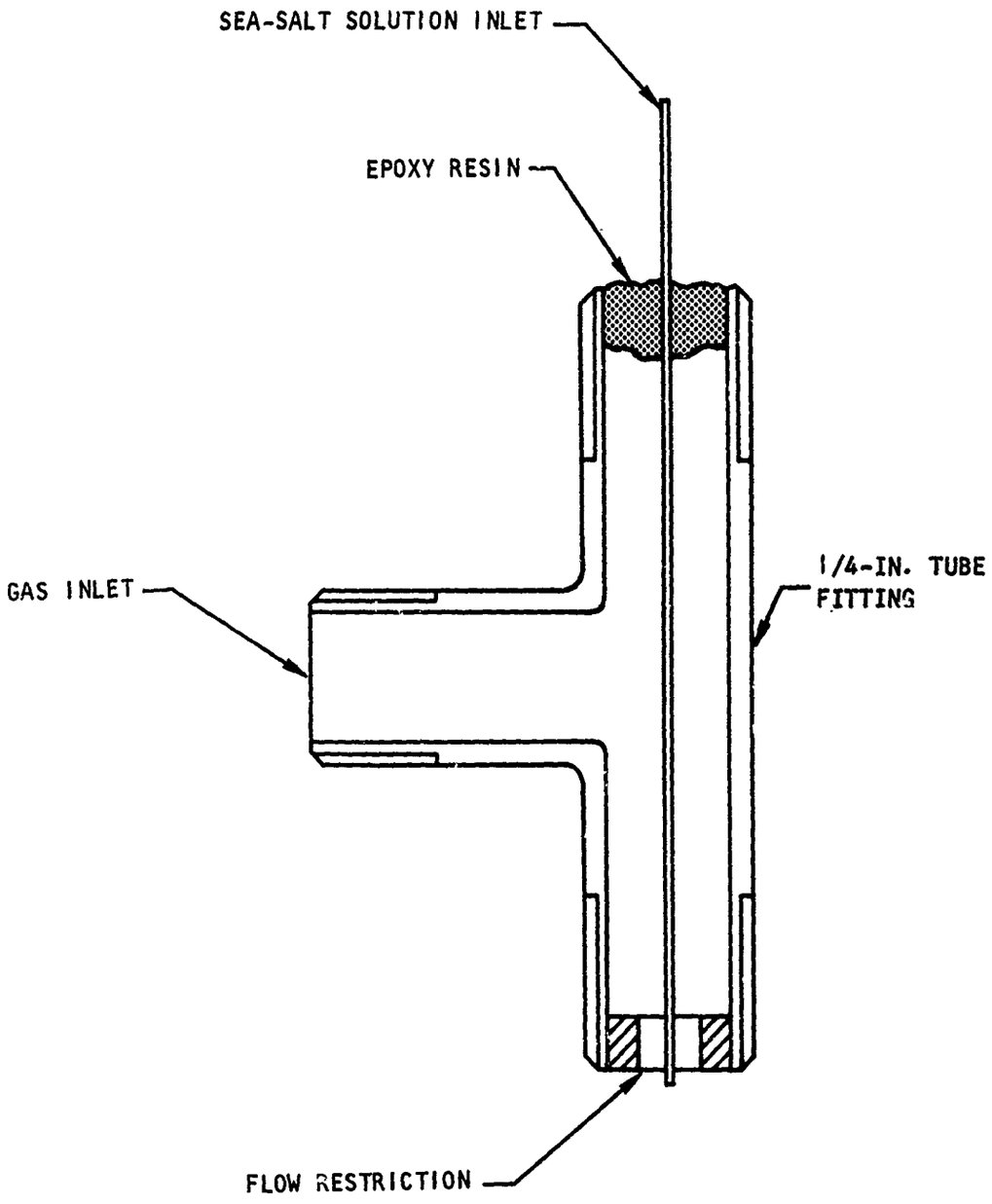

Figure 84. Sea-Salt Solution Injector.

Thermal Cycle Control

A simple timer mechanism was employed to activate solenoid valves and control the operation of the cycles. Figure 85 shows a typical cycle. Beginning at zero time, the furnace is at the operating temperature. The solenoid valves in the reducing and oxidizing gas streams are closed, allowing only nitrogen to flow through the system. The nitrogen purge removes the reducing gases. After 15 min the oxidizing gas solenoid valve is opened, admitting the oxidizing atmosphere into the furnace retort. Two hours later, the timer mechanism closes off the oxidizing gas, electrically isolates the furnace, and opens the valve which admits LN_2 into the retort for 1 min to cool the tubes. The electric current is then restored to the furnace, the LN_2 is turned off, and the reducing gas is turned on.

After the temperature has recovered (which takes 6 min), the reducing gas is turned off and the cycle is repeated. A diagram of the cooling system is shown in Figure 86.

The results of the cyclic hot corrosion tests are presented in Tables XXI through XXV. The stress vs time to rupture results are also plotted in Figures 18 through 22 in the main body of the report.

METALLOGRAPHY

All the tubes were examined visually after testing. Approximately 40 percent of them were selected for more detailed metallographic analysis. Sections from the braze fillet were prepared to determine the effects of corrosion on the joint, and a second specimen taken from the area of failure was examined to ascertain the effects of hot corrosion on the tubing material.

Photomicrographs of the areas examined are presented in Figures 87 through 124, and a commentary on the results is shown in Tables XXVI through XXXV.

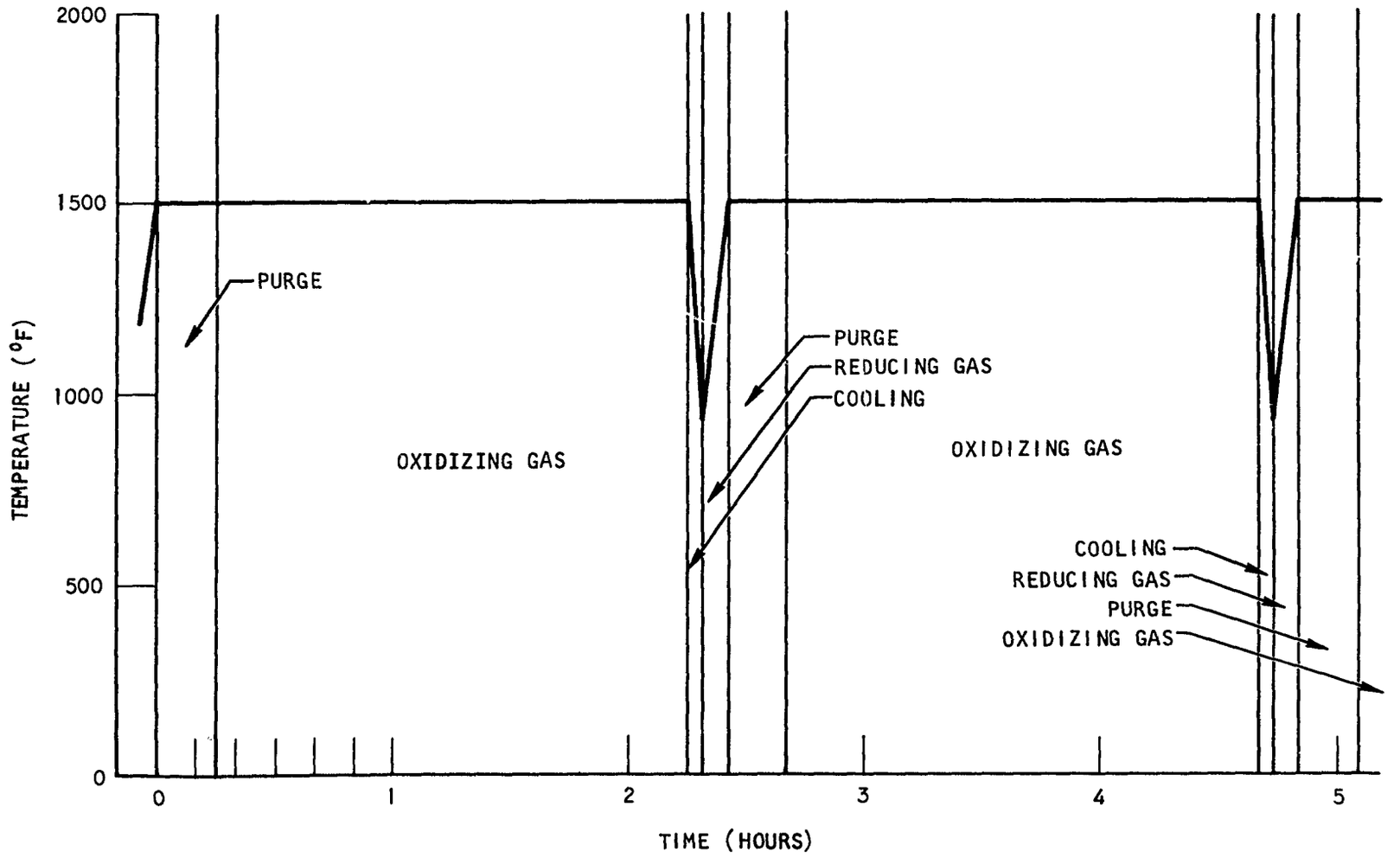

Figure 85. Typical Cyclic Test Program Plan.

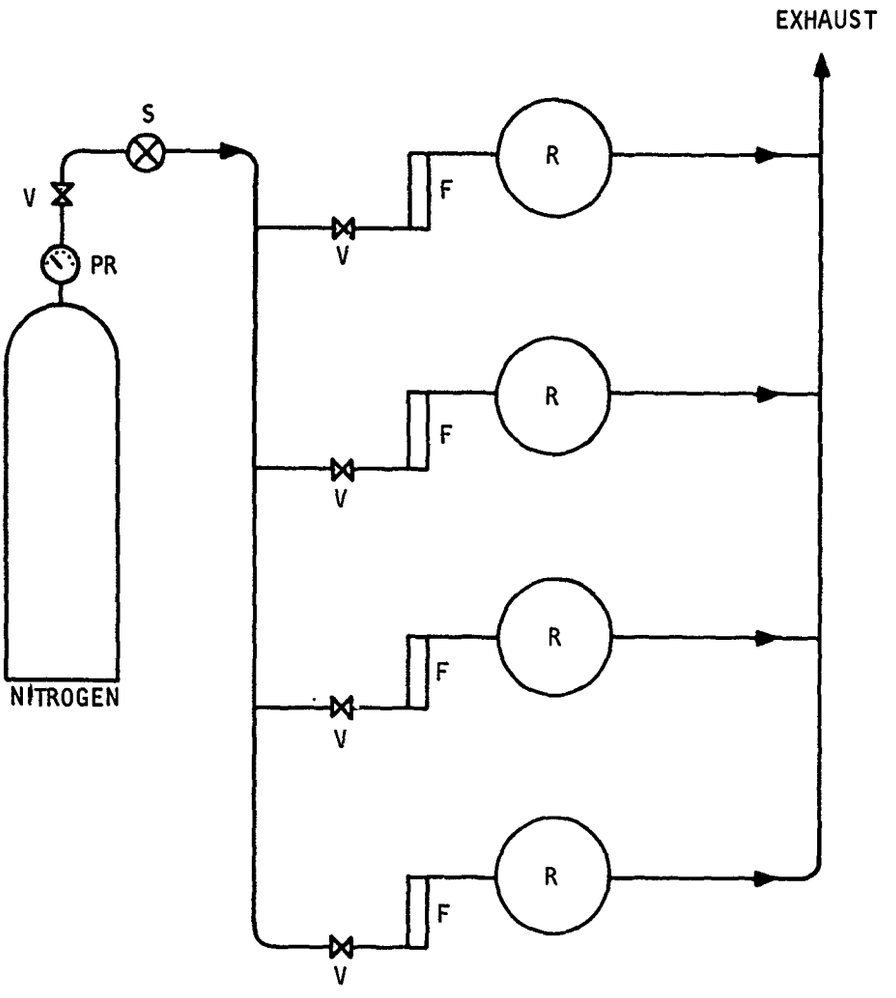

F - FLOW
PR - PRESSURE REGULATOR
R - RETORT
S - SOLENOID VALVE
V - CONTROL VALVE

Figure 86. Schematic Diagram of Cooling System.

TABLE XXI. HASTELLOY X TUBING STRESS-RUPTURE DATA FOR THE THERMAL CYCLIC HOT CORROSION TEST

Temperature (°F)	Stress (ksi)	Time to Rupture (hr)	
		Braze Alloys	
		Palniro 1	J-8100
1500	13.9	13.8 28.1 28.1	22.5 28.1 28.1
	9.0	114.4 114.4 135.9	75 130.5 171.4
	6.5	35.4 222.6 277.0 341.3	141.8 156.6 218.7 -
	4.5	325.8 502.0 562.4	418.9 616.8 623.8
1300	25	- - -	99.1 122.2 147.1
	20.8	87.9 175.2 225.2	204.4 225.4 270.2
	20.0	- - -	344.4 421.7 991.0
	19.1	187.2 343.0 385.6	- - -
	16	424.7 591.0 951.4	- - -
1100	34.7	500 736.1 1121.6	364.2 1164.9* 1507.5*

*Not ruptured, removed from test.

TABLE XXII. INCOLOY 800 TUBING STRESS-RUPTURE DATA FOR THE THERMAL CYCLIC HOT CORROSION TEST

Temperature (°F)	Stress (ksi)	Time to Rupture (hr)	
		Braze Alloys	
		Palniro 7	Coast Metals 50B
1500	8.3	10.6 16.4 28.1	10.6 11.8 29.8
	2.8	88.1 144.1 361.4 -	21.4 222.6 502.0 812
	1.73	- - -	346.5 1174.0* 1174.0*
	1.21	644.3 1501.7* 1501.7*	- - -
1300	15.3	31.9 35.4 37.8	31.9 3.6 37.8
	9.5	166.9 201.7 249.5	217.5 251.0 344.6
	6.1	490.6 1103.3 1538.7*	591.4 740.1 1081.5
1100	30	56.9 68.2 74.5	11.6 43.4 500.0*
	27.8	147.9 253.2 314.5	179.3 420.2 452.2
	24.3	950.0* 1150.0* 1150.0*	1000.0* 1100.0* 1100.0*

*Not ruptured, removed from test.

TABLE XXIII. MULTIMET N-155 TUBING STRESS-RUPTURE DATA FOR THE THERMAL CYCLIC HOT CORROSION TEST

Temperature (°F)	Stress (ksi)	Time to Rupture (hr)	
		Braze Alloys	
		Palniro I	Nicrobraz 200
1500	20	3.4 14.4 15.0	1.5 11.8 24.5
	15.2	25.7 30.3 49.2	17.8 27.9 49.6
	10	83.6 101.4 101.4	81.0 91.8 126.6
	4.5	812.0 908.4 1196.3	908.4 936.6 967.5
1300	30	98.2 110.3 221.9	- - -
	26.7	87.9 127.3 204.4	85 110.7 127.3
	25	- - -	313.4 398.6 410.3
	22.5	106.7 712.2 787.2	221.4 846 852
1100	40	533.7 701.4 760.4	485.2 485.2 1023.6

TABLE XXIV. TYPE 347 STAINLESS STEEL TUBING STRESS-RUPTURE DATA FOR THE THERMAL CYCLIC HOT CORROSION TEST

Temperature (°F)	Stress (ksi)	Time to Rupture (hr)	
		Braze Alloys	
		Palniro 7	Nicrobraz 135
1500	9.2	24.5 31.4 -	37.2 48.9 53.3
		35.0 47.1 49.9	35.0 35.0 125.1
	5.0	103.0 129.4 129.4	142.1 170.2 170.2
	3.0	6.1 6.8 17.8	18.7 77.4 88.1
		128.4 151.8 154.4	141.4 151.8 152.1
1300	13.9	104.1 104.1 127.3	82.7 104.1 107.7
	10.0	294.0 489.5 608.7	221.4 441.1 606.0
	8.0	486.4 533.8 465.4	578.5 667.5 676.2
1100	35.0	36.3 36.3 57.2	228.1 315.0 315.0
	30.0	157.1 250.1 353.7	68.7 248.8 520.9
	26.9	401.7 461.0 1238.7	471.4 846.0 1023.1

TABLE XXV. INCONEL 625 TUBING, STRESS-RUPTURE DATA FOR THE THERMAL CYCLIC HOT CORROSION TEST

Temperature (°F)	Stress (ksi)	Time to Rupture (hr)	
		Braze Alloys	
		J-8100	Nicrobraz 135
1500	14.8	124.3 139.3 213.8	80.3 100.0 101.2
	12.1	146.3 270.2 160.9	85.8 89.5 176.4
	8.7	86.2 187.7 208.9	230.4 230.4 303.4
	6.6	522.6 570.4 699.6	269.8 570.4 669.8
1300	36.5	21.0** 245.6 259.8	55.8 101.1 250.0
	33.0	42.5 146.0 158.1	81.8 169.2 208.0
	26.0	672.0* 774.4* 843.4	320.9 436.3 675.0
	19.1	1278* 1513* 1604*	767* 1604* 1604*

*Not ruptured, removed from test.

**Premature failure.

TABLE XXV. (Continued)

Temperature (°F)	Stress (ksi)	Time to Rupture (hr)	
		Braze Alloys	
		J-8100	Nicrobraz 135
1200	50.4	38.2 43.0 517.8	32.9 56.6 755.7*
	46.4	394.6* 394.6* 394.6*	394.6* 394.6* 394.6*
	41.0	61.7 814.7 955.1*	655.6 1453 776*
	35.7	179.4** 776.4* 1610*	621.5 1306* 1610*

*Not ruptured, removed from test.

**Premature failure.

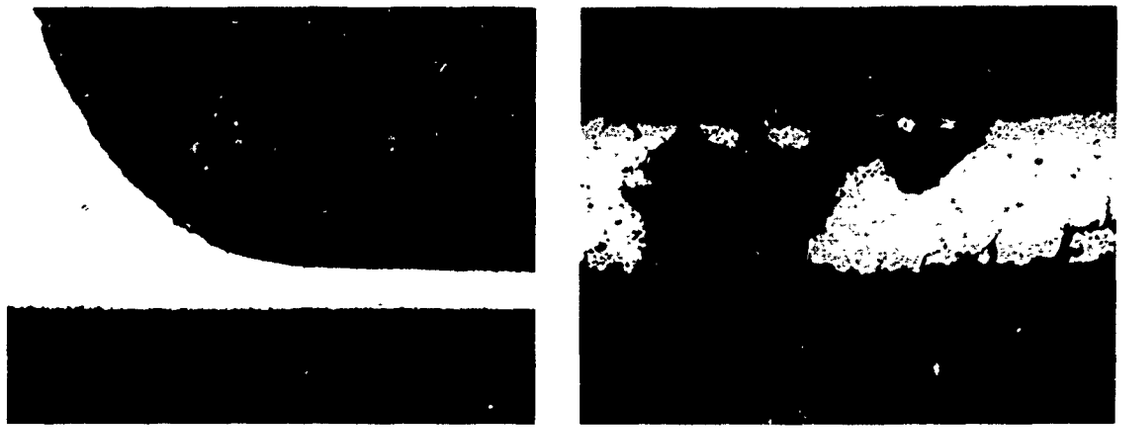

MAG = X75 MAG = X250

1500°F AND 20 KSI, FAILED AFTER 14.4 HOURS

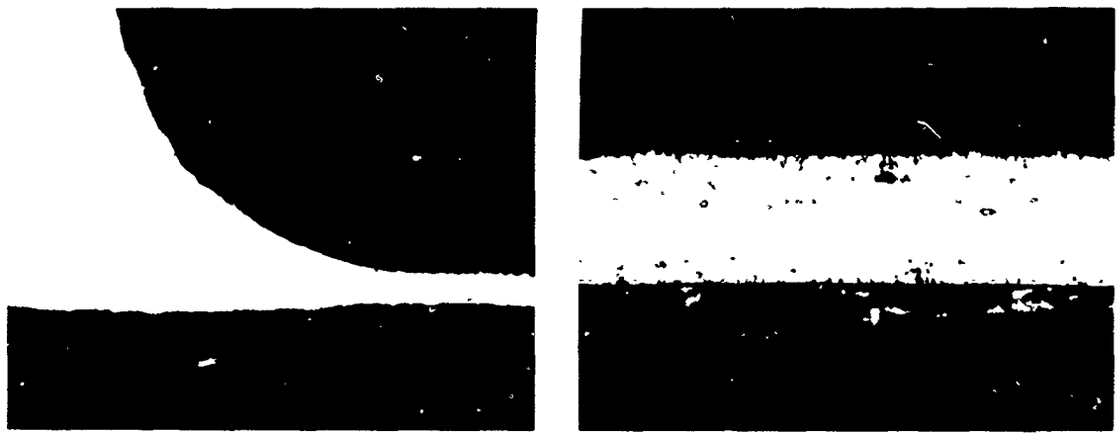

MAG = X75 MAG = X250

1500°F AND 15.2 KSI, FAILED AFTER 25.7 HOURS

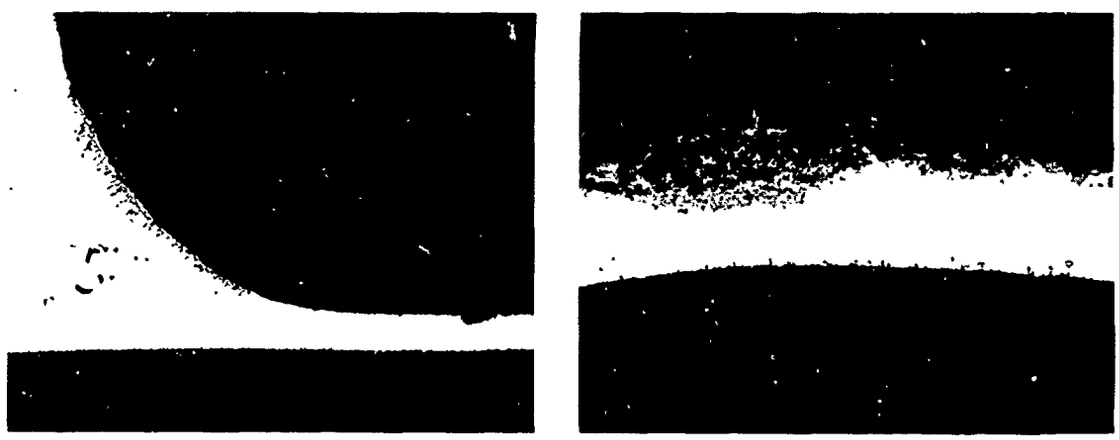

MAG = X75 MAG = X250

1500°F AND 10 KSI, FAILED AFTER 83.6 HOURS

NOTE: FIGURES REDUCED TO 60%.

Figure 87. Photomicrographs of Multimet N-155 Tubes Brazed with Palniro I Brazing Alloy.

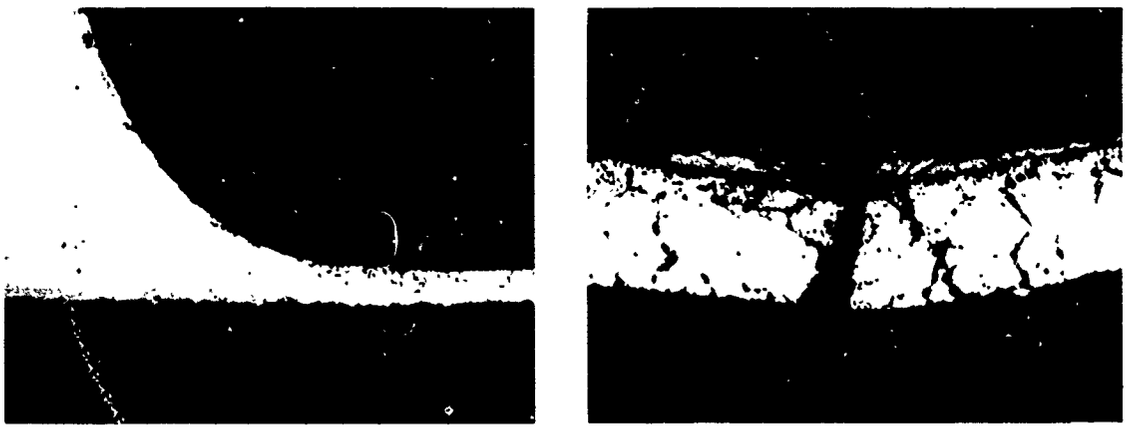

MAG = X75 MAG = X250

1500°F AND 4.5 KSI, FAILED AFTER 119.6 HOURS

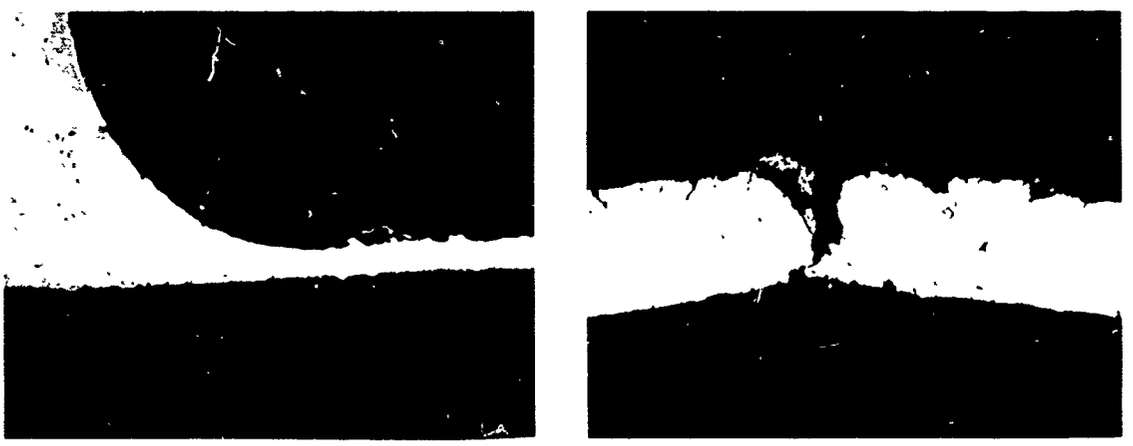

MAG = X75 MAG = X250

1300°F AND 30 KSI, FAILED AFTER 110.3 HOURS

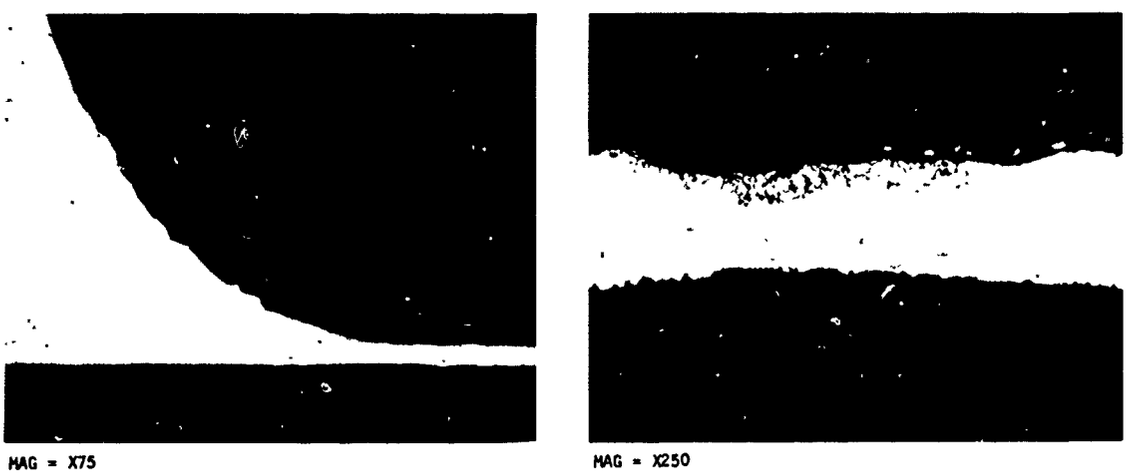

MAG = X75 MAG = X250

1300°F AND 26.7 KSI, FAILED AFTER 87.9 HOURS

NOTE: FIGURES REDUCED TO 60%.

Figure 88. Photomicrographs of Multimet N-155 Tubes Brazed With Palniro I Brazing Alloy.

MAG = X75 MAG = X250

1300°F AND 22.5 KSI, FAILED AFTER 712.2 HOURS

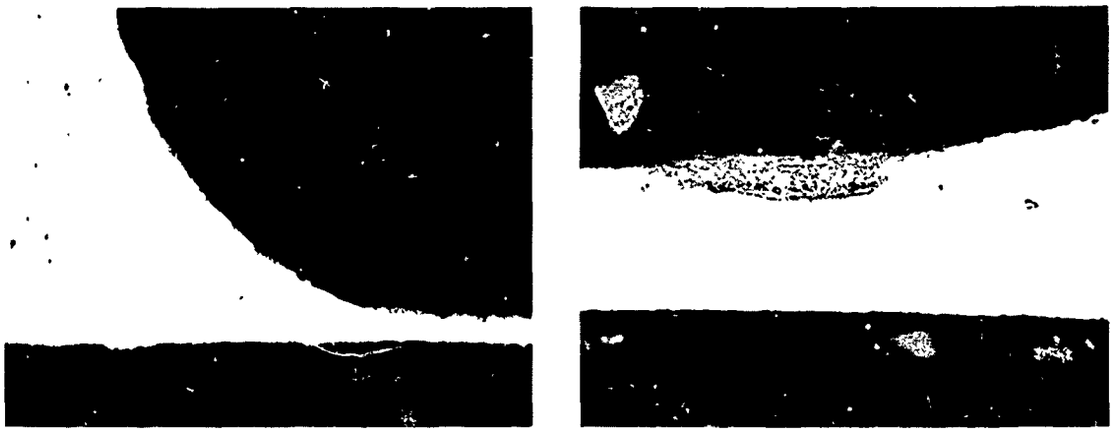

MAG = X250

1300°F AND 22.5 KSI, FAILED AFTER 106.7 HOURS

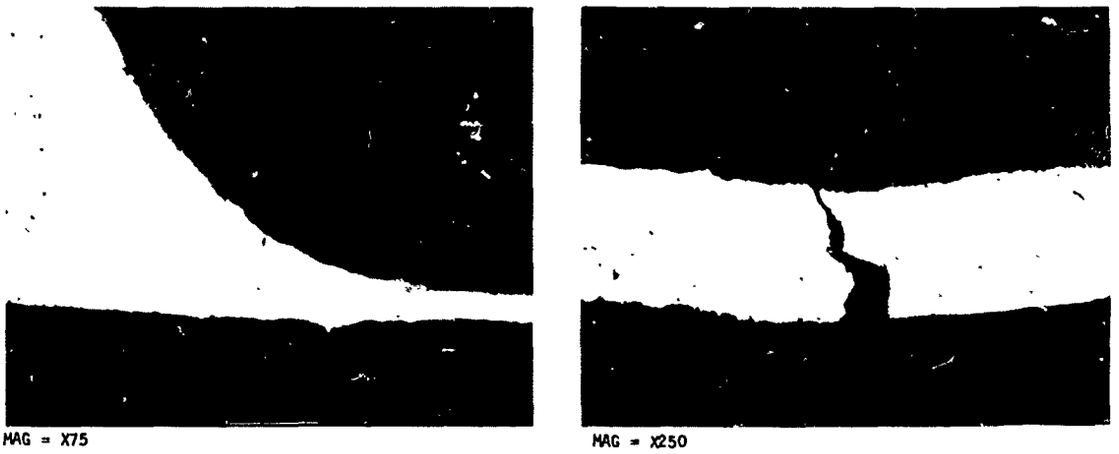

MAG = X75 MAG = X250

1100°F AND 40 KSI, FAILED AFTER 760.4 HOURS

NOTE: FIGURES REDUCED TO 60%.

Figure 89. Photomicrographs of Multimet N-155 Tubes Brazed With Palniro I Brazing Alloy.

TABLE XXVI. MULTIMET N-155 BRAZED WITH PALNIRO I, FAILURE AND CORROSION EXAMINATION

Temperature (°F)	Stress (ksi)	Life (hr)	Visual Examination*			Metallographical Examination		Photomicrograph Figure No.
			Failure		Corrosion	Braze Alloy Fillet	Point of Failure	
			Type	Location				
1500	20	14.4	P	-1	S	No corrosion	Grain boundary oxidation, completely penetrated	87
1500	15.2	25.7	P	J	M	No corrosion	Internal oxidation, slight porosity	87
1500	10	83.6	P	+1/4	M	Intergranular oxide layer	Wart. Metal 1 mil thick	87
1500	4.5	1196.3	P	-3	M	No corrosion	Oxide layer 1/2 mil thick, internal oxidation	88
1300	30	110.3	P	-1	S	No corrosion	Intergranular oxidation	88
1300	26.7	87.9	P	J	S	No corrosion	Internal oxide layer	88
1300	22.5	712.2	P	-1-1/2	M	Heavy oxide layer	Internal attack, oxide layer	89
1300	22.5	106.7	P	J	M	Slight oxidation	Internal oxide layer at tube/braze interface	89
1100	40	760.4	P	-1/2	M	No corrosion	Oxidized fissure	89
1100	40	533.7	P	-4	S	No corrosion	Intergranular oxidation	-

*P = Pinhole leak; R = Tube fracture; J = Braze joint; + = Above J; - = Below J; S = Slight; M = Moderate; H = Heavy

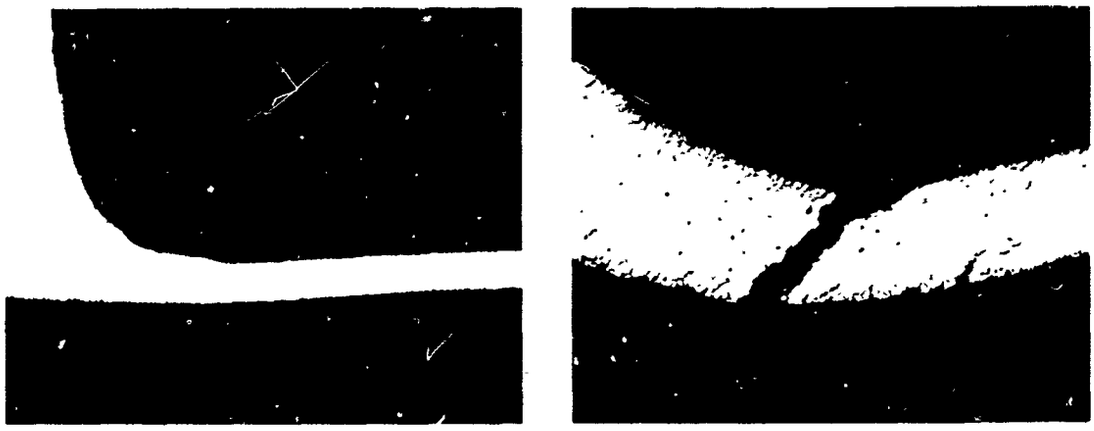

MAG = X75 MAG = X250

1500°F AND 20 KSI, FAILED AFTEF 24.5 HOURS

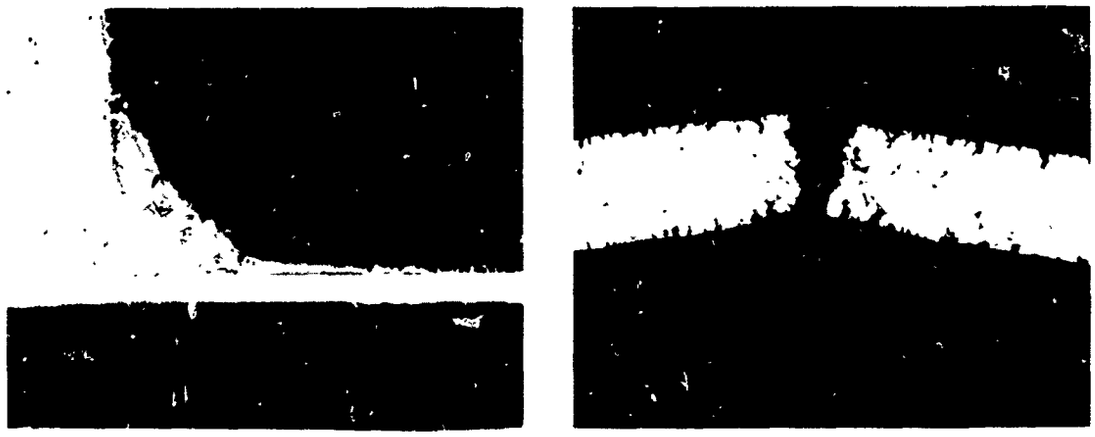

MAG = X75 MAG = X250

1500°F AND 15.2 KSI, FAILED AFTER 7.8 HOURS

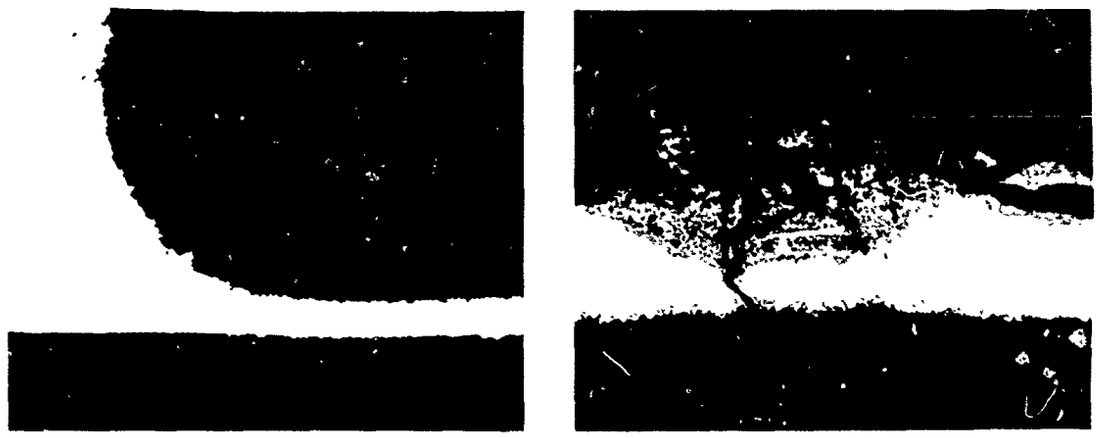

MAG = X75 MAG = X250

1500°F AND 10 KSI, FAILED AFTER 81.0 HOURS

NOTE: FIGURES REDUCED TO 60%.

Figure 90. Photomicrographs of Multimet N-155 Tubes Brazed With Nicrobraz 200 Brazing Alloy.

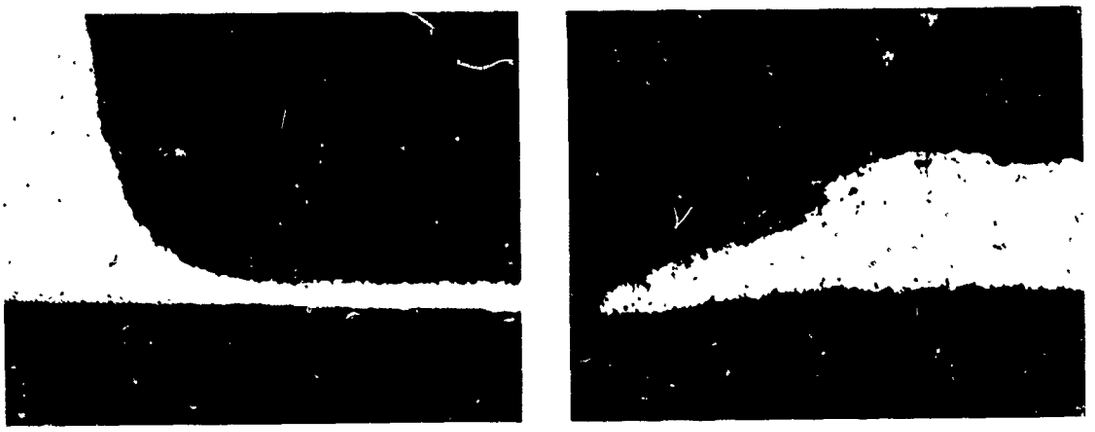

MAG = X75 MAG = X250

1500°F AND 4.5 KSI, FAILED AFTER 908.4 HOURS

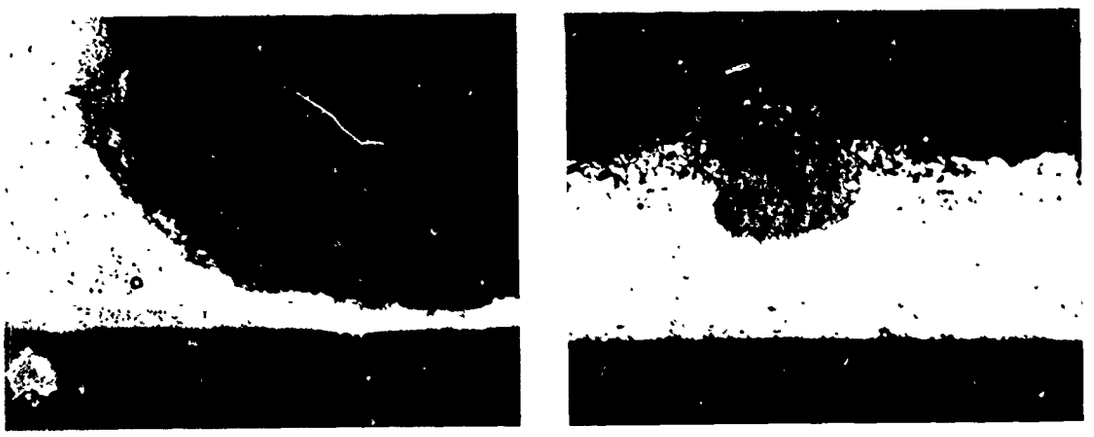

MAG = X75 MAG = X250

1500°F AND 4.5 KSI, FAILED AFTER 967.5 HOURS

MAG = X75 MAG = X250

1300°F AND 26.7 KSI, FAILED AFTER 127.3 HOURS

NOTE: FIGURES REDUCED TO 60%.

Figure 91. Photomicrographs of Multimet N-155 Tubes Brazed With Nicrobraz 200 Brazing Alloy.

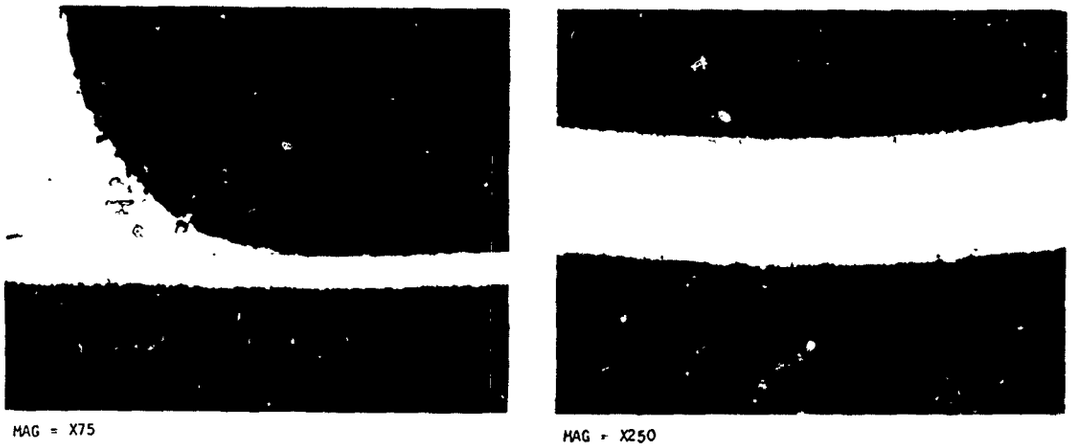

MAG = X75 MAG = X250

1300°F AND 26.7 KSI, FAILED AFTER 85.0 HOURS

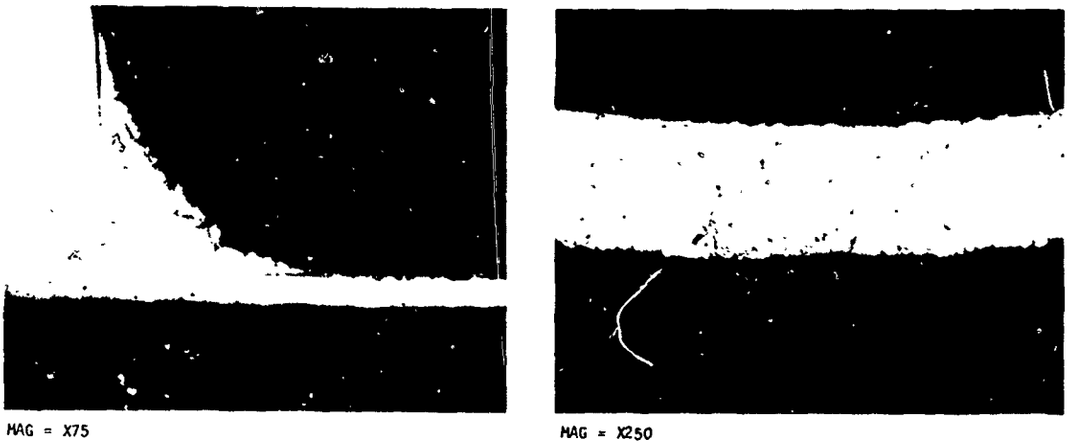

MAG = X75 MAG = X250

1300°F AND 25 KSI, FAILED AFTER 398.6 HOURS

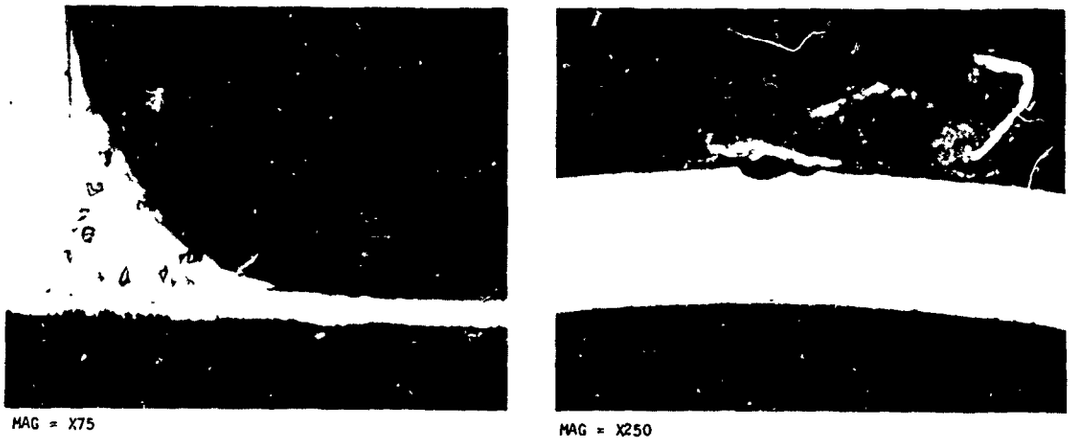

MAG = X75 MAG = X250

1300°F AND 22.5 KSI, FAILED AFTER 221.4 HOURS

NOTE: FIGURES REDUCED TO 60%.

Figure 92. Photomicrographs of Multimet N-155 Tubes Brazed With Nicrobraz 200 Brazing Alloy.

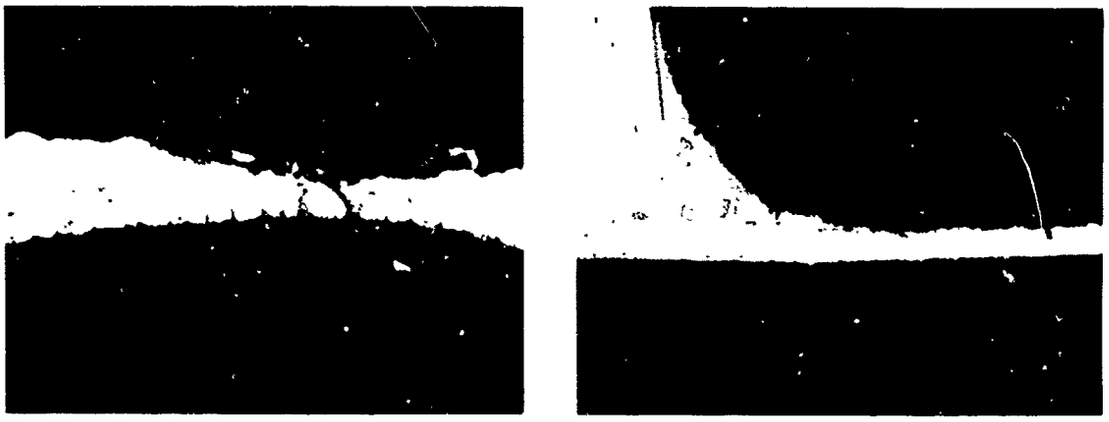

MAG = X75 MAG = X250

1300°F AND 22.5 KSI, FAILED AFTER 852.0 HOURS

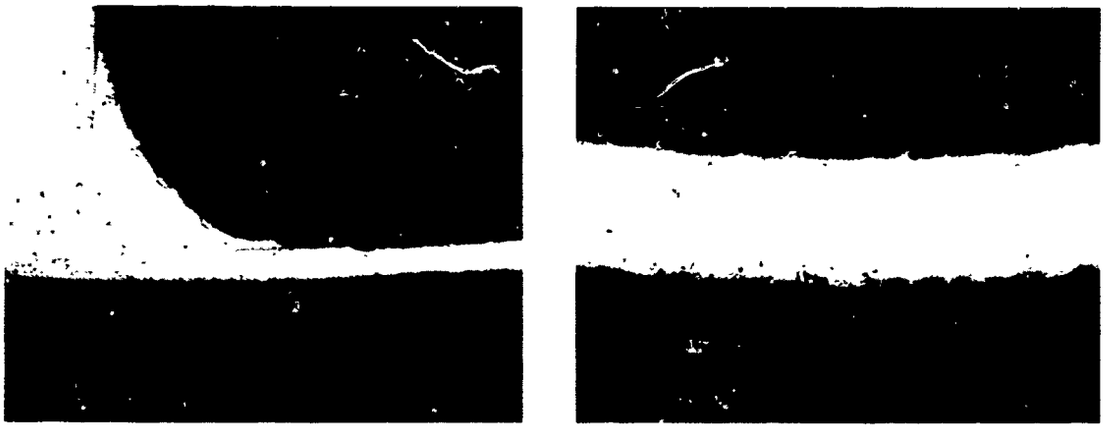

MAG = X75 MAG = X250

1100°F AND 40 KSI, FAILED AFTER 1023.6 HOURS

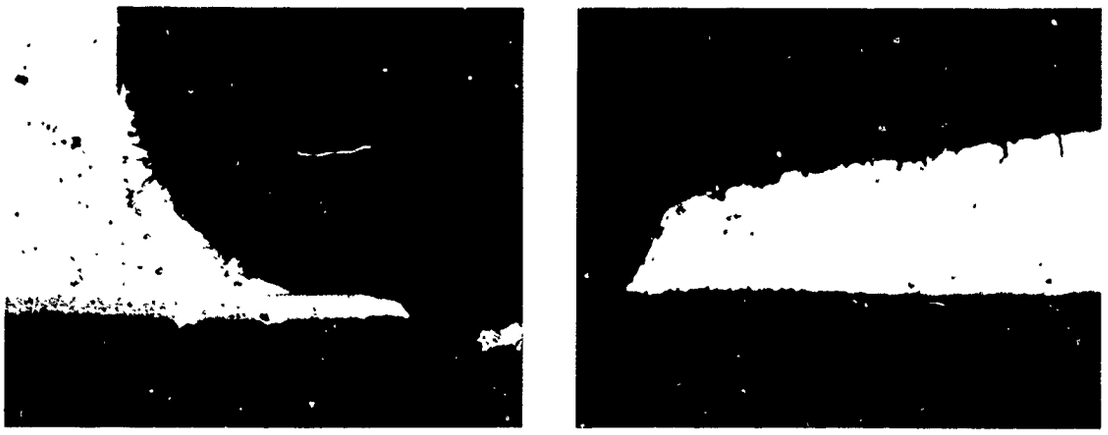

MAG = X75 MAG = X250

1100°F AND 40 KSI, FAILED AFTER 485.2 HOURS

NOTE: FIGURES REDUCED TO 60%.

Figure 93. Photomicrographs of Multimet N-155 Tubes Brazed with Nicrobraz 200 Brazing Alloy.

TABLE XXVII. MULTIMET N-155 BRAZED WITH NICROBRAZ 200, FAILURE AND CORROSION EXAMINATION

Temperature (°F)	Stress (ksi)	Life (hr)	Visual Examination*			Metallographical Examination		Photomicrograph Figure No.
			Failure					
			Type	Location	Corrosion	Braze Alloy Fillet	Point of Failure	
1500	20	24.5	P	-1	S	No corrosion	Intergranular penetration, oxidized fissure	90
1500	15.2	17.8	P	-1	S	No corrosion	Internal oxidation, porous	90
1500	10	81	P	-1/2	M	Some surface oxidation	Intense local attack, wart	90
1500	4.5	908.4	R	-5	M	Little surface corrosion	Internal oxidation, oxidized fissure	91
1500	4.5	967.5	P	J	M	Heavy oxide layer	Intense local attack, wart	91
1300	26.7	127.3	P	-10	S	No corrosion	Slight oxidation, crack	91
1300	26.7	85.0	P	-1/2	S	No corrosion	Slight oxidation, crack	92
1300	25	398.6	P	-5	S	No corrosion	Slight oxidation, intergranular and internal	92
1300	22.5	221.4	P	-9	S	No corrosion	No evidence of failure	92
1300	22.5	852	P	-2	M	No corrosion	Intergranular oxidation, metal thickness = 0.001 in.	93
1100	40	1023.6	P	-4	M	No corrosion	Internal oxidation	93
1100	40	485.6	R	J	S	No corrosion	Intergranular penetration at tube/braze interface	93

*P = Pinhole leak; R = Tube rupture; J = Braze joint; + = Above J; - = Below J; S = Slight; M = Moderate; H = Heavy

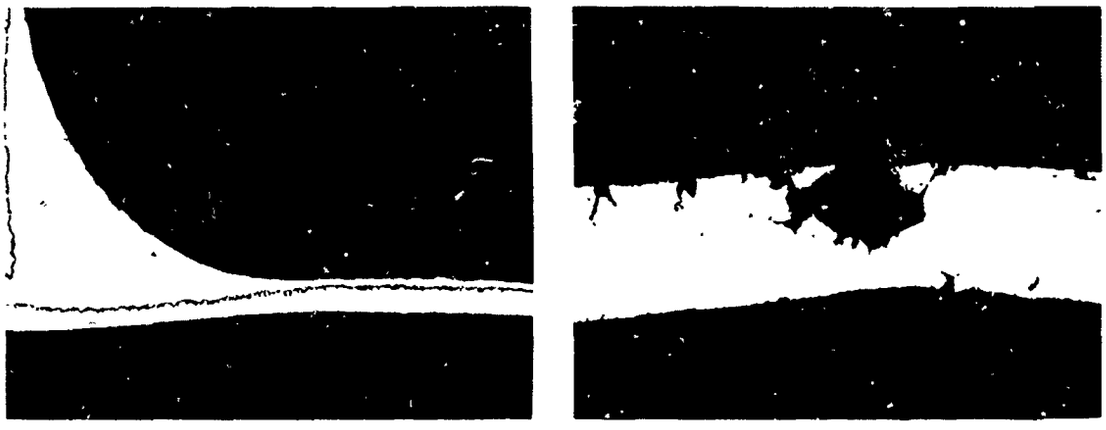

MAG = X75 MAG = X250

1500°F AND 13.9 KSI, FAILED AFTER 13.8 HOURS

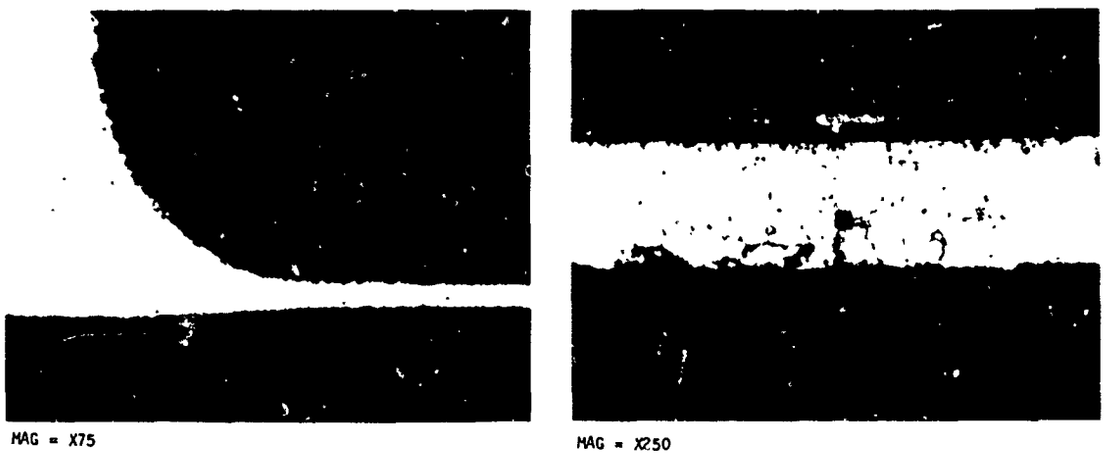

MAG = X75 MAG = X250

1500°F AND 9.0 KSI, FAILED AFTER 114.4 HOURS

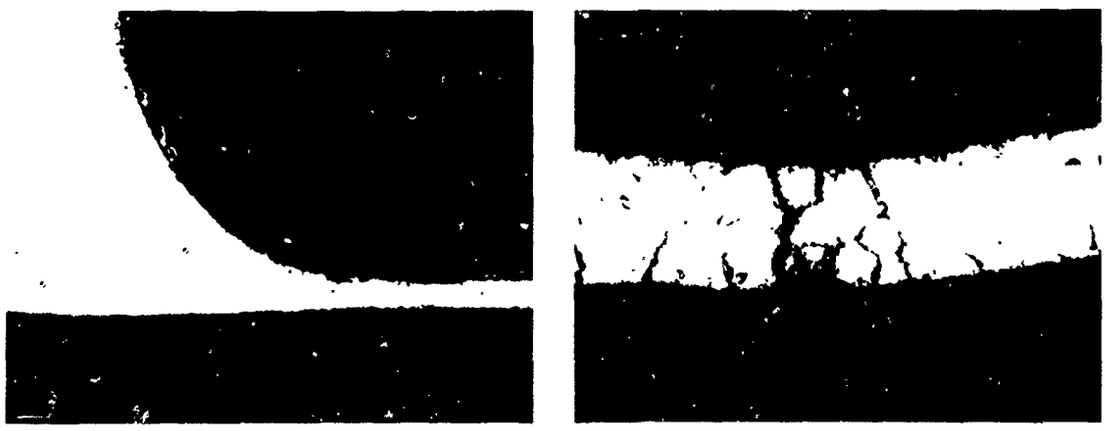

MAG = X75 MAG = X250

1500°F AND 9.0 KSI, FAILED AFTER 135.9 HOURS

NOTE: FIGURES REDUCED TO 60%.

Figure 94. Photomicrographs of Hastelloy X Tubes Brazed With Palniro I Brazing Alloy.

MAG = X75 MAG = X250

1500°F AND 6.5 KSI, FAILED AFTER 277.0 HOURS

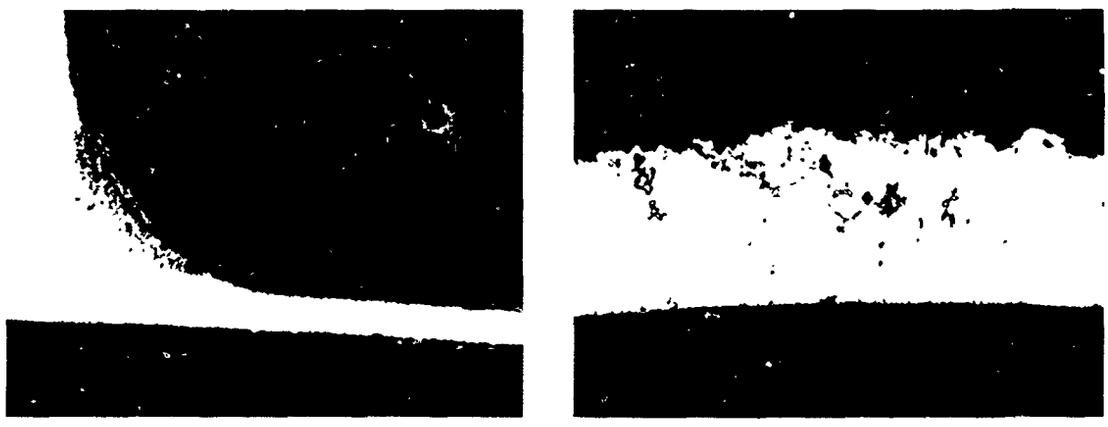

MAG = X75 MAG = X250

1500°F AND 6.5 KSI, FAILED AFTER 341.3 HOURS

MAG = X75 MAG = X250

1500°F AND 4.5 KSI, FAILED AFTER 525.8 HOURS

NOTE: FIGURES REDUCED TO 60%.

Figure 95. Photomicrographs of Hastelloy X Tubes Brazed With Palniro I Brazing Alloy.

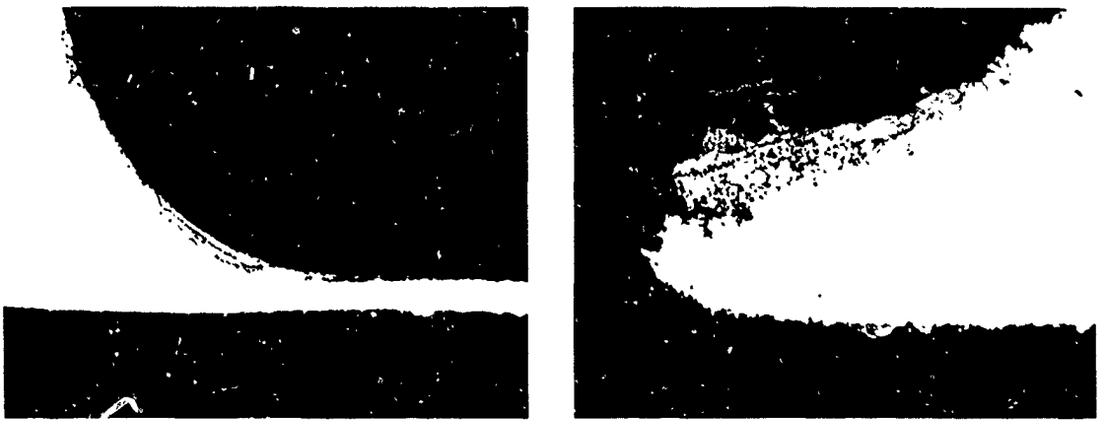

MAG = X75 MAG = X250
1300°F AND 20 8 KSI, FAILED AFTER 175.2 HOURS

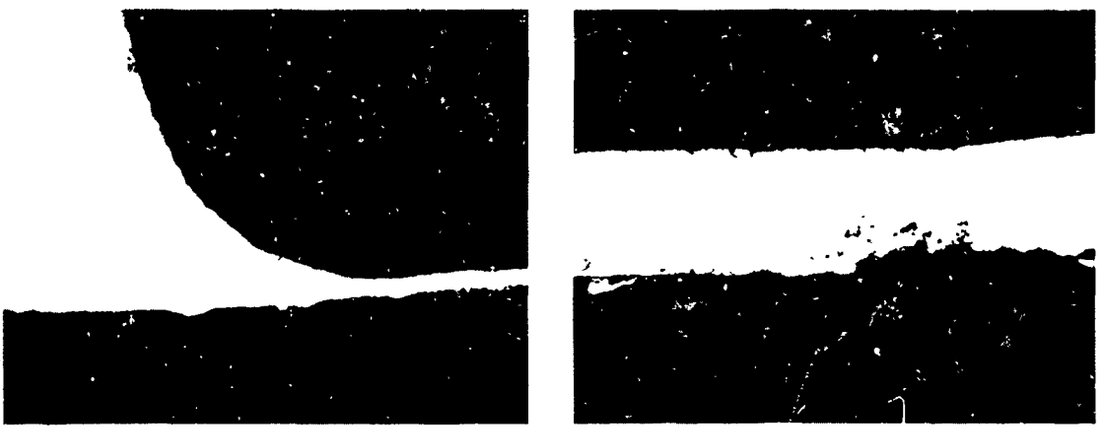

MAG = X75 MAG = X250
1300°F AND 19.1 KSI, FAILED AFTER 187.2 HOURS

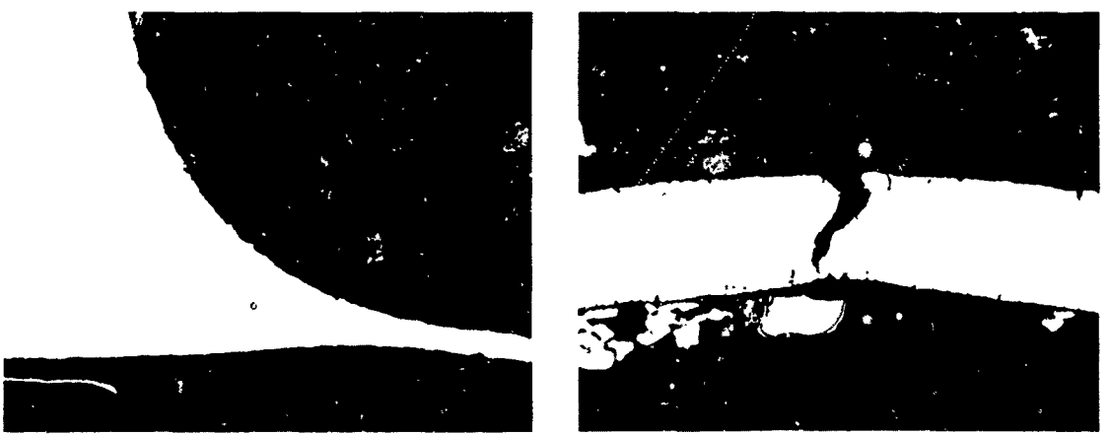

MAG = X75 MAG = X250
1300°F AND 19.1 KSI, FAILED AFTER 385.6 HOURS

NOTE: FIGURES REDUCED TO 60%

Figure 96. Photomicrographs of Hastelloy X Tubes Brazed With Palniro I Brazing Alloy.

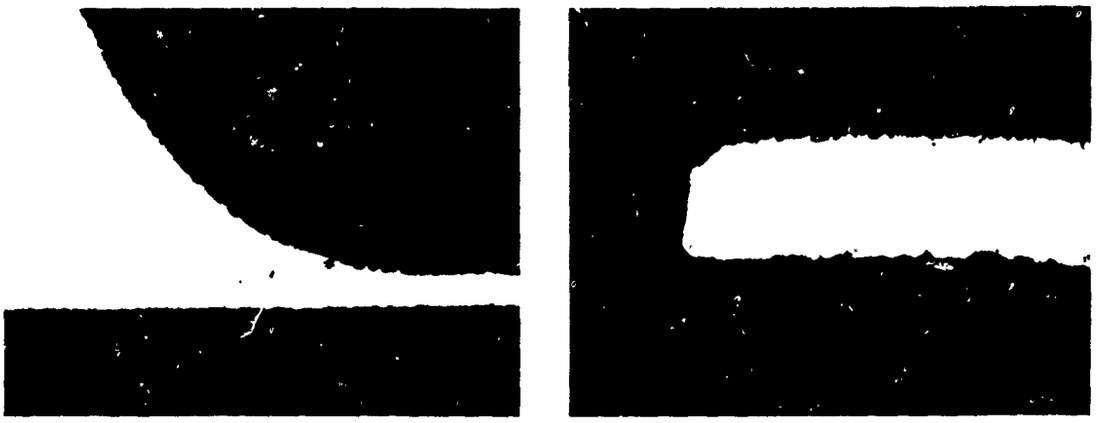

MAG = X75 MAG = X250

1300°F AND 16 KSI, FAILED AFTER 424.7 HOURS

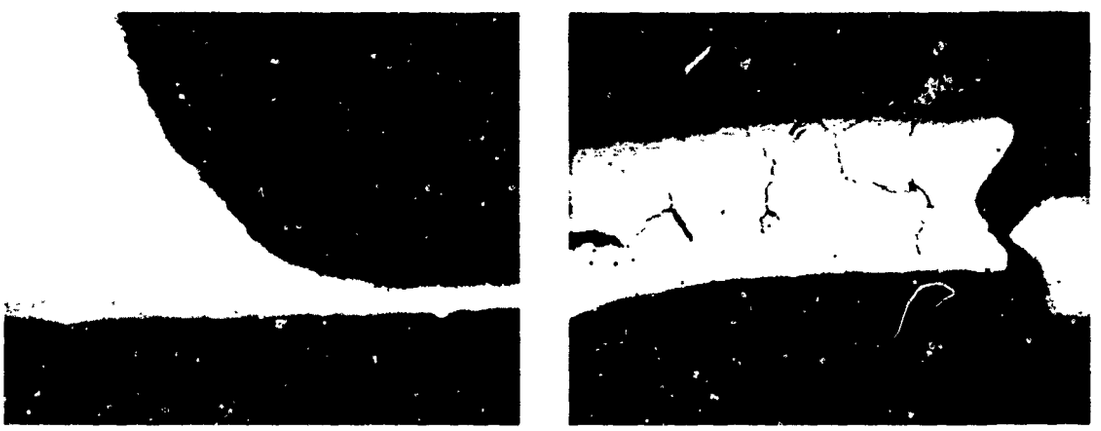

MAG = X75 MAG = X250

1300°F AND 16 KSI, FAILED AFTER 951.4 HOURS

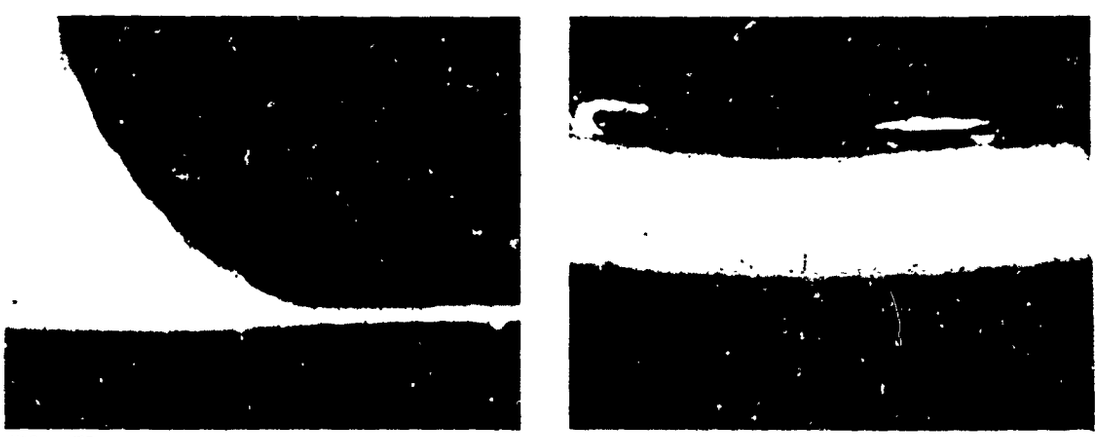

MAG = X75 MAG = X250

1100°F AND 34.7 KSI, FAILED AFTER 1121.0 HOURS

NOTE: FIGURES REDUCED TO 60%.

Figure 97. Photomicrographs of Hastelloy X Tubes Brazed With Palniro I Brazing Alloy.

TABLE XXVIII. HASTELLOY X BRAZED WITH PALNIRO 1, FAILURE AND CORROSION EXAMINATION

Temperature (°F)	Stress (ksi)	Life (hr)	Visual Examination*			Metallographical Examination		Photomicrograph Figure No.
			Failure		Corrosion	Braze Alloy Fillet	Point of Failure	
			Type	Location				
1500	13.9	13.8	P	-2 in.	S	Very light intergranular corrosion	Extensive grain boundary oxidation	94
1500	9.0	114.4	P	J	S	Slight intergranular corrosion	Grain boundary oxidation, some internal oxidation	94
1500	9.0	135.9	P	+1/4	S	Slight intergranular corrosion	Extensive grain boundary oxidation	94
1500	6.5	35.4	P	J	S	Moderate internal oxidation layer	Internal oxidation at interface	
1500	6.5	277	R	-1/2	S	Slight intergranular corrosion	Internal oxidation, porous	95
1500	6.5	341.3	R	J	M	Heavy internal oxidation layer	Internal oxidation, porous	95
1500	4.5	325.8	P	J	M	Slight intergranular corrosion	Internal oxidation, porous	95
1300	20.8	175.2	R	J	S	Some internal oxidation	Internal oxidation at interface	96
1300	19.1	187.2	P	J	M	Very slight internal corrosion	Internal oxidation, porous	96
1300	19.1	385.6	P	-2 in.	M	Very slight internal corrosion	Grain boundary oxidized	96
1300	16.0	424.7	P	+1/4	M	No corrosion	Very little oxidation	97
1300	16.0	951.4	P	+6	M	No corrosion	Extensive grain boundary oxidation	97
1100	34.7	1121	P	+2	S	No corrosion	Slight intergranular oxidation	97

*P = Pinhole leak; R = Tube rupture; J = Braze joint; + = Above J; - = Below J; S = Slight; M = Moderate; H = Heavy

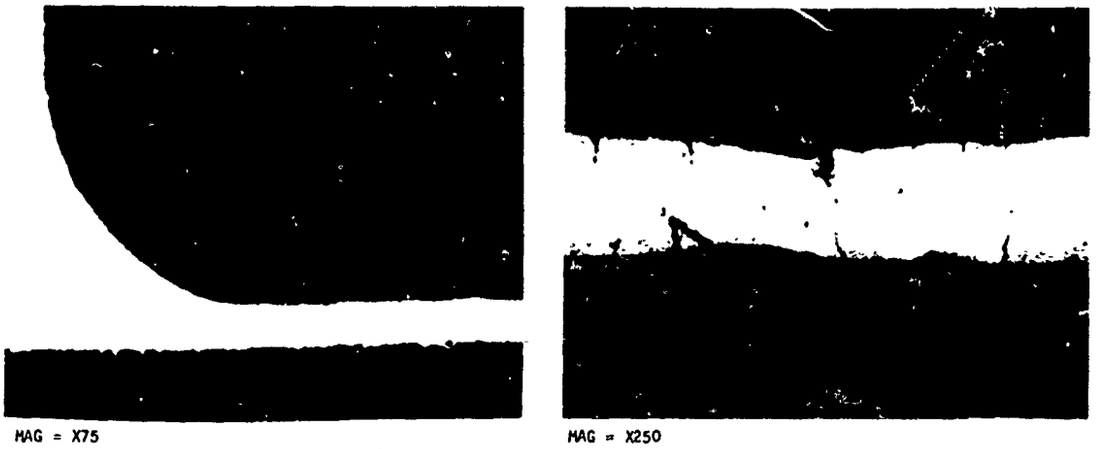

MAG = X75 MAG = X250

1500°F AND 13.9 KSI, FAILED AFTER 28.1 HOURS

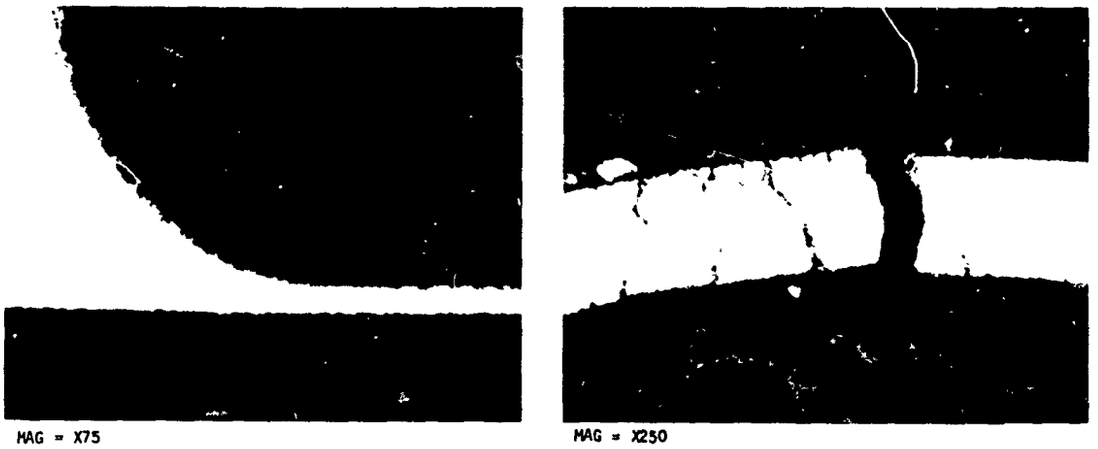

MAG = X75 MAG = X250

1500°F AND 9 KSI, FAILED AFTER 171.4 HOURS

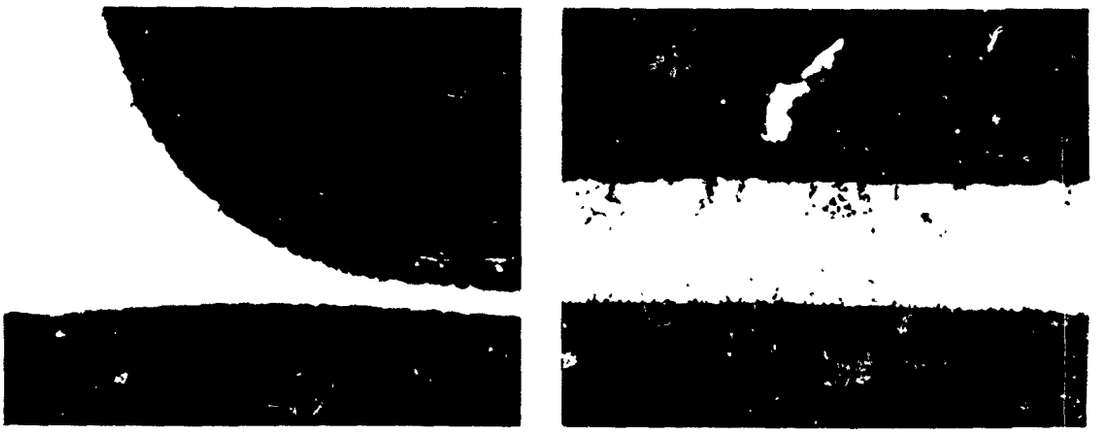

MAG = X75 MAG = X250

1500°F AND 6.5 KSI, FAILED AFTER 156.6 HOURS

NOTE: FIGURES REDUCED TO 60%.

Figure 98. Photomicrographs of Hastelloy X Tubes Brazed With J-8100 Brazing Alloy.

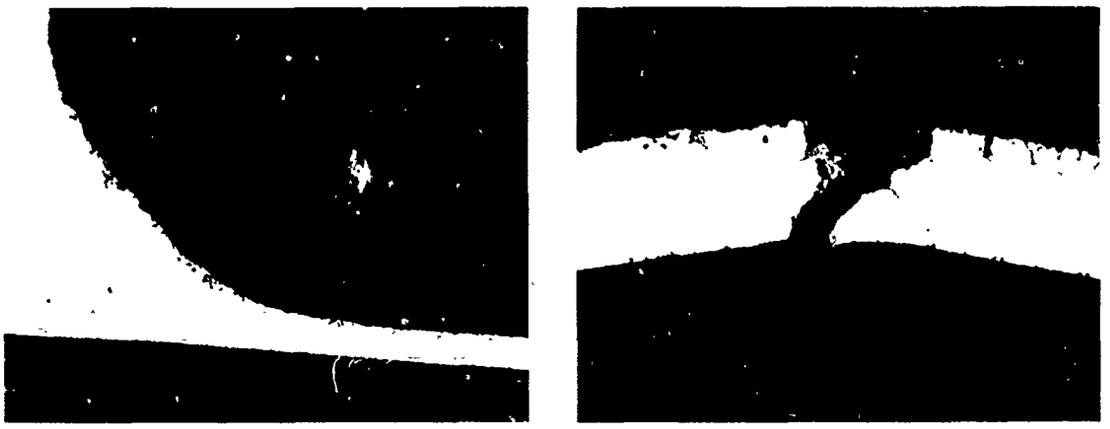

MAG = X75 MAG = X250

1500°F AND 6.5 KSI, FAILED AFTER 141.8 HOURS

MAG = X75 MAG = X250

1500°F AND 4.5 KSI, FAILED AFTER 418.9 HOURS

MAG = X75 MAG = X250

1300°F AND 25 KSI, FAILED AFTER 122.2 HOURS

NOTE: FIGURES REDUCED TO 60%.

Figure 99. Photomicrographs of Hastelloy X Tubes Brazed With J-8100 Brazing Alloy.

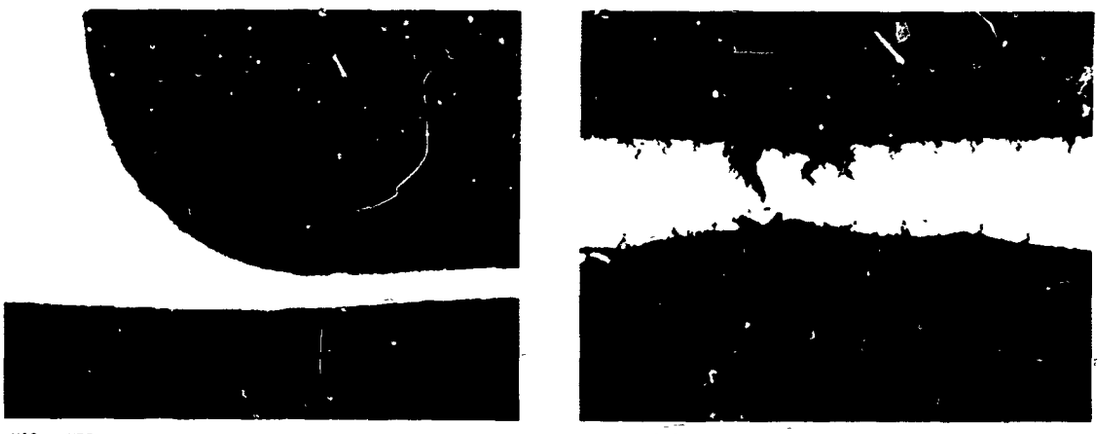

MAG = X75 MAG = X250

1300°F AND 20.8 KSI, FAILED AFTER 204.4 HOURS

MAG = X75 MAG = X250

1300°F AND 20 KSI, FAILED AFTER 344.4 HOURS

MAG = X75 MAG = X250

1300°F AND 20 KSI, FAILED AFTER 991.0 HOURS

NOTE: FIGURES REDUCED TO 60%.

Figure 100. Photomicrographs of Hastelloy X Tubes Brazed With J-8100 Brazing Alloy.

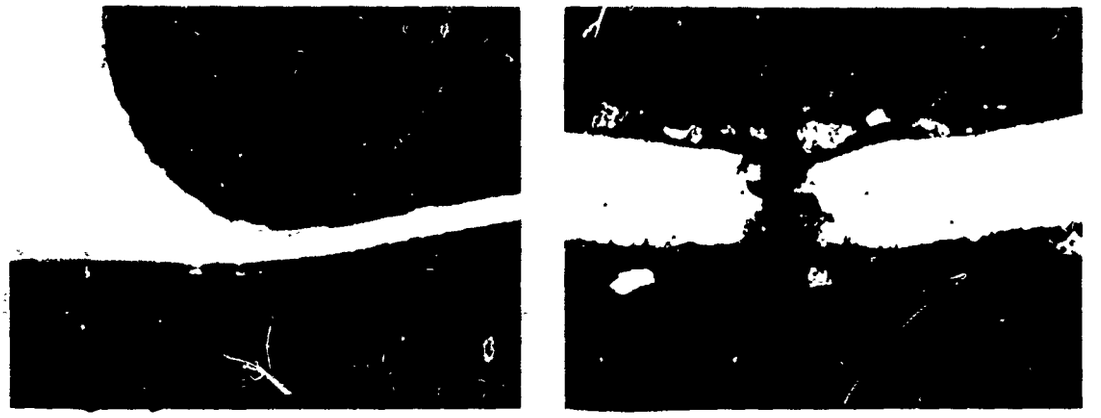

MAG = X75 MAG = X250

1100°F AND 34.7 KSI. FAILED AFTER 364.2 HOURS

MAG = X75 MAG = X250

1100°F AND 34.7 KSI. AFTER 1507.5 HOURS WITHOUT FAILURE

NOTE: FIGURES REDUCED TO 60%.

Figure 101. Photomicrographs of Hastelloy X Tubes Brazed With J-8100 Brazing Alloy.

TABLE XXIX. HASTELLOY X BRAZED WITH J-8100, FAILURE AND CORROSION EXAMINATION

Temperature (°F)	Stress (ksi)	Life (hr)	Visual Examination*			Metallographical Examination		Photomicrograph Figure No.
			Failure		Corrosion	Braze Alloy Fillet	Point of Failure	
			Type	Location				
1500	13.9	28.1	P	-1	S	No corrosion	Intergranular penetration 1/3 way through	98
1500	9.0	171.4	P	-1	M	No corrosion	Intergranular penetration all way through	98
1500	6.5	156.6	P	J	S	No corrosion	Intergranular oxidation, some porosity	98
1500	6.5	141.8	P	-1	M	Slight oxidation	Intergranular penetration all way through	99
1500	4.5	418.9	P	J	M	Slight intergranular oxidation	Some intergranular oxidation	99
1300	25	122.2	P	-1-1/2	S	No corrosion	Intergranular oxidation	99
1300	20.0	204.4	P	-1	S	No corrosion	Intergranular penetration 3/4 way through	100
1300	20.0	344.4	P	-2	M	No corrosion	Intergranular penetration 1/2 way through	100
1300	20.0	991.0	P	-1	M	Slight intergranular attack	Intergranular penetration all way through	100
1100	34.7	364.2	P	-1	S	No corrosion	Intergranular attack , little oxidation	101
1100	34.7	1507.5	No failure		S	No corrosion	Slight surface layer of corrosion products	101

*P = Pinhole leak; R = Tube rupture; J = Braze joint; + = Above J; - = Below J; S = Slight; M = Moderate; H = Heavy

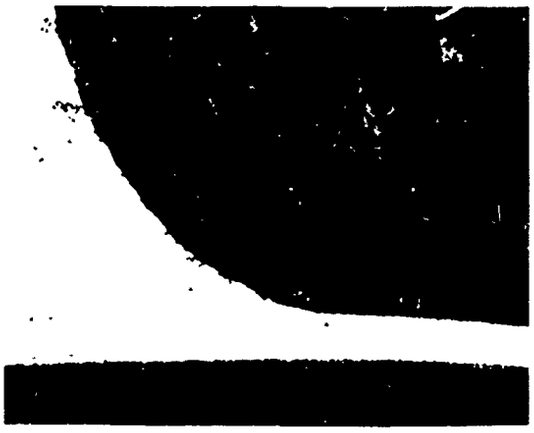

MAG = X75

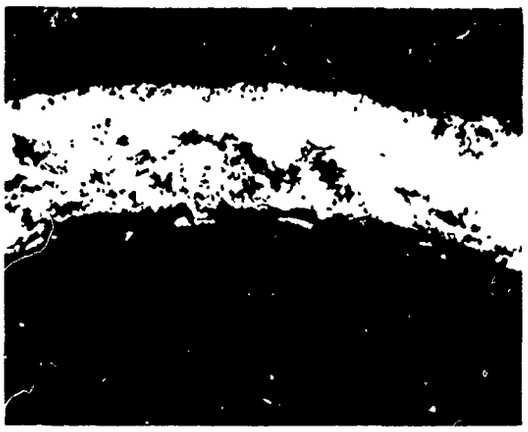

MAG = X250

1500°F AND 8.3 KSI, FAILED AFTER 16.4 HOURS

MAG = X75

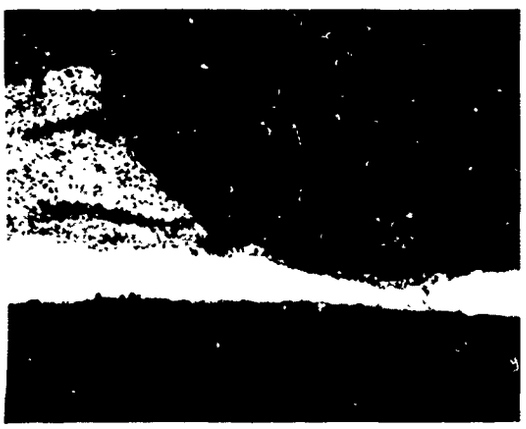

MAG = X250

1500°F AND 2.8 KSI, FAILED AFTER 361.4 HOURS

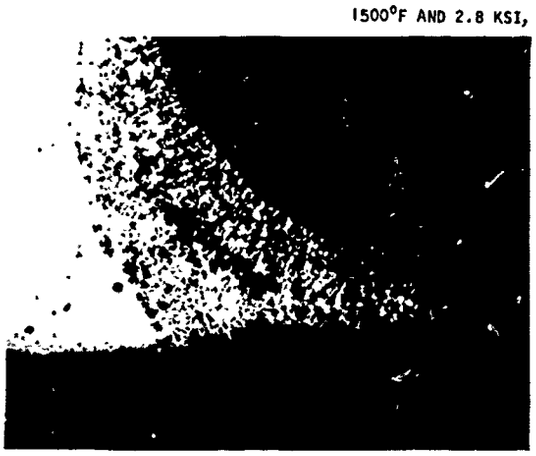

MAG = X75

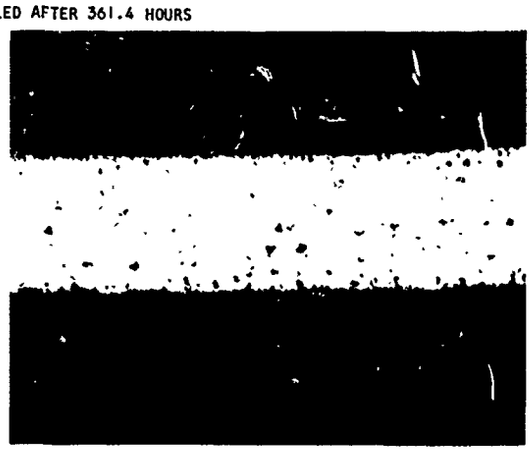

MAG = X250

1500°F AND 1.21 KSI, FAILED AFTER 644.3 HOURS

NOTE: FIGURES REDUCED TO 60%.

Figure 102. Photomicrographs of Incoloy 800 Tubes Brazed With Palniro 7 Brazing Alloy.

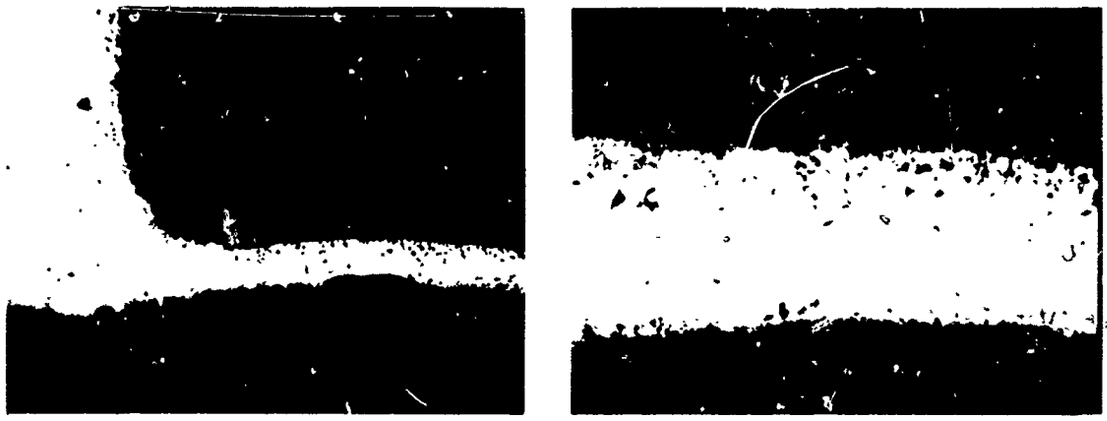

MAG = X75 MAG = X250

1500°F AND 1.2 KSI, AFTER 1501.7 HOURS WITHOUT FAILURE

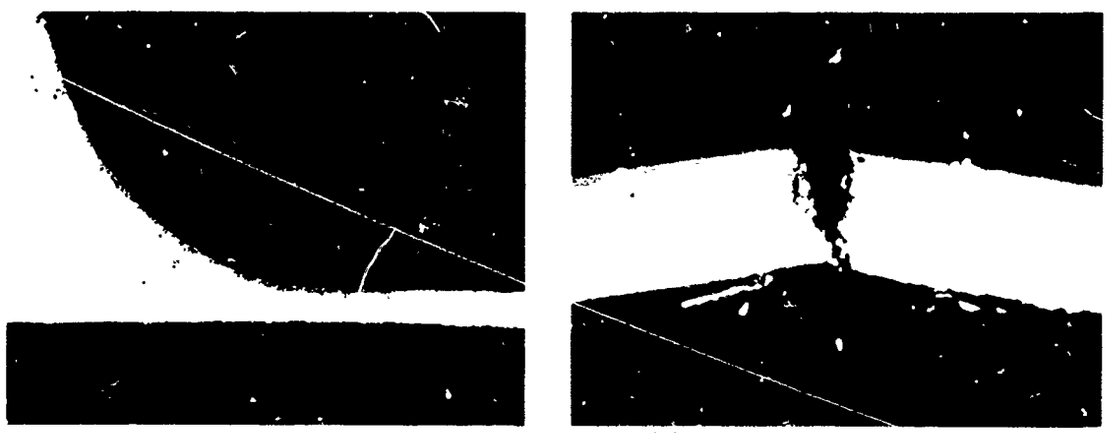

MAG = X75 MAG = X250

1300°F AND 15.3 KSI, FAILED AFTER 35.4 HOURS

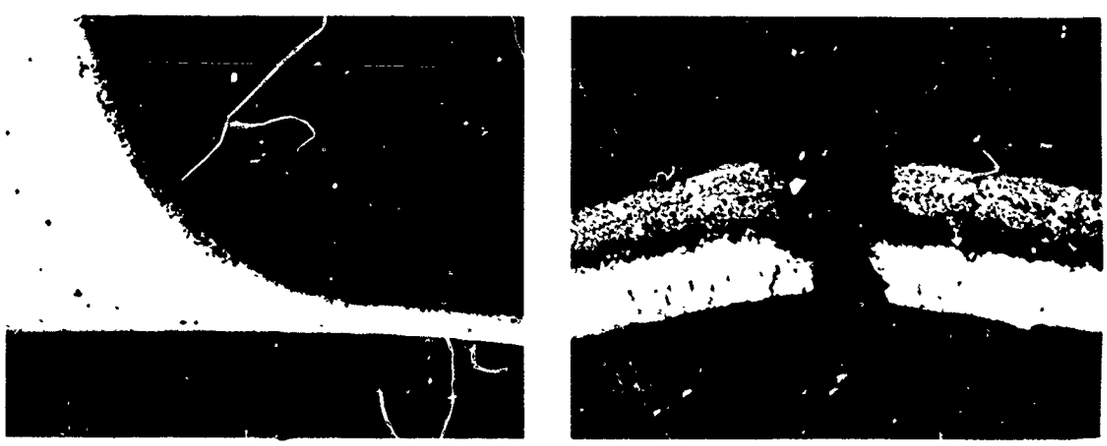

MAG = X75 MAG = X250

1300°F AND 9.5 KSI. FAILED AFTER 201.7 HOURS

NOTE FIGURES REDUCED TO 69%.

Figure 103. Photomicrographs of Incoloy 800 Tubes Brazed With Palniro 7 Brazing Alloy.

MAG = X75

MAG = X250

1300°F AND 6.1 KSI, FAILED AFTER 1103.0 HOURS

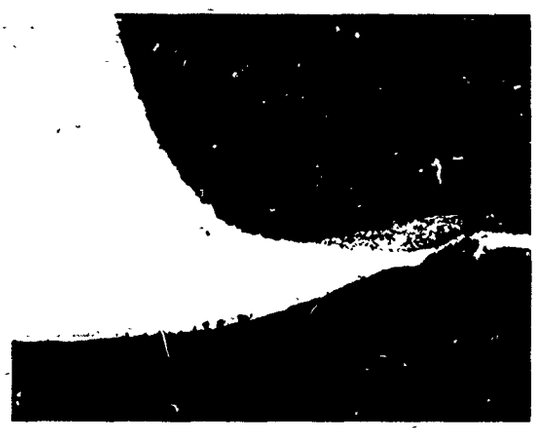

MAG = X75

MAG = X250

1300°F AND 6.1 KSI, FAILED AFTER 490.6

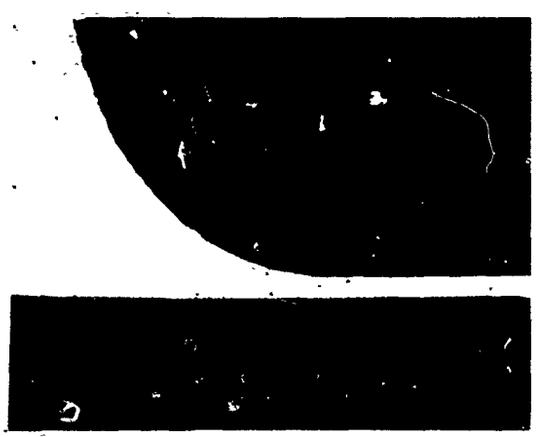

MAG = X75

MAG = X250

1100°F AND 30 KSI, FAILED AFTER 68.2 HOURS

NOTE: FIGURES REDUCED TO 60%.

Figure 104. Photomicrographs of Incoloy 800 Tubes Brazed With Palniro 7 Brazing Alloy.

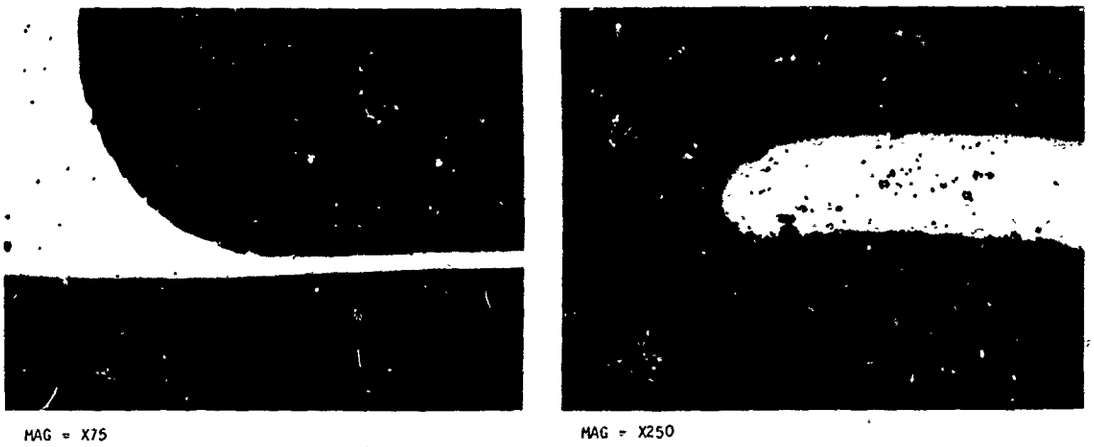

MAG = X75 MAG = X250

1100°F AND 27.8 KSI, FAILED AFTER 314.5 HOURS

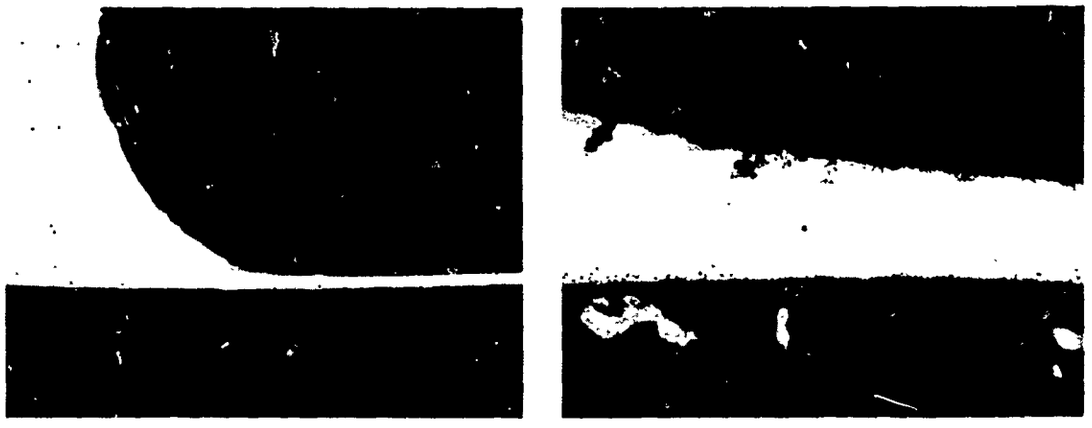

MAG = X75 MAG = X250

1100°F AND 27.8 KSI, FAILED AFTER 147.9 HOURS

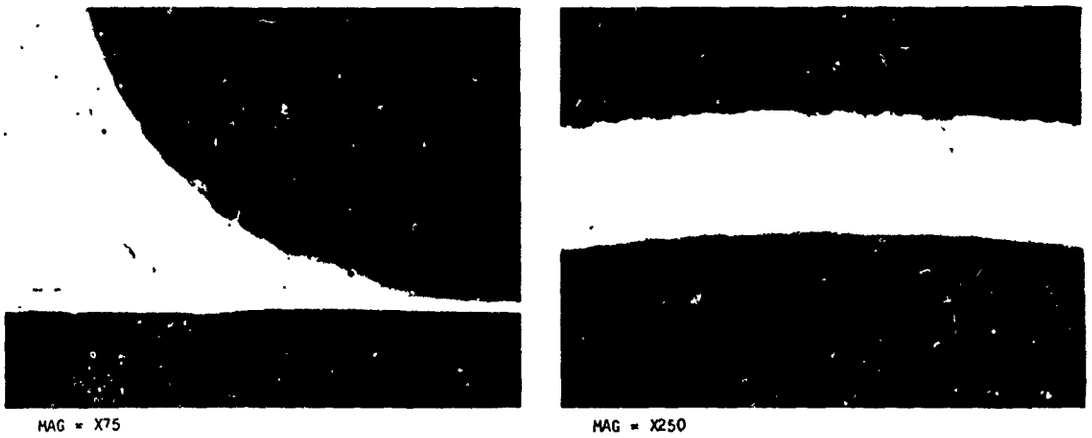

MAG = X75 MAG = X250

1100°F AND 7.2 KSI, AFTER 950.0 HOURS WITHOUT FAILURE

NOTE: FIGURES REDUCED TO 60%.

Figure 105. Photomicrographs of Incoloy 800 Tubes Brazed With Palniro 7 Brazing Alloy.

TABLE XXX. INCOLOY 800 BRAZED WITH PALNIRO 7, FAILURE AND CORROSION EXAMINATION

Temperature (°F)	Stress (ksi)	Life (hr)	Visual Examination*			Metallographical Examination		Photomicrograph Figure No.
			Failure		Corrosion	Braze Alloy Fillet	Point of Failure	
			Type	Location				
1500	8.3	16.4	P	J	S	Slight intergranular corrosion	Oxidized through, porous	102
1500	2.8	361.4	P	+1/4	H	Heavy corrosion	Oxidized through at fillet/tube interface	102
1500	1.2	644.3	R	J	H	Extensive oxidation	Oxidized through, porous	102
1500	1.2	1501.7	No failure		H	Slight intergranular corrosion	Oxidized through, porous	103
1300	15.3	35.4	P	+1-1/4	S	Slight intergranular corrosion	No general penetration, oxidized fissure	103
1300	9.5	201.7	P	J	M	Slight intergranular corrosion	Corrosion layer 1-1/2 mil intergranular penetration	103
1300	6.1	1103	P	J	M	Heavy corrosion	Extensive internal oxidation	104
1300	6.1	490.6	P	J	M	Slight intergranular corrosion	Extensive internal oxidation	104
1100	30	68.2	R	-1	S	No evidence of oxidation	No evidence of oxidation	104
1100	27.8	314.5	R	-1/2	S	No corrosion	Some internal pitting	105
1100	27.8	147.9	R	-1/2	S	No corrosion	No evidence of oxidation	105
1100	7.2**	950.0	No failure		S	No corrosion	No evidence of oxidation	105

*P = Pinhole leak; R = Tube rupture; J = Braze joint; + = Above J; - = Below J; S = Slight; M = Moderate; H = Heavy

**Pressure inadvertently set low by a factor of 3.4.

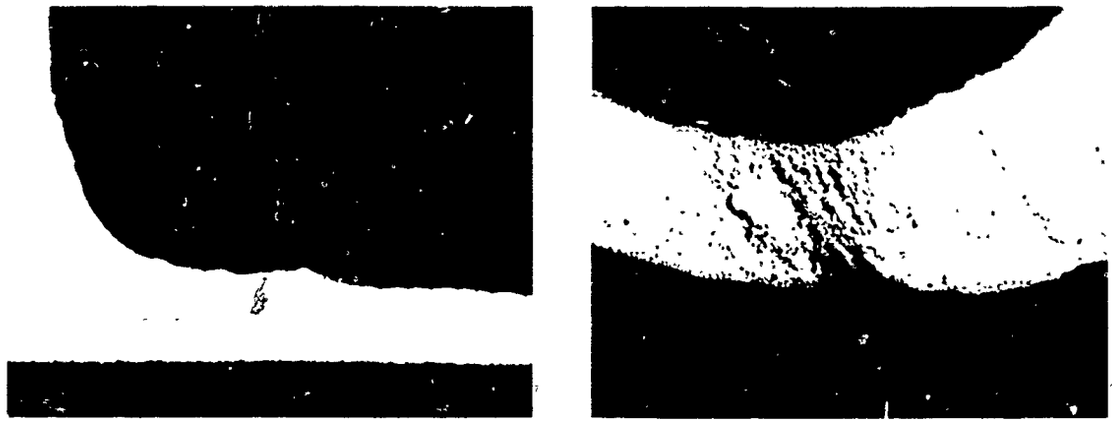

MAG = X75 MAG = X250

1500°F AND 8.3 KSI, FAILED AFTER 29.8 HOURS

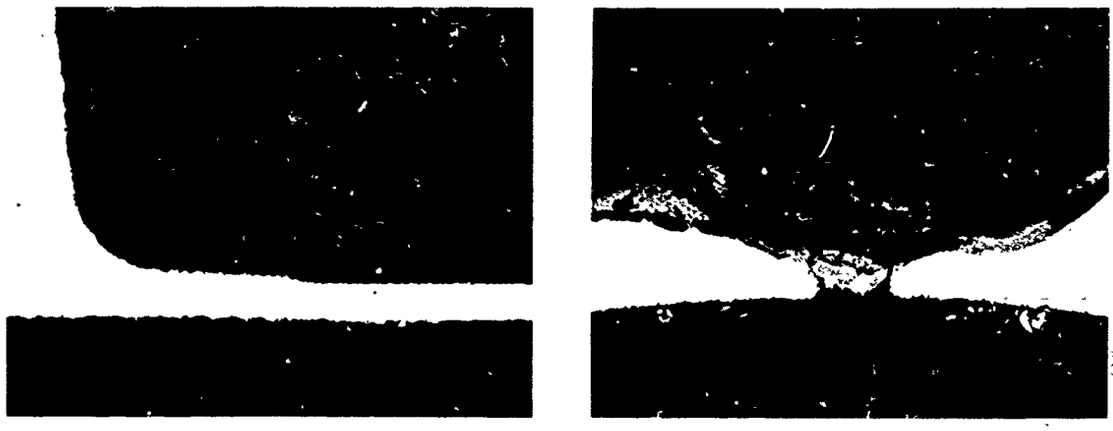

MAG = X75 MAG = X250

1500°F AND 2.8 KSI, FAILED AFTER 21.4 HOURS

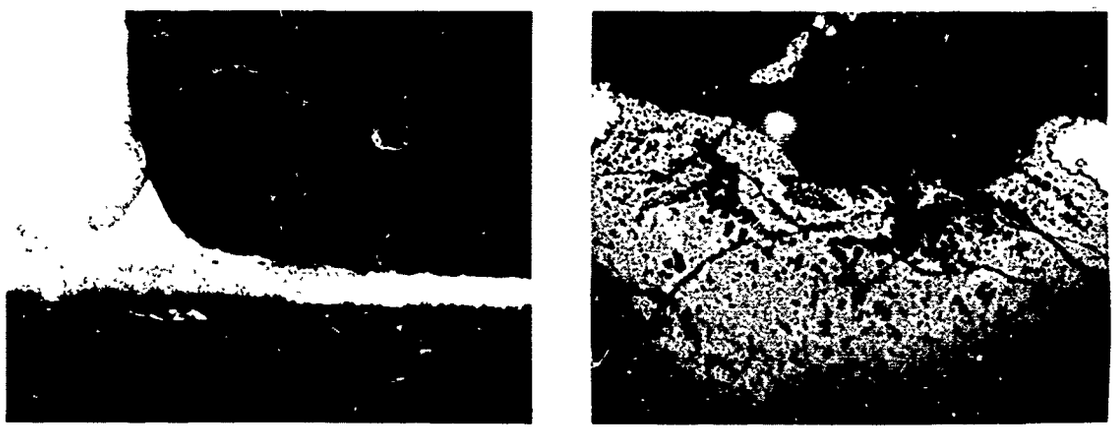

MAG = X75 MAG = X250

1500°F AND 2.8 KSI, FAILED AFTER 222.6 HOURS

NOTE: FIGURES REDUCED TO 60%.

Figure 106. Photomicrographs of Incoloy 800 Tubes Brazed With Coast Metals 50B Brazing Alloy.

MAG = X75 MAG = X250

1500°F AND 2.8 KSI, FAILED AFTER 502.0 HOURS

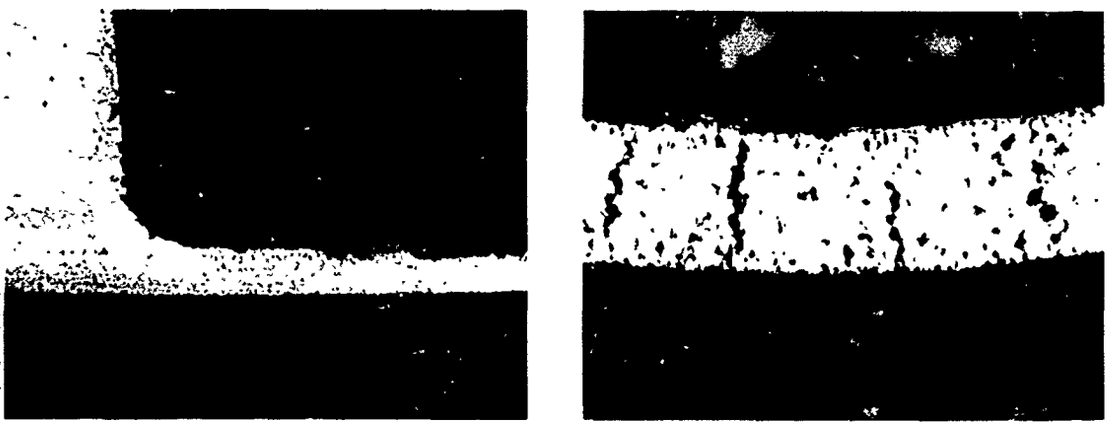

MAG = X75 MAG = X250

1500°F AND 2.8 KSI, FAILED AFTER 812.0 HOURS

MAG = X75 MAG = X250

1500°F AND 1.73 KSI, FAILED AFTER 346.5 HOURS

NOTE: FIGURES REDUCED TO 60%.

Figure 107. Photomicrographs of Incoloy 800 Tubes Brazed With Coast Metals 50B Brazing Alloy.

MAG = X75 MAG = X250

1500°F AND 1.73 KSI, AFTER 1172.4 HOURS WITHOUT FAILURE

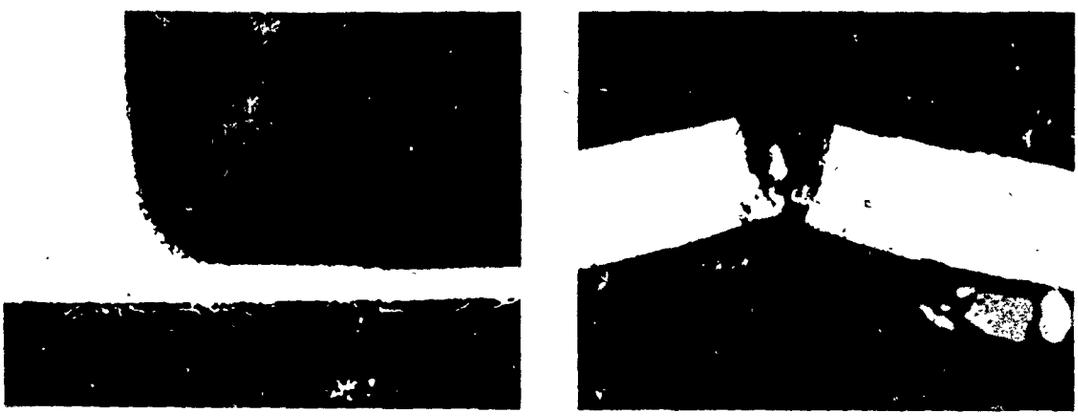

MAG = X75 MAG = X250

1300°F AND 15.3 KSI, FAILED AFTER 33.6 HOURS

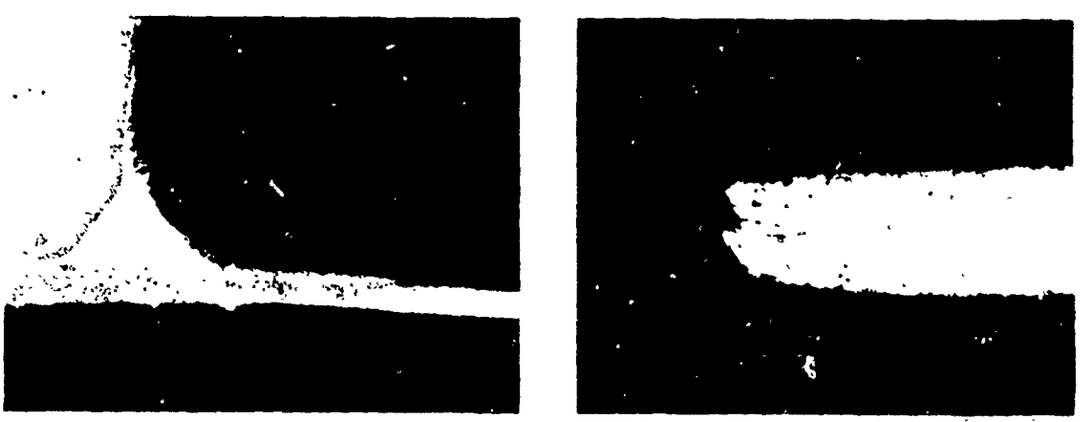

MAG = X75 MAG = X250

1300°F AND 9.5 KSI, FAILED AFTER 217.5 HOURS

NOTE: FIGURES REDUCED TO 60%.

Figure 108. Photomicrographs of Incoloy 800 Tubes Brazed With Coast Metals 50B Brazing Alloy.

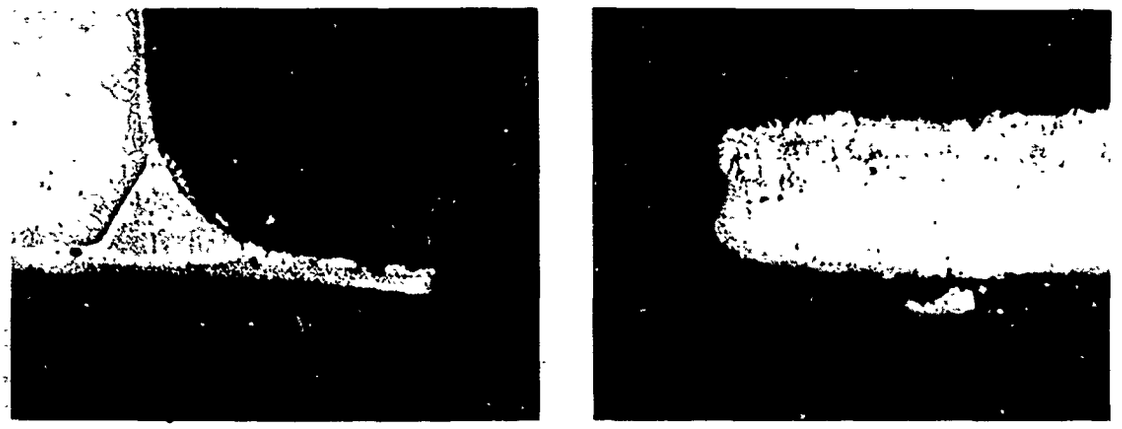

MAG = X75 MAG = X250
1300°F AND 6.1 KSI, FAILED AFTER 1081.5 HOURS

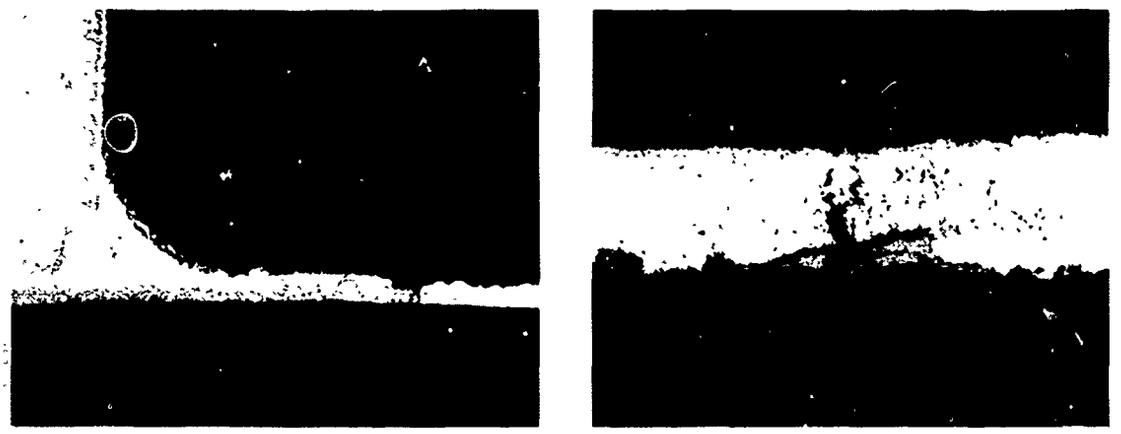

MAG = X75 MAG = X250
1300°F AND 6.1 KSI, FAILED AFTER 740.1 HOURS

MAG = X75 MAG = X250
1100°F AND 30 KSI, FAILED AFTER 11.6 HOURS

NOTE: FIGURES REDUCED TO 60%.

Figure 109. Photomicrographs of Incoloy 800 Tubes Brazed With Coast Metals 50B Brazing Alloy.

MAG = X75 MAG = X250

1100°F AND 30 KSI, FAILED AFTER 43.4 HOURS

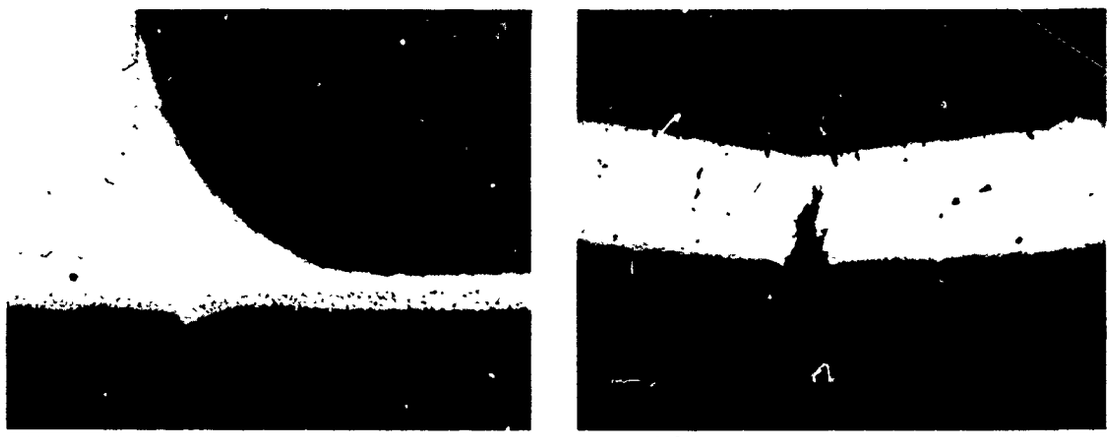

MAG = X75 MAG = X250

1100°F AND 27.8 KSI, FAILED AFTER 420.2 HOURS

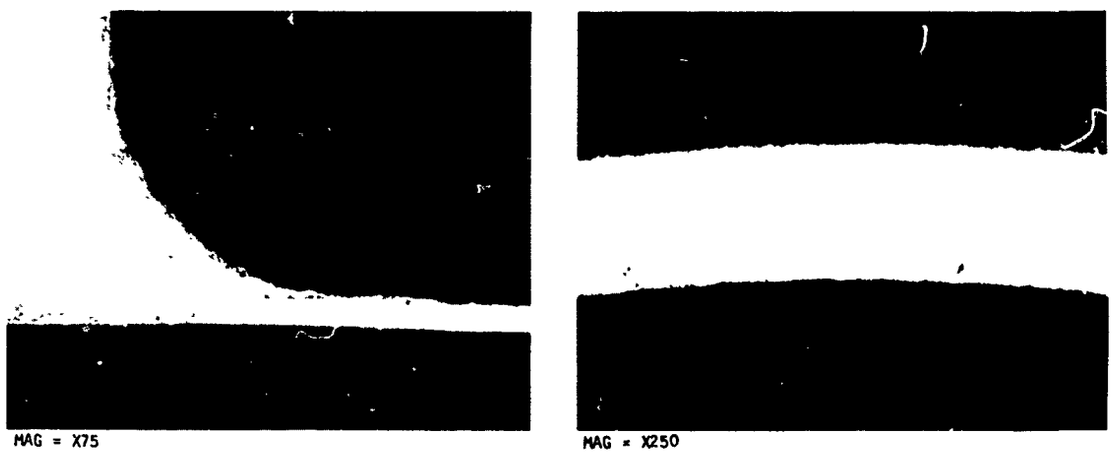

MAG = X75 MAG = X250

1100°F AND 7.2 KSI, AFTER 1100.0 HOURS WITHOUT FAILURE

NOTE: FIGURES REDUCED TO 60%.

Figure 110. Photomicrographs of Incoloy 800 Tubes Brazed With Coast Metals 50B Brazing Alloy.

TABLE XXXI. INCOLOY 800 BRAZED WITH COAST METALS 50B, FAILURE AND CORROSION EXAMINATION

Temperature. (°F)	Stress (ksi)	Life (hr)	Visual Examination*			Metallographical Examination		Photomicrograph Figure No.
			Failure		Corrosion	Braze Alloy Fillet	Point of Failure	
			Type	Location				
1500	8.3	29.8	P	+1	S	No corrosion	Oxidized through, porous	106
1500	2.8	21.4	P	+1	S	No corrosion	Intense localized oxidation	106
1500	2.8	222.6	P	-3	M	No corrosion	Intense localized oxidation	106
1500	2.8	502	P	+1/2	M	Slight intergranular penetration	Internal oxidation, porous	107
1500	2.8	812	P	±1	M	Slight corrosion	Internal oxidation, porous	107
1500	1.73	346.5	P	J	M	Slight corrosion	Slight internal oxidation	107
1500	1.73	1177.4	No failure		H	Pitted	Slight internal oxidation	108
1300	15.3	33.6	P	-1/2	S	Slight corrosion	No general penetration, oxidized fissure	108
1300	9.5	217.5	R	-1-1/2	M	No corrosion	Slight internal oxidation, porous	108
1300	6.1	1081.5	R	J	M	Slight corrosion	Internal oxidation, porous	109
1300	6.1	740.1	P	J	M	Slight corrosion	Internal oxidation, porous	109
1100	30	11.6	P	-3	S	No corrosion	Slight internal oxidation, porous	109
1100	30	43.4	P	-1 -2	S	No corrosion	Slight internal oxidation, porous	110
1100	27.8	420.2	P	-1-1/2	S	No corrosion	Slight internal oxidation, porous	110
1100	7.2**	1100	No failure		S	No corrosion	No evidence of oxidation	110

*P = Pinhole leak; R = Tube rupture; J = Braze joint; + = Above J; - = Below J; S = Slight; M = Moderate; H = Heavy

**Pressure inadvertently set low by a factor of 3.4.

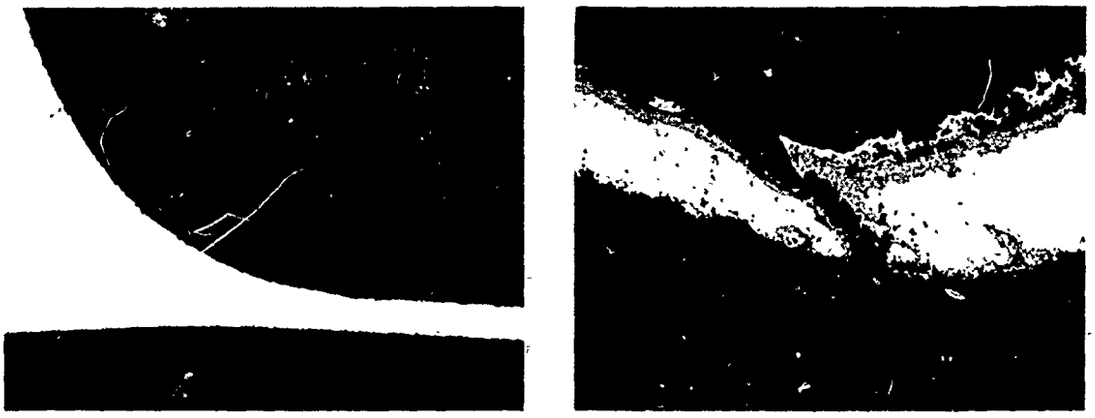

MAG = X75 MAG = X250

1500°F AND 9.2 KSI, FAILED AFTER 31.4 HOURS

MAG = X75 MAG = X250

1500°F AND 9.2 KSI, FAILED AFTER 47.1 HOURS

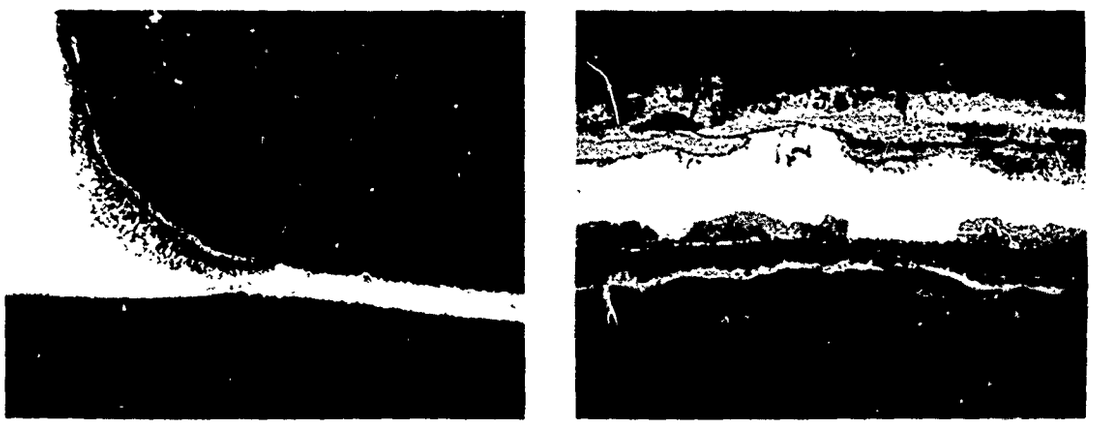

MAG = X75 MAG = X250

1500°F AND 5.0 KSI, FAILED AFTER 129.4 HOURS

NOTE: FIGURES REDUCED TO 60%.

Figure 111. Photomicrographs of Type 347 Stainless Steel Tubes Brazed With Palniro 7 Brazing Alloy.

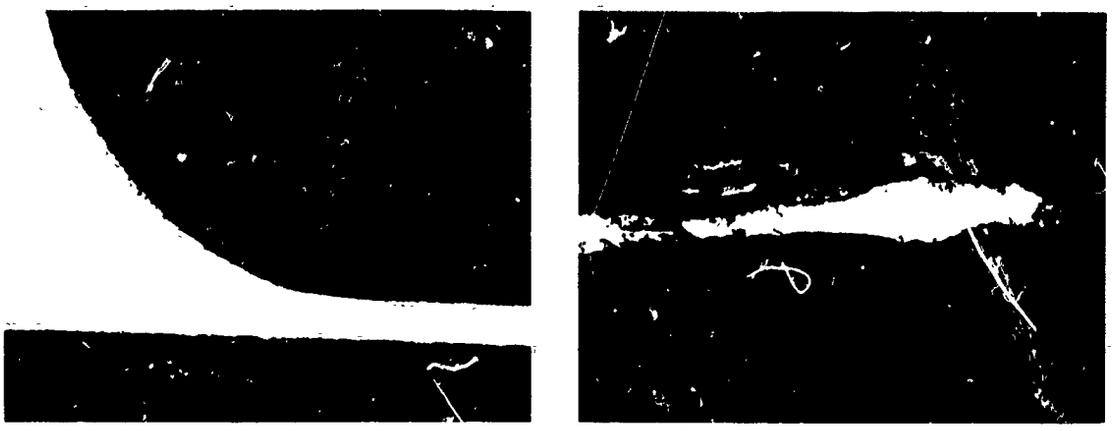

MAG = X75 MAG = X250

1500°F AND 3.0 KSI. FAILED AFTER 6.8 HOURS

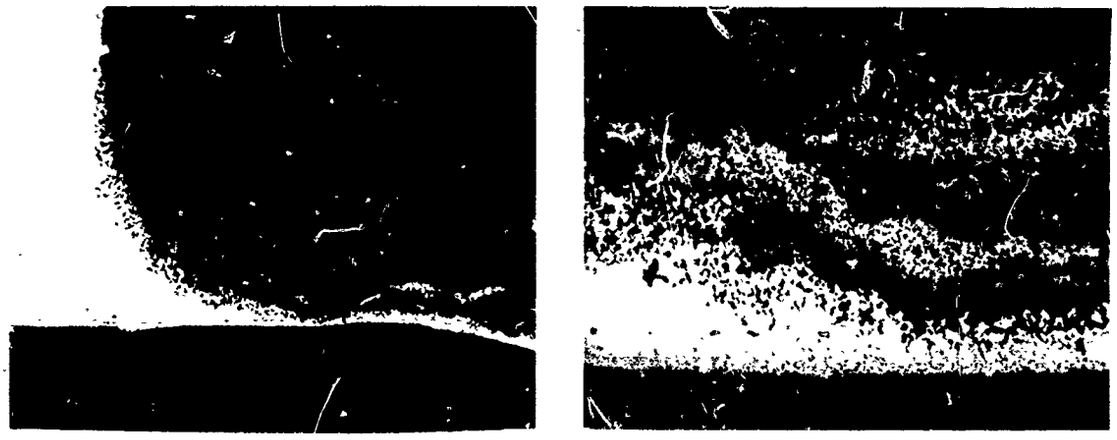

MAG = X75 MAG = X250

1500°F AND 3.0 KSI. FAILED AFTER 154.4 HOURS

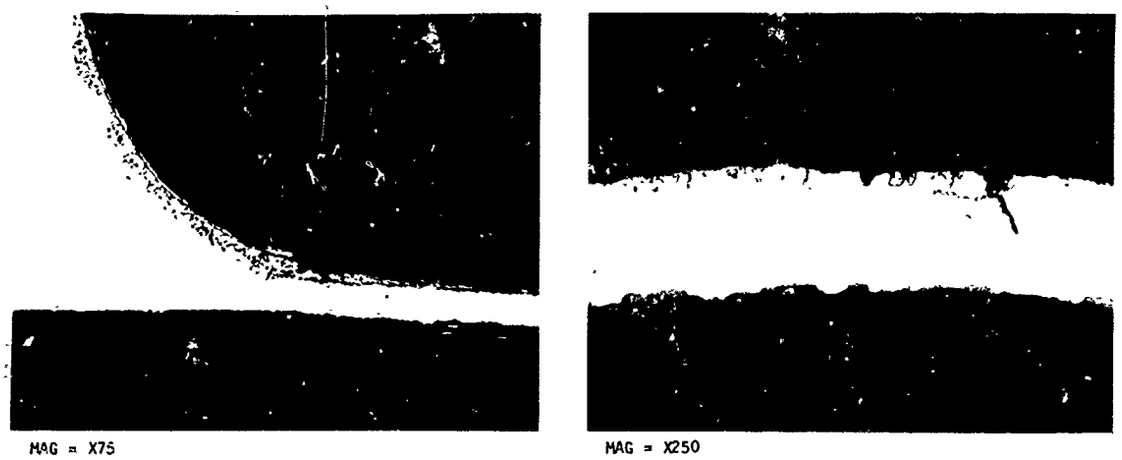

MAG = X75 MAG = X250

1300°F AND 13.9 KSI. FAILED AFTER 104.1 HOURS

NOTE: FIGURES REDUCED TO 60%.

Figure 112. Photomicrographs of Type 347 Stainless Steel Tubes Brazed Wit' Palniro 7 Brazing Alloy.

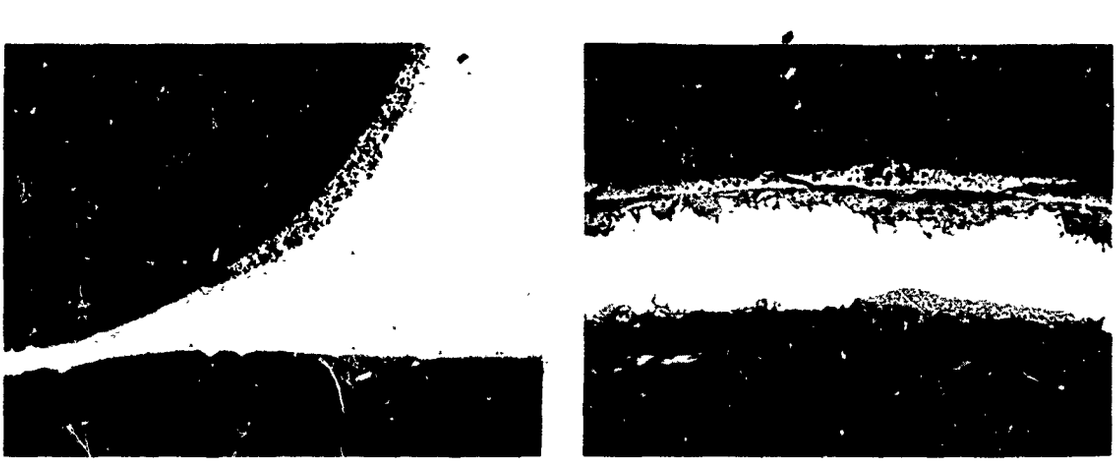

MAG = X75 MAG = X250

1300°F AND 10 KSI, FAILED AFTER 608.7 HOURS

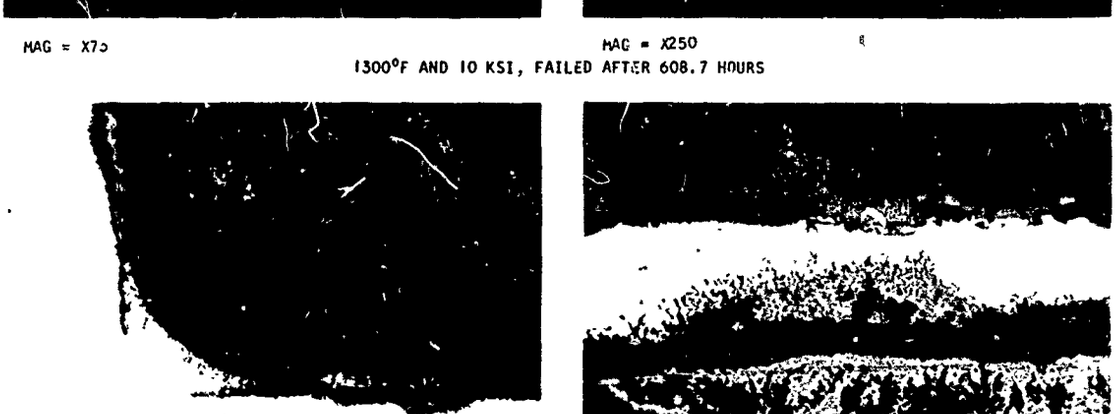

MAG = X75 MAG = X250

1300°F AND 8.0 KSI, FAILED AFTER 486.4 HOURS

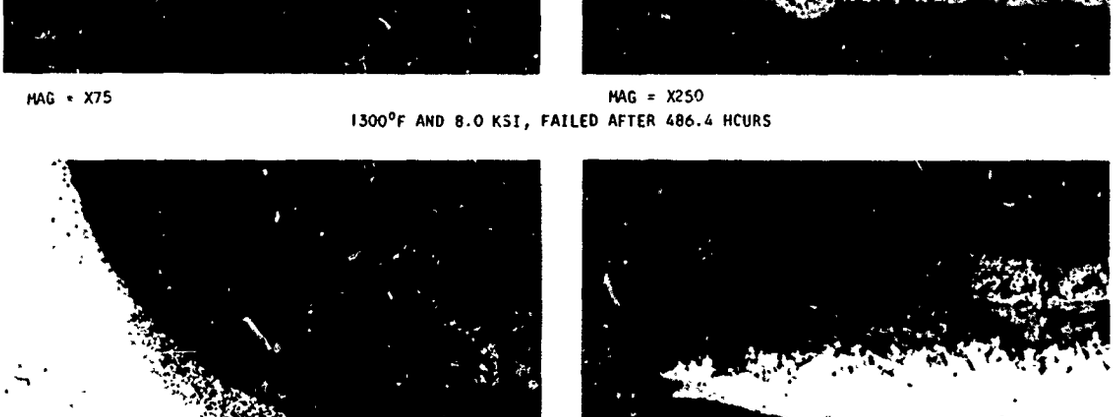

MAG = X75 MAG = X250

1300°F AND 8.0 KSI, FAILED AFTER 465.4 HOURS

NOTE: FIGURES REDUCED TO 60%.

Figure 113. Photomicrographs of Type 347 Stainless Steel Tubes Brazed With Palniro 7 Brazing Alloy.

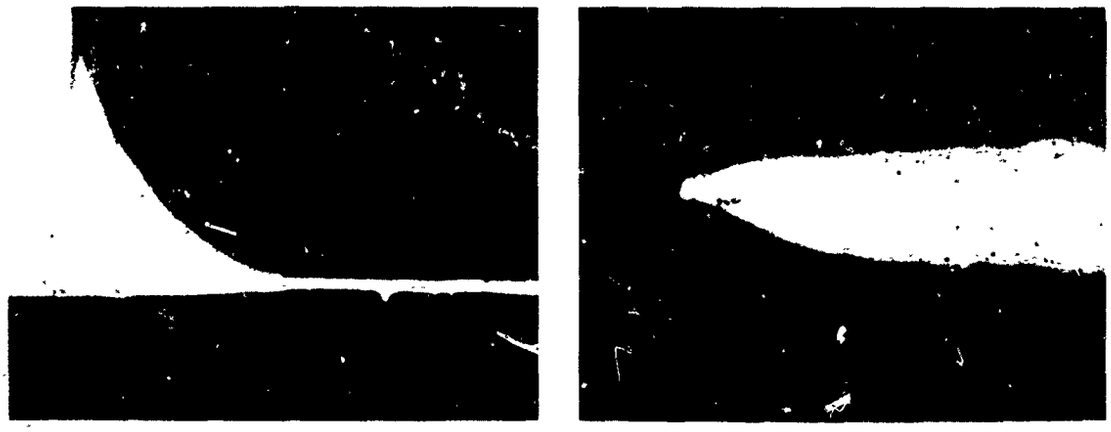

MAG = X75 MAG = X250

1100°F AND 35 KSI, FAILED AFTER 57.2 HOURS

MAG = X75 MAG = X250

1100°F AND 30 KSI, FAILED AFTER 250.1 HOURS

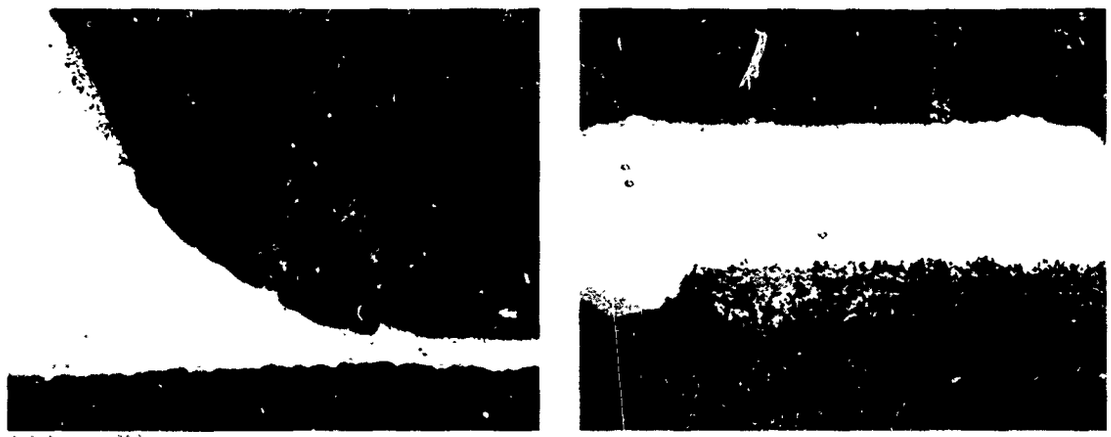

MAG = X75 MAG = X250

1100°F AND 26.9 KSI, FAILED AFTER 1238.7 HOURS

NOTE: FIGURES REDUCED TO 60%.

Figure 114. Photomicrographs of Type 347 Stainless Steel Tubes Brazed With Palniro 7 Brazing Alloy.

TABLE XXXII. TYPE 347 STAINLESS STEEL BRAZED WITH PALNIRO 7, FAILURE AND CORROSION EXAMINATION

Temperature (°F)	Stress (ksi)	Life (hr)	Visual Examination*			Metallographical Examination		Photomicrograph Figure No.
			Failure		Corrosion	Braze Alloy Fillet	Point of Failure	
			Type	Location				
1500	9.2	31.4	P	-1	H	No intergranular corrosion	Heavy oxide layer 1-1/2 mils thick, some intergranular oxidation	111
1500	9.2	47.1	P	-1	H	No corrosion	Slight oxide layer, oxidized fissure	111
1500	5.0	129.4	P	J	H	Heavy internal oxidation	Heavy oxide layer 2 mils thick	111
1500	3.0	6.8	R	-1	H	Slight intergranular oxidation	Oxide layer, almost no metal remaining	112
1500	3.0	154.4	P	J	H	Heavy internal oxidation	Heavy oxide layer 8 mils thick, oxidized all way through tube wall	112
1300	13.9	104.1	P	+1/2	M	Moderate intergranular oxide layer	Deep intergranular penetration	112
1300	10.0	608.7	P	J	H	Heavy intergranular oxide layer	Heavy oxide layer 2 mils thick	113
1300	8.0	486.4	P	-1/4	H	Heavy oxide layer, particularly at interface	Heavy oxide layer, metal 1.0 mil thick	113
1300	8.0	465.4	R	+1	H	Heavy oxide layer, particularly at interface	Heavy oxide layer, metal 0.5 mil thick	113
1100	35	57.2	R	±1	S	No corrosion	Metal thinning, slight corrosion	114
1100	30	250.1	P	-2	S	No corrosion	Slight oxide layer	114
1100	26.9	1238.7	P	+1/4	M	Some intergranular corrosion	Oxide layer 1.0 mil thick	114
1100	26.9	461	P	J	M	No corrosion	Heavy oxide layer, complete penetration	-

*P = Pinhole leak; R = Tube rupture; J = Braze joint; + = Above J; - = Below J; S = Slight; M = Moderate; H = Heavy

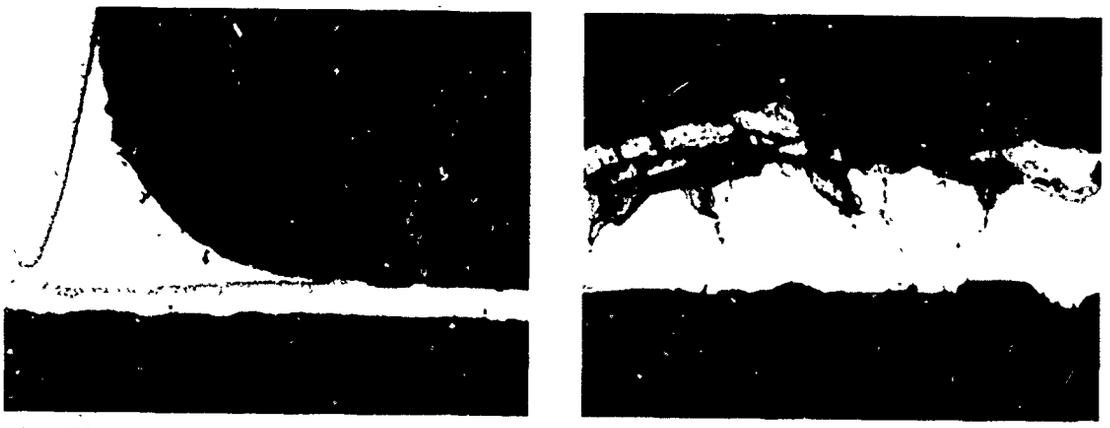

MAG = X75 MAG = X250

1500°F AND 9.2 KSI, FAILED AFTER 35.0 HOURS

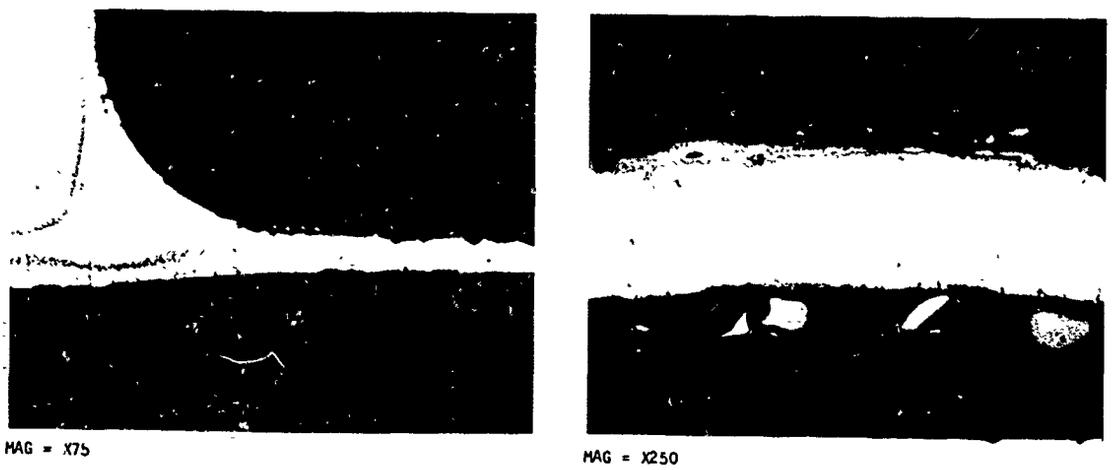

MAG = X75 MAG = X250

1500°F AND 9.2 KSI, FAILED AFTER 125.1 HOURS

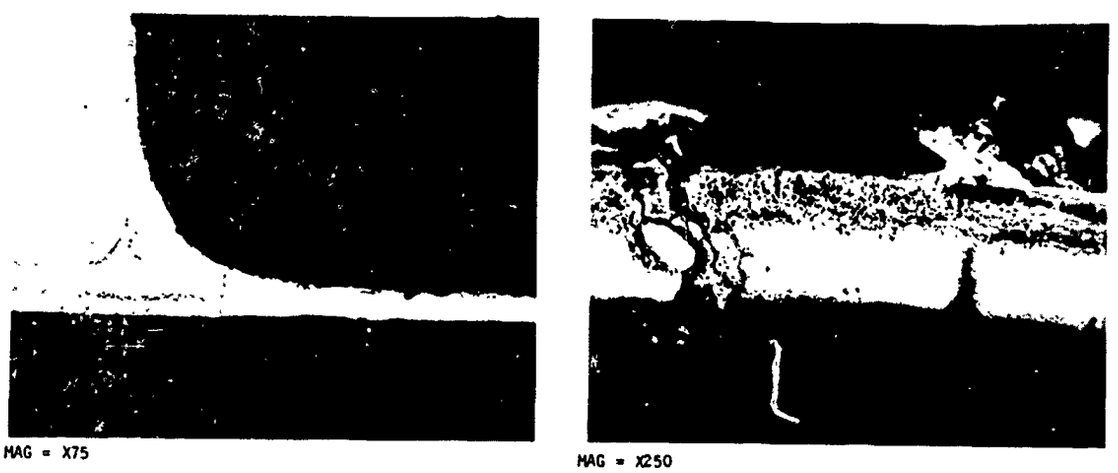

MAG = X75 MAG = X250

1500°F AND 5.0 KSI, FAILED AFTER 170.2 HOURS

NOTE: FIGURES REDUCED TO 60%.

Figure 115. Photomicrographs of Type 347 Stainless Steel Tubes Brazed With Nicrobraz 135 Brazing Alloy.

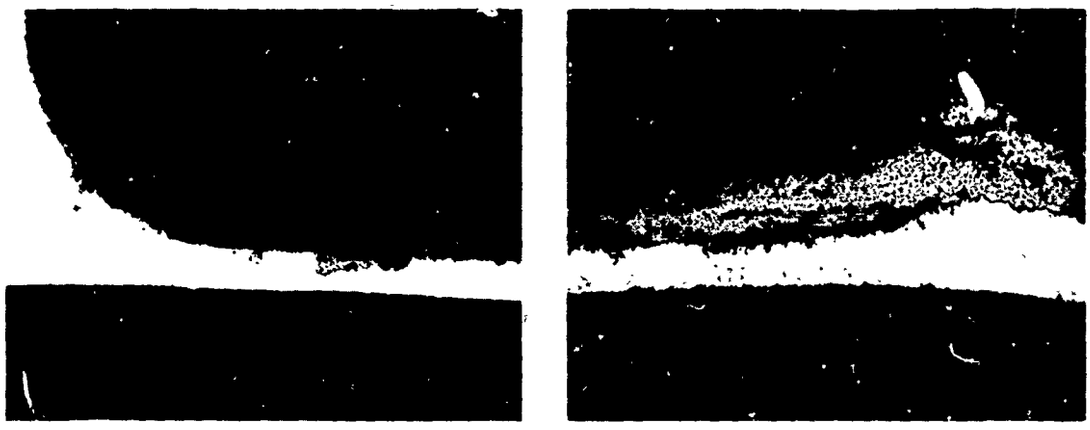

MAG = X75 MAG = X250
1500°F AND 3.0 KSI, FAILED AFTER 17.4 HOURS

MAG = X75 MAG = X250
1300°F AND 13.9 KSI, FAILED AFTER 82.7 HOURS

MAG = X75 MAG = X250
1300°F AND 13.9 KSI, FAILED AFTER 107.7 HOURS

NOTE: FIGURES REDUCED TO 60%.

Figure 116. Photomicrographs of Type 347 Stainless Steel Tubes Brazed With Nicrobraz 135 Brazing Alloy.

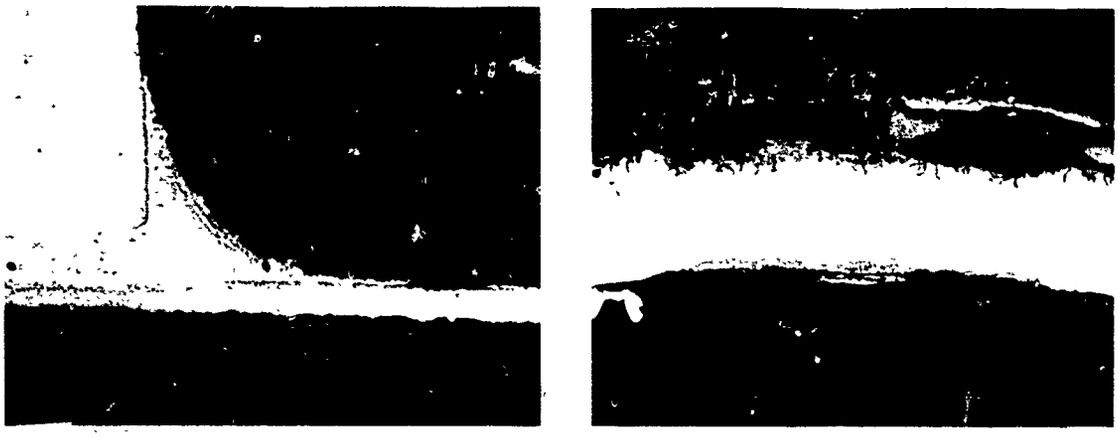

MAG - X75 MAG - X250

1300°F AND 10.0 KSI, FAILED AFTER 441.2 HOURS

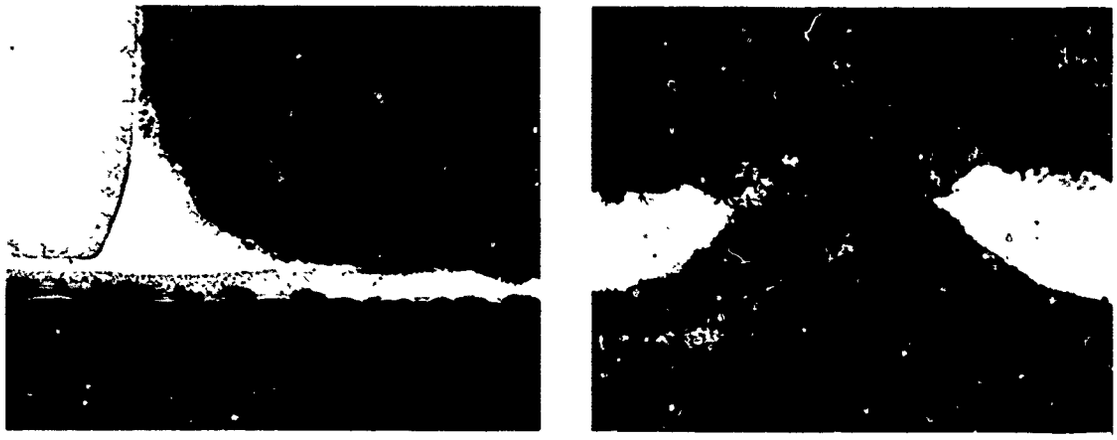

MAG = X75 MAG = X250

1300°F AND 8.0 KSI, FAILED AFTER 676.7 HOURS

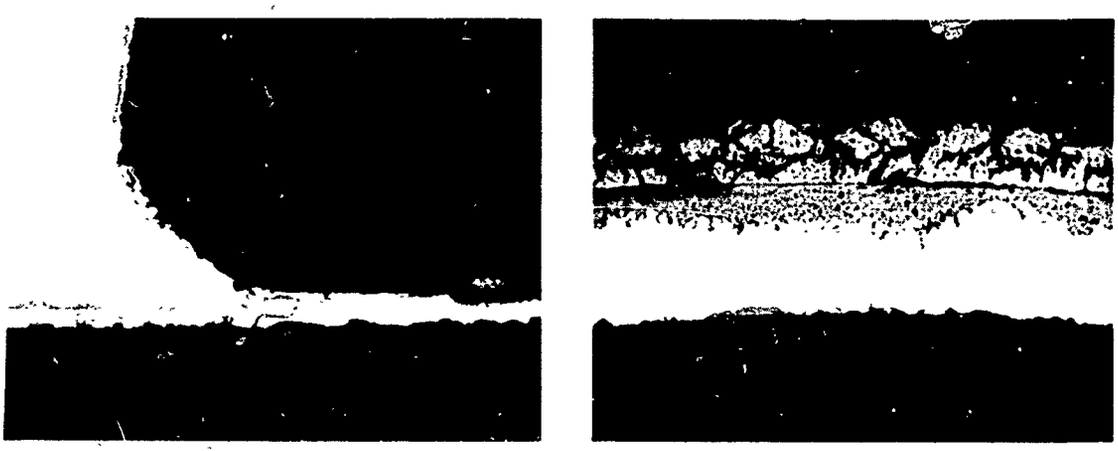

MAG = X75 MAG = X250

1300°F AND 8.0 KSI, FAILED AFTER 578.5 HOURS

NOTE: FIGURES REDUCED TO 60%.

Figure 117. Photomicrographs of Type 347 Stainless Steel Tubes Brazed With Nicrobraz 135 Brazing Alloy.

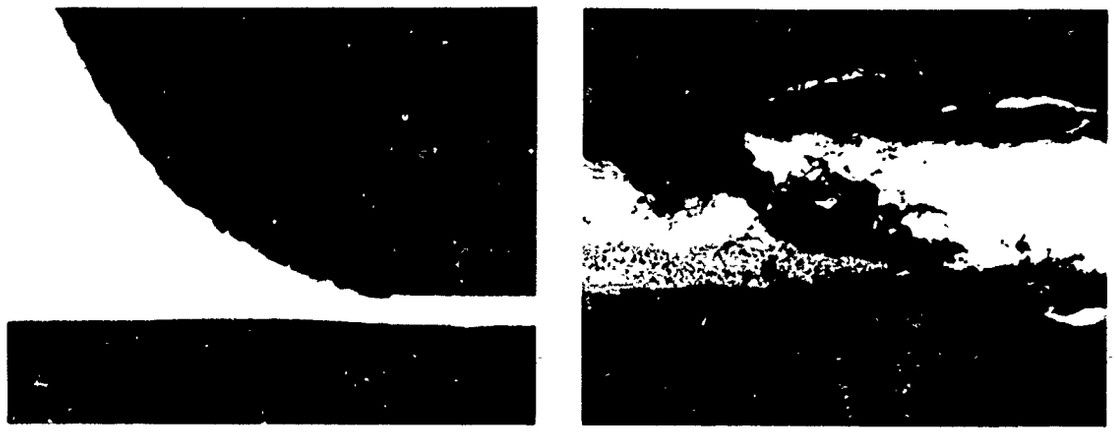

MAG = X75 MAG = X250
1100°F AND 35 KSI, FAILED AFTER 228.1 HOURS

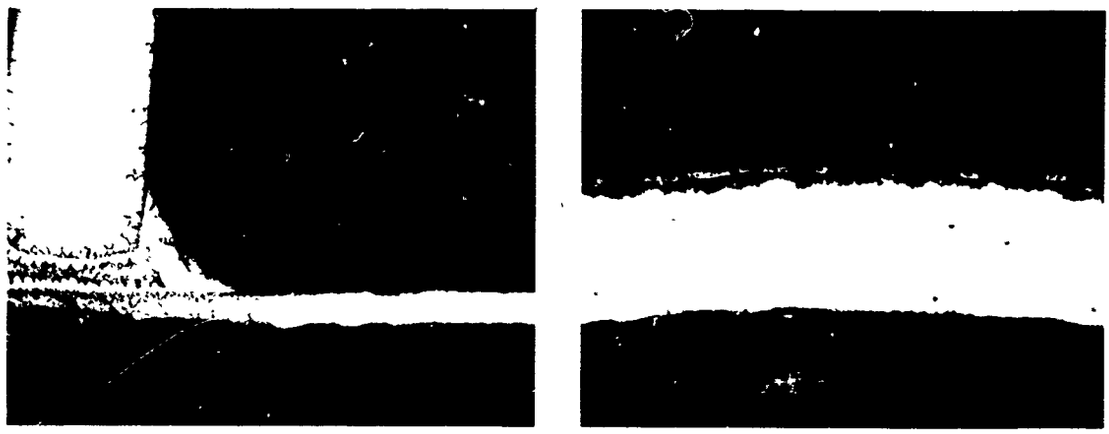

MAG = X75 MAG = X250
1100°F AND 30 KSI, FAILED AFTER 248.8 HOURS

MAG = X75 MAG = X250
1100°F AND 26.9 KSI, FAILED AFTER 1023.0 HOURS

NOTE: FIGURES REDUCED TO 60%.

Figure 118. Photomicrographs of Type 347 Stainless Steel Tubes Brazed With Nicrobraz 135 Brazing Alloy.

TABLE XXXIII. TYPE 347 STAINLESS STEEL BRAZED WITH NICROBRAZ 135, FAILURE AND CORROSION EXAMINATION

Temperature (°F)	Stress (ksi)	Life (hr)	Visual Examination*			Metallographical Examination		Photomicrograph Figure No.
			Failure		Corrosion	Braze Alloy Fillet	Point of Failure	
			Type	Location				
1500	9.2	35.0	P	-1/2	M	Some surface porosity	Heavy oxide layer 1-1/2 mils thick, intergranular oxidation	115
1500	9.2	125.1	P	-1	H	No corrosion	Thin layer, little attack	115
1500	5.0	170.2	P	+1	H	No corrosion	Heavy oxide layer 1-1/2 mils thick, complete intergranular penetration	115
1500	3.0	77.4	P	-3	H	Moderate intergranular corrosion	Heavy oxide layer, 2-1/2 mils thick, some intergranular attack	116
1300	13.9	82.7	R	-3	M	Some surface porosity	Shallow oxide layer, deep intergranular oxidation	116
1300	13.9	107.7	P	+3/4	M	Slight oxide layer	Moderate oxide layer, intergranular penetration	116
1300	10.0	441.2	P	-1	H	No corrosion	Heavy oxide layer 1-1/2 mils thick, some intergranular oxidation	117
1300	8.0	676.7	P	-2	H	Slight intergranular oxidation	Heavy oxide layer	117
1300	8.0	578.5	P	+2	H	Some integranular oxidation	Heavy oxide layer 1-1/2 mils thick	117
1100	35.0	228.1	P	J	S	No corrosion	Oxide layer 1 mil thick, oxidized fissure	118
1100	30.0	248.8	P	+1	S	No corrosion	Thin oxide layer	118
1100	26.9	1023.1	P	+1/2	M	No corrosion	Thin oxide layer	118

*P = Pinhole leak; R = Tube rupture; J = Braze joint; + = Above J; - = Below J; S = Slight; M = Moderate; H = Heavy

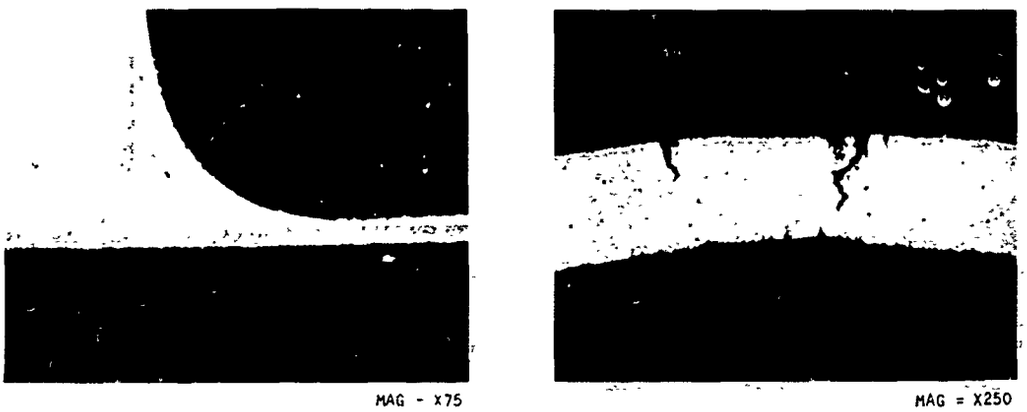

MAG - X75 MAG = X250

1500°F AND 12.1 KSI, FAILED AFTER 89.5 HOURS

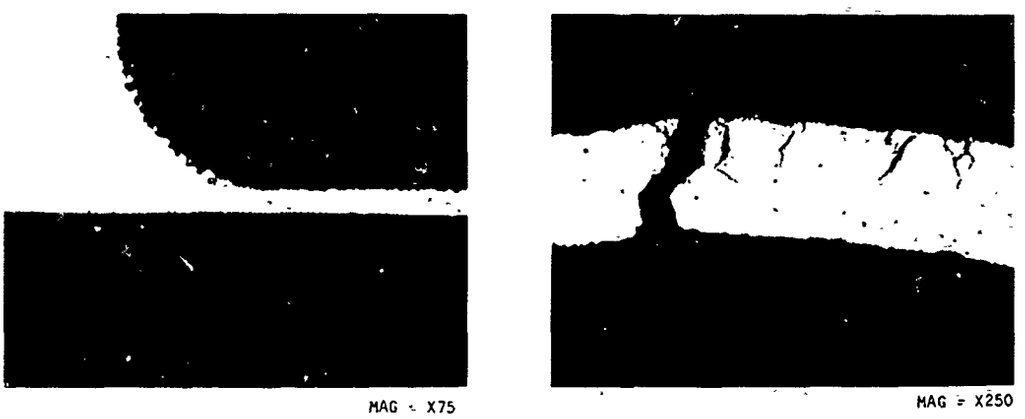

MAG = X75 MAG = X250

1500°F AND 8.7 KSI, FAILED AFTER 230.0 HOURS

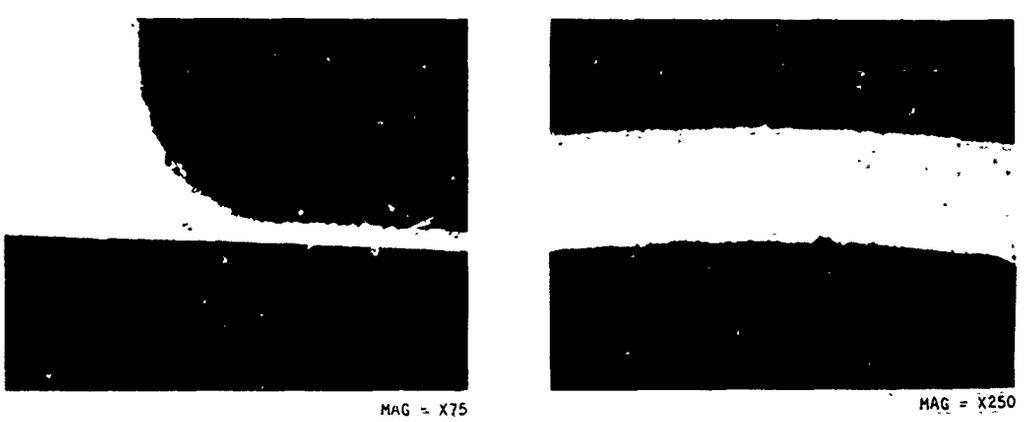

MAG = X75 MAG = X250

1500°F AND 6.6 KSI, FAILED AFTER 570.0 HOURS

NOTE: FIGURES REDUCED TO 60%.

Figure 119. Photomicrographs of Inconel 625 Tubes Brazed With Nicrobraz 135 Brazing Alloy.

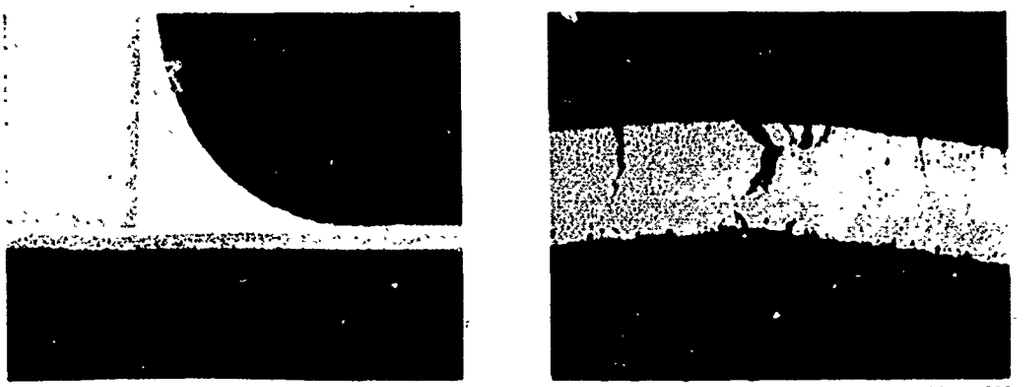

MAG = X75 MAG = X250

1300°F AND 33 KSI, FAILED AFTER 169.0 HOURS

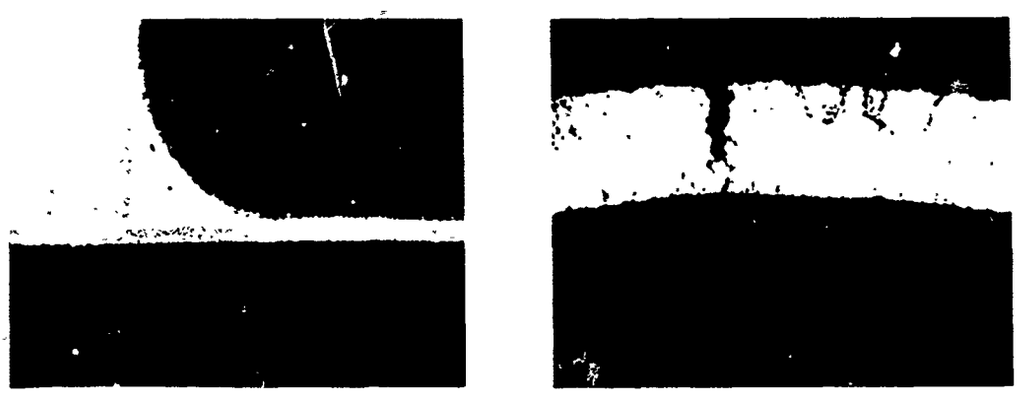

MAG = X75 MAG = X250

1300°F AND 26 KSI, FAILED AFTER 675.0 HOURS

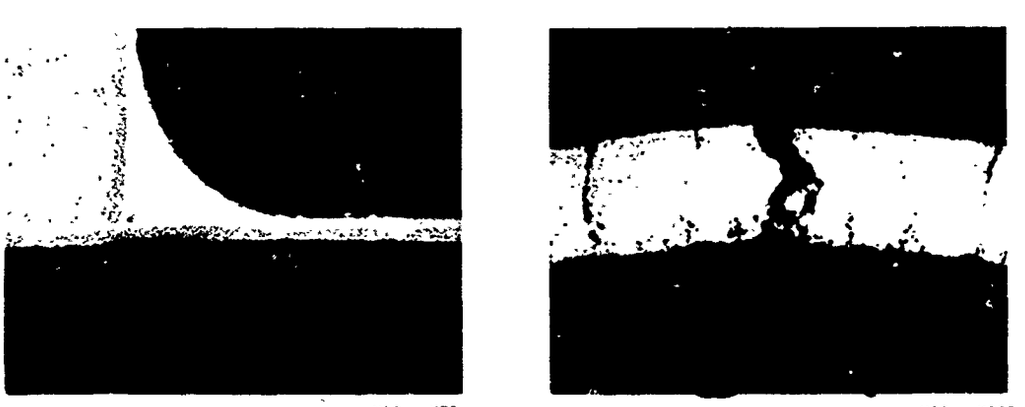

MAG = X75 MAG = X250

1300°F AND 19.1 KSI, NO FAILURE AFTER 1605.0 HOURS

NOTE: FIGURES REDUCED TO 60%.

Figure 120. Photomicrographs of Inconel 625 Tubes Brazed With Nicrobraz 135 Brazing Alloy.

MAG = X75 MAG - X250

1200°F AND 50.4 KSI, FAILED AFTER 56.0 HOURS

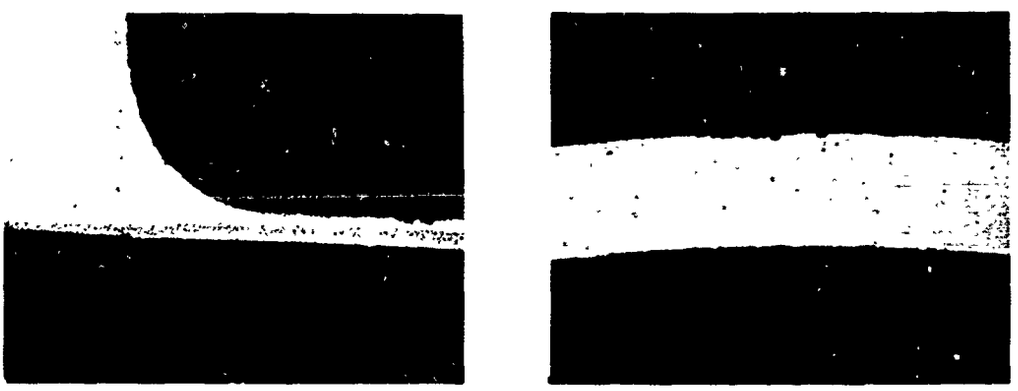

MAG = X75 MAG - X250

1200°F AND 46.4 KSI, FAILED AFTER 394.0 HOURS

MAG - X75 MAG = X250

1200°F AND 34.7 KSI. FAILED AFTER 1610.0 HOURS

NOTE: FIGURES REDUCED TO 60%.

Figure 121. Photomicrographs of Inconel 625 Tubes Brazed With Nicrobraz 135 Brazing Alloy.

TABLE XXXIV. INCONEL 625 BRAZED WITH NICROBRAZ 135, FAILURE AND CORROSION EXAMINATION

Temperature (°F)	Stress (ksi)	Life (hr)	Visual Examination*			Metallographical Examination		Photomicrograph Figure No.
			Failure		Corrosion	Braze Alloy Fillet	Point of Failure	
			Type	Location				
1500	12.1	89.5	P	-1/2	M	No corrosion, no alloy penetration	Oxidation along boundaries at failure site	119
1500	8.7	230.4	P	-1	M	Slight corrosion, no alloy penetration	Oxidation along boundaries at failure site, oxide film 0.5 mil thick	119
1500	6.6	570.4	P	-1	M	Slight corrosion, no alloy penetration	Oxidation along grain boundaries at failure site	119
1300	33.0	169.2	P	-2	S	No corrosion, no alloy penetration	Oxidized grain boundaries along stress-rupture fissure	120
1300	26.0	675	P	+1/2	S	Slight corrosion, no alloy penetration, small fillet	Oxidized grain boundaries and fissure face	120
1300	19.1	160.5	**		M	Slight corrosion, no alloy penetration	No grain boundary oxidation, slight oxide layer 0.1 mil thick	120
1200	50.4	56.6	P	+1/2	S	No corrosion, no alloy penetration, small fillet	No oxidation observed	121
1200	46.4	394.6	**	-	S	No corrosion, slight alloy penetration, small fillet	Discontinuous oxide layer 0.2 mil thick	121
1200	40	655.6	P	-1	S	No corrosion, no alloy penetration, small fillet	No oxidation observed	121
1200	34.7	1610	**		S	No corrosion, slight alloy penetration, small fillet	Discontinuous oxide layer 0.2 mil thick	121

*P = Pinhole leak; R = Tube rupture; J = Braze joint; + = Above J; - = Below J; S = Slight; M = Moderate; H = Heavy;
**No failure

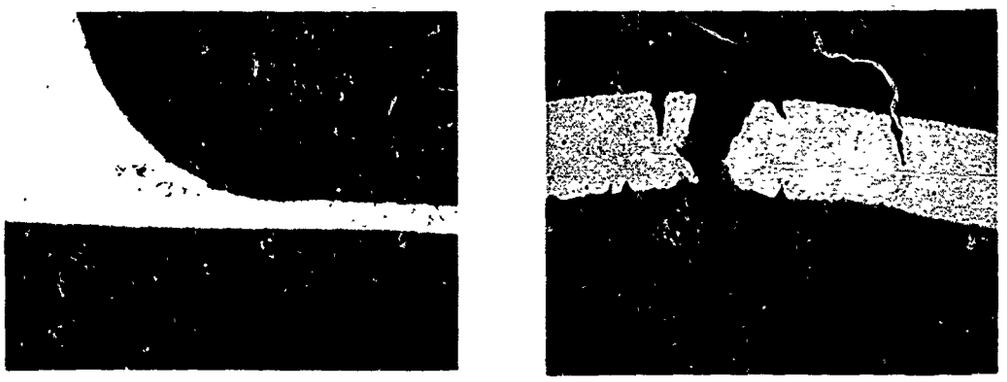

MAG = X75 MAG = X250

1500°F AND 12.1 KSI, FAILED AFTER 146.0 HOURS

MAG = X75 MAG = X250

1500°F AND 8.7 KSI, FAILED AFTER 209.0 HOURS

MAG = X75 MAG = X250

1500°F AND 6.6 KSI, FAILED AFTER 570.0 HOURS

NOTE: FIGURES REDUCED TO 60%.

Figure 122. Photomicrographs of Inconel 625 Tubes Brazed With J-8100 Brazing Alloy.

MAG = X75 MAG = X250

1300°F AND 33.0 KSI, FAILED AFTER 158.0 HOURS

MAG = X75 MAG = X250

1300°F AND 26.C KSI, FAILED AFTER 843.0 HOURS

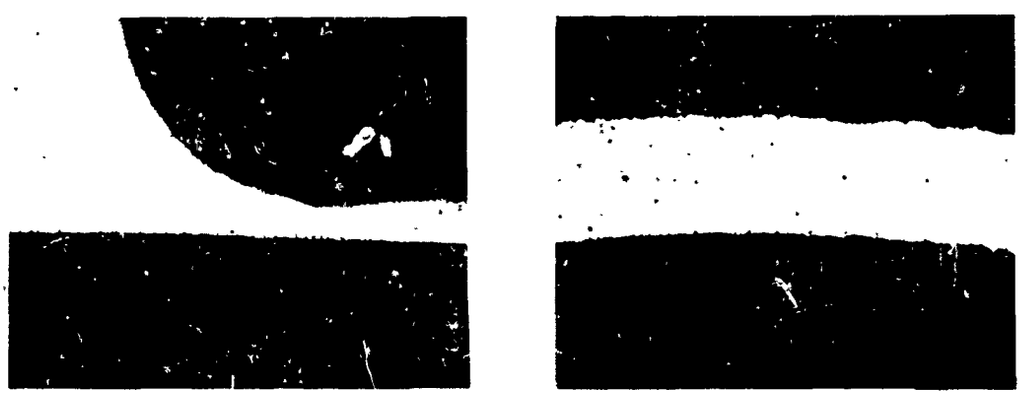

MAG = X75 MAG = X250

1300°F AND 19.1 KSI, FAILED AFTER 1604.0 HOURS

NOTE: FIGURES REDUCED TO 60%.

Figure 123. Photomicrographs of Inconel 625 Tubes Brazed With J-8100 Brazing Alloy.

MAG = X75 MAG = X250

1200°F AND 50 KSI, FAILED AFTER 43.0 HOURS

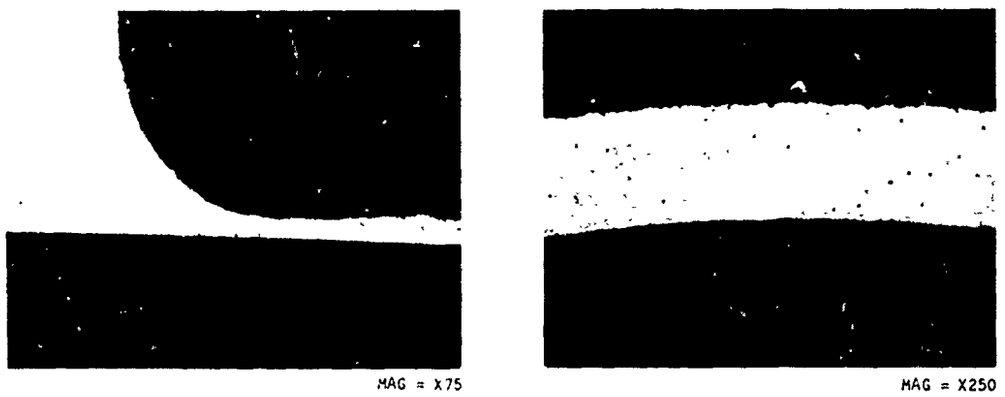

MAG = X75 MAG = X250

1200°F AND 41.0 KSI, FAILED AFTER 955.0 HOURS

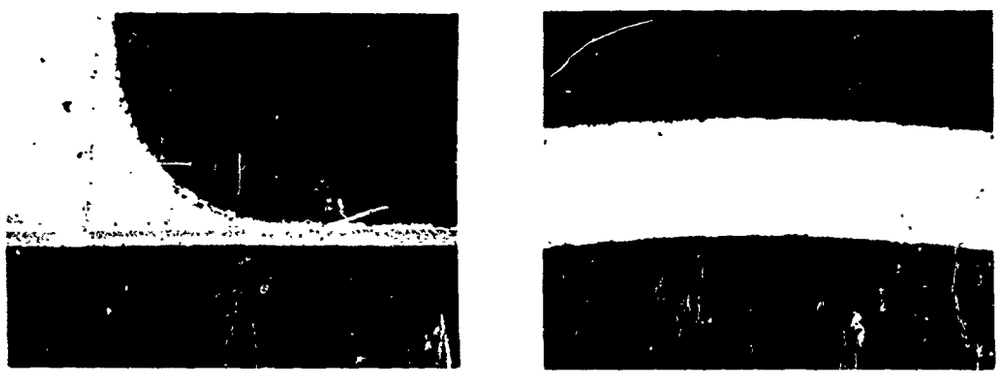

MAG = X75 MAG = X250

1200°F AND 35.0 KSI, FAILED AFTER 1610.0 HOURS

NOTE: FIGURES REDUCED TO 60%.

Figure 124. Photomicrographs of Inconel 625 Tubes Brazed With J-8100 Brazing Alloy.

TABLE XXXV. INCONEL 625 BRAZED WITH J-8100, FAILURE AND CORROSION EXAMINATION

Temperature (°F)	Stress (ksi)	Life (hr)	Visual Examination*			Metallographical Examination		Photomicrograph Figure No.
			Failure					
			Type	Location	Corrosion	Braze Alloy Fillet	Point of Failure	
1500	12.1	146.3	P	-1	M	No oxidation, complete penetration	Grain boundaries oxidized at failure site, no oxide on surface layers	122
1500	8.7	208.9	P	-1-1/2	M	No oxidation, complete penetration	Very thin surface oxide layer, grain boundary oxidation at failure site	122
1500	6.6	570.4	P	-	M	Slight intergranular oxidation, complete penetration	Very thin surface oxide layer, grain boundary oxidation at failure site	122
1300	33.0	158.1	P	-1/2	S	No oxidation, complete penetration of tube wall by brazing alloy	No oxidation observed	123
1300	26.0	843.4	P	-2	M	Some oxidation observed, complete penetration	Some oxidation along stress-rupture fissure	123
1300	19.1	1604	**		M	Slight oxidation of brazing alloy, complete penetration	Oxide film 0.2 mil thick observed, very slight intergranular penetration	123
1200	50.4	43.0	P	-1/2	S	No corrosion, complete penetration of tube by brazing alloy, good filleting	No oxidation observed	124
1200	46.4	394.6	**	-	S	No corrosion, complete penetration of tube by brazing alloy, good filleting	No oxidation observed	124
1200	41.0	955.1	**	-	S	No corrosion, 50 percent penetration of tube by brazing alloy, good filleting	No oxidation observed	124
1200	35.7	1610	**	-	S	Slight oxidation of brazing alloy, good filleting	Very slight oxidation detected (0.1-mil-thick oxide film)	124

*P = Pinhole leak; R = Tube rupture; J = Braze joint; + = Above J; - = Below J; S = Slight; M = Moderate; H = Heavy
**No failure

APPENDIX III

MICROPROBE ANALYSIS

Metallography alone was insufficient to identify the products of corrosion or to determine the extent of diffusion of solute elements across the brazing alloy/tube metal interface. Hence, to gain a better understanding of the diffusion characteristics and hot corrosion mechanisms, electron microprobe analysis was performed on selected samples of tubing materials. Three series of samples were examined:

1. Tubes that had failed in the cyclic hot corrosion test were analyzed in the vicinity of the failure to identify the products of corrosion.

2. Analysis was conducted across the filler metal/tube interface of samples brazed for the cyclic hot corrosion test to ascertain the diffusion characteristics of various elements in the area of the brazed joints.

3. Tubes were taken from the heat exchanger test modules after various exposure times and submitted for microprobe analysis to correlate the corrosion products with those found on the tubes taken from the cyclic hot corrosion test.

EXPERIMENTAL DESCRIPTION

During the analysis, a finely focused electron beam was impinged on the specimen area of interest. The electrons from this beam interact with the orbital electrons associated with the atoms in the specimen, and cause ionization. This leads to the production of X-rays which are characteristic of the elements present within the field of interaction. X-ray intensities, when appropriately corrected for matrix adsorption, secondary fluorescence, and various other electron effects, can be used to quantitatively determine compositions. Various qualitative data collection procedures were employed as follows:

1. Spectral Scans--The specimens were held stationary under the electron beam, and the spectrometers scanned over a range to determine which elements were present under the area of the electron beam. These spot checks were used to classify the elements present at various points on the specimens.

2. Distribution Scans--The spectrometers were set to receive specific X-ray lines, and the specimens were traversed under the beams either continuously or in 1μ or 5μ steps, presenting a record of X-ray intensity for preselected elements along a line traversing the surface of the specimen.

3. Scanning Display--The electron beam was scanned over an area of the specimen, and the X-rays emitted from any predetermined element were used to modulate the brightness of a cathode ray tube having a sweep synchronous with the electron beam. In this manner, photographs can be produced which illustrate the relative distribution density of chosen elements over a comparatively large surface area of 0.05 mm^2.

PROCEDURE AND RESULTS

Evaluation of Brazing Alloy Diffusion and Corrosion

The 10 specimens submitted for characterization studies are shown in Table XXXVI.

TABLE XXXVI. BRAZED SPECIMENS SUBMITTED FOR MICROPROBE ANALYSIS

Tube Material	Brazing Alloy	Specimen Number	
		Before Exposure	After Exposure*
Hastelloy X	Palniro I	12075	12013
Incoloy 800	Coast Metals 50B	12035	12015
Inconel 625	J-8100	11880	12014
N-155	Nicrobraz 200	12082	12016
Type 347 SS	Nicrobraz 135	12083	12017

*Exposure to the 100-hr static hot corrosion test

Spectral scans were obtained from the brazing filler metals and the tube metal interface of the above specimens. The various detected elements, listed sequentially in terms of the amount present, are presented in Table XXXVII.

The presence and approximate distribution of the significant elements were initially surveyed by manual specimen manipulation. Selected X-ray scanning display photomicrographs were then obtained from each of the specimens at a location which included a portion of the tube and adjacent braze material. In addition, X-ray distribution scans were obtained for specific elements along traces which started at the inside tube wall and continued across

TABLE XXXVII. ELEMENTS DETECTED IN SPECTRAL SCANS

Specimen No.	Area	Material	Elements Detected
12075	Braze	Palniro 1	Ni, Au, Pd, Fe, Cr, Mo, Co
12013	Tube	Hastelloy X	Ni, Cr, Fe, Pd, Mo, Au
12013	Braze	Palniro 1	Ni, Au, Pd, Fe, Cr, Mo, Co
12035	Tube	Incoloy 800	Fe, Ni, Cr
12015	Braze	Coast Metals 50B	Fe, Ni, Cr, Pd
11880	Tube	Inconel 625	Ni, Cr, Fe
12014	Braze	J-8100	Ni, Cr, Fe, Si
12082	Tube	N-155	Fe, Co, Cr, Ni, Mn, W
12082	Braze	Nicrobraz 200	Ni, W, Fe, Cr, Co, Mn
12016	Tube	N-155	Fe, Co, Cr, Ni, Mn, W
12016	Braze	Nicrobraz 200	Ni, Fe, Cr, Co, W, Mn
12083	Tube	Type 347 SS	Fe, Cr, Ni, Mn, Si, Co
12083	Braze	Nicrobraz 135	Ni, Co, Fe, Si
12017	Braze	Nicrobraz 135	Ni, Co, Fe, Si

the tube/braze interface into the braze material. The distribution scans were limited to specimens which had undergone corrosive environment exposures.

The various data, which for the most part are self-explanatory, are presented in Figures 125 through 141. The elements for which X-ray scanning display pictures and/or distribution traces were taken are identified in Table XXXVII. The various observations are summarized below:

Hastelloy X - Palniro 1--4-mil interdiffusion zone; uniform distribution of iron, chromium, cobalt, molybdenum, and palladium; inverse variation of gold and nickel in braze; manual scanning identified oxygen, but no sulfur at exterior edge of braze fillet.

Incoloy 800 - Coast Metals 50B--Trace runs from tube wall through braze into attachment; 5-mil interdiffusion zone; uniform nickel; inverse variation of chromium and iron in both tube and braze; braze contains iron-rich and chromium-poor precipitates.

Inconel 625 - J-8100--Indefinite diffusion zone; little variation in silicon, iron, chromium, and nickel intensity between tube and braze matrix; unidentified grain boundary precipitate in braze (perhaps rich in columbium and/or tantalum); molybdenum gradient (10 mils wide) across tube and into braze.

N-155 - Nicrobraz 200--2-mil diffusion gradient; tube has fairly uniform manganese, tungsten, iron, molybdenum, and nickel distributions, with slight variations in all elements; block-like precipitates in braze are rich in tungsten; other braze precipitates are rich in chromium; scanning display pictures which include outer corrosion layer identify the layer as a chromium-iron oxide.

Type 347 Stainless Steel - Nicrobraz 135--1- to 2-mil diffusion gradient; uniform nickel and chromium distributions; chromium enrichment at the inside tube wall; scanning display pictures indicate uniform iron and silicon.

EVALUATION OF CORROSION PRODUCTS

Cyclic Hot Corrosion Test Rig

Eleven of 15 specimens submitted for characterization studies were analyzed by electron microprobe as shown in Tables XXXVIII and XXXIX. Spectral scans were carried out on one specimen of each type of material, and the various elements detected are given in Table XXXIX.

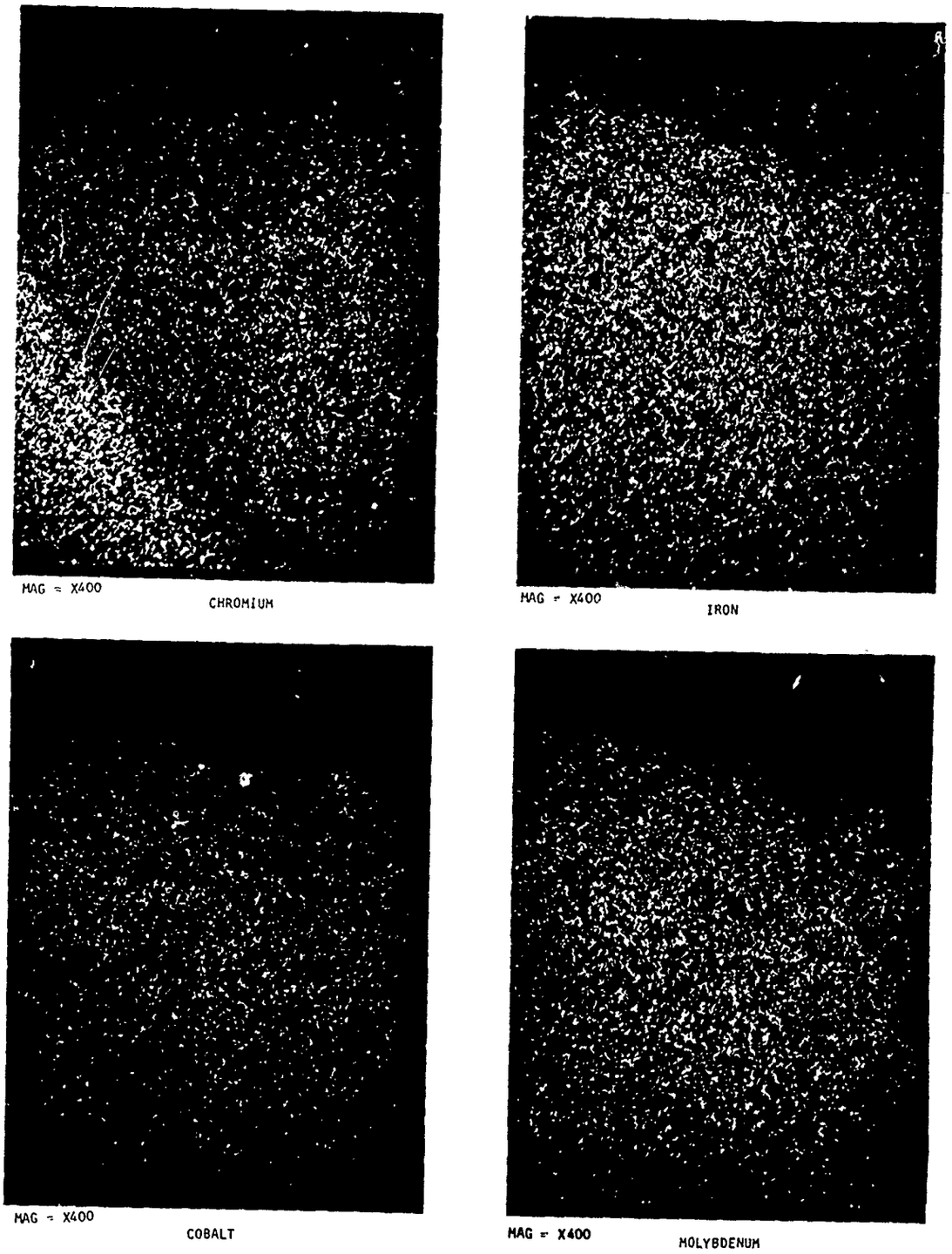

Figure 125. Scanning Display X-ray Images of Hastelloy X Brazed With Palniro 1, Before Exposure. (Tube Wall Is at Lower Right.)

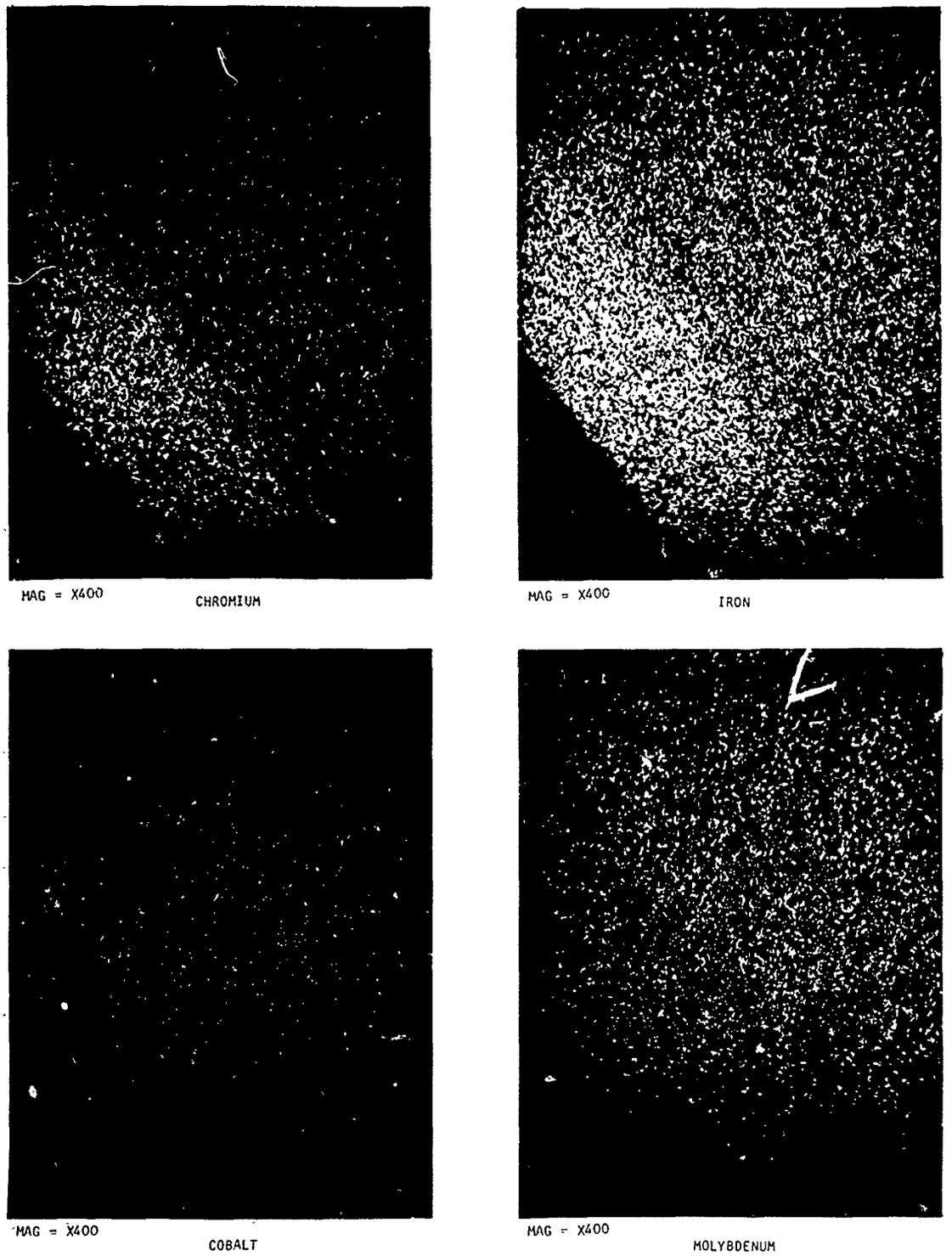

Figure 126. Scanning Display X-ray Images of Hastelloy X Brazed With Palniro I, After Exposure. (Tube Wall Is at Lower Left.)

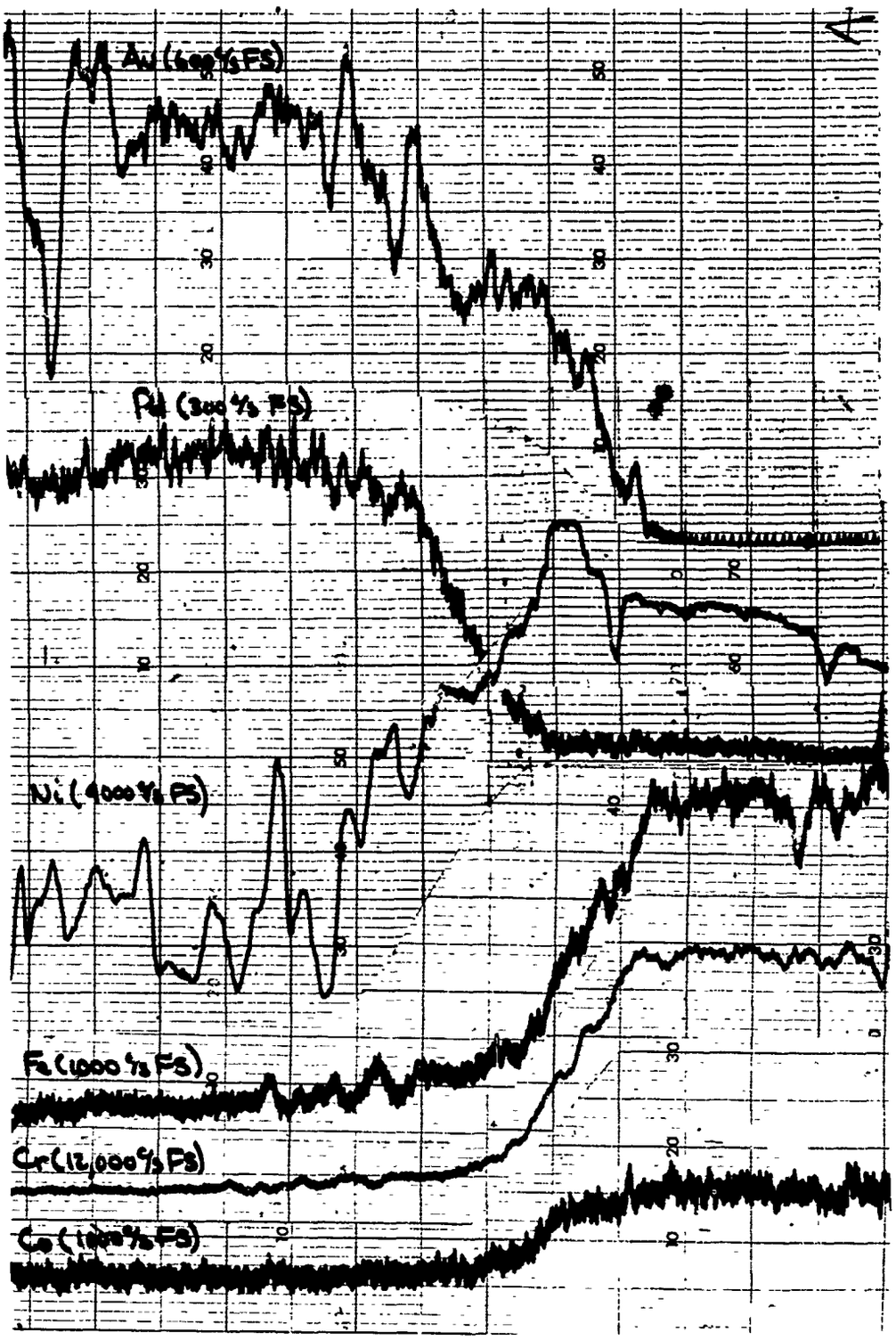

Figure 127. X-ray Distribution Scans Across Hastelloy X - Palniro I Tube Wall/Braze Interface.

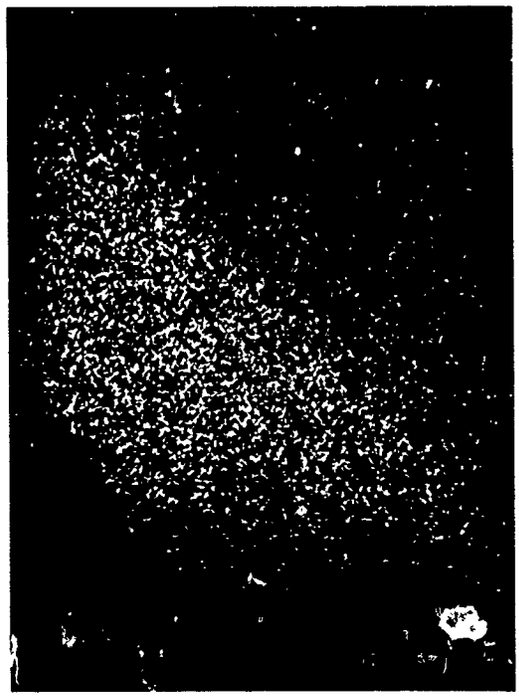

MAG = X400 IRON

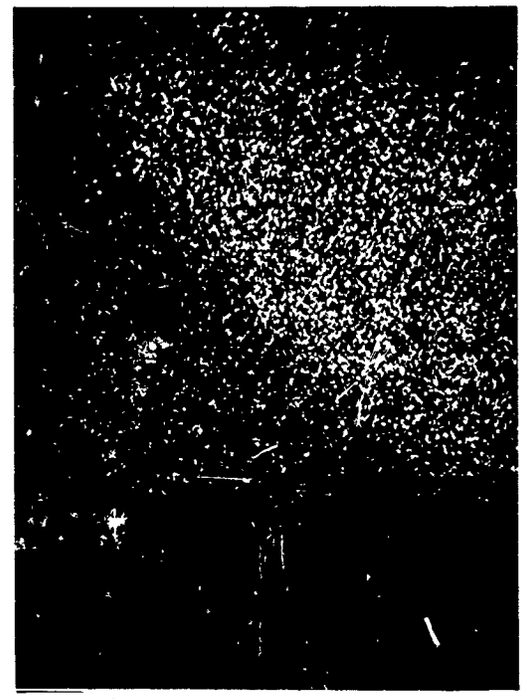

MAG = X400 NICKEL

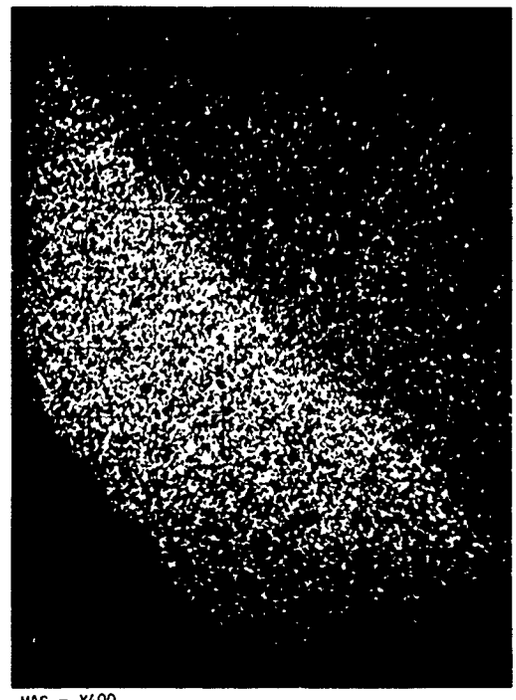

MAG = X400 CHROMIUM

Figure 128. Scanning Display X-ray Images of Incoloy 800 - Coast Metals 50B, Before Exposure. (Tube Wall Is at Lower Left.)

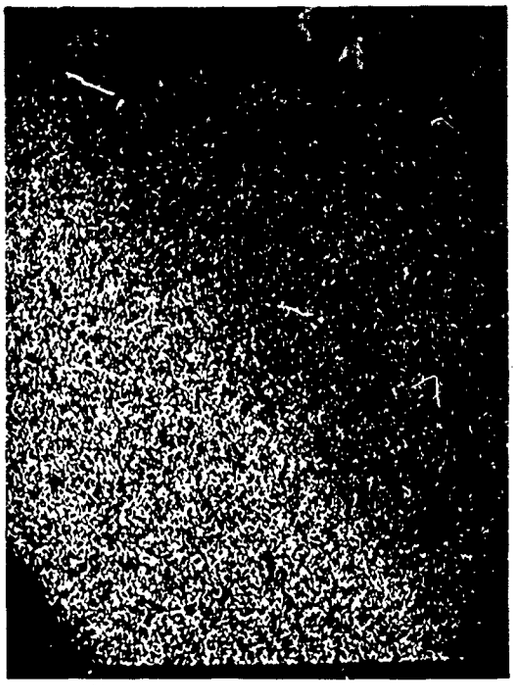

MAG - X400 IRON

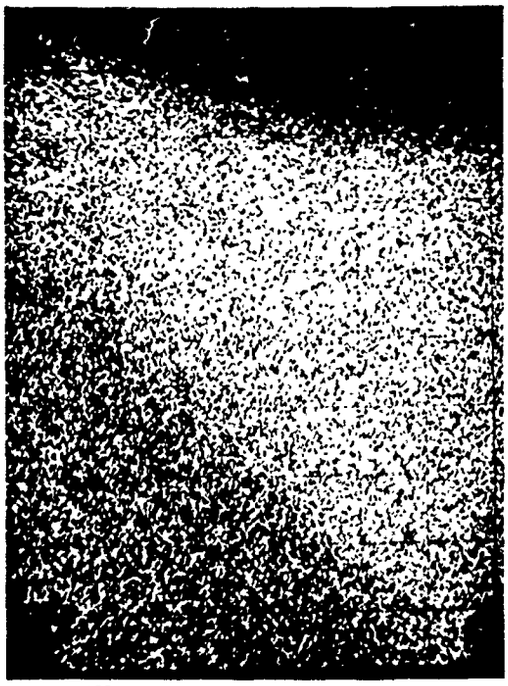

MAG = X400 NICKEL

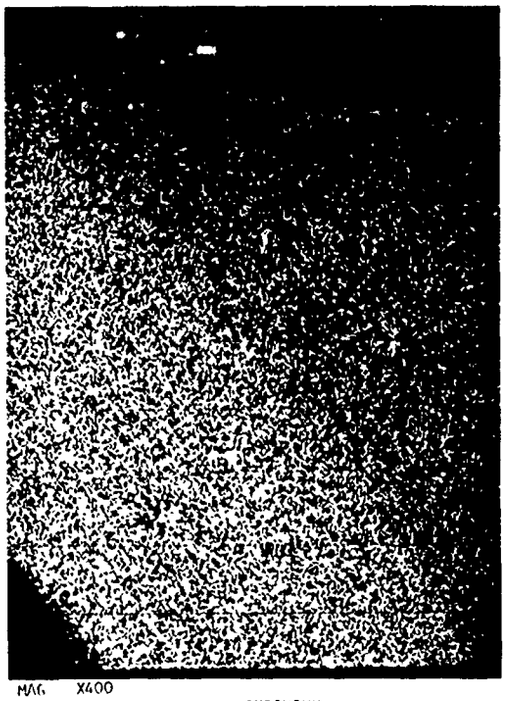

MAG X400 CHROMIUM

Figure 129. Scanning Display X-ray Images of Incoloy 800 - Coast Metals 50B. (Tube Wall Is at Lower Left.)

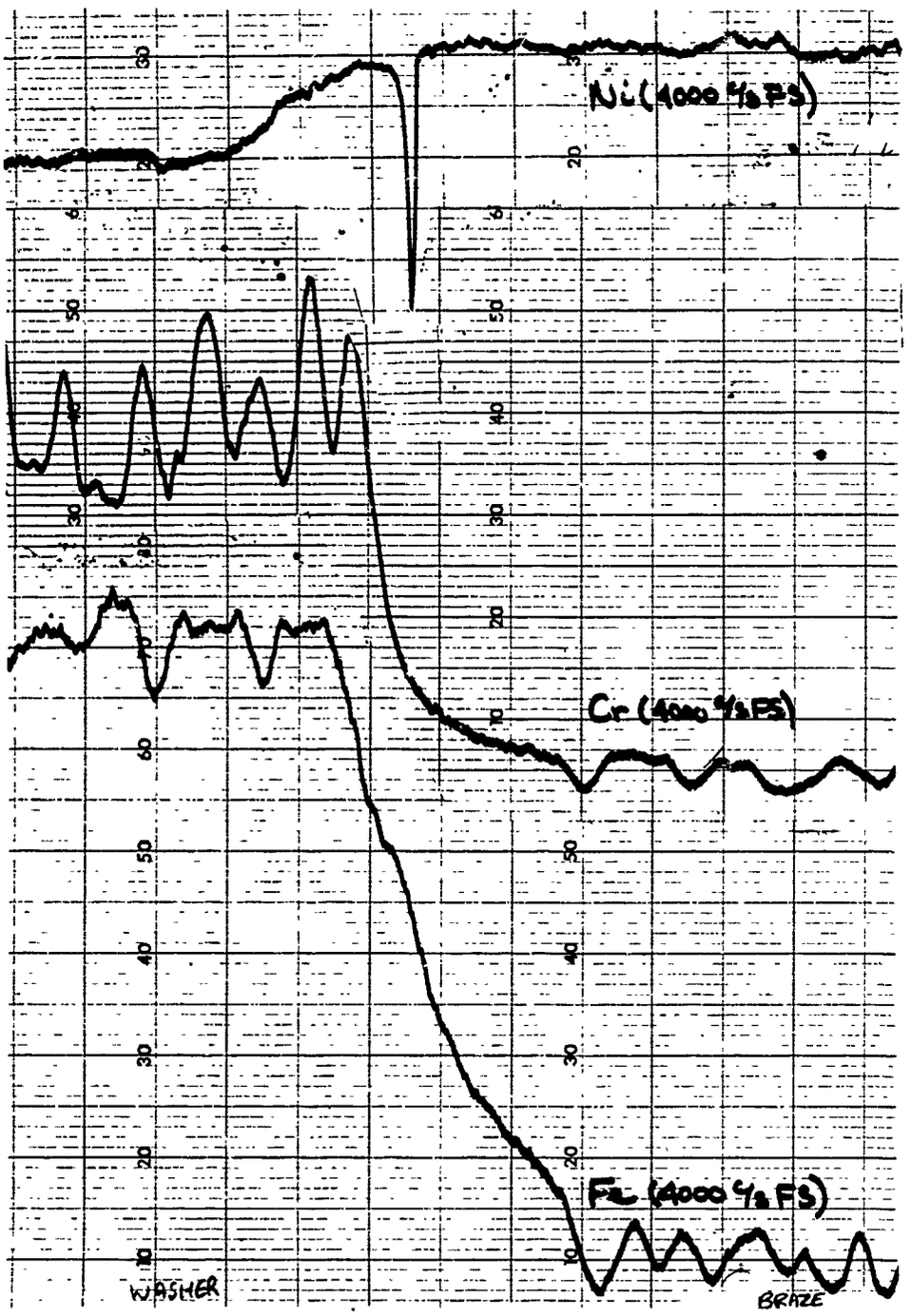

Figure 130. X-ray Distribution Scans Across Tube Wall/Braze Interface, Incoloy 800 - Coast Metals 50B, 2.5 mils per in. of Chart. (Tube Is at Right.)

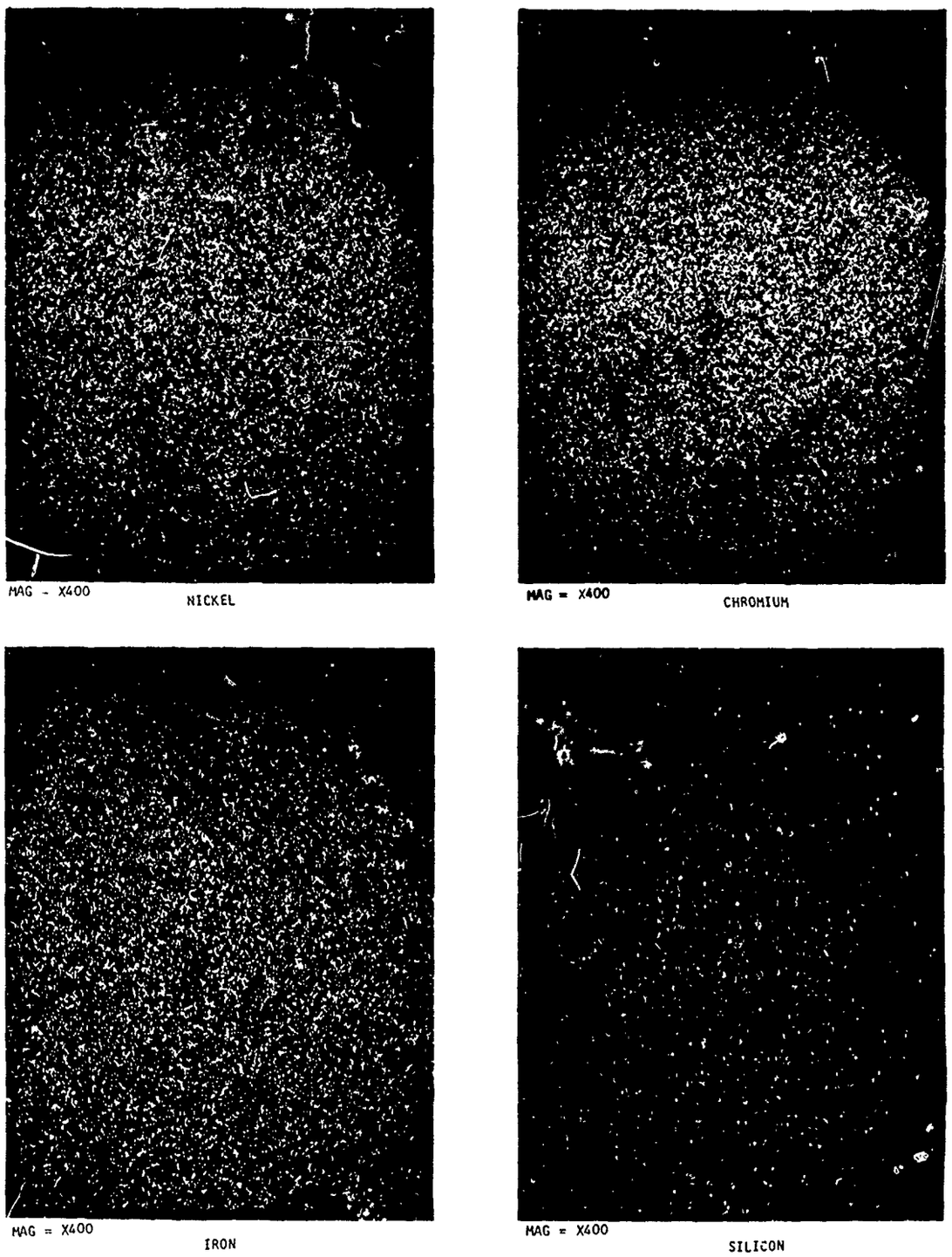

Figure 131. Scanning Display X-ray Images of Inconel 625 - J-8100, Before Exposure. (Tube Wall Is at Lower Left.)

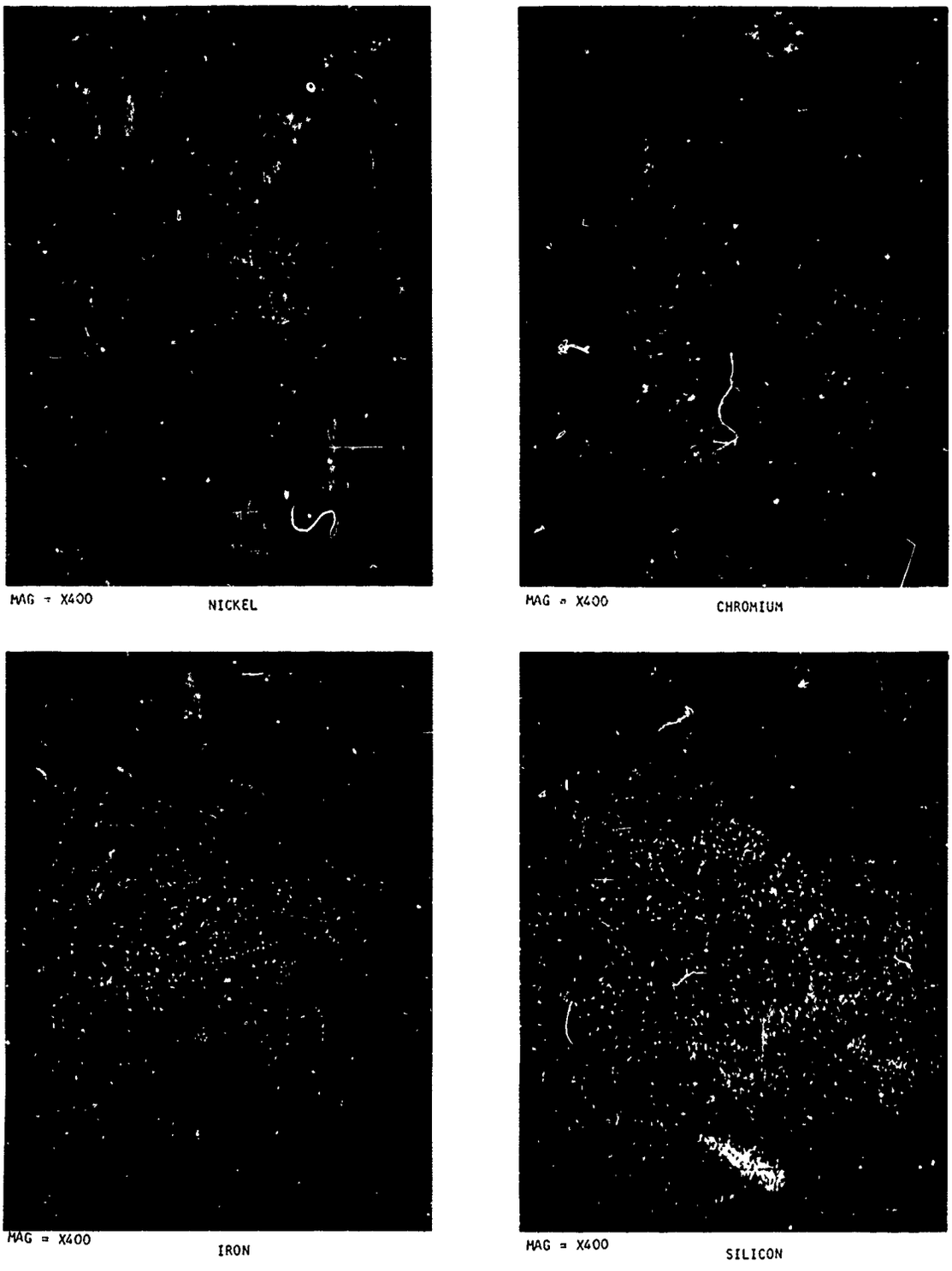

Figure 132. Scanning Display X-ray Images of Inconel 625 - J-8100, After Exposure. (Tube Wall Is at Lower Left.)

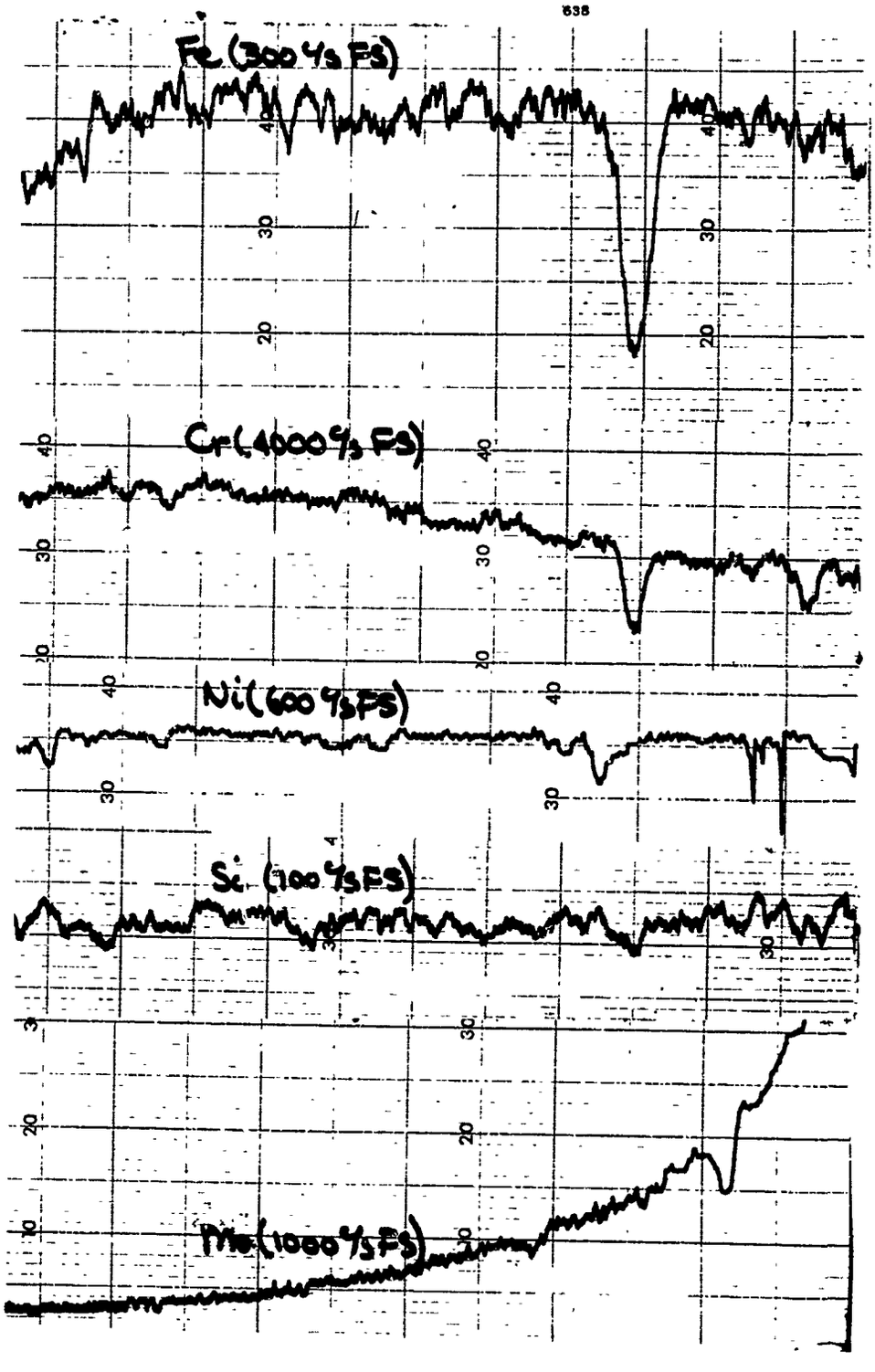

Figure 133. X-ray Distribution Scans Across Tube Wall/Braze Interface, Inconel 625 - J-8100, 2.5 mils per in. of Chart. (Tube Is at Right.)

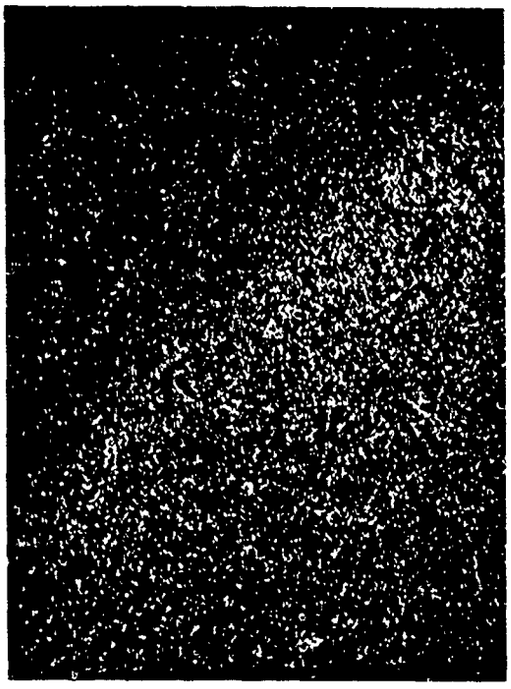

MAG = X400 IRON

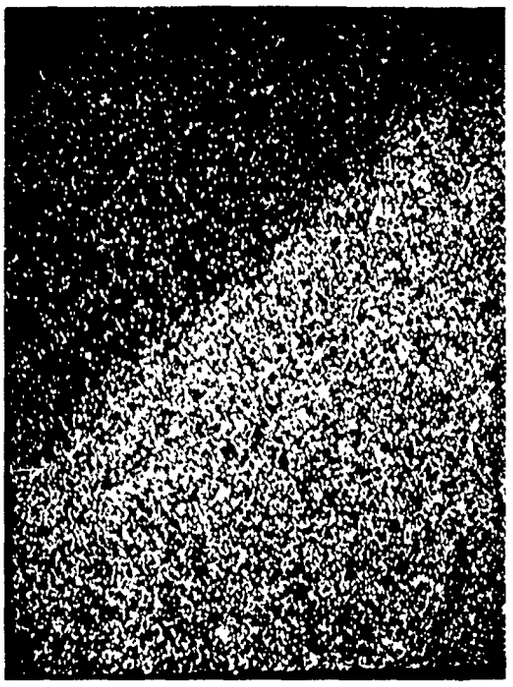

MAG = X400 COBALT

MAG = X400 CHROMIUM

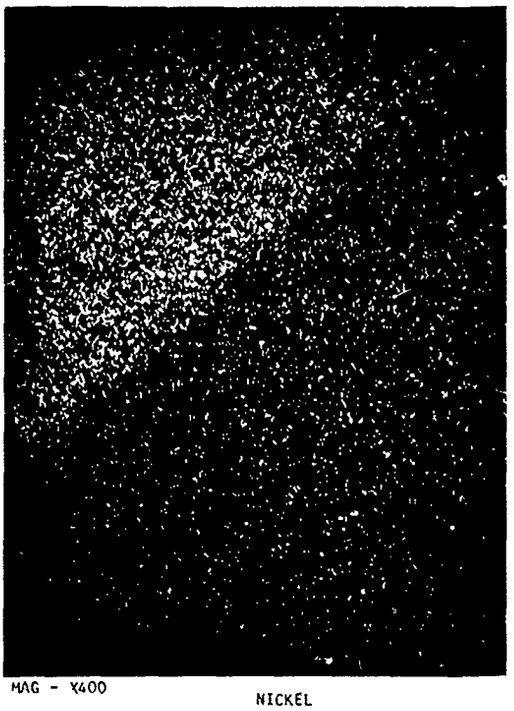

MAG = X400 NICKEL

Figure 134. Scanning Display X-ray Images of N-155 - Nicrobraz 200, Before Exposure. (Tube Attachment Is at Lower Right.)

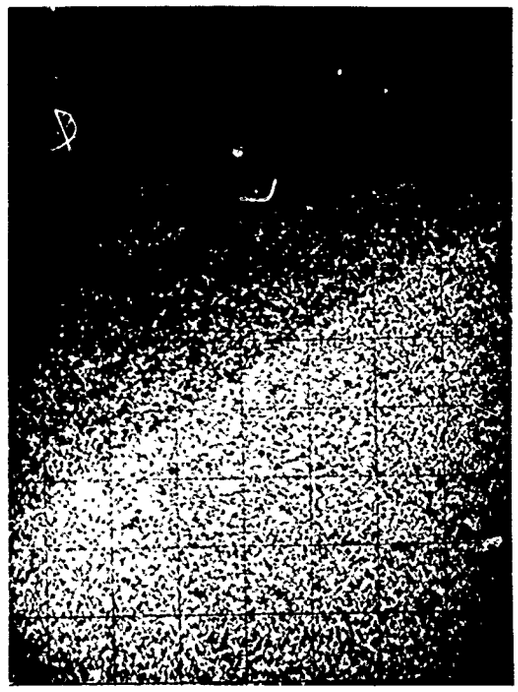

MAG = X400 IRON

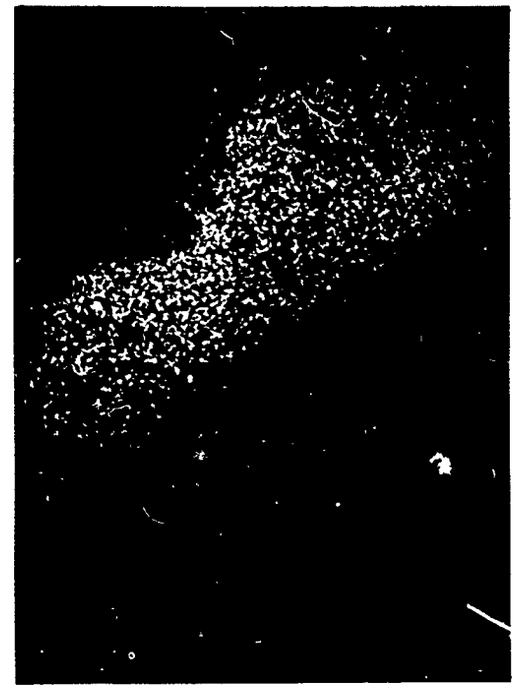

MAG = X400 NICKEL

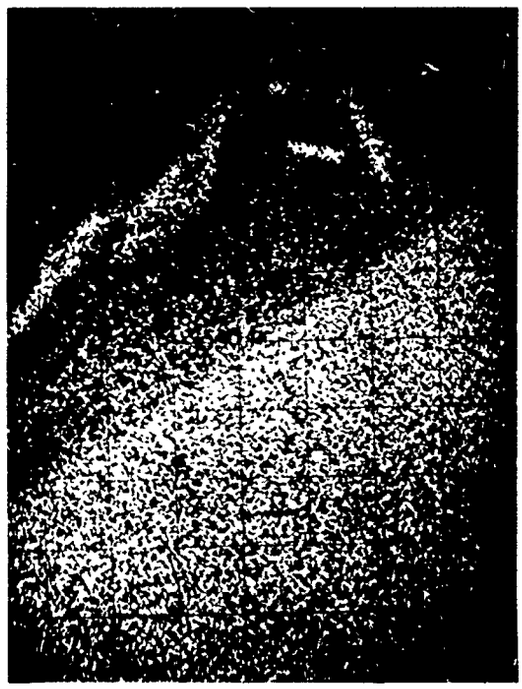

MAG = X400 CHROMIUM

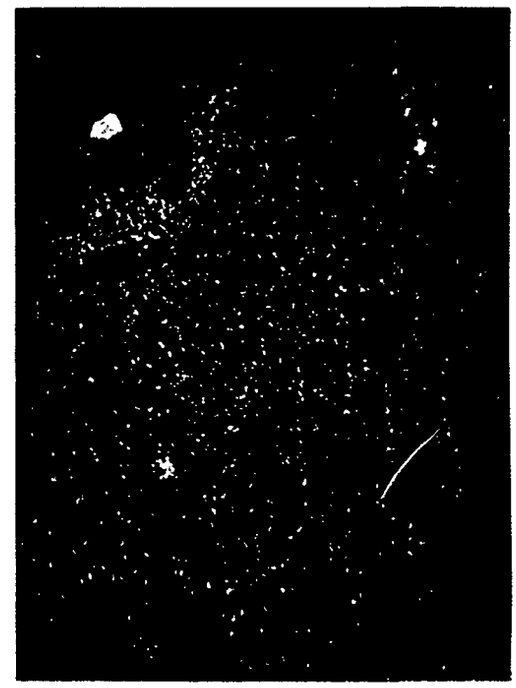

MAG = X400 OXYGEN

Figure 135. Scanning Display X-ray Images of N-155 - Nicrobraz 200, After Exposure. (Tube Attachment Is at Lower Right; Corrosion Product Is Toward Upper Left.)

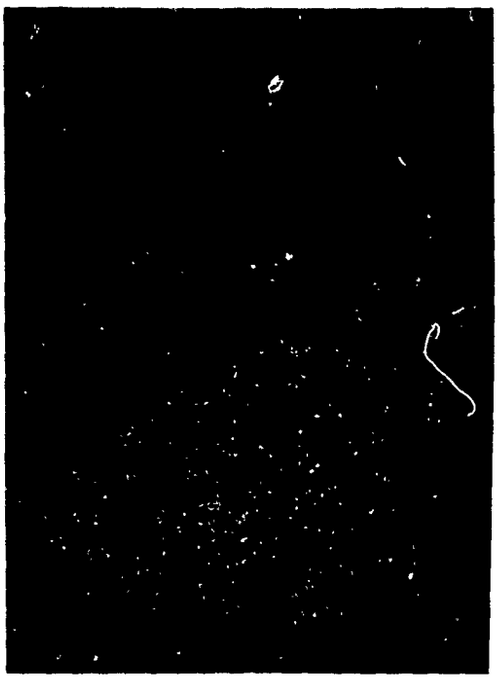

MAG = X400 SILICON

MAG = X400 MANGANESE

MAG = X400 TUNGSTEN

Figure 136. Scanning Display X-ray Images of N-155 - Nicrobraz 200, After Exposure. (Tube Attachment Is at Lower Right; Corrosion Product Is Toward Upper Left.)

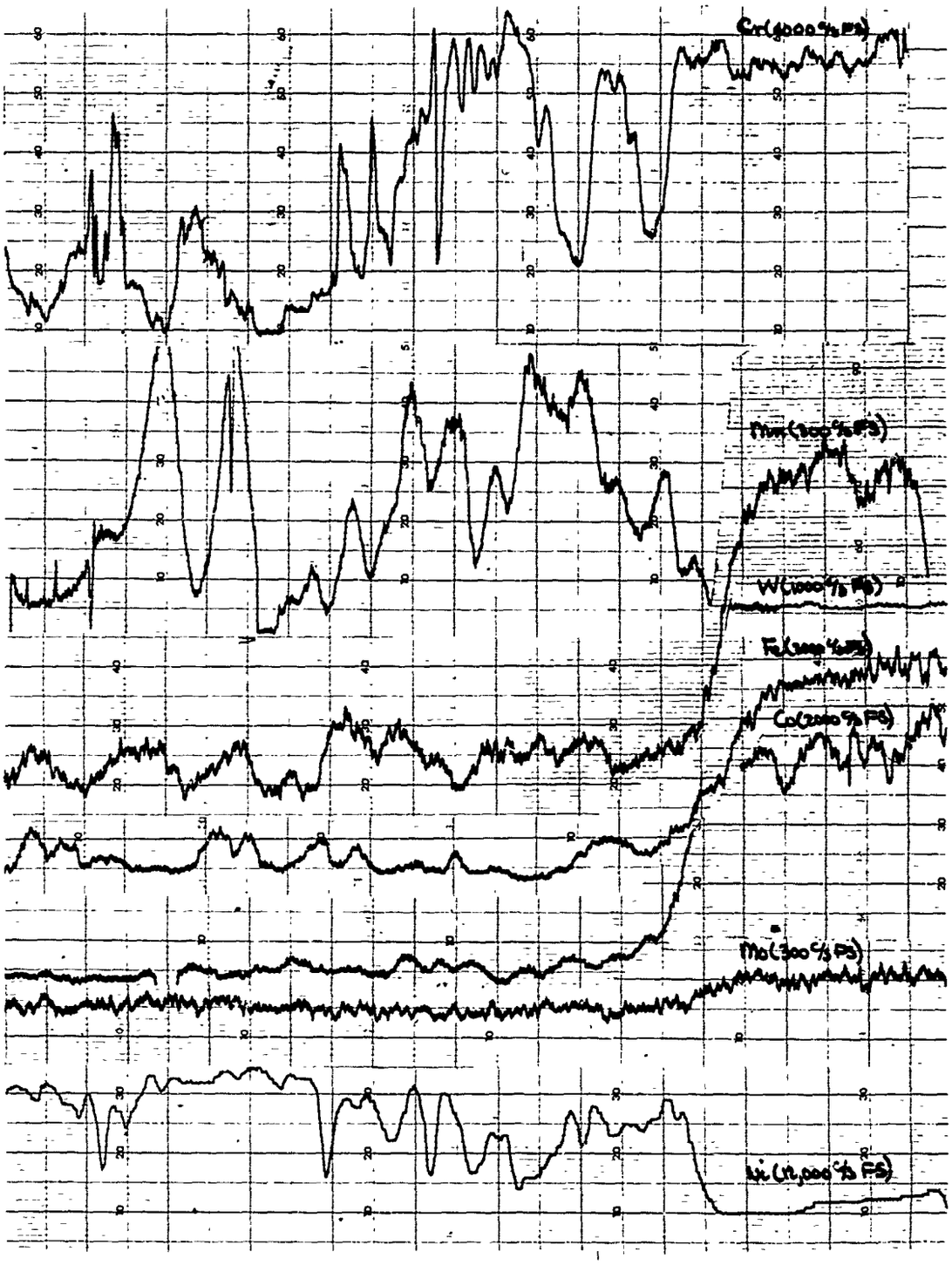

Figure 137. X-ray Distribution Scans Across Tube Wall/Braze Interface, N-155 - Nicrobraz 200, After Exposure, 2.5 mils per in. of Chart. (Tube Is at Right.)

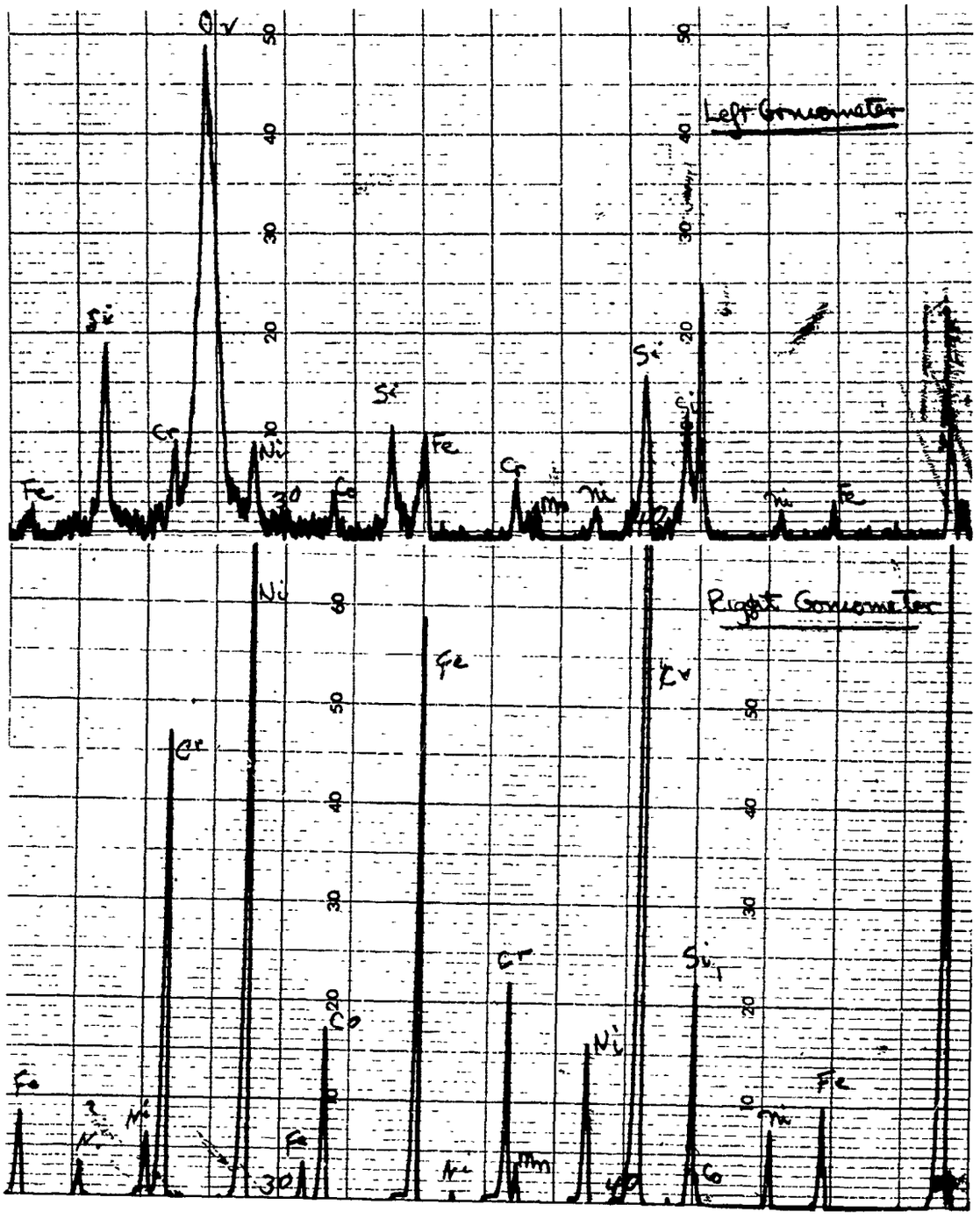

Figure 138. Spectral Scans of Corrosion Film on Outside of Braze Fillet, N-155 - Nicrobraz 200.

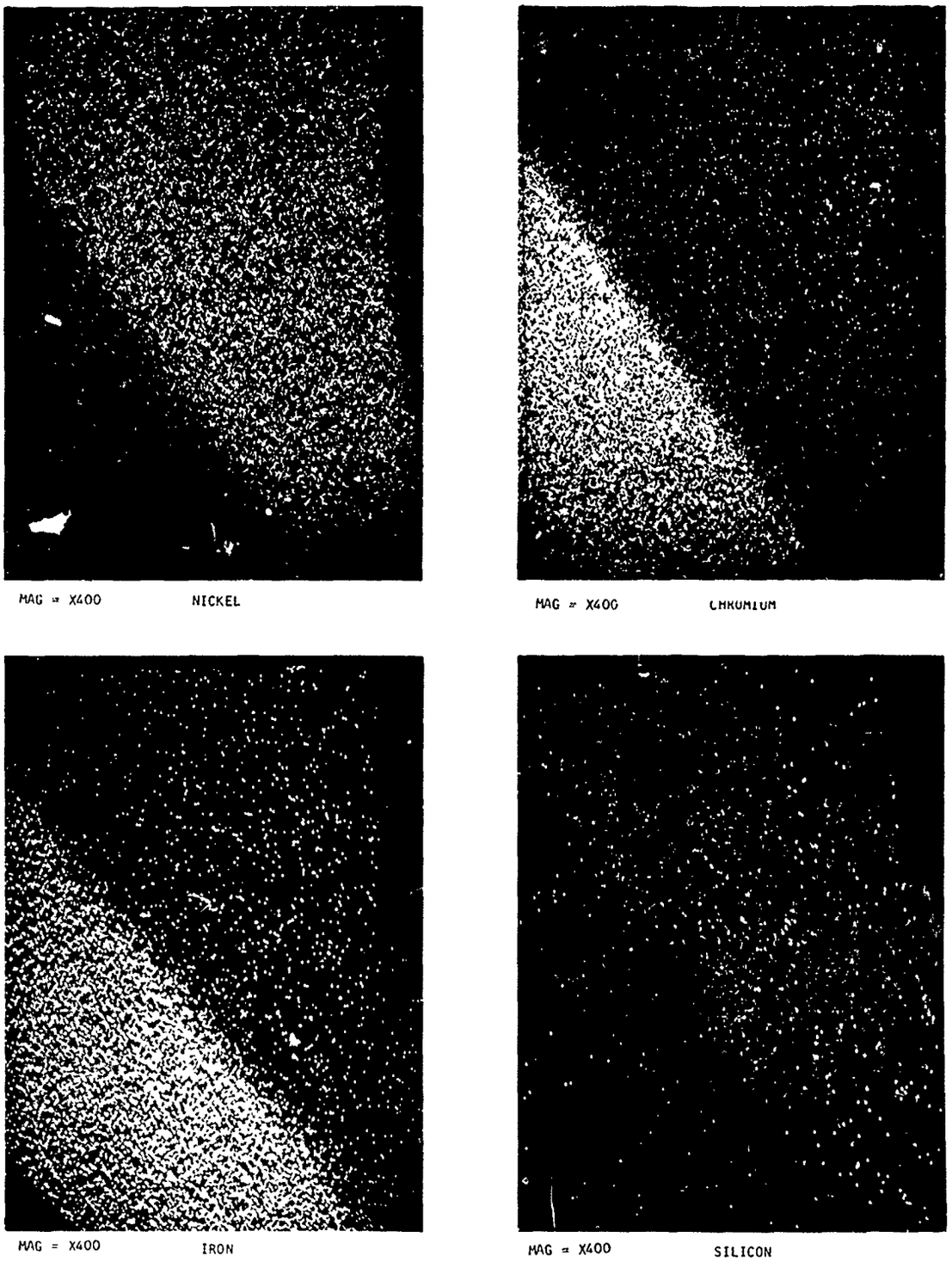

Figure 139. Scanning Display X-ray Images of Type 347 Stainless Steel - Nicrobraz 135, Before Exposure. (Tube wall Is at Lower Left.)

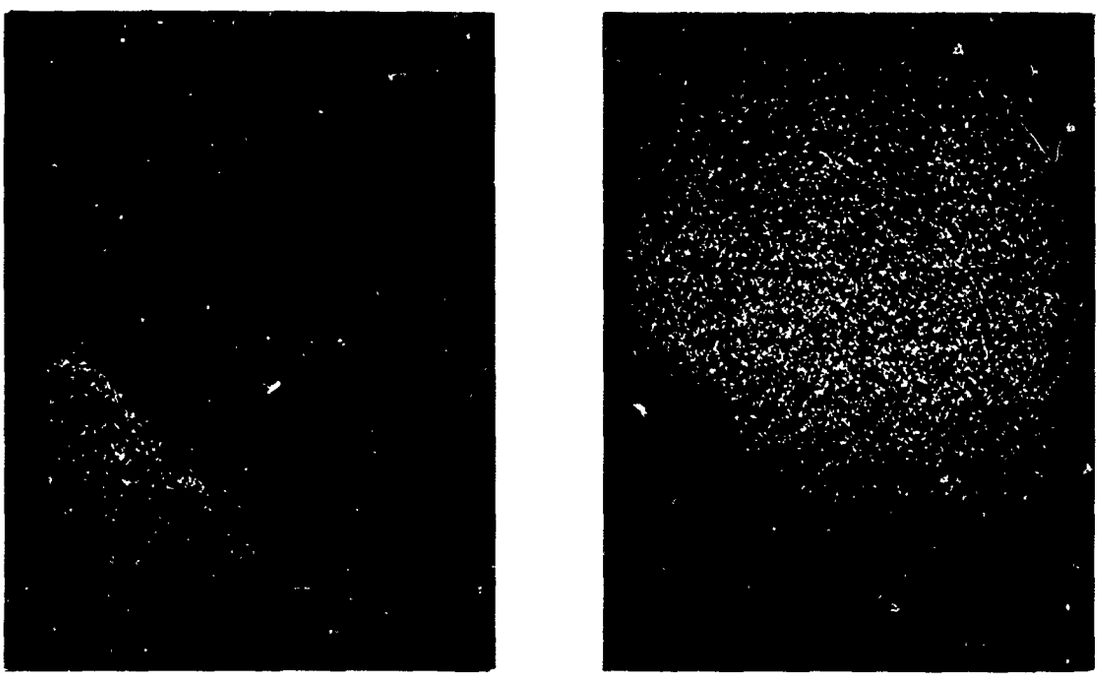

Figure 140. Scanning Display X-ray Images of Type 347 Stainless Steel - Nicrobraz 135, After Exposure. (Tube Wall Is at Lower Left.)

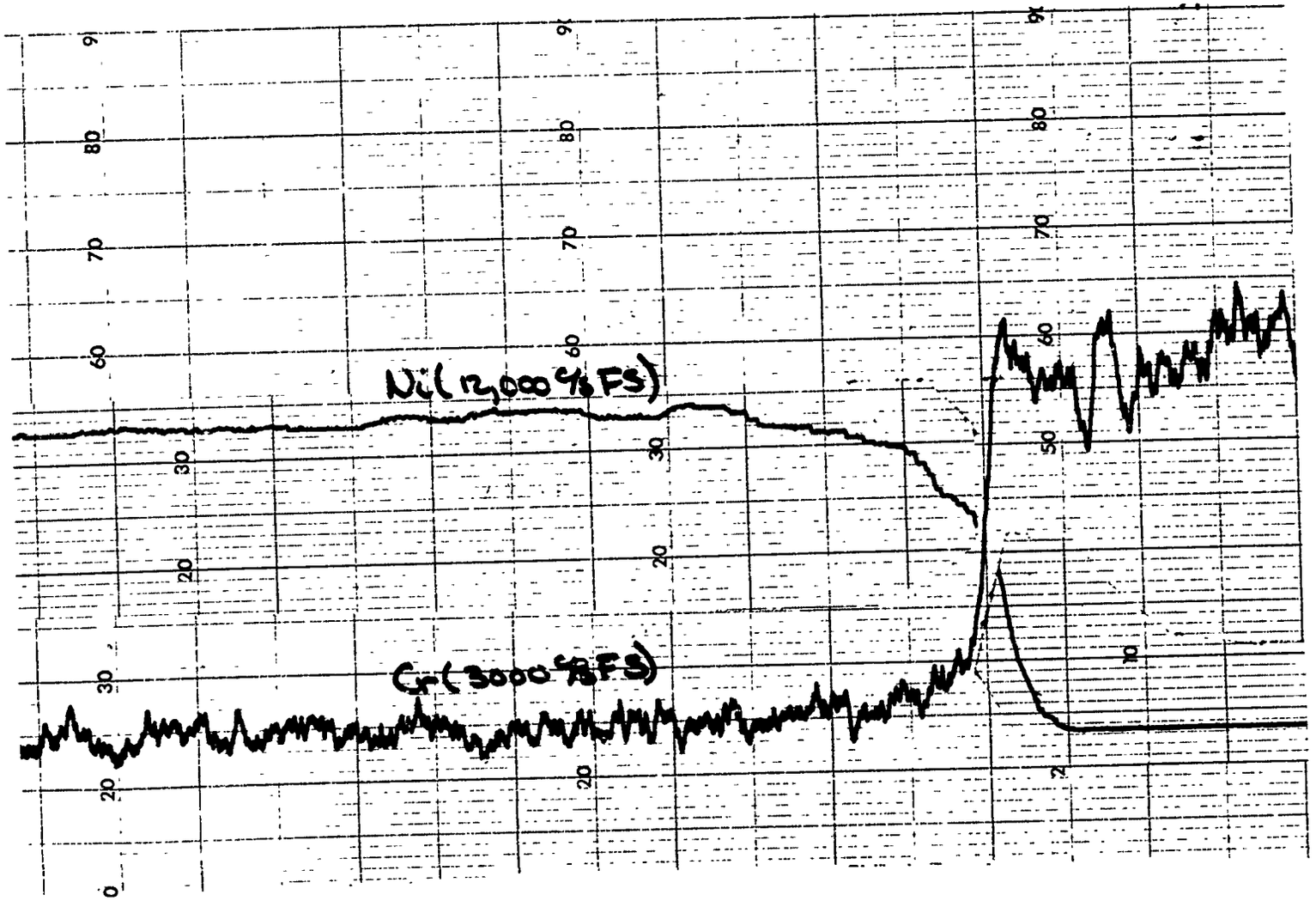

Figure 141. X-ray Distribution Scans Across Tube Wall/Braze Interface, Type 347 Stainless Steel - Nicrobraz 135, After Exposure. (Tube Is at Right.)

TABLE XXXVIII. CYCLIC HOT CORROSION TEST RIG SPECIMENS SUBMITTED TO MICROPROBE ANALYSIS

Specimen No.	Material	Temperature (°F)	Stress (ksi)	Time to Fail (hr)
14298	N-155	1500	4.5	967
13792	N-155	1500	15.2	17
14295	Hastelloy X	1500	9.0	135
13466	Hastelloy X	1300	19.1	187
13787	Type 347 SS	1500	5.0	170
13363	Type 347 SS	1300	13.9	107
13584	Incoloy 800	1500	2.8	502
13360	Incoloy 800	1300	15.3	33.6
16842	Inconel 625	1200	35.0	1610
16869	Inconel 625	1300	19.0	1604
16889	Inconel 625	1500	6.6	570

TABLE XXXIX. ELEMENTS DETECTED IN SPECTRAL SCANS

Specimen No.	Area	Material	Elements Detected
14298	Tube	N-155	Fe, Co, Cr, Ni, Mn, W
13788	Tube	Hastelloy X	Ni, Cr, Fe, Co, Mo
13787	Tube	Type 347 SS	Fe, Cr, Ni, Co, Mn
13998	Tube	Incoloy 800	Cr, Fe, Ni, Mn
12014	Tube	Inconel 625	Ni, Cr, Fe

The results of specific elemental distribution scans and scanning display pictures are presented in Figures 141 through 148. The observed results are summarized as follows:

N-155, 967 hr at 4.5 ksi and 1500°F (Figure 142)--The corrosion material was identified as chromium-manganese oxide; no sulfur was found at any position; manganese and, to a lesser extent, chromium gradients were observed at the tube walls. These elements were depleted by the corrosion exposure; cobalt, nickel, and iron were not depleted; niobium-rich regions, about 10μ in extent, were accompanied by decreases in manganese, chromium, cobalt, nickel, and iron; a spectral scan of a gray precipitate included in the braze area of this specimen is identified as chromium oxide; no tungsten was detected.

N-155, 17 hr at 15.2 ksi and 1500°F (Figure 143)--Distribution scans across the tube for the major elements are shown in Figure 143. (The gradual decrease in metal intensities and increase in oxygen from I to O is due to preferential X-ray absorption due to specimen rounding; i.e., the center of the tube is at a higher elevation than the tube edges.) The inner and outer corrosion zones again appeared to be primarily a chromium oxide, although chromium and oxygen X-ray correspondence is not quite as good as in the previous specimen.

A second series of distribution scans was taken across the wall at a place near the attachment where the wall was especially thick. The scans are presented in Figure 144; a corresponding photomicrograph given in Figure 145b exhibits a gray line where the probe scan was carried out. The inner portion of this thick layer consists of almost pure nickel with one intermediate band high in chromium. The outer portion of the tube at this position is uniform in composition. The presence of a corrosion zone, if any, at this point is not evident under the microscope. Perhaps the corrosion product has been eroded away during metallographic preparation.

Hastelloy X, 135 hr at 9.0 ksi and 1500°F (Figure 146)--The X-ray distribution scan crossed a corrosion band which passed through the tube wall. The corrosion product was identified as a chromium oxide phase which probably contained a small amount of molybdenum, but no iron or nickel. A small depletion of chromium was observed at the edges of the tube; molybdenum, gold, palladium, and sulfur were not detected.

Hastelloy X, 187 hr at 19.1 ksi and 1300°F (Figure 147)--A gray phase passing halfway through the tube was found to be rich in palladium and molybdenum, with depletion in iron and chromium; no oxygen or sulfur was associated with this phase.

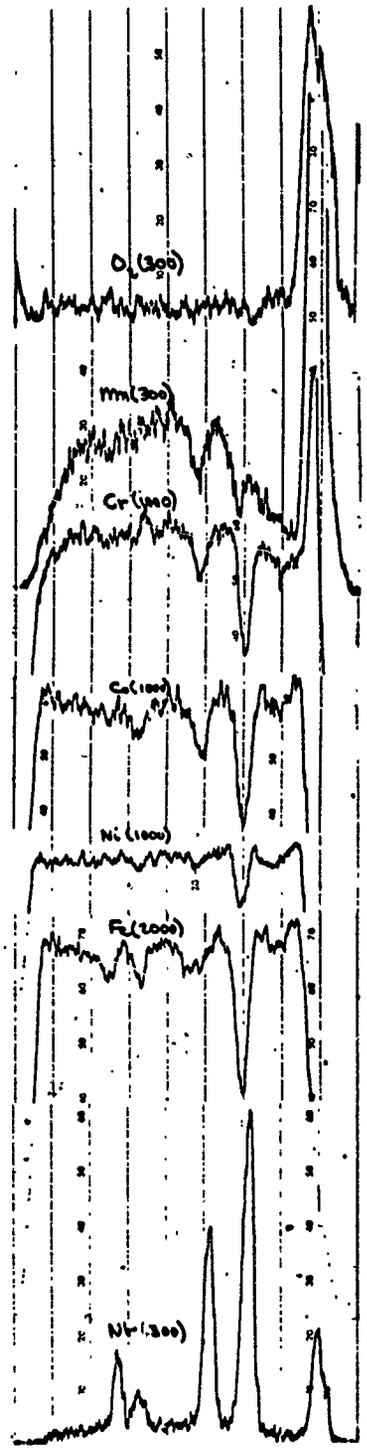

Figure 142. X-ray Distribution Scans Across Tube Wall in Vicinity of Failure Site, Transverse Section, N-155, 967 hr at 4.5 ksi and 1500°F.

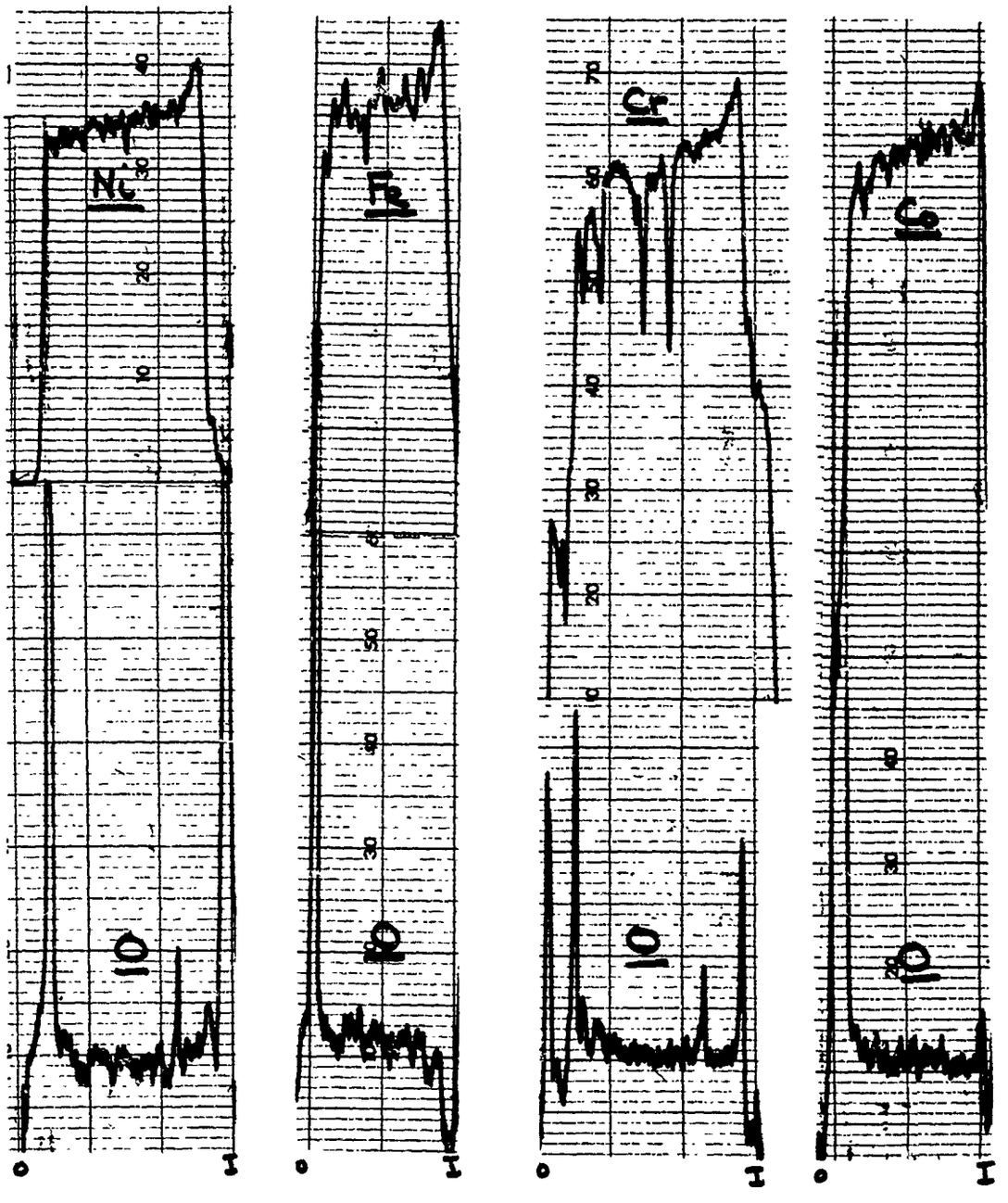

Figure 143. X-ray Distribution Scans Across Thick Wall Section, N-155, 17 hr at 15.2 ksi and 1500°F. (Inside of Wall Is at Right.)

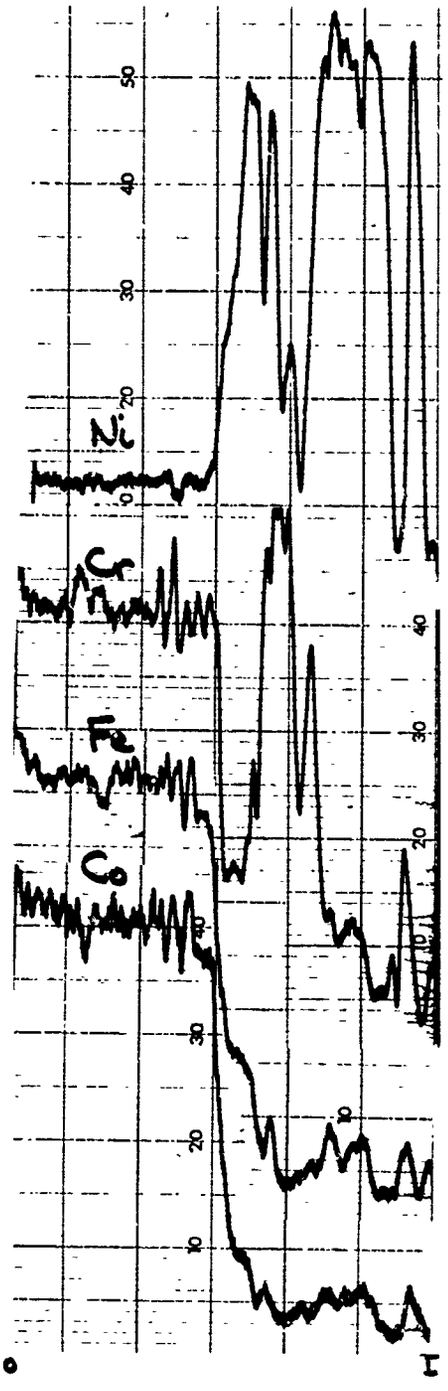

Figure 144. X-ray Distribution Scans Across Tube, N-155, 17 hr at 15.2 ksi and 1500°F. (Inside of Tube Is at Right.)

MAG = X320

(a) BRAZE ALLOY, WITH ATTACHMENT AT LOWER LEFT AND TUBE BODY AT UPPER RIGHT

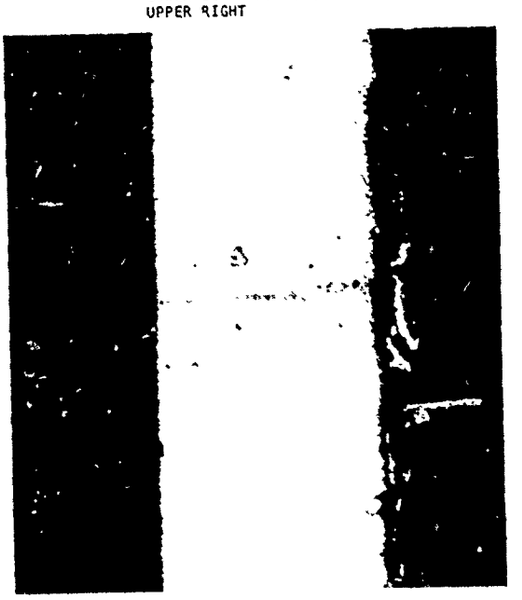

MAG - X250

(b) THICK WALL SECTION, WITH INSIDE WALL OF TUBE AT RIGHT

Figure 145. Photomicrographs of N-155 Exposed for 17 hr at 15.2 ksi and 1500°F.

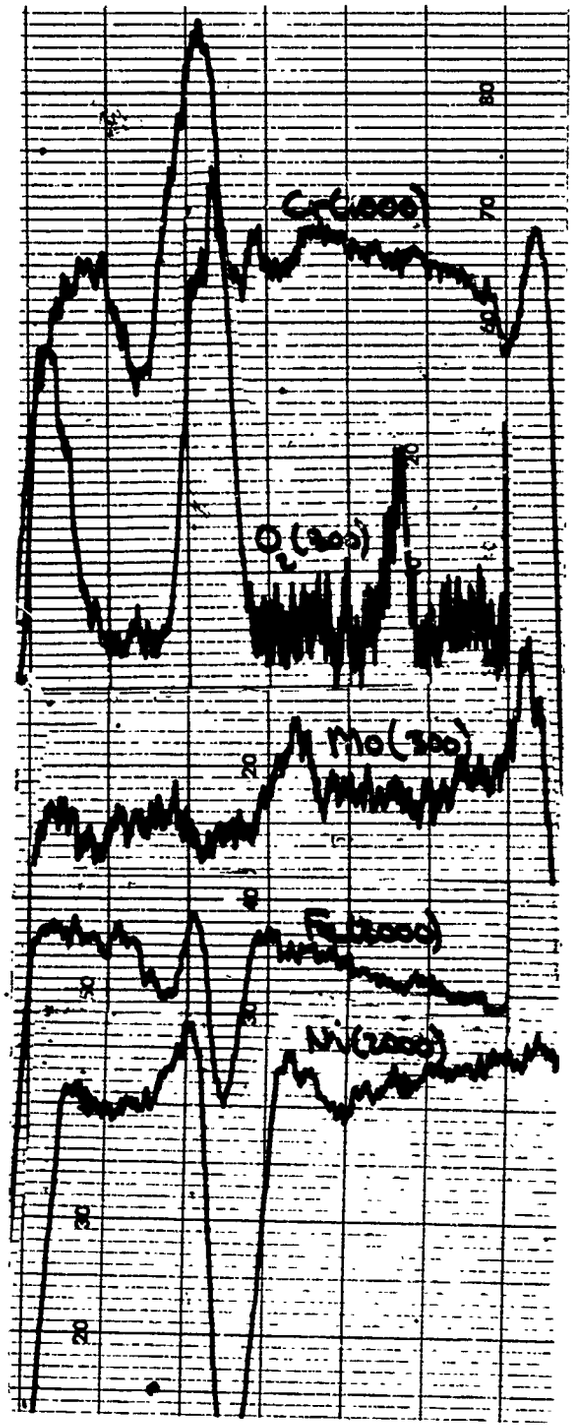

Figure 146. X-ray Distribution Scans Across Tube Wall in Vicinity of Failure Site, Transverse Section, Hastelloy X, 135 hr at 9.0 ksi and 1500°F, 2.5 mils per in. of Chart.

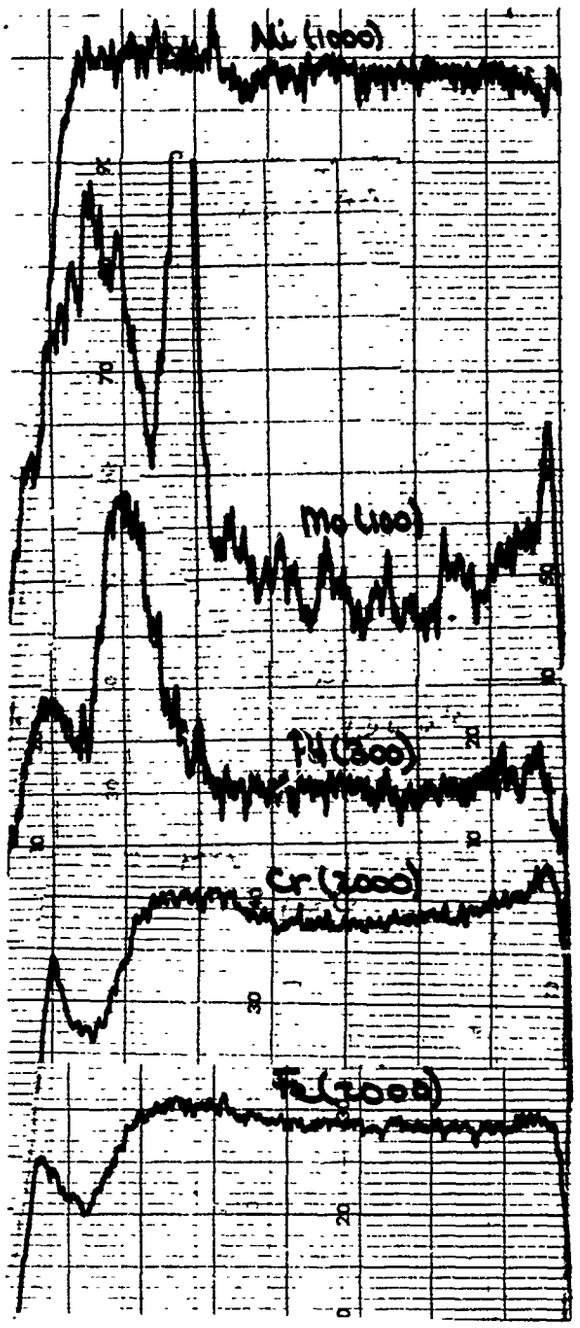

Figure 147. X-ray Distribution Scans Across Tube Wall in Vicinity of Failure Site, Transverse Section, Hastelloy X, 187 hr at 19.1 ksi and 1300°F.

Type 347 Stainless Steel, 170 hr at 5.0 ksi and 1500°F (Figure 148)--The traverse was carried out across a portion of the tube which included a thick inner corrosion product and a thin outer corrosion layer; the former contained a thin nickel oxide layer adjacent to the wall, followed by a chromium-iron oxide zone, and finally by an iron oxide zone; the outer wall corrosion product was identified as an iron oxide; a depletion in chromium and an enrichment in nickel were found at the center at the tube; no sulfur was detected.

Type 347 Stainless Steel, 107 hr at 13.9 ksi and 1300°F--This specimen was manually scanned for iron, nickel, chromium, cobalt, silicon, oxygen, and sulfur. The exterior corrosion phase consisted of an outside layer of chromium oxide and an inner layer of nickel-iron oxide; iron, nickel, manganese, and chromium were quite uniform across the tube; silicon, cobalt, and sulfur were not detected; some oxygen was also observed along the interior tube wall.

Incoloy 800, 502 hr at 2.8 ksi and 1500°F--Manual scanning of corrosion zones which intruded into the outer tube wall identified the corrosion material as chromium oxide; one large gray precipitate adjacent to the inner wall was identified as silicon dioxide, perhaps introduced during polishing. Elemental point counting was carried out at the center and outside edge of the tube to detect depletion at the wall; the following X-ray counts were obtained:

Cr		Fe		Ni	
Edge	Center	Edge	Center	Edge	Center
39217	42013	48970	48570	30167	28353
40895	39274	47226	49100	30017	28546
40235	40607	49321	48994	29415	28143

There is no evidence of surface depletion of any of these elements; nickel is perhaps slightly enriched at the surface.

A second set of distribution scans was taken in the vicinity of the failure site in a transverse section. The region of the scans is pictured in Figure 149d, which also shows the inner corrosion layer. The traces are presented in Figure 150. Oxygen and chromium were observed to increase in the vicinity of the crack, indicating a chromium oxide layer along the crack.

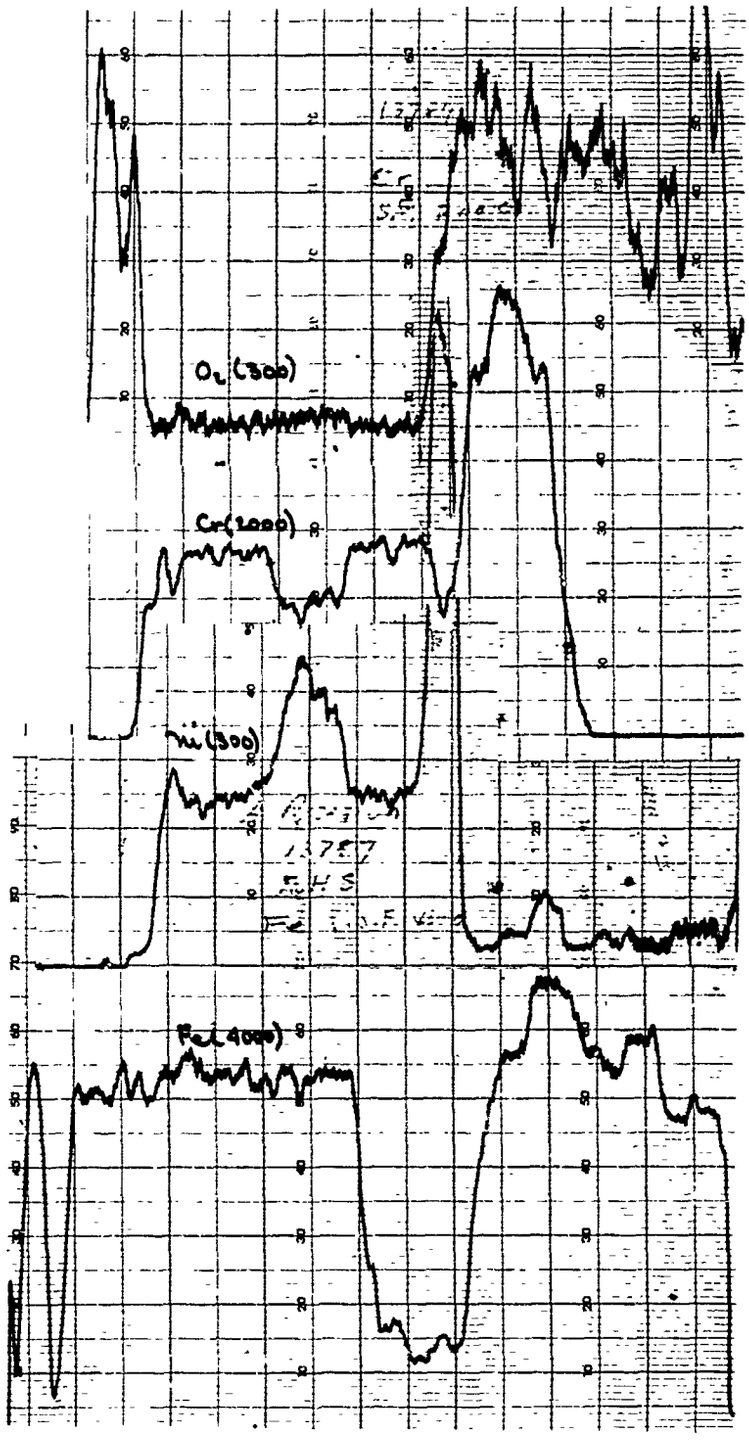

Figure 148. X-ray Distribution Scans Across Tube Wall in Vicinity of Failure Site, Transverse Section, Type 347 Stainless Steel, 170 hr at 5.0 ksi and 1500°F, 2.5 mils per in. of Chart.

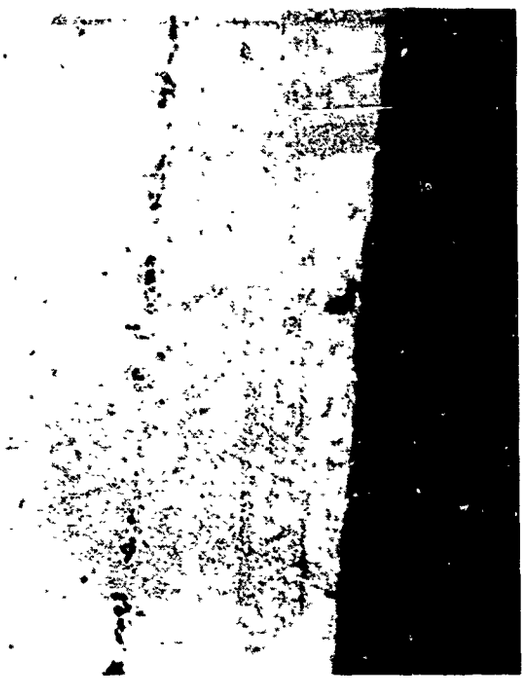

MAG - X320

(a) TUBE BODY (INSIDE WALL OF TUBE IS AT RIGHT)

MAG = X400

(b) INTERFACE BETWEEN BRAZE ALLOY AND ATTACHMENT, WITH ALLOY AT UPPER RIGHT

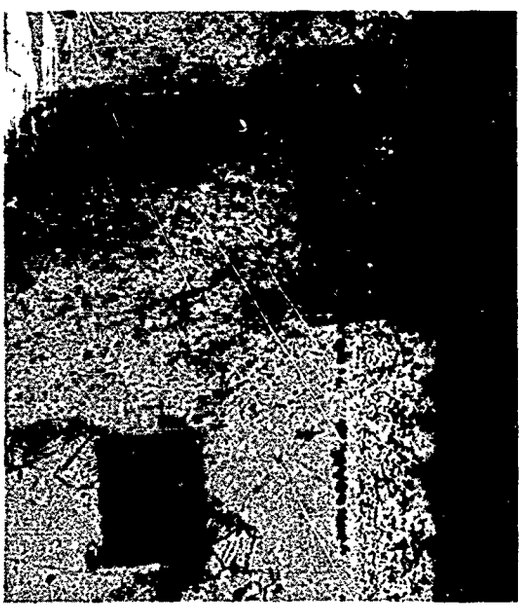

MAG = X150 (c) AREAS SHOWN IN (a) AND (b)

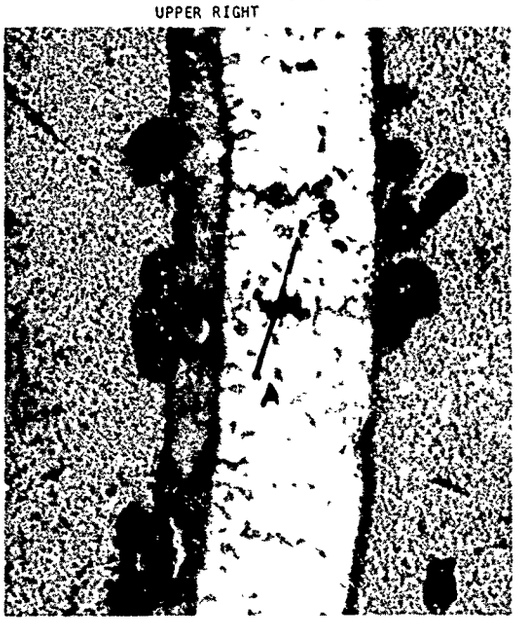

MAG = X250 (d) TUBE FAILURE SITE, TRANSVERSE SECTION

Figure 149. Photomicrographs of Incoloy 800, 502 hr at 2.8 ksi and 1500°F.

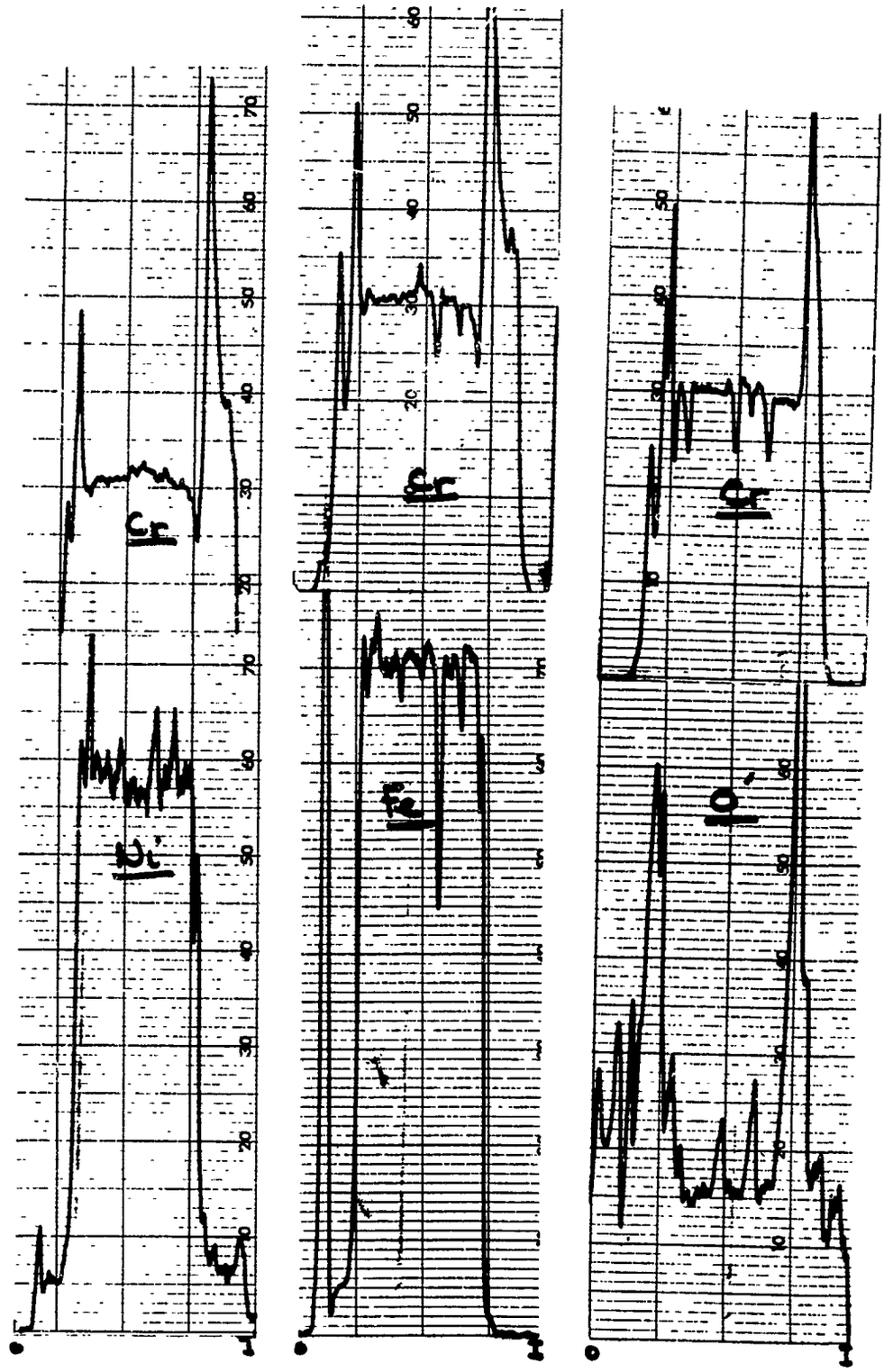

Figure 150. X-ray Distribution Scans Across Tube, Incoloy 800, 502 hr at 2.8 ksi and 1500°F. (Inside of Tube Is at Right.)

Scanning display X-ray images were taken at two sites corresponding to the inner film, tube, and braze alloy and to the grain boundary phase in the attachment adjacent to the braze. Photomicrographs of these regions are presented in Figure 149, where the darkened areas represent the scanning display regions. The very edge of the tube yields an increase in iron, nickel, and chromium. The corrosion layer, which corresponds to the right one-fourth of the images, presents isolated patches rich in iron and nickel and a large precipitate (≈1 mil in cross section) of pure silicon. The portion of the corrosion layer corresponding to the lower right side of the images was considerably below the level of the tube; X-rays emerging from this area were completely absorbed by the tube and are not observed on the images. Manual scanning indicated that most of the layer, which was especially thick at this point, corresponded to chromium oxide.

Incoloy 800, 33.6 hr at 15.3 ksi and 1300°F--A scan at one location, where the gray film was thicker than average, yielded high chromium and manganese contents and low amounts of iron, nickel, and titanium. Sulfur was not detected at any position in either the inner or the outer film.

Distribution scans for the principal elements were run across the tube wall; data were collected for chromium, iron, nickel, and oxygen, where chromium was used as a monitor to indicate changes from one scan to the next due to slight changes in beam positioning. Both the inner and outer corrosion films are identified as chromium oxide. Across the tube wall, there are a few spots showing an increase in nickel (and possibly in oxygen), with a corresponding decrease in chromium and iron.

Inconel 625, 1610 hr at 35.0 ksi and 1200°F--Very little oxidation was observed on this specimen. The 1μ-step scan through the surface of the tube showed an oxide film about 5μ thick (Figure 151). The oxide present was rich in chromium and contained traces of iron and nickel. There was a layer about 5μ thick below the oxide which was depleted in molybdenum, nickel, and chromium. There had been no diffusion of oxygen into the matrix of the tube. Figure 152 shows an X-ray display photograph, indicating the distribution of sulfur in the corroded area. Note that there is no correlation between the sulfur distribution and the corrosion products.

Inconel 625, 1604 hr at 19.0 ksi and 1300°F--Figure 153 shows that very little oxide was detected on the surfaces of the tube exposed for 1604 hr at 1300°F. The 1μ step scan illustrated that there was a layer approximately 5μ thick below the surface which became depleted in molybdenum and nickel, which presumably were volatilized. No sulfur was detected on the surface of the tubes, and no oxygen had diffused into the tube wall.

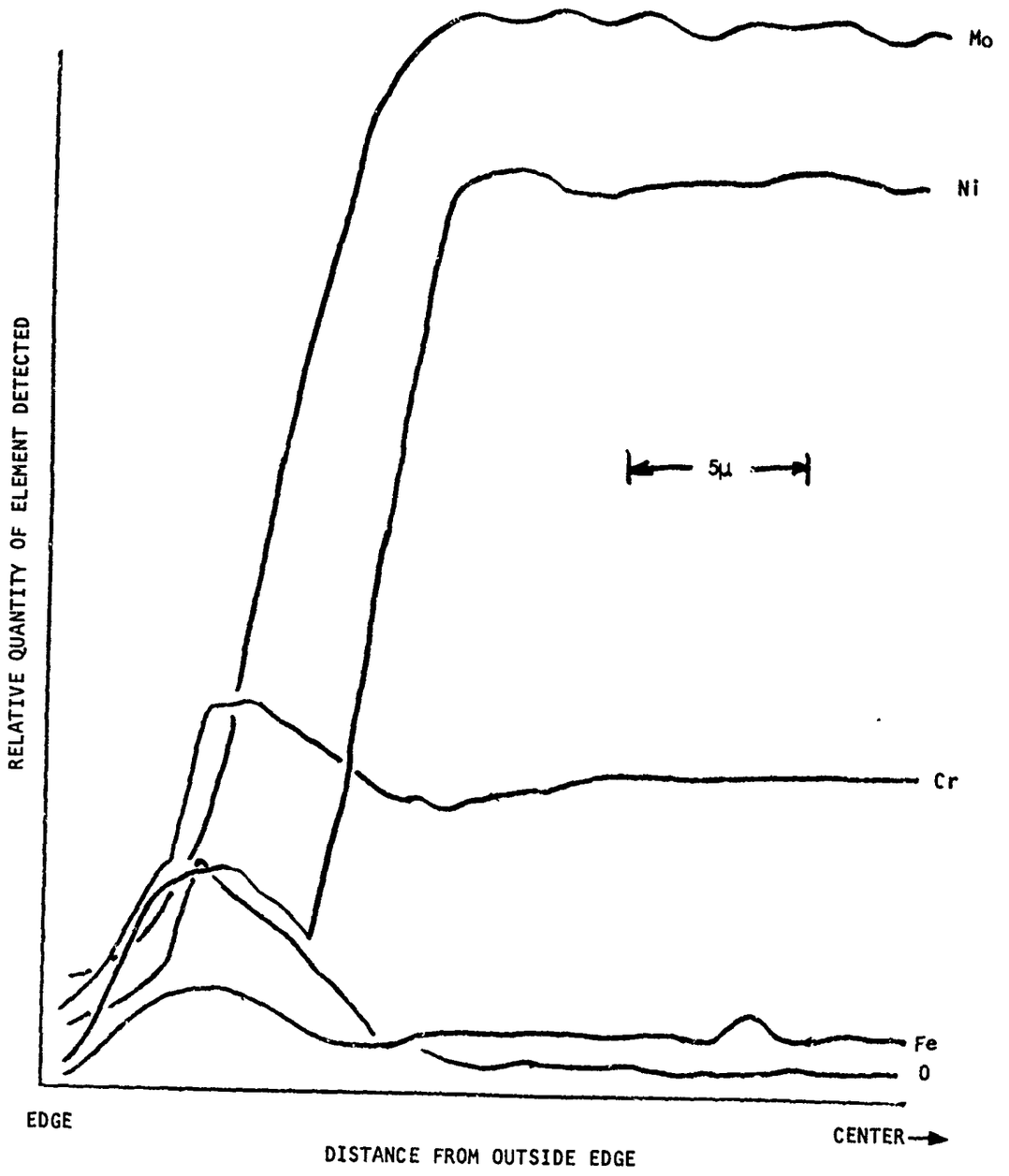

Figure 151. 1μ Step Scan, Inconel 625 Cyclic Hot Corrosion Test, Specimen 16842, Exposed 1610 hr at 35.0 ksi and 1200°F.

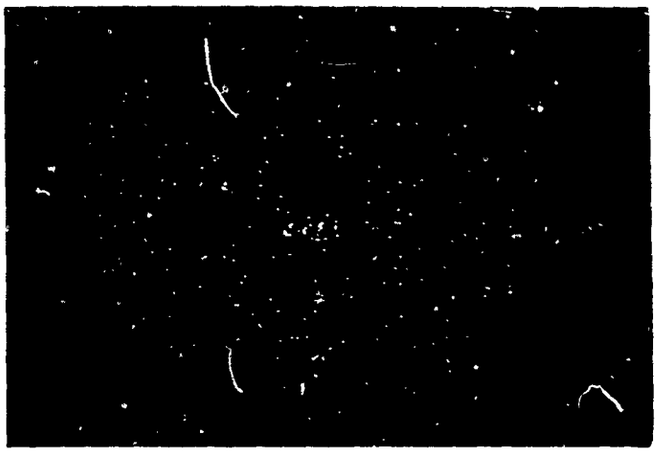

Figure 152. Scanning Display X-ray Image Showing Sulfur Distribution in Inconel 625 Exposed 1610 hr at 35.0 ksi and 1200°F in the Cyclic Hot Corrosion Test Rig. (Note Uniform Distribution of Sulfur, Indicating No Sulfides Were Produced by the Corrosive Test Atmosphere.)

Inconel 625, 570 hr at 6.6 ksi and 1500°F--Again, little or no oxide layer was detected on the external surfaces of the tubes, although the chromium depletion layer extended 15 to 20μ below the surface. A thin nickel oxide layer approximately 5μ thick was detected on the inner surface of the tube by the 1μ step scan (Figure 154).

RECUPERATOR TEST RIG

The five specimens which were submitted for characterization studies are shown in Table XL.

TABLE XL. PHASE II RECUPERATOR TEST RIG SPECIMENS SUBMITTED FOR MICROPROBE ANALYSIS

Testing Time		Total Exposure Time (hr)	Sea-Salt Concentration (ppm)	Specimen Number	
On (hr)	Off (hr)			N-155	Incoloy 800
0	36	36	5.0	17280	17284
36	150	114	0.022	17174	17172
300	500	200	0.10	17298	17300
36	500	464	Up to 0.10	17288	17291
0	500	500	5.0 (36 hr 0.0 (36 hr) Up to 0.1 (428 hr)	17302	17301

Step scans were conducted on all of the specimens in an attempt to identify the products of corrosion. In addition, the degree of diffusion of oxygen into the base metal was assessed to determine the amount of sound metal remaining after exposure. The various observations are summarized below:

N-155, 36-hr Exposure, 5.0-ppm Sea Salts--Figure 155 shows the 1μ step scan taken through the surface layers of the corroded tube. It indicates that the outer surface of the tube was covered with a layer of chromium oxide about 15μ thick and that oxygen had not penetrated the oxide layer.

N-155, 114-hr Exposure, 0.022-ppm Sea Salts (Maximum)--An oxide layer about 8μ thick was measured on this specimen. Figure 156 shows the results of a 1μ step scan which indicates that the oxygen did not penetrate the oxide film.

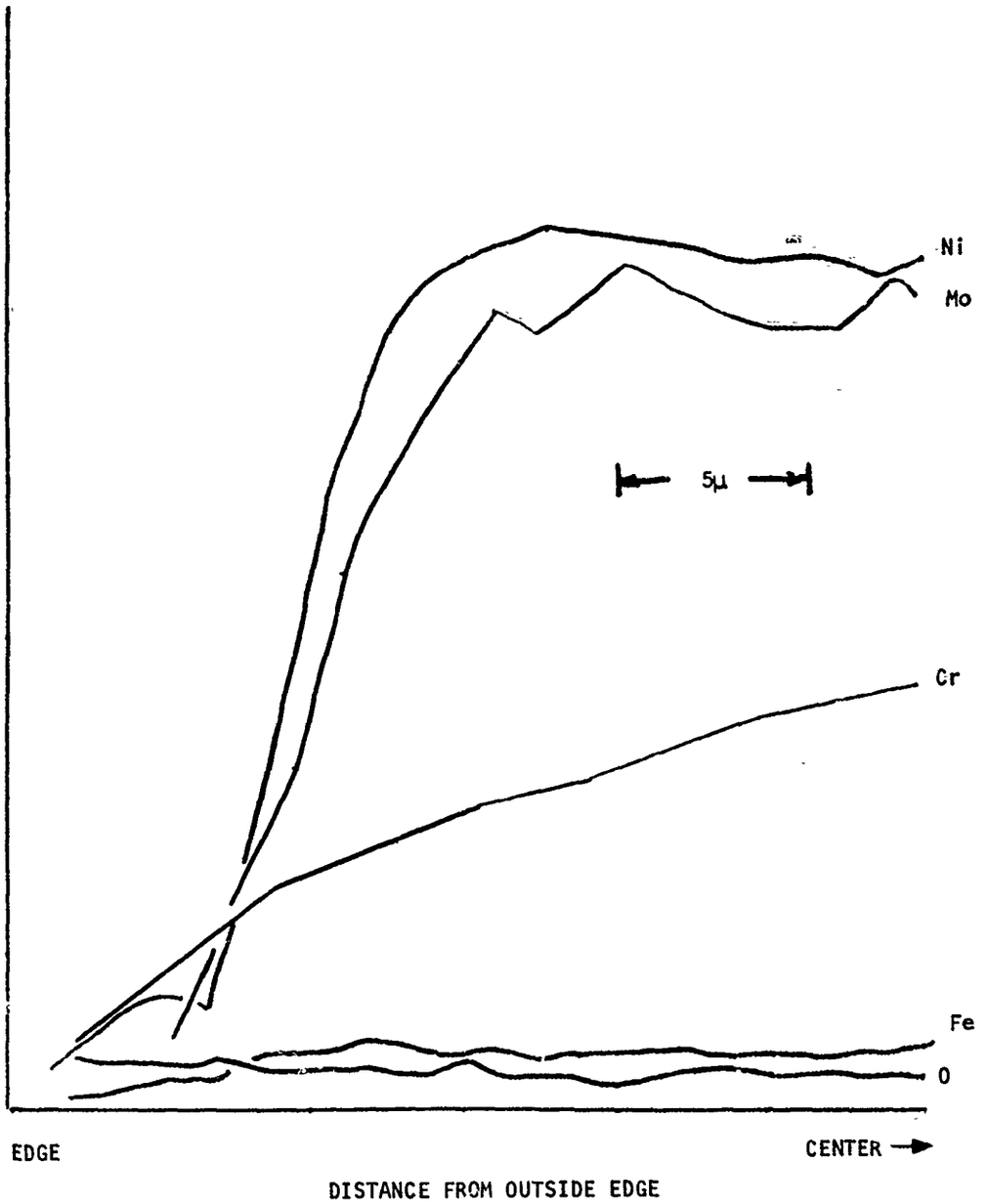

Figure 154. 1μ Step Scan, Inconel 625 Cyclic Hot Corrosion Test, Specimen 16889, Exposed 570 hr at 6.6 ksi and 1500°F.

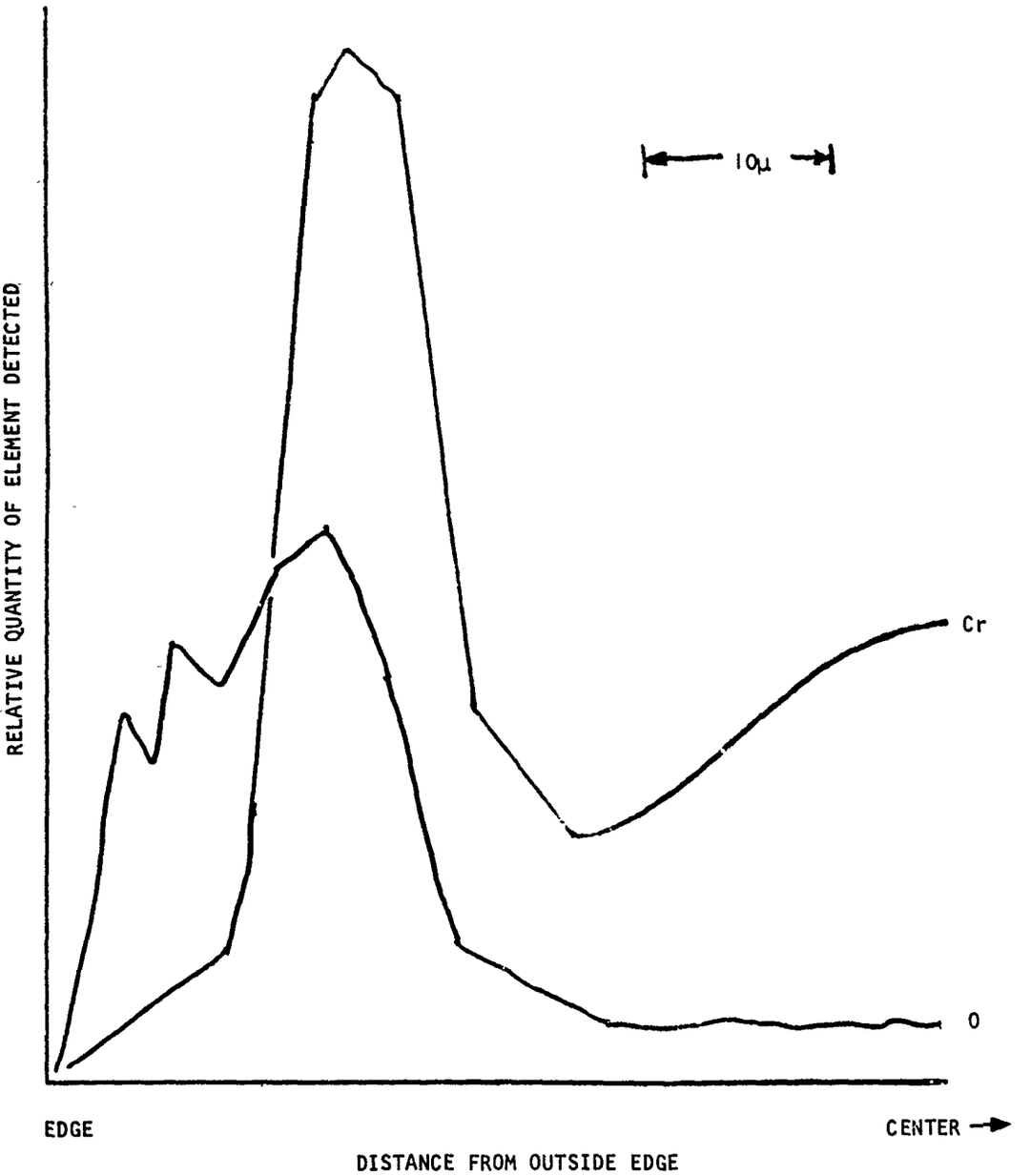

Figure 155. 1μ Step Scan, N-155 Recuperator Test Rig, Specimen 17280, Exposed 36 hr at Approximately 1500°F and 5-ppm Sea Salts.

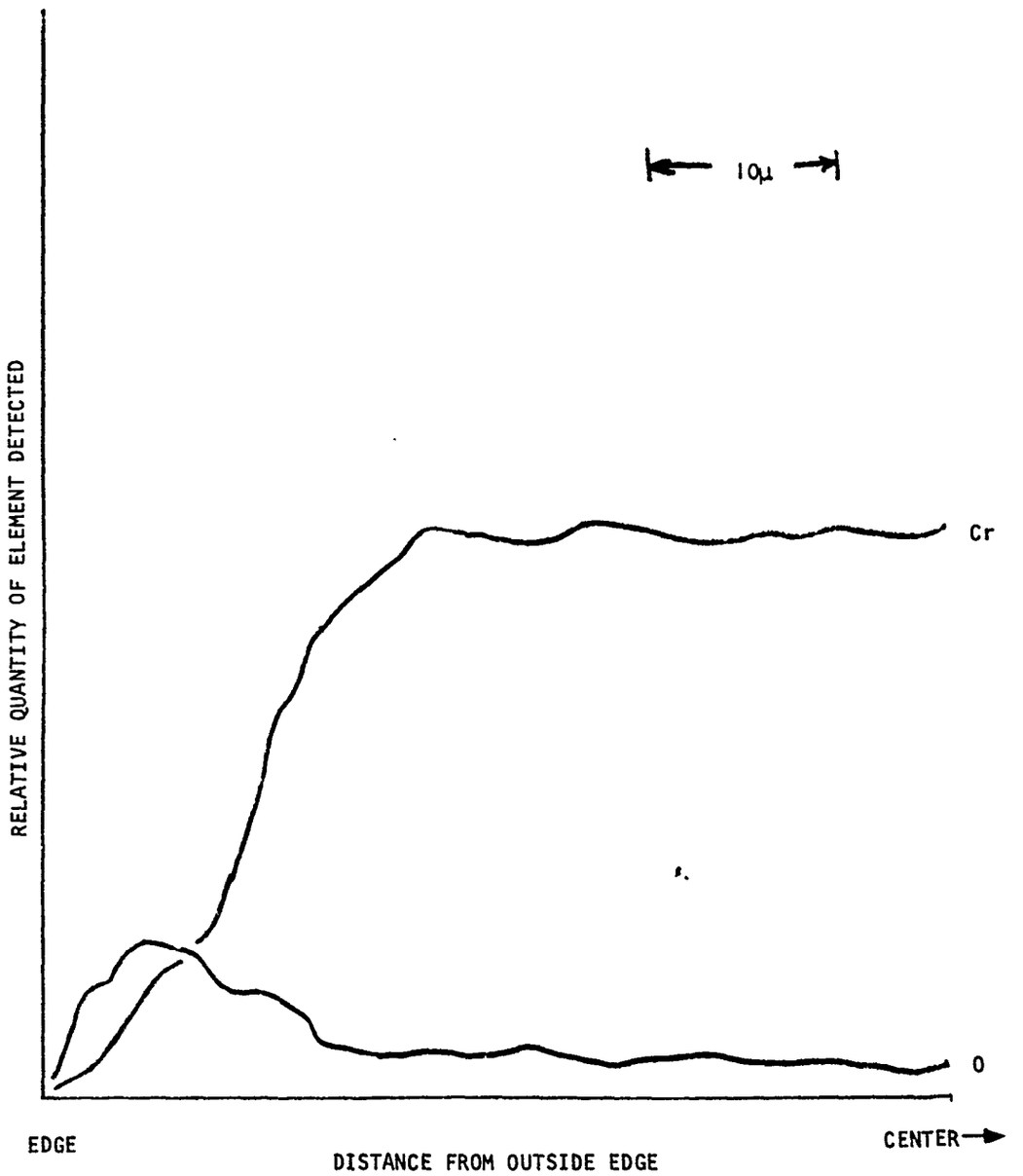

Figure 156. 1μ Step Scan, N-155 Recuperator Test Rig, Specimen 17174, Exposed 114 hr at Approximately 1500°F and 0.022-ppm Sea Salts Maximum.

N-155, 200-hr Exposure, 0.10-ppm Sea Salts--Figure 157 shows the 1μ step scan through the oxide layer on the outer surface of the tube. It illustrates that the oxide layer was 10 to 15μ thick and consisted essentially of chromium oxide. The N-155 had suffered no internal oxidation.

N-155, 464-hr Exposure, 0.10-ppm Sea Salts (Maximum)--A layer of chromium oxide 30μ thick was found on this tube specimen by the 1μ step scan. Figure 158 again shows that the outer oxide film was impervious to oxygen.

N-155, 500-hr Exposure, First [illegible] hr at 5.0-ppm and Subsequent Time at 0.1-ppm Sea Salts (Maximum)--The chromium oxide layer, approximately 20μ thick, covered a 10μ-deep zone of chromium-depleted matrix. X-ray display photographs were made on this specimen in an effort to detect sulfur, but no more than the normal amount which contaminates N-155 wrought material was found. The 1μ step scan is shown in Figure 159, and Figure 160 depicts the X-ray display photograph of the sulfur distribution.

Incoloy 800, 36-hr Exposure, 5.0-ppm Sea Salts--Figure 161, the 1μ step scan through the oxide layer, shows that the chromium oxide film was 8 to 10μ thick, that there was a chromium-depleted layer, and that no internal oxidation had taken place.

Incoloy 800, 114-hr Exposure, 0.022-ppm Sea Salts (Maximum)--Elements nickel and iron were also determined on this specimen in conjunction with chromium and oxygen. The 5μ step scan indicated that the outer oxide layer consisted of iron oxide superimposed upon a chromium-nickel oxide layer. The total oxide layer was about 50μ thick and covered a layer of metal rich in nickel but depleted in iron and chromium. No oxygen had penetrated the oxide film (Figure 162).

Incoloy 800, 200-hr Exposure, 0.10-ppm Sea Salts--The 1μ step scan through the surface layers of the tube revealed an oxide layer 18μ thick superimposed upon a 5 to 8μ deep layer of chromium-depleted metal (Figure 163).

Incoloy 800, 464-hr Exposure, 0.10-ppm Sea Salts (Maximum)--An oxide layer 30μ deep was found on the tube specimen which had been exposed for 464 hr in the recuperator test rig. Oxygen had not penetrated the oxide layer, and there was little or no depletion of chromium in the underlying layer of metal. The 1μ step scan is shown in Figure 164, and the X-ray display photograph is shown in Figure 165. The photograph shows that there was an even distribution of sulfur, which did not appear to be associated with the corrosion products.

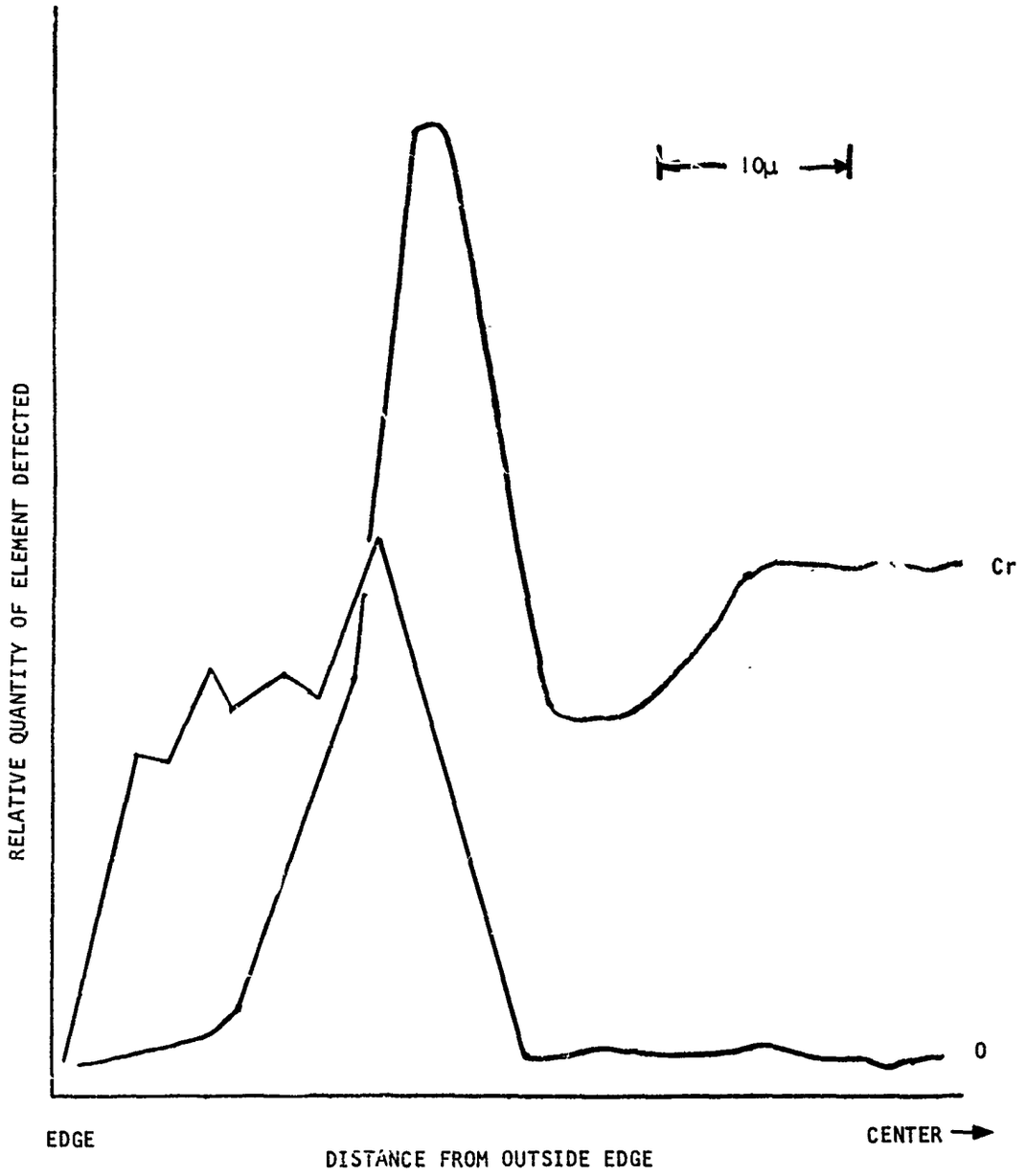

Figure 157. 1μ Step Scan, N-155 Recuperator Test Rig, Specimen 17298, Exposed 200 hr at Approximately 1500°F and 0.10-ppm Sea Salts.

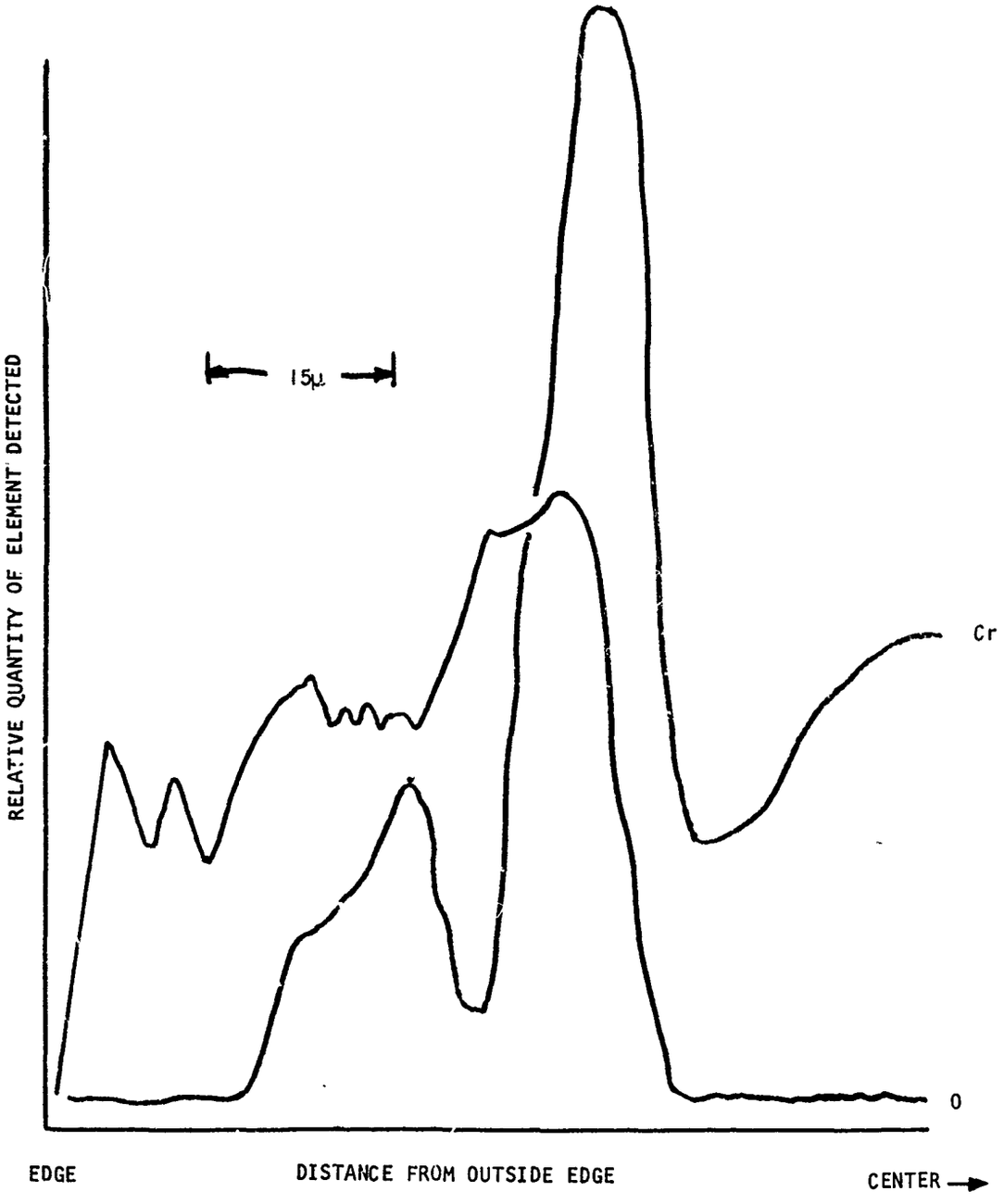

Figure 158. 1μ Step Scan, N-155 Recuperator Test Rig, Specimen 17288, Exposed 464 hr at Approximately 1500°F and 0.10-ppm Sea Salts Maximum.

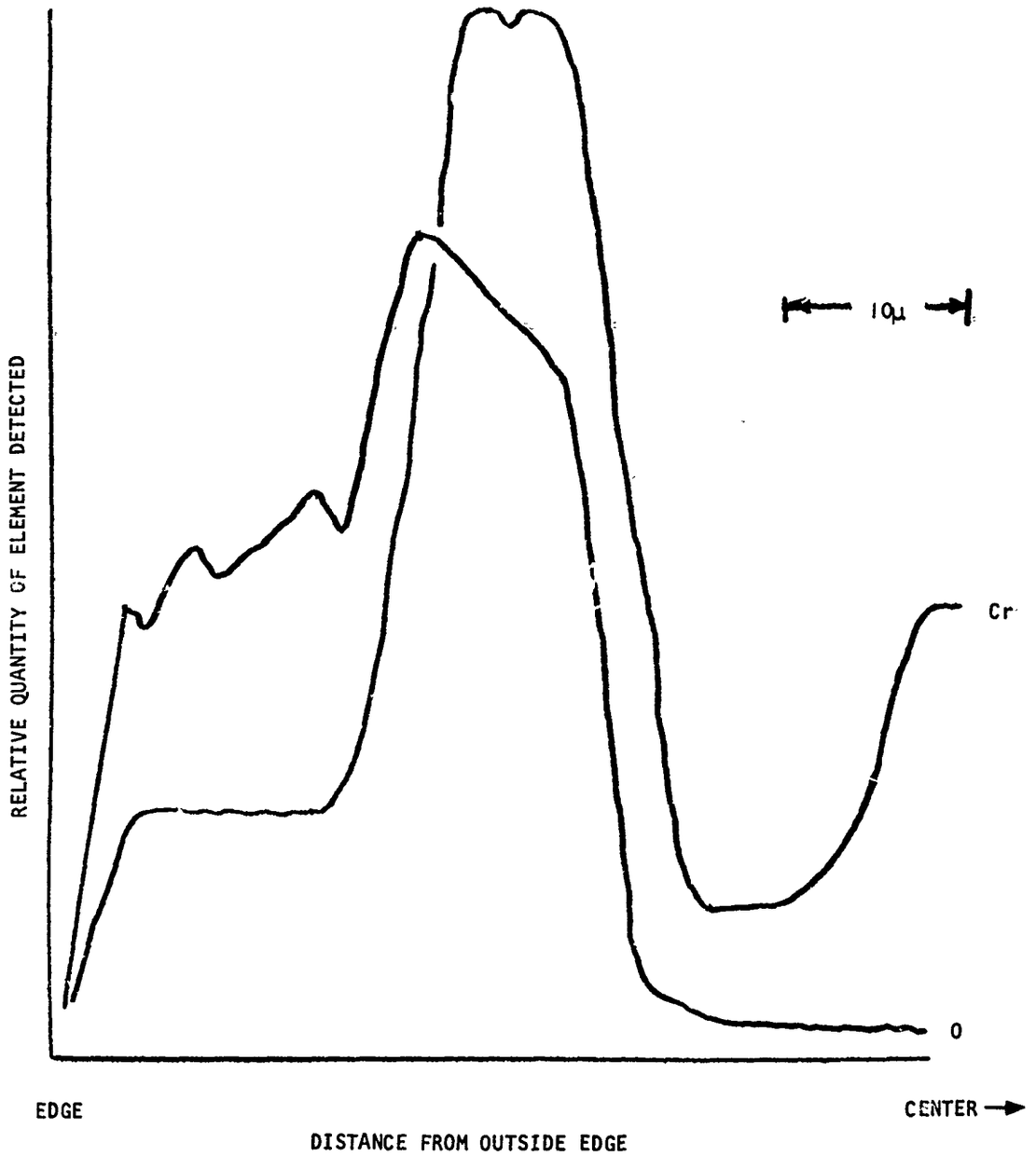

Figure 159. 1μ Step Scan, N-155 Recuperator Test Rig, Specimen 17302, Exposed 500 hr at Approximately 1500°F.

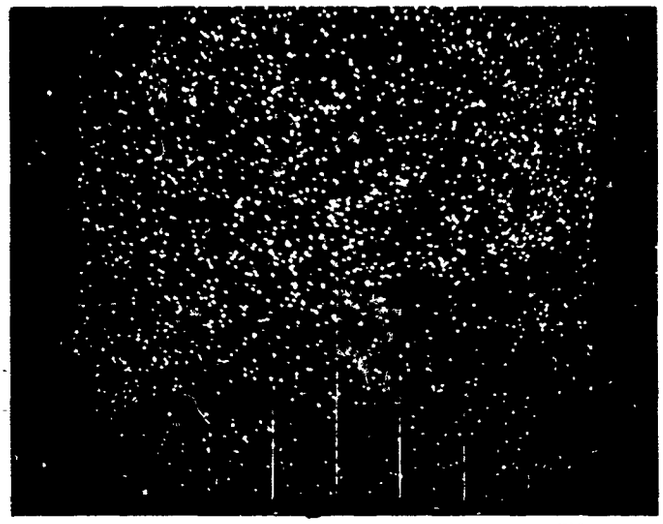

Figure 160. Sulfur Distribution in N-155 Exposed 300 hr in Recuperator Test Rig. (Note Uniform Distribution of Sulfur, Indicating No Sulfides Were Produced by the Corrosive Test Atmosphere.)

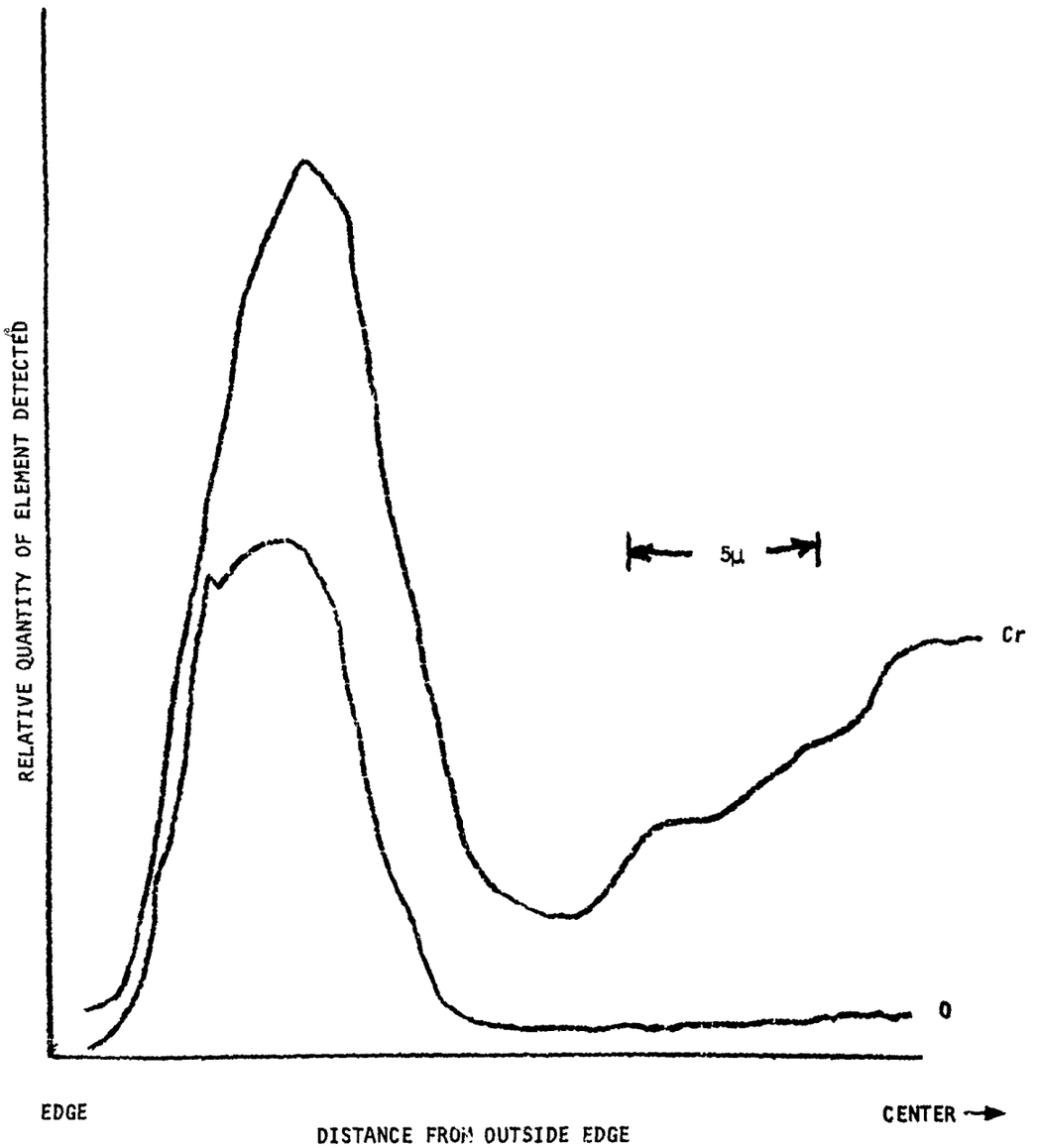

Figure 161. 1μ Step Scan, Incoloy 800 Recuperator Test Rig, Specimen 17284, Exposed 36 hr at Approximately 1500°F and 5.0-ppm Sea Salts.

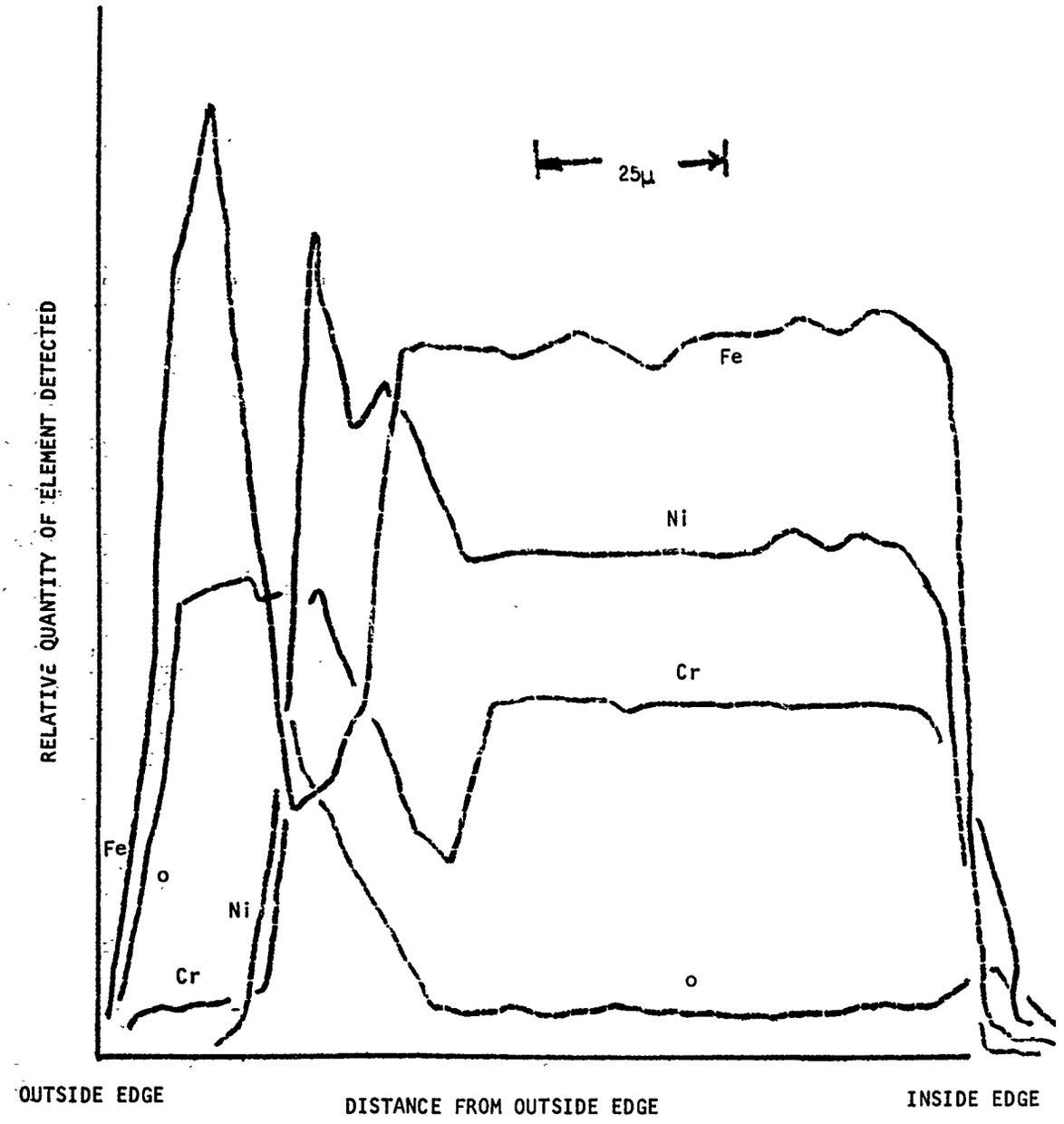

Figure 162. 5μ Step Scan, Incoloy 800 Recuperator Test Rig, Specimen 17172, Exposed 114 hr at Approximately 1500°F and 0.022-ppm Sea Salts Maximum.

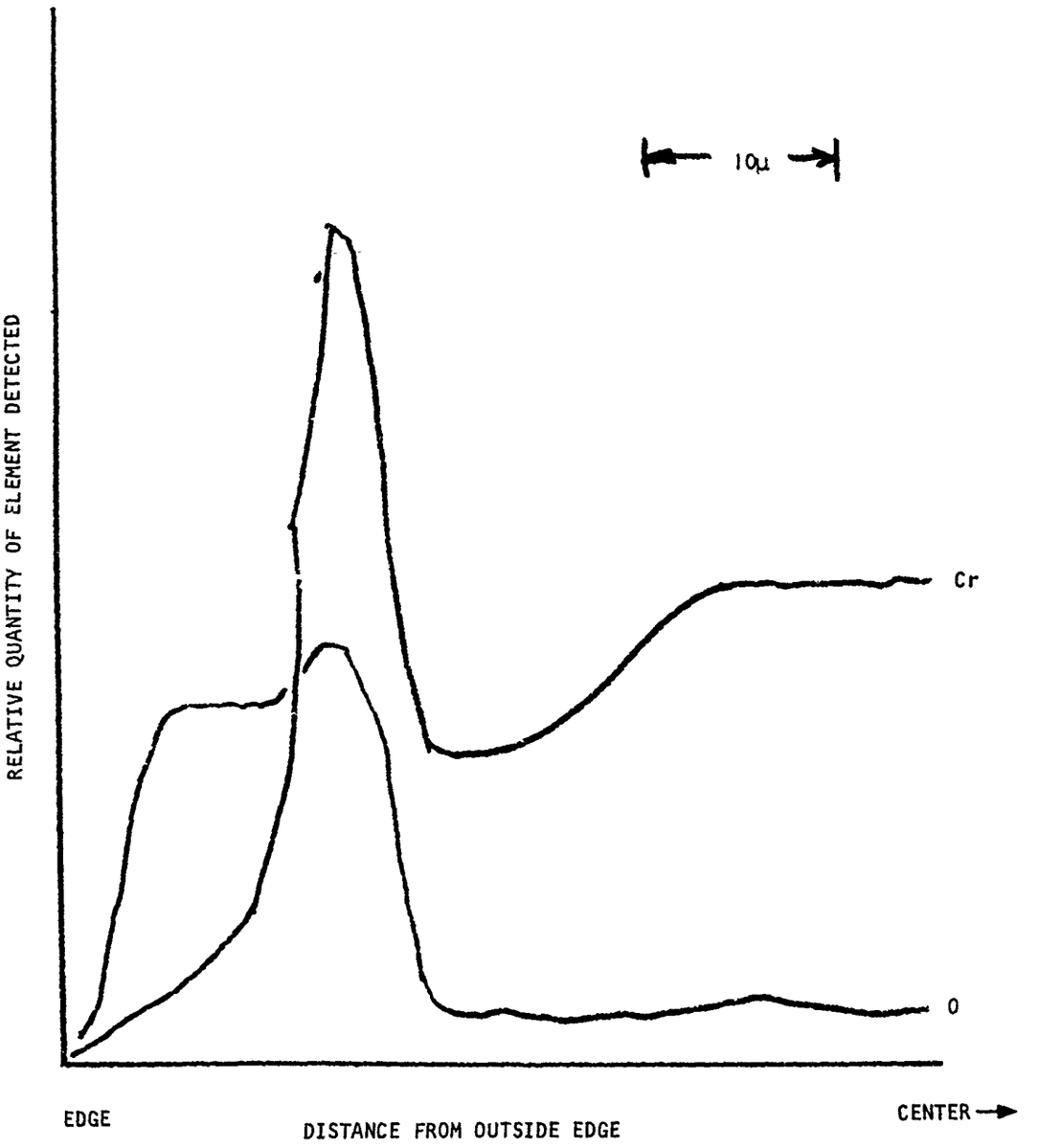

Figure 163. 1μ Step Scan, Incoloy 800 Recuperator Test Rig, Specimen 17300, Exposed 200 hr at Approximately 1500°F and 0.10-ppm Sea Salts.

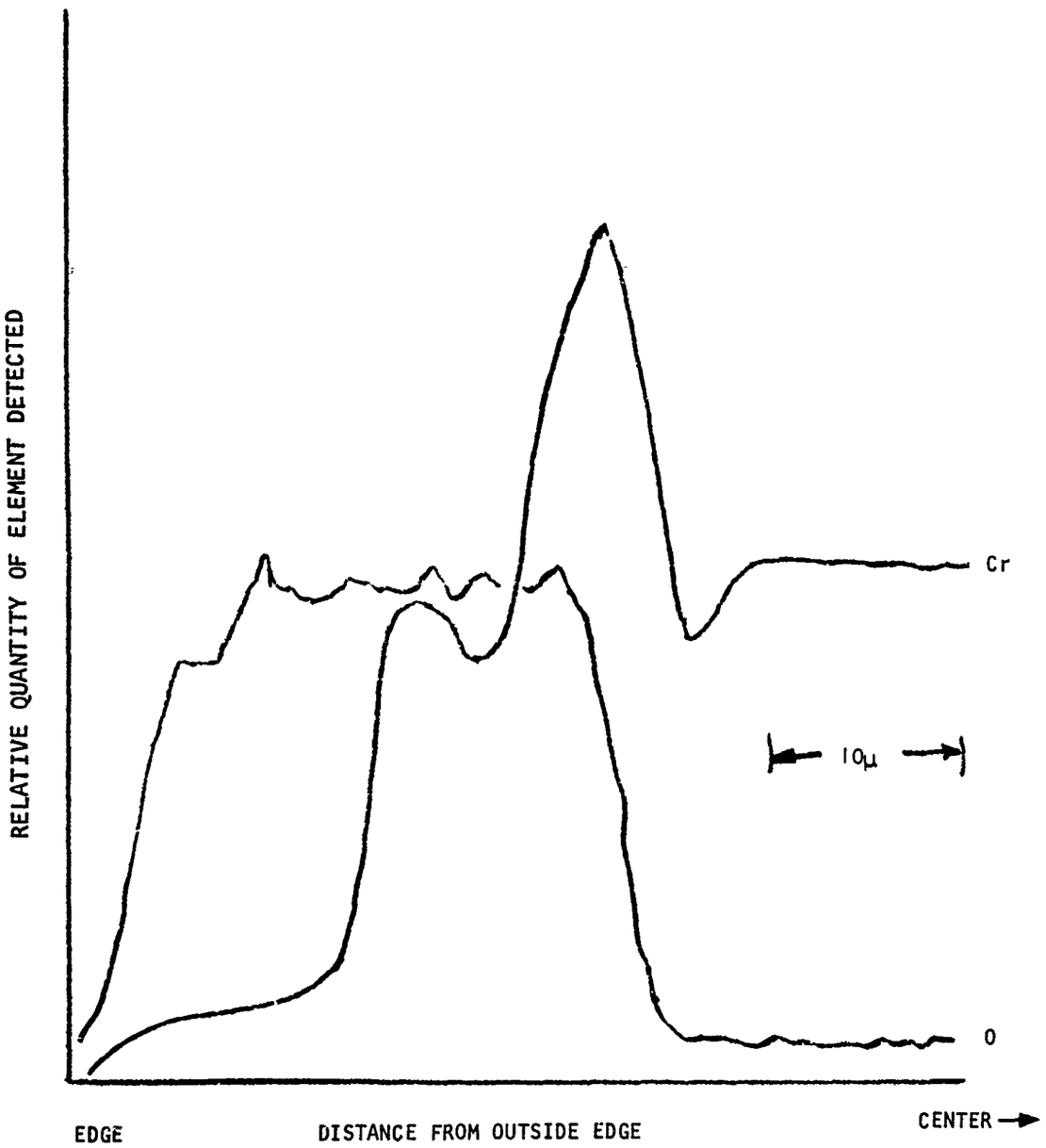

Figure 164. 1μ Step Scan, Incoloy 800 Recuperator Test Rig, Specimen 17291, Exposed 464 hr at Approximately 1500°F and 0.10-ppm Sea Salts Maximum.

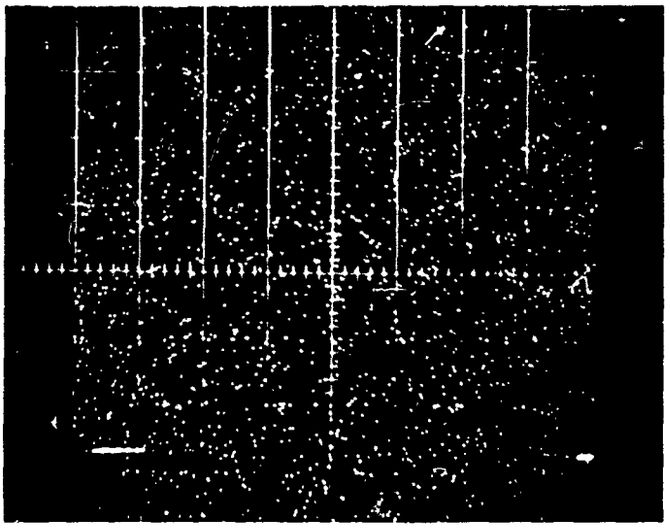

Figure 165. Sulfur Distribution in Incoloy 800 Exposed 464 hr in Recuperator Test Rig. (Note Uniform Distribution of Sulfur, Indicating No Sulfides Were Produced by the Corrosive Test Atmosphere.)

Incoloy 800, 500-hr Exposure, First 36 hr at 5.0-ppm and Subsequent Time at 0.1-ppm Sea Salts (Maximum)--Figure 166 shows that an oxide layer 16μ thick was produced on the outer surface of the tube. No internal oxidation was detected, although an extensive layer of chromium-depleted metal was revealed.

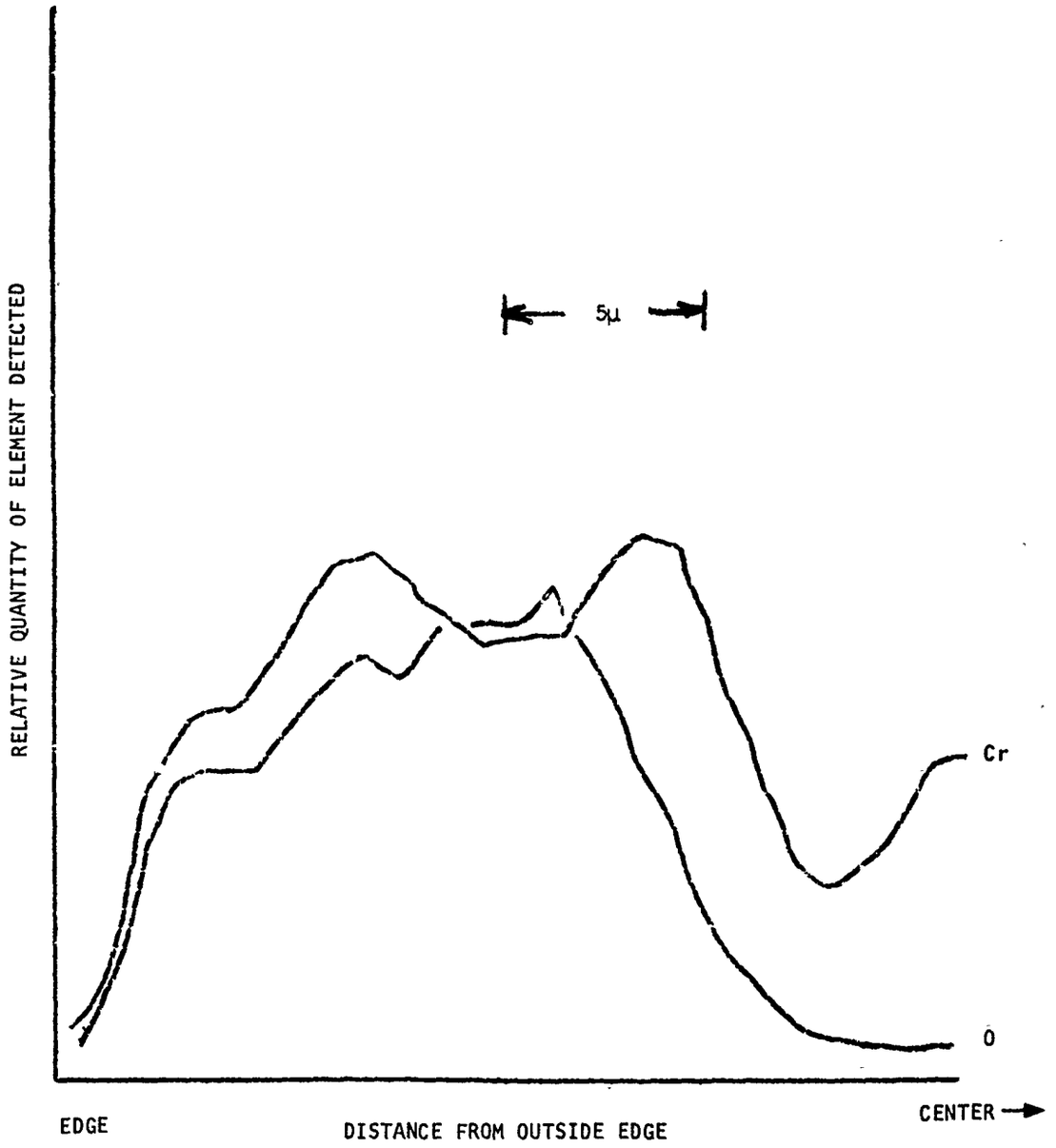

Figure 166. 1μ Step Scan, Incoloy 800 Recuperator Test Rig, Specimen 17301, Exposed 500 hr at Approximately 1500°F.

LITERATURE CITED

1. Wheeler, A. J., Dolf, H. R., Klein, V. J., and Acurio, J., SMALL GAS TURBINE ENGINE COMPONENT TECHNOLOGY REGENERATOR RESEARCH, The Boeing Company; USAAVLABS Technical Report 66-90, U.S. Army Aviation Materiel Laboratories, Fort Eustis, Virginia, January 1967, AD 809557L.

2. Haryslak, L. W., and Pollini, R. J., MARINE ENVIRONMENT INFLUENCE ON GAS TURBINE HOT CORROSION, Hot Corrosion Problems Associated with Gas Turbines, ASTM STP 421, 1967, pp. 146-168.

3. Simons, E. L., Browning, G. V., and Liebhafsky, H. A., SODIUM SULPHATE IN GAS TURBINES, Corrosion, Vol. 11, December 1955, p. 505.

4. Sykes, C., and Shirley, H. T., SCALING OF HEAT RESISTING STEELS, INFLUENCE OF COMBUSTIBLE SULPHUR AND OIL FUEL ASH CONSTITUENT, Iron and Steel Institute Special Report No. 43, 1951, p. 153.

5. Shirley, H. T., EFFECTS OF SULPHATE-CHLORIDE MIXTURES IN FUEL ASH CORROSION OF STEELS AND HIGH NICKEL ALLOYS, Journal of the Iron and Steel Institute, February 1956, p. 144.

6. Roush, M. S., MATERIALS STUDY OF PROTECTIVE COATINGS FOR GAS TURBINE HOT SECTION COMPONENTS, AiResearch Manufacturing Division of Arizona Report MP5092 MR, September 1963.

7. General Electric Company, HOT CORROSION MECHANISM STUDY, February 1966, AD 629598.

8. Dean, A. V., RESISTANCE OF NICKEL AND COBALT BASED ALLOYS TO SEA SALT CORROSION AT ELEVATED TEMPERATURE, Ministry of Aviation N.G.T.E. (Pyestock) Report R267, May 1965.

9. Foster, A. D., FUELS, Journal of Engineering for Power, Trans ASME, Series A, July 1959, p. 234.

10. Rentz, W. A., Downer, J. B., and Russel, R. N., AN INVESTIGATION OF SULPHIDATION OF TURBINE BLADE MATERIALS, Pratt and Whitney Aircraft, Formal Report No. 1843.

11. Niles, W. D., HIGH-TEMPERATURE SULPHUR CORROSION, Esso Report, December 1960.

12. Danek, G. J., STATE OF THE ART SURVEY ON HOT CORROSION IN MARINE GAS TURBINE ENGINES, Marine Engineering Laboratory R&D Report 32/65, March 1965.

13. Curbishley, G., and Price, M. H., THE EFFECTS OF THERMAL CYCLING ON SULPHIDATION OF NICKEL AND COBALT BASED SUPERALLOYS, unpublished report at Lucas Gas Turbine Equipment, Ltd. (Burnley), 1966.

14. Bergman, P. A., HOT CORROSION OF GAS TURBINE ALLOYS, Corrosion, March 1967.

15. Hancock, P., THE CORROSION OF NICKEL CHROMIUM ALLOYS IN SULPHUR CONTAINING ATMOSPHERES AT HIGH TEMPERATURES, First International Congress on Metallic Corrosion, Butterworths, London, 1961.

16. Bradbury, E. J., Hancock, P., and Lewis, H., THE CORROSION OF NICKEL BASE MATERIAL IN GAS TURBINE AND BOILER ATMOSPHERES, Metallurgia, January 1963.

17. Lewis, H., and Smith, R. A., CORROSION OF HIGH TEMPERATURE NICKEL BASE ALLOYS BY SULPHATE-CHLORIDE MIXTURES, First International Congress on Metallic Corrosion, Butterworths, London, 1961.

18. Davin, A., Coutsouradis, D., and Habraken, L., DRY CORROSION OF COBALT CHROMIUM ALLOYS AT HIGH TEMPERATURE--INFLUENCE OF TERNARY ADDITIONS, Cobalt 35, June 1967, p. 69.

19. Bergman, P. A., Sims, C. T., and Beltran, A. M., DEVELOPMENT OF HOT CORROSION RESISTANT ALLOYS FOR MARINE GAS TURBINE SERVICE, General Electric Company, January 1966, AD 629786.

20. Davin, A., and Coutsouradis, D., DRY CORROSION OF COBALT, CHROMIUM AND Co-Cr, Ni-Cr AND Fe-Cr ALLOYS IN HYDROGEN SULPHIDE, Cobalt 17, December 1962.

21. Schirmer, R. M., and Quigg, H. T., EFFECT OF JP-5 FUEL CONTENT ON HOT CORROSION OF SUPERALLOYS IN MARINE ENVIRONMENT, ASTM Paper No. 105, presented to 69th Annual Meeting, June 1966.

22. Donachie, M. J., Sprague, R. A., Talboom, F. P., and Bradley, E. F., EFFECTS OF TURBINE ATMOSPHERES ON SULPHIDATION CORROSION, A.S.M.E. publication 67-GT-2, presented at Gas Turbine Conference, Houston, Texas, November 1966.

23. Bergman, P. A., DEVELOPMENT OF HOT CORROSION RESISTANT ALLOYS FOR MARINE GAS TURBINE SERVICE, General Electric Co., January 1966, AD 629786.

24. Wheaton, H. L., STUDY OF HOT CORROSION OF SUPERALLOYS, Avco Lycoming Division Report 2195.8.2, December 1966.

25. Walters, J. J., STUDY OF THE HOT CORROSION OF SUPERALLOYS, Avco-Lycoming Division, September 1967, AD 822779.

26. de Crescente, M. A., and Bornstein, N. S., FORMATION AND REACTIVITY THERMODYNAMICS OF SODIUM SULPHATE WITH GAS TURBINE ALLOYS, Corrosion, Vol. 24, May 1968.

27. Quigg, H. T., and Schirmer, R. M., EFFECT OF SULPHUR IN JP-5 FUEL ON HOT CORROSION OF COATED SUPERALLOYS IN MARINE ENVIRONMENTS, Phillips Petroleum Co., May 1968, AD 834682.

28. Steverding, B., INTERGRANULAR SULPHUR CORROSION OF NICKEL TUBES, Corrosion, December 1962, p. 433.

29. Mason, B. J., THE PHYSICS OF CLOUDS, Oxford, The Clarendon Press, 1957, pp. 57-63.

Unclassified

Security Classification

DOCUMENT CONTROL DATA - R & D

(Security classification of title, body of abstract and indexing annotation must be entered when the overall report is classified)

1. ORIGINATING ACTIVITY *(Corporate author)* AiResearch Manufacturing Company 9851 - 9951 Sepulveda Blvd. Los Angeles, California 90009	2a. REPORT SECURITY CLASSIFICATION Unclassified 2b. GROUP

3. REPORT TITLE

Hot Corrosion Resistance of Materials for Small Gas Turbine Recuperators

4. DESCRIPTIVE NOTES *(Type of report and inclusive dates)*

5. AUTHOR(S) *(First name, middle initial, last name)*

George Curbishley Erich Gellersen
William Larson
Don McGrath

6. REPORT DATE	7a. TOTAL NO. OF PAGES	7b. NO. OF REFS
December 1969	284	29

8a. CONTRACT OR GRANT NO. DAAJ02-67-C-0048 b. PROJECT NO. 1G162203D142 c. d.	9a. ORIGINATOR'S REPORT NUMBER(S) USAAVLABS Technical Report 69-92 9b. OTHER REPORT NO(S) *(Any other numbers that may be assigned this report)* 69-5351

10. DISTRIBUTION STATEMENT

This document is subject to special export controls, and each transmittal to foreign governments or foreign nationals may be made only with prior approval of US Army Aviation Materiel Laboratories, Fort Eustis, Virginia 23604.

11. SUPPLEMENTARY NOTES	12. SPONSORING MILITARY ACTIVITY
	U. S. Army Aviation Materiel Laboratories Fort Eustis, Virginia

13. ABSTRACT

Hot corrosion tests were carried out on various brazed recuperator tubing materials to determine their suitability for service in gas turbine exhaust environments.

Five tubing materials (Hastelloy X, Inconel 625, Incoloy 800, N-155, and Type 347 stainless steel) and three types of brazing alloy (nickel based, nickel-manganese based and gold based) were selected for evaluation on the basis of economics, corrosion resistance, and mechanical properties.

Thin wall tubes, having simulated headers brazed to them, were exposed at temperatures between 1100° and 1500°F to synthetic turbine exhaust gases containing sea salts. In this environment, stress-rupture properties were measured under thermal cycling conditions for periods up to 1000 hours. Following these tests, a recuperator, fabricated from N-155 and Incoloy 800 using a nickel based brazing alloy, was operated in the salt contaminated exhaust of a JP-4 fuelled combustor for a period of 500 hours, with tube temperatures ranging from 900 to 1500°F.

Nickel chromium brazing alloys proved to be the most resistant to hot corrosion. Inconel 625 and Hastelloy X exhibited the best stress-rupture properties and hot corrosion resistance. Type 347 stainless steel had inadequate corrosion resistance above 1300°F. Incoloy 800 and N-155 suffered from localized oxidation and their integrity over prolonged periods is questionable. Sea salt concentration had a strong effect on corrosion rate in the recuperator test.

DD FORM 1 NOV 68 1473 REPLACES DD FORM 1473, 1 JAN 64, WHICH IS OBSOLETE FOR ARMY USE.

Unclassified

Security Classification

14. KEY WORDS	LINK A		LINK B		LINK C	
	ROLE	WT	ROLE	WT	ROLE	WT
Hot corrosion						
Thin wall tubes						
Recuperator						
Stress rupture properties						
Brazing alloy selection						
Sea salt contaminated exhaust gas						

454-70